REC

REPORT DOCUMENTATION PAGE

AFRL-SR-AR-TR-04-

0263

1. AGENCY USE ONLY (Leave blank)	2. REPORT DATE	3. REPORT TYPE AND DATES COVERED
	April 15, 2004	FINAL, 10/1/98 to 9/30/01

4. TITLE AND SUBTITLE

Studies of Anomalous Shock Wave Propagation And Dispersion in Weakly Ionized Plasmas

5. FUNDING NUMBERS

AFOSR Grant No. F49620-99-1-0023

6. AUTHOR(S)

I. V. Adamovich, W. R. Lempert, V. V. Subramaniam, and J. W. Rich

7. PERFORMING ORGANIZATION NAME(S) AND ADDRESS(ES)

Dept. of Mech. Eng., The Ohio State University
650 Ackermann Road, Suite 255
Columbus, OH 43202

8. PERFORMING ORGANIZATION REPORT NUMBER

736784

9. SPONSORING / MONITORING AGENCY NAME(S) AND ADDRESS(ES)

Air Force Office of Scientific Research
AFOSR/NA
4015 Wilson Blvd.
Arlington, VA 22203-1954

10. SPONSORING / MONITORING AGENCY REPORT NUMBER

11. SUPPLEMENTARY NOTES

12a. DISTRIBUTION / AVAILABILITY STATEMENT

Approved for public release, distribution unlimited

20040520 059

13. ABSTRACT *(Maximum 200 words)*

The effects of weak ionization on the strength of shock waves in supersonic gas flows were studied in an experimental program. Claims that weak ionization can substantially reduce shock wave strength, independently of any plasma heating effects, were evaluated. Experiments were conducted in both shock tubes and in supersonic, steady flow, plasma wind tunnels. Temperatures and ionization levels in the flows were measured. It was demonstrated that shocks can be weakened by creating an electric discharge in the flow, but this effect is purely a consequence of the Joule heating of the plasma. Without heating, ionization alone does not weaken the shock.

14. SUBJECT TERMS

Plasma aerodynamics, weakly ionized gases, shock waves in ionized gases

15. NUMBER OF PAGES

16. PRICE CODE

17. SECURITY CLASSIFICATION OF REPORT	18. SECURITY CLASSIFICATION OF THIS PAGE	19. SECURITY CLASSIFICATION OF ABSTRACT	20. LIMITATION OF ABSTRACT

STUDIES OF ANOMALOUS SHOCK WAVE PROPAGATION AND DISPERSION IN WEAKLY IONIZED PLASMAS

FINAL REPORT

by

Igor V. Adamovich, Walter R. Lempert, Vish V. Subramaniam, and J. William Rich

Nonequilibrium Thermodynamics Laboratories
Dept. of Mechanical Engineering
The Ohio State University

Prepared for

Air Force Office of Scientific Research
Unsteady Aerodynamics and Hypersonics Program

SUMMARY

The research program reported here is an experimental investigation of the effects on shock wave strength in supersonic gas flows, created by weakly ionizing the gas. Prior to the inception of the present program, an interesting effect was noted in the aerodynamics and plasma literature. It was reported that when various molecular and atomic gases, including air, argon, carbon dioxide, and many others, were weakly ionized, the strength of a shock wave propagating through the gas was substantially weakened. These previous experiments were in unsteady environments, and were of two basic types: 1) Normal shocks were created in shock tubes, and the shock was allowed to propagate through the weakly ionized gas. 2) Models (normally, small spheres) were fired into ballistic test ranges, and again allowed to propagate through weakly ionized gas. In both classes of experiments, the shock wave strength and structurewere monitored. It was discovered that there were strong effects of the ionization on the shock waves in most of the experiments. Basically, in the shock tube experiments, the strength of the shock wave substantially decreased, and, also, the shock wave appeared to be dispersed, breaking up into more that a single normal shock. In the ballistic test range experiments, the bow shock on the test models was substantially weakened, the shock stand-off distance increased, and, in some cases, the bow shock mostly disappeared. Enormous reductions in the supersonic wave drag were reported. While most of these results were reported in the Russian literature, some key points were reproduced in experiments at USAF laboratories, although it was noted that various important features required further measurement and test.

In most all these experiments, gas ionization levels were low, with approximately 10^{-8} to 10^{-6} of the gas molecules being ionized in these plasmas. Furthermore, it was believed that the gas temperatures in these experiments remained rather low. To achieve ionization levels of 10^{-6} in atmospheric air in a thermal plasma requires heating to several thousand degrees. However, in the typically low pressure environments of the experiments, the plasma conditions were more those of a glow discharge plasma, characterized by rather cold gas kinetic temperatures. The low temperatures were a critical point for interpretation of the observed shock wave weakening. This is because if there was substantial heating of the gas by the electric discharge creating the ionization, such heating alone could cause the observed weakening effects. With such heating, the speed of sound in the gas would increase, and even for a constant shock velocity or model velocity, the Mach number of the flow would decrease, and the shock strength would decrease to the values characteristic of the lower Mach number flow. Such a purely thermal effect is, of course, a well-known and trivial result in compressible gas dynamics. Similarly, even without substantial heating of the entire bulk gas, if creating the plasma resulted in substantial thermal gradients, local "hot pockets", and/or non-uniform boundary layer interactions, the shock weakening could be understood within the framework of conventional gas dynamic theory.

On the other hand, if there were no substantial gas heating in the previous experiments, and if the plasma were uniform, the observed weakening would be truly "anomalous"; researchers began to seek an explanation in basic plasma theory. Such an anomaly would

not be just of theoretical interest. Inasmuch as huge reductions in wave drag were reported for what was initially thought to be rather modest plasma power requirements, these results have major potential for achievement of more efficient hypersonic flight.

The goal of the present program was to find out if the observed anomalous shock weakening effects were the result of gas heating and/or gas flow field thermal nonuniformities, or, whether, they were solely the result of the presence of a very small fraction of electrons and ions ($< 10^{-6}$) in the flow. For this test, experiments have been designed in which varying levels of ionization can be created and controlled in the test gases, independently of causing significant changes in test gas temperature. Ionization fractions up to 10^{-6} can be produced in air and other gases, and electrons and ions can be almost totally removed in our test flows, with variation of gas temperatures of, at most, a few tens of degrees. Further, care was taken to create very spatially uniform plasmas, to avoid arc filaments or local hot spots producing density inhomogeneities. There were careful measurements of flow field temperature and electron density to demonstrate this level of control.

Two classes of experiments have been conducted in the program. In the first class, described in Sections 1-1 through 1-6 of this report, a shock tube was set up, and both glow and optically pumped plasmas were created in the tube. Normal shock wave propagation in the tubes was measured, and shock strength and structure determined. There were careful measurements to characterize the plasma parameters, and results were interpreted in terms of a fluid dynamic analysis (Section 1-1). It was found that all the shock weakening and dispersive effects were, indeed the effect of thermal gradients and heating of the test gases. It was also shown that in the absence of thermal gradients, viscous effects (i.e. wall shear) produces similar effects on shock propagation and structure.

Sections 2-1 through 2-5 are unlike any of the previous experiments in this research area, in that a continuous flow supersonic plasma wind tunnel was built. In this tunnel, steady state flows in the M=2 to M=4 range could be created. Upstream electric discharges created an ionized gas flow; the flow in the supersonic test section was essentially a flowing "afterglow". Small models, usually sharp nosed wedges or cones, were installed in the test section. The bow shock position and strength were monitored, as the gas temperature and the electron density of the flow were independently varied. While, in these experiments, it was possible to significantly weaken the bow shock on the models, this could only be accomplished with the appropriate amount of flow heating. The experiments demonstrate that the presence of ions and electrons alone in the flow do not change the strength of the bow shocks in these flows. The conclusions are therefore the same as those of our shock tube experiments of Section 1, and those of similar shock tube experiments at Princeton University; there is no effect of weakly ionizing the gases on supersonic shock waves, independent of simultaneously heating the flow. In effect, there is no pure "plasma magic", as has been previously hypothesized.

1. Unsteady Normal Shocks

Studies in Shock Tubes

1.1 On the Characteristics of a Spark Generated Shock Wave

PHYSICS OF FLUIDS VOLUME 12, NUMBER 4 APRIL 2000

On the characteristics of a spark generated shock wave

S. M. Aithal[a] and V. V. Subramaniam[b]
Center for Advanced Plasma Engineering, Non-Equilibrium Thermodynamics Laboratories, The Ohio State University, 206 West 18th Avenue, Columbus, Ohio 43210

(Received 18 May 1999; accepted 28 December 1999)

Recent experiments involving shock waves propagating through weakly ionized plasmas have raised questions regarding interpretation of the experimental results. In aid of analyzing these experimental results, shock waves initiated by a simulated spark and their subsequent propagation in a cylindrical tube containing argon initially at 30 Torr and 300 K, have been analyzed numerically in this paper. Numerical solutions to the compressible Navier–Stokes equations are considered under the four conditions of induced flow (a) without wall friction, (b) with wall friction, (c) with wall friction and purely axial thermal gradients, and (d) with wall friction and both axial and radial thermal gradients. Although plasma processes have not been simulated, it is found that the effects of wall shear and thermal gradients alone are sufficient to explain most of the experimental observations. This work represents a first step in the analysis of this problem before plasma effects can be modeled. © *2000 American Institute of Physics.* [S1070-6631(00)01804-3]

I. INTRODUCTION

Electric sparks set off by sudden and intense capacitive discharges in gases have been used for generation of shock waves. They provide a means of studying shock propagation through plasmas and reacting gases. Interest in spark-generated shock waves stems from recent measurements involving their interactions with plasmas.[1–3] Some of these interactions may possibly arise due to the electrostatic properties of the plasma,[3] or due to thermal gradients arising from Ohmic heating.[4–10] Before plasma–shock interactions can be studied in detail, it is necessary to thoroughly understand the influence of thermal effects alone. The aim of this paper is to examine thermal and viscous effects on shock propagation, independently of any plasma effects. In this paper, we examine the behavior of spark-generated shock waves propagating through a nonionized gas under four different conditions, using numerical solutions of the compressible Navier–Stokes equations. The four conditions are shock propagation (i) without wall shear and in the absence of thermal gradients, (ii) with wall shear and no thermal gradients, (iii) with wall shear and purely axial thermal gradients, and (iv) with wall shear and with both axial and radial thermal gradients. These cases allow the effects of thermal gradients and wall shear on shock propagation to be isolated.

In the experiments reported in Refs. 1–3, a capacitor is discharged across a spark gap in argon or nitrogen at pressures on the order of 30 Torr. The process of energy addition to the gas by the discharging capacitor ultimately resulting in a spark, has been analyzed previously.[11] The electrons are initially heated to high temperatures by electron–electron collisions energized by the applied electric field, and subsequently transfer energy to the gas atoms or molecules via electron–neutral collisions. This process is found to result in rapid heating of the gas within time scales on the order of a microsecond and drive a shock wave. Experimental measurements reported in Refs. 1 and 2 use a He–Ne laser beam to record passage of the propagating shock wave by deflection of the beam either onto or away from a photo-detector caused by the density gradient across the shock front. Since the signal intensity is proportional to the magnitude of the density gradient, a sharp signal resembling a Delta function is recorded. This photo-acoustic deflection (PAD) technique has been used to experimentally investigate the effects of ionization on propagation of spark-generated shocks.[1,2] Sample PAD signals reported in Ref. 1 are displayed here in Fig. 1 for illustrative purposes.

Spark-generated shock waves have been analyzed within the framework of one-dimensional propagation,[8] and two-dimensional inviscid propagation using Euler's equations.[6,7] These calculations suggest that many of the experimental observations reported in Refs. 1 and 2 can be explained by shock curvature in the presence of radial temperature gradients, without the need to invoke plasma effects. Earlier work also posits this notion that thermal effects explain the characteristics of shock propagation and structure in the presence of weakly ionized plasmas.[4,5] There has since been compelling experimental evidence provided for the importance of gas heating and radial thermal gradients,[10] but the effects of viscosity and wall shear are not known. The behavior of the shock speed versus current in the glow discharge plasma as reported in Refs. 1 and 2 exhibits nonlinear behavior that cannot be explained by thermal effects alone. The focus of this paper is on the characteristics of spark-generated shock waves including the effects of viscosity and more importantly, wall friction. In addition, we examine the behavior of

[a]Presently Technical Specialist, CFD Research Corporation, Cummings Research Park, 215 Wynn Drive, Suite 501, Huntsville, Alabama 35805; Telephone: 256-726-4963; Fax: 256-726-4806; Electronic mail: sma@cfdrc.com
[b]Professor, Department of Mechanical Engineering & Chemical Physics Program; Telephone: 614-292-6096; Fax: 614-292-3163; Electronic mail: subramaniam.1@osu.edu

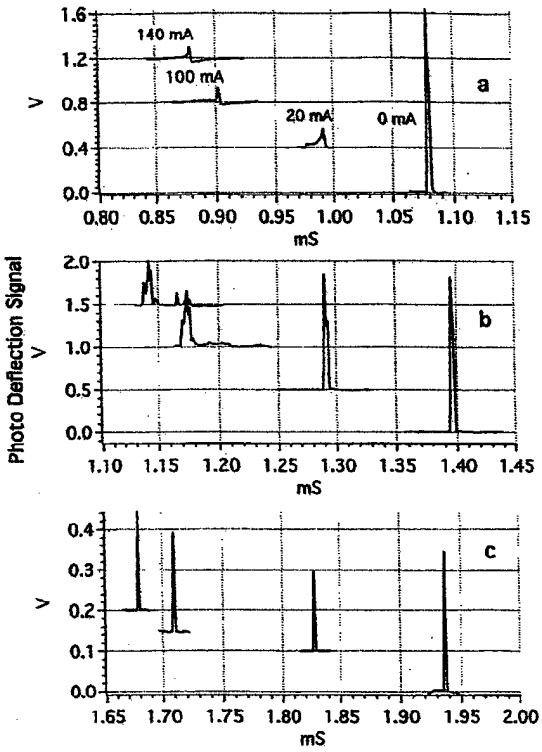

FIG. 1. Experimentally measured PAD signals recorded as a spark-generated shock wave traverses through a glow discharge and re-emerges into a cold gas (from Ref. 1).

such spark-generated shocks in the presence of thermal gradients (purely axial thermal gradients as well as axial and radial gradients), in order to understand the propagation of spark-generated shocks in the presence of thermal gradients better. In contrast to earlier work,[6,7] we examine the effects of thermal gradients (including pure axial thermal gradients) on shock propagation using numerical solutions to the compressible Navier–Stokes equations. The intent of this work is not to model the experiments reported in Refs. 1–3, but to lay the foundation for its proper interpretation. This work is viewed as a first step before modeling the spark discharge leading to formation of the shock and the glow discharge through which the shock traverses.

This paper is organized as follows. Formulation of the problem is discussed in Sec. II including the governing equations and numerical method used. Section III then provides the results of our numerical calculations and discusses them in detail. Finally, a summary is provided in Sec. IV.

II. PROBLEM FORMULATION

A. Governing equations

We consider here a cylindrical tube, 5 cm in diameter, containing argon at a pressure of 30 Torr. Launching of a spark-generated shock wave is simulated by means of volumetric energy addition at a specified location for a specified period of time. The governing equations determining the subsequent response of the gas to this volumetric heat addition is described by the compressible Navier–Stokes equations, in conjunction with conservation of energy. These equations in two-dimensional (2D), axi-symmetric form are

$$\frac{\partial \rho}{\partial t}+\frac{1}{r}\frac{\partial}{\partial r}(r\rho u)+\frac{\partial}{\partial x}(\rho w)=0, \tag{1}$$

$$\frac{\partial}{\partial t}(\rho u)+\frac{1}{r}\frac{\partial}{\partial r}(r\rho u^2)+\frac{\partial}{\partial x}(\rho uw)-\frac{\rho V^2}{r}$$
$$=-\frac{\partial p}{\partial r}+\frac{\partial}{\partial r}\left[2\eta\frac{\partial u}{\partial r}-\frac{2}{3}\eta\nabla\cdot\mathbf{u}\right]$$
$$+\frac{\partial}{\partial x}\left[\eta\left(\frac{\partial u}{\partial x}+\frac{\partial w}{\partial r}\right)\right]+\frac{2\eta}{r}\left(\frac{\partial u}{\partial r}-\frac{u}{r}\right), \tag{2}$$

$$\frac{\partial}{\partial t}(\rho w)+\frac{1}{r}\frac{\partial}{\partial r}(r\rho uw)+\frac{\partial}{\partial x}(\rho w^2)$$
$$=-\frac{\partial p}{\partial x}+\frac{\partial}{\partial x}\left[2\eta\frac{\partial w}{\partial x}-\frac{2}{3}\eta\nabla\cdot\mathbf{V}\right]$$
$$+\frac{1}{r}\frac{\partial}{\partial r}\left[r\eta\left(\frac{\partial u}{\partial x}+\frac{\partial w}{\partial r}\right)\right], \tag{3}$$

$$\frac{\partial e_T}{\partial t}+\frac{1}{r}\frac{\partial}{\partial r}([e_T+p]ur)+\frac{\partial}{\partial x}([e_T+p]w)$$
$$=\frac{1}{r}\frac{\partial}{\partial r}\left(kr\frac{\partial T}{\partial r}\right)+\frac{\partial}{\partial x}\left(k\frac{\partial T}{\partial x}\right)+\eta\Phi+QtH(t_0-t)$$
$$\times[H(x-x_0)-H(x-x_1)], \tag{4}$$

where the energy equation is written for transport of total energy, i.e., internal energy and kinetic energy per unit volume, with $e_T=e+\rho(u^2+w^2)/2$. The internal energy per unit volume, e, is given by $e=\frac{3}{2}nk_BT$ for monatomic gases, where n is the total number density, k_B is Boltzmann's constant, and T is the temperature. In Eqs. (1)–(4), u is the radial component of velocity, V is the azimuthal component of velocity (set to 0 here), w is the streamwise or axial component of velocity, ρ is the mass density, $p=nk_BT$ is the pressure, η is the coefficient of dynamic viscosity which varies with temperature to the 3/2 power according to mean free path theory, x is the axial coordinate, r is the radial coordinate, t is time, and k is the thermal conductivity of the gas. Φ is the viscous dissipation function and its expression can be found in Ref. 12. $H(t_0-t)$ is the Heaviside step function in time with $t_0=1$ μs, and $[H(x-x_0)-H(x-x_1)]$ ensures that the energy added by the simulated spark is confined to a region between $x_0\leqslant x\leqslant x_1$. For the cases considered in this paper, $x_0=19.95$ cm, $x_1=20.05$ cm, and $Q=4.413\times10^{14}$ W/m^3/s. This corresponds to an energy density of 0.221 J/cm^3 or 0.433 mJ added over the 1 μs time interval. It is important to point out that this value is three orders of magnitude lower than the energy of several Joules released by the spark in the experiments of Refs. 1–3. Addition of energy on the order of several Joules within a microsecond would require extremely fine grids to resolve the steep spatial gradients in the vicinity of the spark in the first few microseconds. It would also require taking prohibitively small time steps to accurately resolve the temporal changes necessary for stability. How-

ever, the regions of interest in this work are those near the propagating shock fronts formed as a result of this rapid release of energy, and not the regions where the energy release actually occurs. Equations (1)–(4) do not account for turbulence, and the implicit assumption of laminar flow is verified *a posteriori*. For the weak shocks propagating at low pressure considered in this work, the induced streamwise components of velocity are less than 100 m/s and the kinematic viscosity at 30 Torr is on the order of 5×10^{-3} m^2/s for argon. Consequently, the Reynolds number based on a tube diameter of 5 cm (0.05 m) is expected to be on the order of 10^3 or less. Since this is less than the critical Reynolds number for internal flows in tubes of circular cross section, the assumption of laminar flow is justified.

As initial conditions, zero velocities are prescribed everywhere in the domain, the temperature of the undisturbed gas is taken to be a uniform 300 K, and the pressure is set to 30 Torr. Implicit extrapolation is used for the temperature and velocity components at both axial boundaries, while pressure is prescribed as constant. The density is then calculated using the ideal gas equation of state ($p=nk_BT;\rho=mn$, where m is the atomic mass of argon). In the radial direction, no-slip boundary conditions (i.e., zero velocity) are prescribed at $r=r_0$, the outer radial boundary, and symmetry boundary conditions are prescribed at the centerline. Also by symmetry, the centerline is an adiabat and $\partial T/\partial r=0$ at $r=0$. At the outer wall, $r=r_0$, the adiabatic boundary condition is applied. Similarly, $\partial p/\partial r=0$ at $r=0$ and at $r=r_0$. As described by the source term in Eq. (4), heat is added over a period of one microsecond (i.e., $t_0=1$ μs), and the subsequent temporal response as determined by Eq. (1)–(4) is calculated numerically.

B. Numerical method

The governing equations [Eqs. (1)–(4)] are solved using the linearized block implicit (LBI) of Briley and McDonald.[13] This method is described in detail elsewhere,[14] and therefore, only a brief summary is provided here. Equations (1)–(4) are discretized in time using Crank–Nicolson differencing, and the spatial derivatives are central differenced in space. The two-dimensional operator is split using the Douglas–Gunn alternating direction implicit (ADI) procedure, resulting in a block tridiagonal matrix equation in each of the coordinate directions.[15] The block tridiagonal matrix is solved in each coordinate direction at each time step, using LU (lower-upper) decomposition.

The addition of energy over a period as short as one microsecond gives rise to steep gradients in the vicinity of the region of energy addition, during the early portion of the transient. Consequently, fine grids are required to adequately resolve these early, steep gradients. Use of fine grids is computationally expensive, especially at later times when gradients in the dependent variables are relatively less steep and coarser grids would suffice. In this work, we use a specific procedure to avoid prohibitive computational cost. This procedure consists of initially using a 1000×25(axial×radial) grid over a spatial region 10 cm×2.5 cm. Following the initial, rapid heat release and initiation of the shock wave, this grid is used until the shock waves have traveled approximately half the domain. At this instant, the solution is mapped onto another grid of the same size (1000×25), but double in spatial extent, which is equivalent to doubling the spatial step size Δx in the axial direction. This procedure is repeated with further advancement in time, until the shock waves have traversed the spatial location of interest. For the calculations reported here, the axial step size Δx varied from 0.1 mm to a maximum of 0.4 mm using this procedure, and a $\Delta t=31$ ns was used.

Three cases of spark-generated shock propagation are considered here. In all cases, the shock wave is produced in Argon initially at 30 Torr and 300 K. The effects of viscosity and wall friction are explored using two different boundary conditions. The first set of boundary conditions (i.e., first case) is $\partial u/\partial r=0$ and $\partial w/\partial r=0$ applied at the wall of the tube in order to examine viscous effects independently of wall friction. The second set of boundary conditions (i.e., second case) is with the usual no-slip boundary conditions ($u=w=0$) applied at the wall to simulate real viscous flow in a tube including the effects of wall shear. The first set of boundary conditions, i.e., *unconfined* shock propagation without wall friction, is shown to be similar in nature to quasi one-dimensional shock propagation despite the inclusion of viscosity. The second set of boundary conditions (second case), with no-slip conditions applied at the wall, also considers the effects of purely axial thermal gradients. In this second case, the rightward propagating spark-generated shock is initiated in a region of relatively cold temperature (300 K) and launched into a region (between $x=25$ cm and $x=30$ cm) where the temperature is initially at 1000 K. Beyond $x=30$ cm, the temperature is reduced back to 300 K. This is a purely axial temperature gradient, since the heated region is extended all the way to the wall. This initial distribution does relax in time due to heat conduction as the shock is initiated upstream and launched, but there is insufficient time to change appreciably. This is because the time required for the shock to travel from the location of initiation to the edge of the heated region is on the order of 100 μs while the relaxation time by heat conduction is on the order of 10 milliseconds. In the third case, the effects of a radial temperature gradient are examined as the temperature distribution in the hot region is varied from 1000 K at the centerline to 300 K at the wall in a parabolic manner. As before, the shock is initiated in a region initially maintained at 300 K. In this last case, the shock is made to encounter both an axial gradient as well as radial gradient as it enters the heated region. The temperature distributions in the last case resemble the expected temperature variations in a uniform glow discharge.

III. RESULTS AND DISCUSSION

A. Propagation into a uniform gas in the absence of wall friction

In this case, a shock is initiated in argon at 30 Torr and 300 K by energy addition over a prescribed time interval of 1 μs as described in Sec. II. Such energy addition over one microsecond simulates the generation of a shock wave trig-

gered by a capacitively discharged spark. The governing equations for compressible, viscous flow are solved with boundary conditions that mimic an *unconfined* viscous gas, i.e., one without the presence of a wall. These boundary conditions are used in order to examine the effects of viscosity independently of wall friction and in the absence of thermal gradients, a situation not considered in previous analyses of the problem using numerical solutions to Euler's inviscid equations of motion.[6,7] This solution is compared with solutions to the quasi one-dimensional equations of motion, and contrasted later in Sec. III B with the realistic case of viscous flow in a bounded cylindrical tube where boundary effects (i.e., wall friction) are considered.

The governing equations for this problem [Eqs. (1)–(4)] are solved numerically using the LBI method described in Sec. II. In this first case, the usual no-slip boundary conditions at the wall are replaced by $\partial u/\partial r=0$ and $\partial w/\partial r=0$. These conditions effectively simulate the absence of a boundary so that wall friction is absent while the flow is still viscous, i.e., this is an *unconfined* gas into which a spark-generated shock wave is launched. The resulting profiles of density at $r=0$ nondimensionalized by the undisturbed gas density, $\rho_0=0.0641\ \mathrm{kg/m^3}$, at 100, 200, 300, and 400 μs, are shown as a function of the axial coordinate x in Fig. 2(a). Formation of two propagating shocks, one to the right and one to the left, are clearly evident in this figure. The passage of the shock is often detected in experiments using methods such as laser deflection or PAD[1,2] that are sensitive to the density gradient, and it is, therefore, instructive to examine the axial derivative of the density integrated along the radial direction (i.e., along the transverse line of sight[6,7]). Thus, the observed signal in an experimental realization of this problem would be proportional to $\partial\rho/\partial x$. This derivative integrated in the radial direction, referred to here as the simulated PAD signal, is plotted in Fig. 2(b). In practice, the detector sensitivity is limited to a minimum value of this axial density gradient. Hence, an experimental counterpart of Fig. 2(b) would appear similar except that in some neighborhood around $\partial\rho/\partial x=0$ it would be truncated, as shown for illustrative purposes by the dotted horizontal lines in Fig. 2(b). As expected, it can be seen from Figs. 2(a) and 2(b) that the pulse waveform spreads out, while the magnitude of the leading compression front decreases with increasing distance from the location of shock initiation. Note however that the simulated PAD signal in Fig. 2(b) maintains a sharp feature similar to a delta function, while decreasing in magnitude, but does not spread out as the density profile does. Moreover, there is no evidence of splitting of the simulated PAD signal. Figure 2(c) shows the calculated pressure profile along the centerline at 300 μs for illustrative purposes, and resembles the density profile in shape.

B. Propagation into a heated region, followed by a colder region: Effects of purely axial temperature gradients

We now consider shock waves initiated in argon at 30 Torr and 300 K using energy release from a simulated spark at $x=20$ cm, and propagating in a cylindrical tube under the action of wall friction. Unlike the case discussed in Sec. III A, the present case considers the realistic case of viscous flow induced by a propagating shock wave in a 5 cm diam cylindrical tube, with the usual no-slip boundary conditions applied at the wall. Of the two shock waves resulting from the simulated spark, the rightward propagating wave is launched into a heated region situated at $25\ \mathrm{cm}<x<30\ \mathrm{cm}$. The heated region is maintained at the same pressure of 30 Torr but at a temperature of 1000 K. After traversing this heated region, the shock re-emerges into cold argon at 300 K and 30 Torr beyond $x=30$ centimeters. The corresponding leftward moving wave propagates into undisturbed argon at 30 Torr and 300 K. This case allows us to simultaneously examine the effects of wall friction (for the leftward moving wave) and a purely axial temperature gradient combined with wall friction (for the rightward moving wave). The rightward propagating wave encounters purely axial temperature gradients on the order of +7000 K/mm at $x=25$ cm and −7000 K/mm at $x=30$ cm, respectively. At these locations, the temperature is raised from 300 to 1000 K within 1 mm, and lowered from 1000 to 300 K within 1 mm, respectively. The calculated profiles of $\rho(x)$ along the centerline ($r=0$) as well as the corresponding simulated PAD signal (proportional to $\partial\rho/\partial x$) are shown in Figs. 3(a) and 3(b), respectively, at 100, 150, 300, and 400 μs. Several interesting characteristics are evident in these solutions, and are discussed next.

We begin first by observing the leftward moving wave, which is affected by wall friction alone, in the absence of any thermal gradients. Three effects are clearly visible. First, the simulated PAD signal for the leftward propagating wave shows effects of "splitting" of the simulated PAD signal or non-monotonic variation of $\rho(x)$ in the *absence of any thermal gradients*, within 10 cm of the initiation point. These profiles are clearly different from the numerical results obtained for a propagating shock in the absence of a wall [see Figs. 2(a) and 2(b)]. Second, the simulated PAD signal is attenuated more than its counterpart, the shock propagating in the absence of wall friction, as can be seen in Figs. 2(a), 2(b), 3(a), and 3(b). Third, there is substantial spreading of the axial density profile behind the front when wall friction is present as can be seen by comparing Fig. 3(a) with Fig. 2(a). Multiple structures are also evident in Fig. 3(b), indicative of departure from monotonic behavior of the instantaneous axial density profile. All three effects, apparent splitting of the shock as observed in the simulated PAD signal, spreading of the signal, and decrease in amplitude are due to the effects of wall friction. It is important to point out that such splitting of the PAD signal due to wall friction alone was not reported in the experiments of Refs. 1 and 2. It is due to the difference in the magnitude of the initial energy loading between the simulations and experiments, eventually leading to the formation of the shock (0.433 mJ is added in this simulation as opposed to the several Joules typically deposited into the gas in the experiments of Refs. 1–3). The reason for the apparent splitting in the PAD signal of the leftward moving wave subjected only to wall shear, can be seen in Fig. 3(c) which shows the density profiles at the centerline ($r=0$) and at $r=1.5$ cm, at 300 μs. The density profiles at r

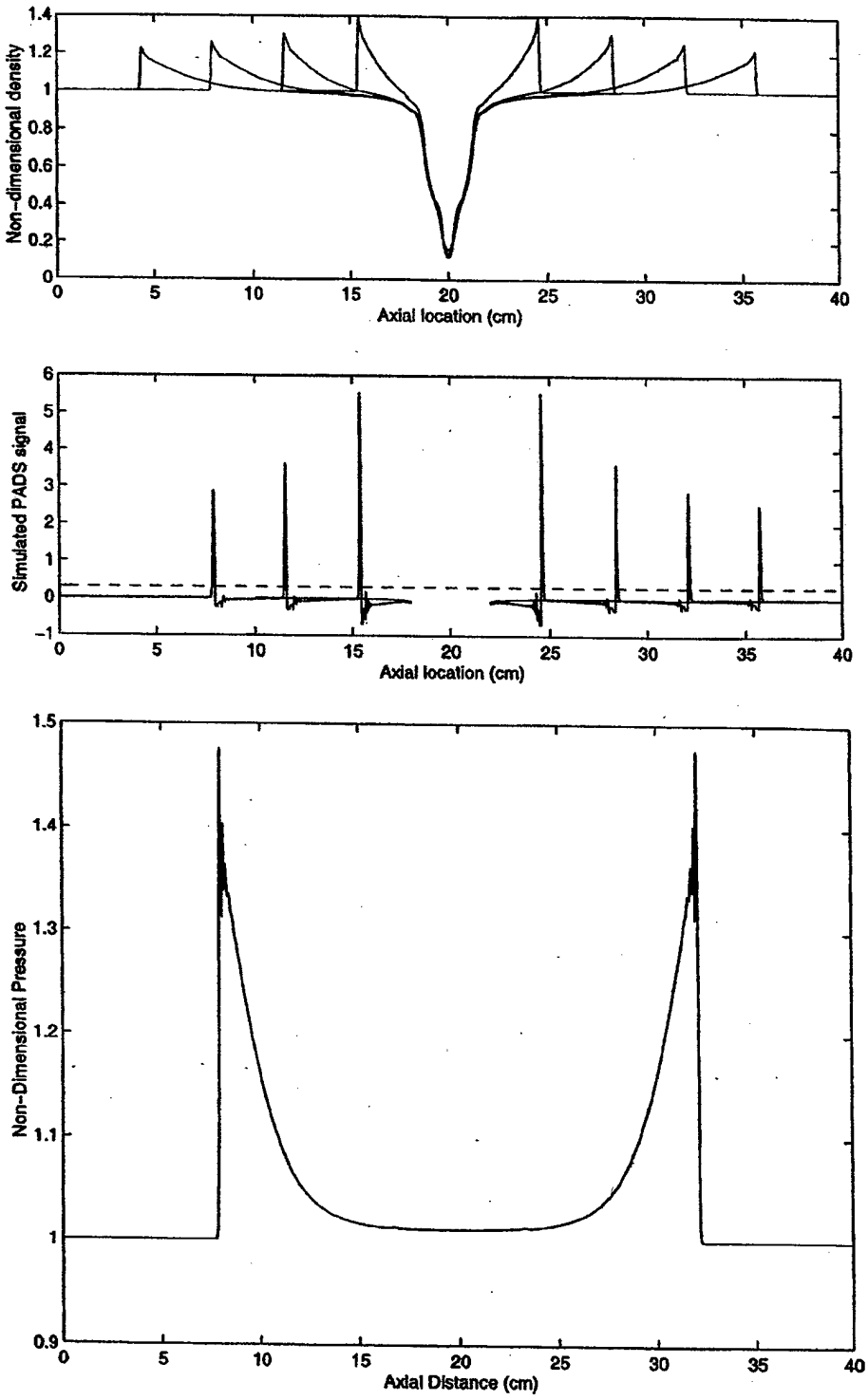

FIG. 2. (a) Profiles of mass density along $r=0$ nondimensionalized by the undisturbed gas density, $\rho_o = 0.0641\ \text{kg/m}^3$, are shown here vs the axial coordinate, x, at several instants (100, 200, 300, and 400 μs, respectively) after energy addition leads to formation of a propagating shock. This result is for the case of shock propagation in an *unconfined* gas with $\partial u/\partial r = 0$ and $\partial w/\partial r = 0$ applied at the walls instead of the usual no-slip boundary conditions. (b) Simulated PAD signal obtained by integrating the axial derivative of density (see 2(a)) in the transverse, i.e., radial, direction. The horizontal dotted line is used to show that experimental limitations on sensitivity would have the effect of truncating the PAD signal in a neighborhood around $\partial p/\partial x = 0$. (c) Profile of pressure along $r=0$ nondimensionalized by the undisturbed pressure, $P = 4000$ Pa, is shown here vs the axial coordinate, x, at 300 μs after energy addition leads to formation of a propagating shock. This result is for the case of shock propagation in an *unconfined* gas with $\partial u/\partial r = 0$ and $\partial w/\partial r = 0$ applied at the outer boundary of the computational domain instead of the usual no-slip boundary conditions. Note the similarity of the shape of the pressure profile to the density profiles shown in (a).

$=0$ and at $r=1.5$ cm. can be seen in Fig. 3(c) to be displaced in space (and hence in time). The shock front near the wall is decelerated due to wall friction, leading to curvature of the shock front. This is what gives the appearance of splitting in the PAD signal as the portion of the shock near the wall is slowed due to wall friction.

The rightward moving wave is also subject to the effects of wall friction, but encounters a heated region before it has a chance to display a split PAD signal. It is important to point out that since the viscosity is temperature-dependent, the heated region is also a region of increased viscosity. It can be seen from these solutions that the amplitude is substantially reduced within the heated region, and partially recovers upon emergence from the heated region. This is to be expected since the heated region has a higher temperature relative to the unheated region. Consequently at the same

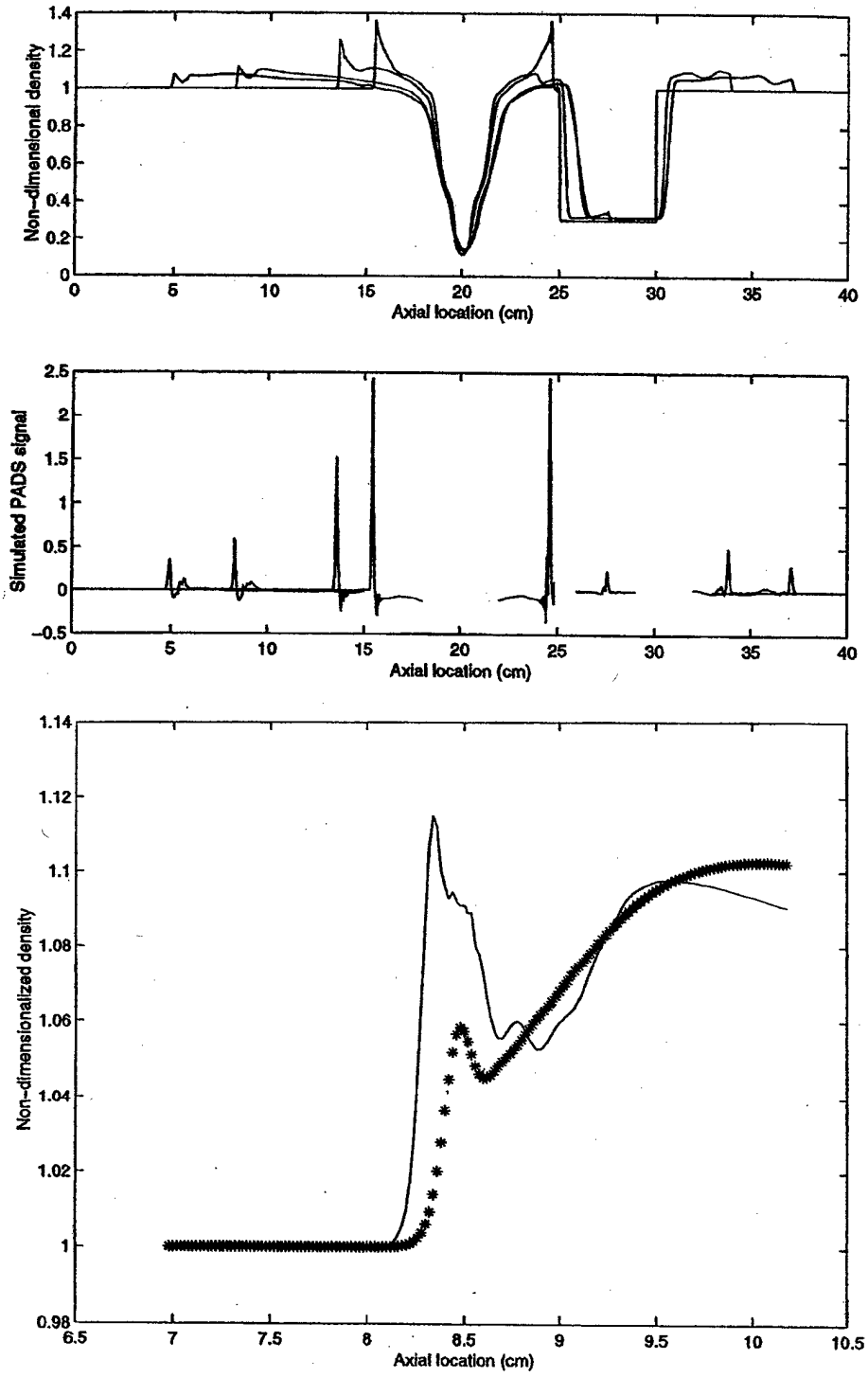

FIG. 3. (a) Profiles of mass density along $r=0$ nondimensionalized by the undisturbed gas density, $\rho_o = 0.0641$ kg/m^3, are shown here vs the axial coordinate, x, at several instants (100, 150, 300, and 400 μs, respectively) after energy addition leads to formation of a propagating shock. This result is for the case of shock propagation in Argon initially at 30 Torr and 300 K, with no-slip conditions applied at the walls. This case considers the realistic bounded viscous flow induced by a traveling shock in a 5 cm diam tube, where the rightward traveling wave encounters a heated region *with no radial temperature gradients*. (b) Simulated PAD signal obtained by integrating the axial derivative of density (corresponding to (a)) in the transverse, i.e., radial, direction. (c) Profiles of density for the leftward moving wave are shown here at 300 μs, at two different radial locations: $r=0$, and $r = 1.5$ cm. It is the radial staggering of these density profiles that gives rise to apparent splitting in the PAD signal. In this case, the portion of the shock wave nearest the wall is retarded due to wall friction and lags behind its counterpart at the centerline. This gives the appearance of two or more split structures in the PAD signal.

pressure, the density must be lower compared to its corresponding level in the colder regions. Within the heated region, the simulated PAD signal exhibits splitting at 150 μs, whereas its corresponding leftward moving twin does not, at the same instant of time. This is really due to increased wall shear resulting from an increase in viscosity arising from the higher temperature. Hence, the rightward moving wave exhibits splitting in the simulated PAD signal before the leftward moving wave, in this case of purely axial thermal gradients. The leftward moving wave shows evidence of splitting in the absence of thermal gradients due to the effect of wall friction alone, but at a later time. Finally, acceleration of the rightward moving wave is clearly evident in Figs. 3(a) and 3(b) when the corresponding axial locations of the two waves are compared at 150, 300, and 400 μs. The heated region has also clearly altered the trailing structure of the rightward moving wave in an irreversible manner.

As a point of further comparison and contrast, we

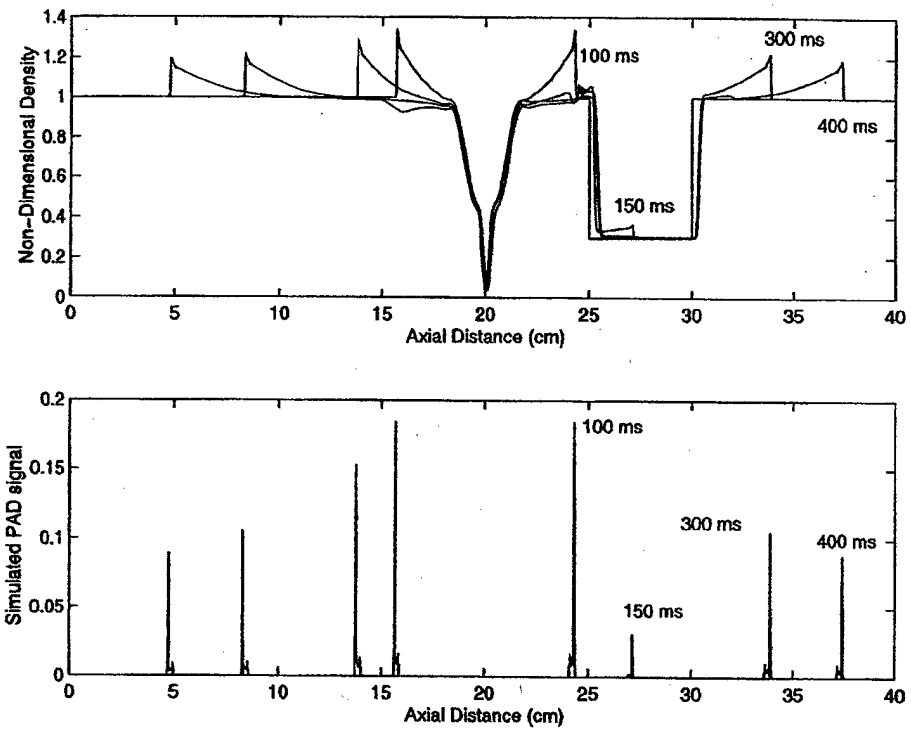

FIG. 4. (a) Quasi 1D calculations for a propagating shock in a tube in the absence of wall friction. Note the similarity between the leftward traveling wave and the 2D shock propagation in an *unconfined* gas [Fig. 2(a)]. The rightward traveling shock encounters the same heated region as in the case shown in Fig. 3(a), but clearly remains intact even upon reemergence into the cold gas. (b) Simulated PAD signal obtained by differentiating the density profile shown in Fig. 4(a).

present solutions of the (inviscid) quasi one-dimensional equations for this case in Figs. 4(a) and 4(b). As in the 2D case presented in this section, energy release occurs at $x = 20$ cm. resulting in two propagating shocks. The rightward moving shock wave is made to encounter a heated region exactly as for the shock shown in Figs. 3(a) and 3(b), while the leftward moving wave is not. It can be seen from Figs. 4(a) and 4(b) that while the quasi 1D (one-dimensional) solution predicts the acceleration of the rightward moving wave, it shows no splitting in the simulated PAD signal due to the purely axial thermal gradients. The same features observed in the 2D viscous solution for shock propagation in *unconfined* Argon (i.e., in the absence of wall shear) are found in numerical solution of the quasi one-dimensional inviscid equations as well. This can be seen in Fig. 4(a) along with the associated simulated PAD signal in Fig. 4(b). The quasi one-dimensional solution is seen to be virtually identical to the 2D viscous solution without wall shear. This serves to confirm that viscous effects in the absence of a boundary or wall serve to diminish the amplitude of the simulated PAD signal *but do not introduce any splitting or spreading of the signal.*

Figure 5 shows the radial profiles of the axial component of flow velocity induced by the leftward moving shock wave at $t = 150\,\mu$s, for three different locations. As can be seen from Fig. 5, a jet-like velocity profile is produced at $x = 13.6$ cm, just behind the shock front. This is typical of the flow behind weak shock waves considered in this work ($M_s \leq 2$), for which the induced flow is laminar and vorticity generation via the baroclinic effect caused by the $(\nabla\rho) \times (\nabla p)$ term in the momentum equation (see Ref. 7) is suppressed due to viscous effects as shown first in Ref. 16. Consequently, it can be seen that vorticity generation leading to shock curvature, as suggested in Ref. 7, is not the mechanism responsible for the curvature of a weak shock leading to an apparently split PAD signal. The baroclinic term may indeed be important for strong shocks, and is in fact implicitly included in the present work. The velocity profile of the induced flow behind the shock front can be seen to relax in Fig. 5 to a more rounded profile at $x = 16$ cm, typical of a laminar flow, and is consistent with previous analyses of flows induced behind weak shocks.[16] Immediately behind the

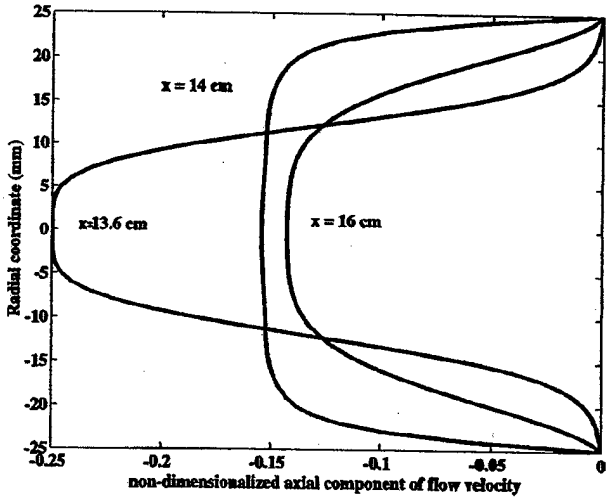

FIG. 5. Radial profiles of the axial component of flow velocity induced by passage of the shock are shown here for the leftward moving wave of the second case, 150 μs after the initiation of the shock wave, for three different spatial locations. The location $x = 13.6$ cm refers to the position just behind the shock front, while $x = 14$ cm and $x = 16$ cm refer to locations further behind the shock front.

shock however, the velocity profile begins developing a point of inflection at the wall. This indicates that a higher shock Mach number would have generated flow reversal near the boundary and induced vorticity behind the shock.

Several conclusions can be drawn from these important pedagogical cases. First and foremost, it has been shown that a bounding wall alone with its associated wall shear can produce splitting in the PAD signal in the absence of any thermal gradients. However, this effect of wall shear depends on the initial loading of energy by the spark into the gas and the length of travel. In other words, an amount of energy larger than the 0.433 mJ added in the present simulations would delay splitting of the PAD signal in the presence of wall shear alone, to longer distances of travel. This is the case in the experiments of Refs. 1–3. Second, axial thermal gradients produce split PAD signals whose trailing structures appear to be diminished in magnitude compared to their counterparts produced by wall friction. This splitting is again due to wall shear magnified by the increased viscosity resulting from the higher temperature in the heated region. The split simulated PAD signal structure also comprises a primary peak or leader, followed by multiple peaks that are smaller in magnitude compared to the leader. Third, wall friction and purely axial thermal gradients both produce simulated PAD signal structures that have zero crossings between the leading and trailing structures. In contrast, experimental PAD signals show no such zero crossing. Finally and expectedly, wall friction slows down the shock wave whereas heating accelerates it. These effects are examined next in the presence of radial thermal gradients.

C. Propagation into a heated region, followed by a colder region: Effects of axial and radial temperature gradients

It has previously been suggested that the presence of radial thermal gradients can explain the structure of observed PAD signals as a spark-generated shock wave propagates through a glow discharge.[6,7] However, these analyses were conducted in the absence of wall friction, which has been shown here to be as important as thermal gradients in influencing the structure of the simulated PAD signal. It is important to also note that earlier analyses have considered radial thermal gradients, but without isolating the effects of purely axial thermal gradients. Furthermore, when a shock is initiated using a spark in a region of initially uniform temperature and then launched into a region with radial thermal gradients, it must *necessarily* encounter axial thermal gradients as well. The effects of purely axial thermal gradients have been delineated in Sec. III B, and we now examine the effects of radial thermal gradients in the presence of viscosity and wall shear.

Equations (1)–(4) are solved as described in Sec. II with no-slip boundary conditions for the 5 cm diam cylindrical tube described earlier. Figures 6(a) and 6(b) show the centerline profiles of normalized density, $\rho(x,r=0)$, and the simulated PAD signal, at 100, 150, 300, and 400 μs, respectively. As in the previous case discussed in Sec. III B, the rightward moving wave is launched into a heated region, where the temperature varies from 300 to 1000 K along the centerline at $x=25$ cm and from 1000 K back to 300 K at $x=30$ cm. Within this region, $25\text{ cm}\leqslant x\leqslant 30\text{ cm}$, a parabolic radial distribution in temperature is prescribed varying from 1000 K at the centerline to 300 K at the wall. The leftward moving wave by contrast, encounters no thermal gradients and propagates into the uniform gas and is subjected solely to the effects of viscosity and wall shear. The leftward moving wave shows the same behavior in Figs. 6(a) and 6(b) as discussed in Sec. III B [see Figs. 3(a) and 3(b)]. The rightward moving wave displays the effects of splitting and spreading in the simulated PAD signal, as can be seen in Figs. 6(a) and 6(b). However, there are some differences in the present case due to the additional presence of radial thermal gradients. First, radial thermal gradients can be seen to diminish the PAD signal in addition to axial thermal gradients. Second, the split PAD signal structures are spread further apart by the additional presence of radial gradients in temperature. Radial gradients in temperature produce curvature of the shock front since different portions of the front are subjected to different temperatures. Third, the split PAD signal does not show a zero crossing between the leading and the trailing structures, as in the cases discussed earlier. Finally, the leader has a smaller amplitude compared to the trailing structures in the presence of radial thermal gradients, but this situation reverses only a 100 μs later. In contrast, in the case of wall shear and purely axial thermal gradients, the leader always has a higher magnitude than the trailing structures in the PAD signal. The significance of the relative magnitudes of the leading and trailing peaks of the PAD signal is unclear since no definite trend has been reported experimentally.[1,2]

The effects on shock propagation of a bounding wall with associated wall friction, purely axial thermal gradients, and radial thermal gradients, may now be summarized. It has been shown that the effect of a bounding wall, i.e., wall shear, is capable of producing split PAD signals *in the absence* of any thermal gradients. This apparent splitting is caused by retardation of the propagating shock in the neighborhood of the wall as compared with the centerline. This leads to shock curvature near the wall manifesting itself as a split PAD signal. The case of a shock wave traversing through a heated region and subjected to purely axial thermal gradients has shown that wall shear can cause apparent splitting in the PAD signal. This is an effect that is at least two-dimensional, and cannot be observed in quasi-1D solutions. The case of a shock wave propagating through a heated region and subjected to both axial and radial thermal gradients also shows that the effects of wall friction are important. However, as observed in the earlier inviscid simulations reported in Refs. 6 and 7, radial thermal gradients influence the shock propagation in a manner similar to what has been found here to be due to wall friction, as far as splitting of the PAD signal is concerned. It is clear why the earlier inviscid (Euler) simulations[6,7] of this problem required radial thermal gradients to explain splitting of the experimentally observed PAD signal. There is no wall shear in the inviscid calculations, which resemble the case discussed in Sec. III A of this paper. Splitting of the PAD signal requires either a retarding

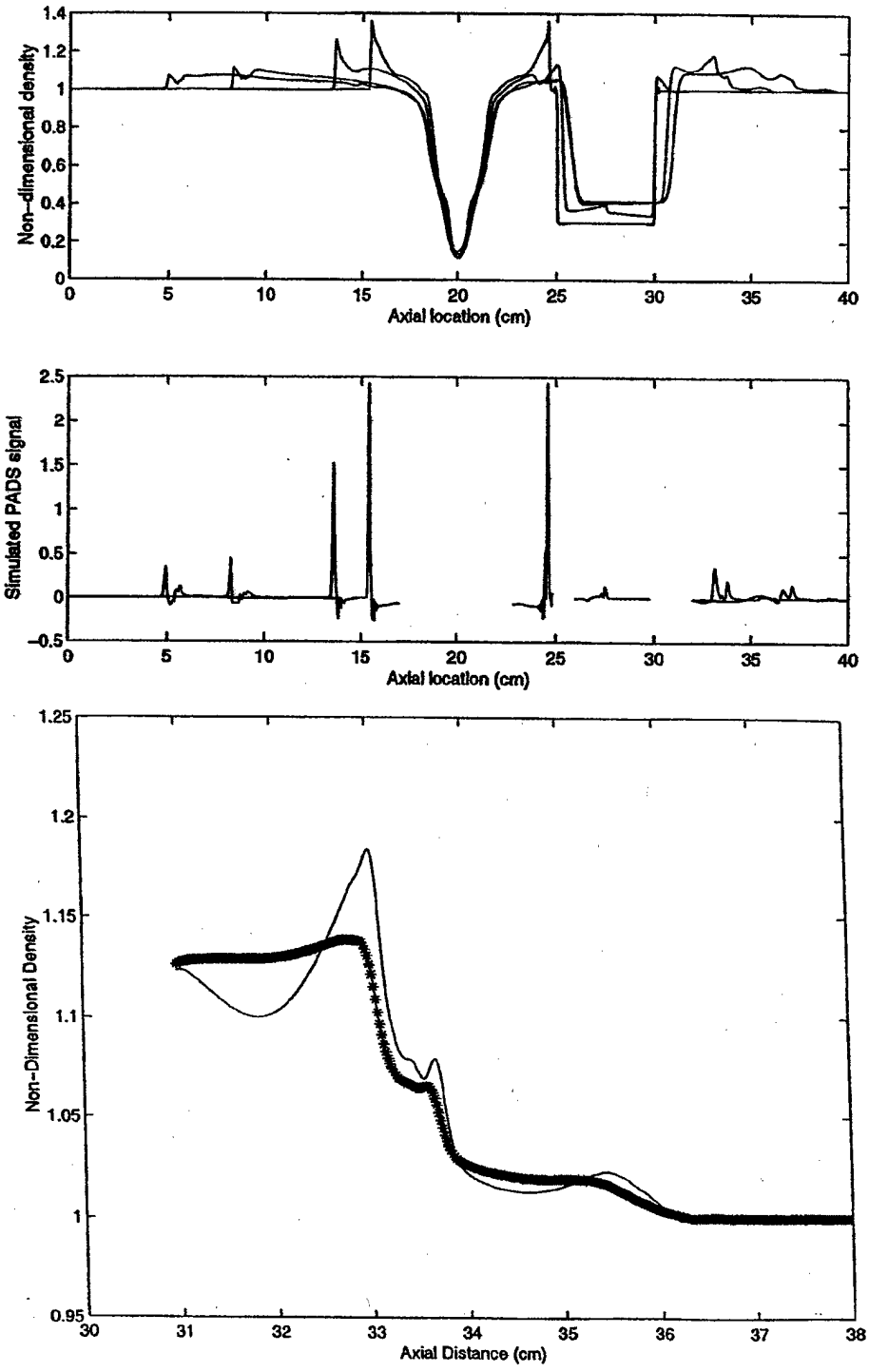

FIG. 6. (a) Profiles of mass density along $r=0$ nondimensionalized by the undisturbed gas density, $\rho_o = 0.0641$ kg/m^3, are shown here vs the axial coordinate, x, at several instants (100, 150, 300, and 400 μs, respectively) after energy addition leads to formation of a propagating shock. This result is for the case of shock propagation in Argon initially at 30 Torr and 300 K, with no-slip conditions applied at the walls. This case considers the realistic bounded viscous flow induced by a traveling shock in a 5 cm diam tube, where the rightward traveling wave encounters a heated region *with an initial radial distribution of temperature*. This case considers the effects of both axial and radial thermal gradients as well as wall shear. (b) Simulated PAD signal obtained by integrating the axial derivative of density (corresponding to (a)) in the transverse, i.e., radial direction. (c) Profiles of density for the rightward moving wave are shown here at 300 μs, at two different radial locations: $r=0$, and $r = 1.5$ cm. It is the radial staggering of these density profiles that gives rise to apparent splitting in the PAD signal. In this case, the portion of the shock wave nearest the wall is retarded relative to its counterpart at the centerline due to the lower temperatures near the wall, and therefore, lags behind in space (and in time). This gives the appearance of two or more split structures in the PAD signal.

force at the wall or a colder temperature near the wall relative to the centerline, in order to produce axially staggered density profiles in the radial direction as shown in Figs. 3(c) and 6(c). There are also noticeable differences in the relaxation of the density profiles between the cases discussed in Secs. III A and III B, as the shock re-emerges from the heated region into the colder gas. As can be seen in Figs. 3(a)–3(c) and 6(a)–6(c), there appears to be a characteristic relaxation distance (or equivalently, a relaxation time) for the PAD signal to recover its sharp Delta function-like character as the shock emerges from the heated region. This relaxation distance (or time) is influenced by thermal gradients as the shock wave propagates down the tube. A distinct relaxation distance (or time) can also be seen to exist for momentum relaxation, as can be seen by comparing the respective positions of the shock front at 300 and 400 μs in Figs. 3(b), 4(b), and 6(b). The shock speed reduces to approximately the same value upon emergence from the heated region in all

cases, *independent* of its velocity as it leaves the heated region. This strongly suggests that there are two distinct relaxation distances (and hence relaxation times). One dictates the relaxation of the distortion in the profiles themselves, and is indicative of *energy relaxation*. The other governs the speed of propagation of the shock front, and is indicative of *momentum relaxation*.

Given this detailed understanding of wall shear, axial thermal gradients, and radial thermal gradients, the measurements of Refs. 1 and 2 can be better interpreted and understood. The PAD signals reported in Refs. 1 and 2 are clearly proportional to the axial density gradient, as suggested in Refs. 6 and 7. The small negative spike observed in the trailing portion of a peak in the simulated PAD signal and not observed in all cases in experiments can be understood as a limitation in sensitivity in the PAD measurement technique itself. In other words, only a minimum or threshold value of the magnitude of $\partial\rho/\partial x$ leads to a detectable signal. This is why the experimentally measured PAD signals exhibit the sharp delta function-like character where the corresponding density profiles are roughly triangular in shape. The experimental PAD signals are sensitive to the steep slope in the rising portion of the density profiles and either less sensitive or not sensitive at all to the shallower, trailing portions of the propagating shock structure. Attenuation of the experimentally observed PAD signals within the glow discharge can indeed be explained by the effects of heating within the glow discharge, as previously suggested first in Ref. 6, and subsequently in Ref. 7. However, the most interesting features of shock propagation appear to occur downstream of the glow discharge in the experiments of Ref. 2 and downstream of the heated regions in the simulations reported in this work. This work suggests that there exist two distinct relaxation times for relaxation of energy and momentum within the propagating shock structure, which are profoundly affected by heat addition and external forces such as wall friction. In this regard, the recent direct simulation Monte Carlo (DSMC) analysis reported in Ref. 17, which considers the effects of electrostatic forces caused by charge separation across the shock front on the propagating shock structure, is most relevant. As the shock traverses the electrode in the glow discharge in Refs. 1–3, it encounters the sheath region near the electrode with its associated relatively high electric fields. The presence of fields of this magnitude (on the order of kV/cm) can induce substantial charge separation across the shock front, and must affect the relaxation of momentum of the propagating structure. In fact, the presence of an electrostatic body force is completely analogous to the presence of wall friction considered in this work, and raises the possibility of altering shock structure and shock propagation characteristics in the presence of ionization and externally applied electric fields. The possibility of mitigating the strength of propagating detonation shocks by application of electric fields was first suggested by J. J. Thomson as early as 1910,[18] but met with mixed success in experimental attempts to verify his idea.[19,20]

IV. SUMMARY AND CONCLUSIONS

The characteristics of shock waves generated by rapid heat addition, such as from a capacitively discharged electric spark, have been numerically simulated in argon initially at 30 Torr and 300 K. Instantaneous spatial profiles of density, induced flow velocity, temperature, and pressure have been calculated by solving the compressible Navier–Stokes equations using the linearized block implicit (LBI) method of Briley and McDonald. Shock waves initiated by a simulated spark and their subsequent propagation in a cylindrical tube have been analyzed in this paper, under four different conditions: (a) Without wall friction, (b) with wall friction, (c) with wall friction and purely axial thermal gradients, and (d) with wall friction and both axial and radial thermal gradients.

Three important conclusions can be drawn from the analysis presented in this paper:

(1) First, wall friction alone, in the absence of thermal gradients, can produce splitting in simulated photo-acoustic deflection (PAD) signals. Such splitting has been shown in this work to be caused by deceleration of the shock wave in the near-wall regions relative to the centerline, resulting in mild curvature of the shock front. Note that a split PAD signal does not imply splitting of the shock wave but indicates curvature or tilting of the shock front. A significant implication of this conclusion is that external forces (i.e., body forces such as electrostatic forces or boundary effects such as wall shear) may be useful in modification of shock structure or inclinations. However, it remains to be shown whether this is possible to implement independently of any thermal effects. Splitting of the PAD signal due to wall friction alone was not observed in the experiments of Refs.1 and 2, and is due to the difference in the magnitude of the initial energy loading between our simulations (0.433 mJ) and experiments of Refs. 1 and 2 (typically on the order of several Joules). Nevertheless, the analysis presented in this paper aids in interpreting experimental measurements such as those reported in Refs. 1 and 2 by delineating the contributions of various phenomena to the observed PAD signal.

(2) Secondly, the effects of wall friction and radial thermal gradients have been shown to be similar, with the latter augmenting and enhancing the effects of friction at a boundary. Earlier inviscid (Euler) simulations have proposed the presence of radial thermal gradients as the cause of splitting of the PAD signal.[6,7] Recently, compelling experimental evidence for the importance of thermal gradients has been published.[10]

(3) Thirdly, the results of these simulations suggest the presence of two distinct relaxation times with regard to shock propagation, a relaxation time for momentum, and a relaxation time for energy. In the simulations, the speed of a shock wave as it emerges from a heated region into the cold gas is found to assume similar values regardless of the initial velocity of the shock as it leaves the heated region. However, a significantly longer time (or equivalent distance) elapses before the PAD signal recovers its sharp, delta function-like feature. In other words, a significantly longer time (or equivalent distance) elapses before the curvature of the shock wave vanishes and a straight front is restored.

Detailed experimental measurement of shock velocities and relaxation of shock characteristics downstream of the glow discharge would be invaluable in understanding the momentum and energy relaxation phenomena implied by the recovery of the PAD signal. Additionally, spatially and temporally resolved temperature measurements would serve to provide information regarding the magnitude of thermal gradients and their associated impact on shock propagation and relaxation phenomena.

ACKNOWLEDGMENTS

The authors gratefully acknowledge many helpful discussions with Dr. B. N. Ganguly and Dr. P. Bletzinger of AFRL, and Professor W. Bailey of AFIT. This work was supported by AFOSR Grant No. F49620-99-1-0023, and in part by the DDR&E within the Air Plasma Ramparts MURI Program managed by AFOSR.

[1]B. N. Ganguly, P. Bletzinger, and A. Garscadden, "Shock wave dispersion in nonequilibrium plasmas," Phys. Lett. A **230**, 218 (1997).
[2]B. N. Ganguly and P. Bletzinger, "Acoustic shock wave propagation in nonequilibrium nitrogen and argon plasmas," Proceedings of the Workshop on Weakly Ionized Gases, pp. HH5-HH13, U.S. Air Force Academy, 9–13 June 1997.
[3]A. Garscadden, P. Bletzinger, and B. N. Ganguly, "Acoustic shock interaction in a positive column plasma," Paper AIAA-99-4973 presented at the 9th International Space Planes and Hypersonic Systems and Technologies Conference and 3rd Weakly Ionized Gases Workshop, Norfolk, Virginia, 1–5 November 1999.
[4]P. A. Voinovich, A. P. Ershov, S. E. Ponomareva, and V. M. Shibkov, High Temp. **29**, 468 (1990).
[5]S. A. Bystrov, I. S. Zaslonko, Yu. K. Mukoseav, and F. V. Shugaev, Sov. Phys. Dokl. **35**, 39 (1990).
[6]W. F. Bailey, and W. M. Hilbun, "Baseline of thermal effects on shock propagation in glow discharges," Proceedings of the Workshop on Weakly Ionized Gases, pp. GG3–GG18, U.S. Air Force Academy, 9–13 June 1997.
[7]S. O. Macheret, L. Martinelli, and R. B. Miles, "Shock wave propagation and structure in non-uniform gases and plasmas," paper AIAA 99-0598 presented at the 37th AIAA Aerospace Sciences Meeting and Exhibit, Reno, Nevada, 11–14 January 1999.
[8]I. Adamovich, V. V. Subramaniam, J. W. Rich, and S. O. Macheret, "Phenomenological analysis of shock waves in weakly ionized gases," AIAA J. **36**, No. 5, 5816 (1998).
[9]R. B. Miles, S. O. Macheret, and P. Efthimion, "Mechanisms of shock propagation and stability control in low temperature plasmas," Proceedings of the Workshop on Weakly Ionized Gases, pp. X3–X33, U.S. Air Force Academy, 9–13 June 1997.
[10]Y. Z. Ionikh, N. V. Chernysheva, A. V. Meshchanov, A. P. Yalin, and R. B. Miles, "Direct evidence for thermal mechanism of plasma influence on shock wave propagation," Phys. Lett. A **259**, 387 (1999).
[11]R. G. Fowler, G. W. Paxton, and H. G. Hughes, "Electrons as a shock driver gas," Phys. Fluids **4**, No. 2, 234 (1961).
[12]N. E. Todreas and M. S. Kazimi, *Nuclear Systems I-Thermal Hydraulic Fundamentals* (Taylor and Francis, Washington, DC, 1990), p. 115.
[13]W. R. Briley and H. McDonald, "Solution of the multidimensional compressible Navier–Stokes equations by a generalized implicit method," J. Comput. Phys. **24**, 372 (1977).
[14]S. M. Aithal, V. V. Subramaniam, J. Pagan, and R. Richardson, "Numerical model of a transferred plasma arc," J. Appl. Phys. **84**, No. 7 1 (1998).
[15]D. A. Anderson, J. C. Tannehill, and R. H. Pletcher, *Computational Fluid Mechanics and Heat Transfer* (McGraw-Hill, New York, 1984), p. 515.
[16]H. Mirels, "Laminar boundary layer behind shock advancing into stationary fluid," NACA TN 3401, Washington, March 1955.
[17]A. H. Auslender and R. Rubinstein, "Shock wave propagation in a gas far from equilibrium," Proceedings of the 2nd Weakly Ionized Gases Workshop, pp. 119–126, Norfolk, Virginia, 24–25 April 1998.
[18]W. E. Garner and S. W. Saunders, "Ionization in gas explosions," Faraday Soc. Trans. **22**, 281 (1926). See citation J. J. Thomson, B. A. Report on Gaseous Combustion, p. 501, 1910, therein.
[19]Dixon, Campbell, and Slater, Proc. R. Soc. London, Ser. A **90**, 506 (1914).
[20]Malinowski, J. Chim. Phys. **21**, 469 (1924).

1.2 Effect of Wall Shear on the Propagation of a Weak Spark-Generated Shock Wave in Argon

Effect of wall shear on the propagation of a weak spark-generated shock wave in argon

A. R. White and V. V. Subramaniam
Non-Equilibrium Thermodynamics Laboratories, Center for Advanced Plasma Engineering, Department of Mechanical Engineering and Chemical Physics Program, The Ohio State University, Columbus, Ohio 43210

(Received 16 June 2000; accepted 22 March 2001)

Photo-acoustic deflection (PAD) measurements are presented for a weak spark-generated shock wave propagating in argon at 40 Torr in a cylindrical tube. Measurements indicate that for a given shock strength, there is a maximum distance of travel beyond which the shock front is nonplanar, consistent with the predictions of numerical calculations reported recently [S. M. Aithal and V. V. Subramaniam, Phys. Fluids **12**, 924 (2000)]. The initially planar shock wave exhibits curvature at downstream locations in the shock tube in the absence of any imposed temperature gradients. Since the PAD signal is a line-of-sight measurement, it is sensitive to the axial gradient of density at all radial locations, and shock curvature manifests itself as a split and spread PAD signal. In contrast, a planar shock registers a sharp, delta-function-like PAD signal. The curvature of weak shocks observed in the present experiments is due to viscous action alone, as the wall shear retards the near-wall portions of the front relative to its near-axis portions. The PAD signal associated with shock curvature due to wall shear alone is found to closely resemble that due to externally imposed radial temperature gradients such as in a glow discharge plasma. © *2001 American Institute of Physics.* [DOI: 10.1063/1.1378033]

Experiments in the former Soviet Union[1–4] and, more recently, in the United States[5–11] have documented certain characteristics of shock waves propagating through a weakly ionized ($n_e/n \sim 10^{-8}$–10^{-6}) plasma in a shock tube. These include an increase in shock propagation velocity within the plasma and an apparent broadening of the shock front as recorded by photo-acoustic deflection (PAD) measurements. Recent work[9,12] has attributed the former effect to heating of the gas by the glow discharge and the latter to the presence of radial temperature gradients within the glow region. Radial temperature gradients can indeed produce different velocities for the shock front on the tube axis and the region near the wall. It has been suggested that this results in curvature of the shock front and explains the apparent broadening and splitting observed in photoacoustic deflection signals. Recently, numerical calculation of the characteristics of spark-generated shock waves has shown that wall shear can also produce curvature of the shock front in the absence of any radial thermal gradients, depending on the shock strength and available length of the tube. In this Brief Communication, we present experimental measurements verifying the predictions of Ref. 12 for a weak spark-generated shock wave propagating in argon at 40 Torr and 300 K, under the action of viscous effects alone and in the absence of radial thermal gradients.

The experimental apparatus comprises a pyrex glass tube (1 m long and 5 cm in diameter), with a Kolb tube for generating the shock at one end (see Refs. 5–8 for further details). As shown in Fig. 1, the shock is produced by a high-voltage spark discharge (lasting on the order of microseconds) in argon gas at a pressure of 40 Torr. This rapid energy addition into the gas results in a sudden rise in gas temperature and pressure, and produces compression waves that steepen to form shock waves traveling in opposite directions. The shock tube has three flanges labeled 1–3 in Fig. 1, starting from closest to the Kolb tube, and shock characteristics are explored at various axial locations downstream from the first flange (position 1) using photoacoustic deflection.[5–8] Typically, spark discharge voltages in excess of about 3 kV are required to reliably produce shock waves which then are capable of traveling the entire length of the tube. The numerical results of Ref. 12 show that the maximum distance traveled by such a shock before succumbing to the effects of wall shear depends on the amount of energy initially imparted to the gas by the spark discharge. Unfortunately, it is extremely difficult to control the energy loaded into the gas by the spark in a repeatable manner simply by adjusting the spark duration or supply voltage. Consequently, another means to observe the effects of wall shear on weak shock waves is used in the present work. When the spark is discharged in the gas, two shock waves are produced, one traveling to the right along the shock tube and one traveling to the left, as described in Ref. 12. The leftward moving shock reflects off the short end of the tube and follows the primary shock that travels to the right. This secondary, reflected shock, is weaker (M=1.009) than the primary shock wave (M=1.025) and lags approximately 265 μs behind. The secondary shock wave is further weakened by passing it through a constriction with an axially centered orifice, 6 mm in diameter, located at position 1 (see Fig. 1). The primary shock wave also passes through this orifice. After the primary shock wave emerges as a curved front and then steep-

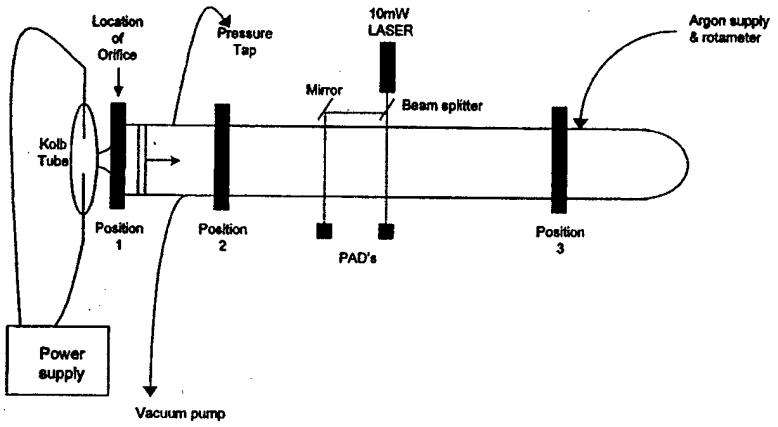

FIG. 1. Schematic of shock tube apparatus. A spark discharge in the Kolb tube at the left results in the formation of a primary shock traveling to the right. A secondary shock traveling to the left is also produced, which then reflects off the left boundary and follows the primary shock to the right. An orifice is placed at the first flange (position 1) in order to weaken the secondary shock wave.

ens into a planar shock, it remains planar for the remainder of the tube. The secondary shock also emerges as a curved front that then straightens into a planar shock front propagating along the shock tube (see Fig. 2). However, this secondary shock wave is much weaker than the primary and does not sustain itself as a planar front beyond a certain location along the tube. It was shown in Ref. 12 that a shock of given strength will succumb to viscous effects after traveling a certain length along the tube. A weaker shock will therefore exhibit effects of curvature for shorter lengths of travel compared to stronger shocks, despite the fact that wall shear increases with shock strength. Since the shock tube used in the present experiments is 1 m long, the distance of travel over which shock curvature due to viscous effects can be studied is limited. For this reason, the characteristics of the weaker secondary shock are examined in this work in order to study its formation and propagation in the presence of viscous effects alone.

Figure 2 shows both the primary shock and the secondary shock from the same experiment at a location of 57.5 cm from position 1. It can be seen from their sharp delta-function-like PAD signal shown in Fig. 2 that both are planar. Note that the secondary shock is significantly weaker (i.e., has a lower amplitude) than the primary shock and is 8.56 cm (265 μs) behind the location of the primary shock. The location of the secondary shock (and, hence, its arrival time), relative to the primary shock at a given downstream location, is repeatable. The separation between the two shock waves is observed to increase as they travel down the length of the shock tube. The secondary shock lags the primary shock by ~265 μs downstream of position 1, but lags by as much as 280 μs towards the end of the shock tube. Figures 3(a)–3(c) show PAD signal data for the secondary shock wave at various axial locations downstream from the orifice (position 1). In Fig. 3(a), it can be seen from the split and spread PAD signal that the secondary shock is curved immediately downstream of the orifice. It then steepens into a planar shock front [note the delta-function-like appearance in Fig. 3(b)], and is subsequently nonplanar, as can be seen from the split and spread PAD signal 63 cm downstream from position 1, shown in Fig. 3(c). Figure 4 shows details of the PAD signal of both the primary and secondary shock from the same experiment at a location of 63 cm downstream of the orifice. Figures 3 and 4 clearly show that the secondary shock is nonplanar immediately after it emerges from the orifice, straightens out, and that it becomes nonplanar again further downstream due to the action of wall shear.

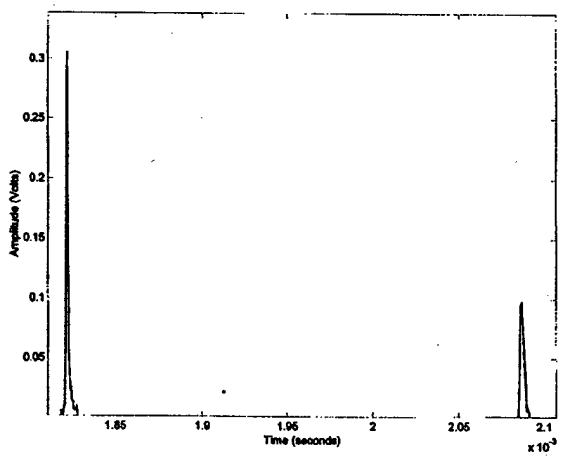

FIG. 2. PAD signal vs absolute arrival time, showing the primary and secondary shock waves from the same experiment, at a location of 57.5 cm downstream of the orifice located at position 1 (see Fig. 1). Note the sharp delta-function-like appearance of the signals indicating planar fronts. Note also the smaller amplitude of the secondary shock (right) compared to the primary shock (left) indicating its weakness.

The PAD signal is generated as the shock traverses the path of the transverse laser beam. The streamwise density gradient across the passing shock front causes the laser beam to be deflected onto the detector, resulting in the generation of a sharp peak. The amplitude of this peak is proportional to the magnitude of the density gradient. Thus, we may write

$$I_{\mathrm{PAD}} \propto \int_{-R}^{R} \frac{\partial \rho}{\partial x} dr. \tag{1}$$

For a perfectly planar front $\partial\rho/\partial x$ is constant versus r, the radial coordinate. In this case, a split or spread PAD signal is indicative of curvature of the front itself since the signal samples various radial locations along the line of sight. On the other hand, if $\partial\rho/\partial x$ exhibits nonmonotonic variation with x, this can contribute to splitting and spreading of the

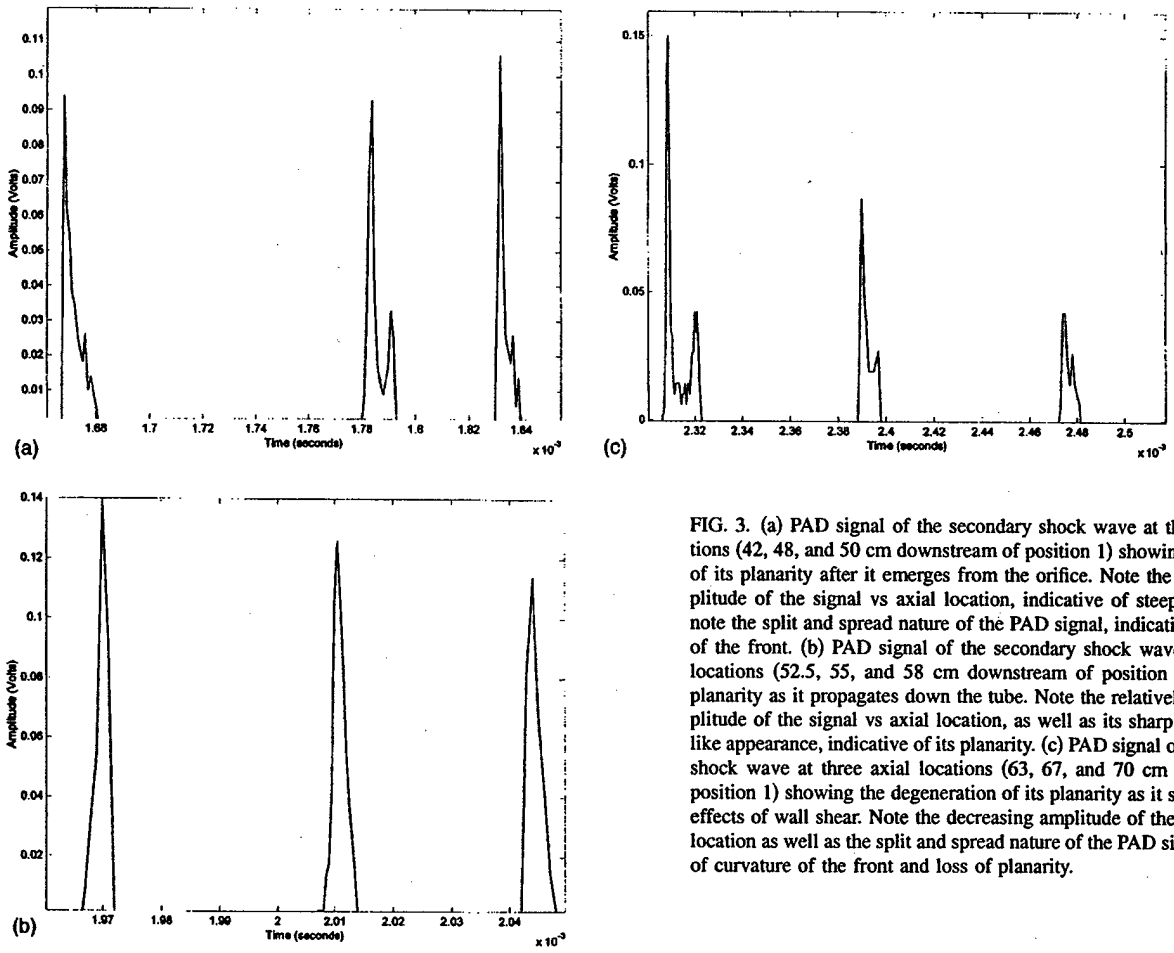

FIG. 3. (a) PAD signal of the secondary shock wave at three axial locations (42, 48, and 50 cm downstream of position 1) showing the evolution of its planarity after it emerges from the orifice. Note the increasing amplitude of the signal vs axial location, indicative of steepening. Further, note the split and spread nature of the PAD signal, indicative of curvature of the front. (b) PAD signal of the secondary shock wave at three axial locations (52.5, 55, and 58 cm downstream of position 1) showing its planarity as it propagates down the tube. Note the relatively constant amplitude of the signal vs axial location, as well as its sharp delta-function-like appearance, indicative of its planarity. (c) PAD signal of the secondary shock wave at three axial locations (63, 67, and 70 cm downstream of position 1) showing the degeneration of its planarity as it succumbs to the effects of wall shear. Note the decreasing amplitude of the signal vs axial location as well as the split and spread nature of the PAD signal, indicative of curvature of the front and loss of planarity.

PAD signal as well. The numerical calculations reported in Ref. 12 show that both effects are present, but that nonplanarity of the front has a greater influence on PAD signal structure. Furthermore, nonmonotonic variation of the density with x would result in multiple PAD signal peaks that are on the order of 30 μs apart, with the troughs approaching zero signal. In contrast, PAD signals in the present experiments exhibit split peaks that are on the order of 10 μs or less apart and troughs with *nonzero* amplitude [see Figs. 3(c) and 4]. We can therefore be reasonably certain that the observed splitting and spreading of the PAD signals is indeed due to nonplanarity of the shock front.

It has been observed experimentally that shock waves of moderate strength travel a greater distance before succumbing to wall shear, compared to weak (M~1) shocks. Their corresponding PAD signals remain sharply peaked compared to the weaker shocks, which exhibit split and spread PAD signals. There are two possible explanations for this observation. First, since wall shear is greater for the stronger shock, it is expected to be smeared near the wall. In this instance, the shock would remain largely planar until the near-wall regions where it would simply disappear, thereby resulting in a single sharp PAD signal. This is analogous to classical Fanno flow, where a supersonic flow can be reduced to subsonic speeds without shock formation, by the action of wall shear alone. The second possible reason involves sensitivity of the PAD measurement itself. Equation (1) shows the true nature of the PAD signal, which is comprised of contributions from streamwise density gradients at various radial locations. Consequently, the axial density gradients near the

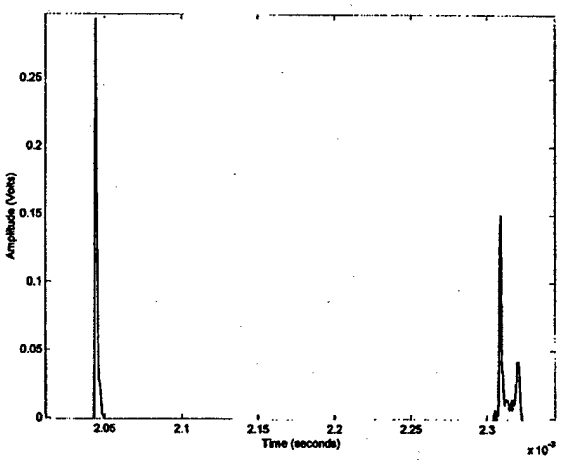

FIG. 4. PAD signal vs absolute arrival time, showing the primary and secondary shock waves from the same experiment at a location of 63 cm downstream of the orifice. Note that the primary shock (on the left) is still planar while the secondary shock (on the right) exhibits a split and spread structure, indicative of shock curvature. This figure should be compared to Fig. 2, where both shocks are planar upstream of the location presented in this figure.

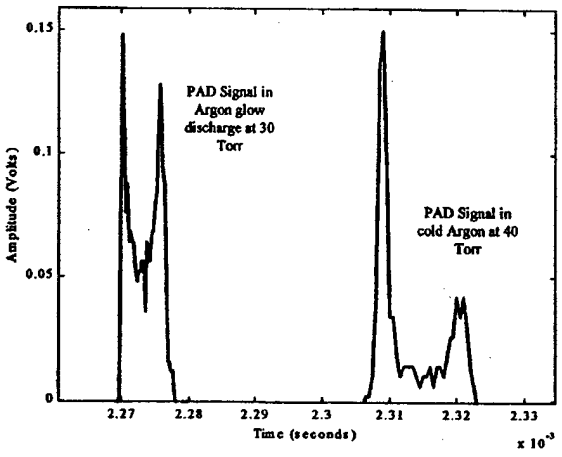

FIG. 5. Comparison of PAD signals with and without a plasma. The PAD signal on the left is for a M=1.4 shock wave launched into a glow discharge plasma in argon (10 mA, 4.5 kV) at 30 Torr. The PAD signal on the right is for a M=1.009 shock wave propagating in neutral argon at 40 Torr. Note the similar effect on shock structure of radial temperature gradients (left) and wall shear in the absence of temperature gradients (right).

centerline of the tube as well as near the walls contribute to the PAD signal. In the case of moderately strong shocks, the axial density gradient at the centerline is considerably larger than that near the walls, and hence dominates the PAD signal. In contrast, for weaker shocks (i.e., M~1), the axial density gradients in the near-wall regions are comparable to those near the centerline, and hence contribute significantly to the PAD signal. Thus, no effects on the PAD signal may be observed for a shock of moderate strength although its curvature may actually be greater than that of a weaker shock. In other words, while shock curvature due to wall shear may occur in shocks of all strength, it is more noticeable the weaker the shock strength, resulting in a split and spread PAD signal.

Radial temperature gradients that exist in a glow discharge have been shown to cause curvature of the shock front.[9,12] However, curvature of the shock front has also been shown to occur in numerical calculations due to the presence of a retarding force such as wall shear.[12] In the present experiments without a glow discharge, and with no externally imposed thermal gradients, wall shear can be the only cause of the observed split and spread PAD signals. Figure 5 shows the PAD signal of a primary shock wave (M~1.4) in the presence of a glow discharge plasma in argon (10 mA, 4.5 kV, 30 Torr). Also shown in Fig. 5 is the PAD signal of the secondary shock wave (M~1.009) previously displayed in Fig. 4 in the absence of a glow discharge. Note that the trailing peak is smaller in magnitude compared to the leading peak, consistent with the near wall portion of the shock having a shallower axial density gradient compared to the near axis portion of the shock. Although the two shock strengths in Fig. 5 are different, this figure serves to highlight the similarities between these PAD signals and shows that shock curvature can arise either from radial thermal gradients or due to wall shear alone. It is important to mention that the comparison in Fig. 5 could have been made for similar shock strengths. However, a much longer (several meters long) shock tube would have been required in order to observe the effects of wall shear alone on a M~1.4 shock wave. This work has experimentally verified the predictions of the numerical calculations reported in Ref. 12 regarding the influence of wall shear on the structure of weak propagating shock waves, and suggests that modification of shock structure by application of an external force is possible even in the absence of any thermal effects. Imaging of the shock front using laser-induced fluorescence would provide further valuable insight into the structure of the shock front itself.

ACKNOWLEDGMENTS

This work was supported by Grant No. F49620-99-1-0023 from AFOSR, under the direction of Dr. Steven Walker.

[1] A. I. Klimov, A. N. Koblov, G. I. Mishin, Y. L. Serov, and I. P. Yavor, "Shock wave propagation in a glow discharge," Sov. Tech. Phys. Lett. **8**, 192 (1982).
[2] A. I. Klimov, A. N. Koblov, G. I. Mishin, Y. L. Serov, K. V. Khodataev, and I. P. Yavor, "Shock wave propagation in a decaying plasma," Sov. Tech. Phys. Lett. **8**, 240 (1982).
[3] N. V. Evtyukhin, A. D. Margolin, and V. M. Shmelev, "On the nature of shock wave acceleration in glow discharge plasma," Sov. J. Chem. Phys. **3**, 2080 (1986).
[4] P. A. Voinovich, A. P. Ershov, S. E. Ponomareva, and V. M. Shibkov, "Propagation of weak shock waves in plasma of longitudinal flow discharge in air," High Temp. **29**, 468 (1991).
[5] B. N. Ganguly, P. Bletzinger, and A. Garscadden, "Shock wave damping and dispersion in nonequilibrium low pressure argon plasmas," Phys. Lett. A **230**, 218 (1997).
[6] B. N. Ganguly and P. Bletzinger, "Acoustic shock wave propagation in non-equilibrium nitrogen and argon plasmas," in *Proceedings of the Workshop on Weakly Ionized Gases*, U.S. Air Force Academy, 9–13 June 1997, pp. HH-3–HH-13.
[7] P. Bletzinger and B. N. Ganguly, "Local acoustic shock velocity and shock structure recovery measurements in glow discharges," Phys. Lett. A **258**, 342 (1999).
[8] A. R. White, S. M. Aithal, and V. V. Subramaniam, "Experimental studies of shock generated shock waves," paper AIAA-99-3670 presented at the AIAA 30th Plasmadynamics and Lasers Conference, Norfolk, VA, 28 June–1 July 1999.
[9] Y. Z. Ionikh, N. V. Chernysheva, A. V. Meschanov, A. P. Yalin, and R. B. Miles, "Direct evidence for thermal mechanism of plasma influence on shock wave propagation," Phys. Lett. A **259**, 387 (1999).
[10] Y. Z. Ionikh, N. V. Chernysheva, A. P. Yalin, S. O. Macheret, L. Martinelli, and R. B. Miles, "Shock wave propagation through glow discharge plasmas: Evidence of thermal mechanism of shock dispersion," paper AIAA-2000-0714 presented at the 38th Aerospace Sciences Meeting and Exhibition, Reno, NV, 10–13 January 2000.
[11] S. O. Macheret, L. Martinelli, and R. B. Miles, "Shock wave propagation and structure in non-uniform gases and plasmas," paper AIAA-99-0598 presented at the 37th Aerospace Sciences Meeting and Exhibition, Reno, NV, 11–14 January 1999.
[12] S. M. Aithal and V. V. Subramaniam, "On the characteristics of a spark generated shock wave," Phys. Fluids **12**, 924 (2000).

1.3 Effects of Thermal Gradients and Ionization on the Propagation of Spark-Generated Shock Waves

AIAA – 99 - 4855

EFFECTS OF THERMAL GRADIENTS AND IONIZATION ON THE PROPAGATION OF SPARK-GENERATED SHOCK WAVES

by
A. R. White, K. A. Essenhigh, I. Adamovich, W. Lempert, and V. V. Subramaniam
Center for Advanced Plasma Engineering
Non-Equilibrium Thermodynamics Laboratories
Department of Mechanical Engineering
The Ohio State University
Columbus, Ohio 43210, U.S.A.

9th International Space Planes and Hypersonic Systems and Technologies Conference
and
3rd Weakly Ionized Gases Workshop
1-5 November 1999
Norfolk, VA

Abstract

The behavior of spark-generated shock waves propagating through weakly ionized glow-discharge plasmas has been recently examined experimentally[1-4]. The shock wave is observed to exhibit curvature of the front[1-4], non-monotonic variation of velocity along distance of travel[1,2], a propagation velocity that possibly shows a mild dependence on the direction of the electric field[1,2], and recovery lengths on the order of several tube diameters downstream of the discharge before the front straightens out[1,2]. Analysis of these experiments reveals that most of the observations can be explained by the combined presence of radial temperature gradients within the glow discharge[2-8], as well as wall shear[2,8]. It is clear that if any electrostatic effects impact the shock wave propagation, they are well masked by the dominant effects of radial thermal gradients and wall shear. In this paper, we report on shock propagation in two different types of discharges containing Argon with 3.3% CO, a standard DC glow discharge and an electrodeless optically pumped discharge[9]. The presence of CO leads to formation of C_2 that allows approximate determination of gas temperature via radiative emission from the Swan bands in both discharges. A shock wave is launched into the two discharges as described in ref.[2], and passage of the shock wave is detected using photoacoustic deflection (PAD) of a HeNe laser beam as described in refs.[1,2]. It is found that the shock wave behavior as determined by the PAD signal characteristics in both discharges with the same CO/Ar gas mixture are very similar, and that the maximum temperatures are comparable in both discharges, on the order of 1000 ± 200 K. The optically pumped discharge is shown to be an excellent environment for isolating thermal effects from any plasma effects that may be masked.

I. Introduction

Spark-generated shock waves propagating through weakly ionized glow discharge plasmas exhibit several features when observed using photoacoustic deflection (PAD). Recent experiments[1,2] show that among the more significant effects observed are that:

(1) the shock accelerates within the plasma, reaching a maximum average speed within the positive column, and decreasing thereafter;
(2) the shock front is initially planar before entering the discharge and subsequently becomes slightly convex within the discharge[8];
(3) the PAD signal is diminished in amplitude, spread, and split, within the glow discharge. In the absence of a discharge, the PAD signal is a sharp peak resembling a Delta function;
(4) the shock promptly decelerates upon exiting the glow discharge but exhibits a split and spread PAD signal for up to 2 or 3 tube diameters before recovering its initial Delta function – like shape[8];
(5) the average shock speed increases non-linearly and concave-down as the discharge current is increased; and
(6) the average shock speed depends on the orientation of the electric field within the glow discharge.

Interpretation of the PAD signal measurements was greatly aided by earlier one-dimensional models and 2-D inviscid simulations [5-7]. These calculations showed that a two-dimensional effect, notably the radial temperature gradient existing within the glow discharge was responsible for most, if not all of the aforementioned experimental observations. The most compelling evidence for the importance of radial temperature gradients is the recent work reported in ref.[4]. Of course, effects such as the non-linear variation of the shock speed versus discharge current and long recovery lengths for the shock to recover its flat front, cannot be explained without including wall shear (viscous effects). Wall shear has since been shown to be important, in recent compressible Navier-Stokes simulations of spark-generated shock waves in Argon[2,8]. Moreover, it has been shown recently that depending on the energy loading by the spark and the length of the shock tube, wall shear alone can produce split and spread PAD signals in a manner similar to radial temperature gradients, confirming once again that curvature or tilting of the propagating shock wave results in split and spread PAD signals[8]. The significance of this finding is the suggestion that shock curvature or shock tilt within a shock tube may be produced by external forces such as friction at a boundary or body force, even in the absence of thermal effects[8]. In the experiments of refs.[1-4], both thermal gradients and wall shear are present and influence the propagating characteristics of spark-generated shock waves. The long recovery lengths (on the order of two or three tube diameters) downstream of the glow discharge

are also observed in the compressible Navier-Stokes calculations reported in ref.[8] showing that plasma effects do not need to be invoked to explain the experimental observations.

For illustrative purposes, some key results from ref.[8] are reproduced here. Figure 1 shows the propagation of shock waves produced by rapid energy addition in Ar at 30 Torr. Figure 1a shows density (non-dimensionalized by $\rho_0 = 0.0641$ kg/m^3) along the tube centerline as a function of axial location, while Fig. 1b shows the corresponding simulated PAD signal (proportional to $\partial\rho/\partial x$ integrated over the radial direction, along the line of sight). As can be seen, the leftward moving wave propagates subject only to wall shear, whereas the rightward moving wave encounters a region (between x = 25 cm. and x = 30 cm.) where the temperature varies radially from 1000 K at the centerline to 300 K at the wall. Note that the aforementioned points (1) through (4), are evident in Figs. 1a and 1b. Moreover, point (5) can be understood to arise from the opposing effects of heating and wall friction. As the current in the discharge is raised, the temperature increases as the square of the current while the shock speed scales as the square root of temperature for a given Mach number. Hence, the shock speed should scale linearly with the discharge current if thermal effects alone were dominant. However, wall shear also increases as the shock speed increases, ultimately limiting the speed to less than a linear increase versus current. It would be natural to expect then that the shock speed should exhibit a local maximum and concave-down variation with discharge current. Figure 2 shows the calculated radial variations of the axial component of induced flow velocity at several locations behind the leftward propagating shock wave in 30 Torr of Argon (from ref.[8]). Note that viscous effects are quite prominent at this pressure, and cannot be ignored.

The only remaining point to be addressed is the weak dependence of the shock speed on the direction of the electric field (point (6)). Since all the calculations and simulations thus far have considered non-ionized gases, this point cannot be addressed. Experimental measurements show that the average shock speed within the glow discharge is higher when the electric field is opposed to the direction of shock propagation[2]. This too may be understood in terms of thermal effects since in this orientation (i.e., electric field opposed to the direction of shock propagation), the cathode is the upstream electrode and is expected to be the hotter of the two electrodes in a glow discharge. In this paper, preliminary average temperature measurements are made in a 3.3% CO/96.7% Ar mixture at 30 Torr, using the Swan band emission from C_2. The characteristics of a spark-generated shock launched into such a plasma are discussed and contrasted with earlier measurements in a pure Ar discharge[2]. An optically pumped, electrodeless plasma is created in the same CO/Ar gas mixture using irradiation from a CO laser[9]. Infrared radiation from the CO laser is absorbed by the low-lying vibrational levels of the CO molecules and re-distributed to higher vibrational levels via anharmonic VV pumping collisions[10]. As a result, the CO molecules react, leading ultimately to formation of C_2. In addition, associative ionization by pooling of vibrational energies between CO molecules results in the production of electrons and molecular ions such as $(CO)_2^+$ or CO^+[11]. The electron production in this optically pumped plasma discharge can be controlled by limiting the up-pumping within CO, by the simple addition of inert gases such as He[11].

This paper is organized as follows. The experimental apparatus is briefly described in Sections IIA, IIB, and III, since the essential details are provided in refs.[1,2]. Some additional measurements related to the local velocity minimum in the vicinity of the upstream-most electrode discussed in ref.[2] for shock propagation through a glow discharge plasma in a straight shock tube, are given in Section IIA. Measurements of average shock speeds and average temperatures for shocks propagating through a glow discharge in pure Ar as well as in a 3.3% CO/96.7% Ar mixture at 30 Torr, are made in the same shock tube but fitted with a T-shaped Kolb tube for generating the shock wave. These results are provided in Section IIB. Experiments are done in this geometry to ensure that shock propagation characteristics are unaffected by the change in the geometry of the spark-generating section upstream. The same T-tube geometry is then used to create an optically pumped CO/Ar plasma, into which a spark-generated shock wave is launched. These results are discussed in Section III. A summary is then provided in Section IV.

II. Experiments in DC Glow Discharges

IIA. Shock tube with straight shock generating spark section

The experimental apparatus used in the present work is the same as that discussed in ref.[2], and is nearly identical to that described in ref.[1]. It consists of a 5 cm. diameter closed pyrex tube comprising a central glow discharge section. A Kolb tube at one end houses the spark gap used to generate a shock wave. The spark gap consists of a pair of

tungsten electrodes with a gap distance of 1 cm. The electrodes are cylindrical rods 0.3175 cm. (1/8 in.) in diameter. The gas is Argon maintained at a pressure of 30 Torr. As described in ref.[2], a voltage of 10 kV is typically impressed across the spark gap, discharging approximately 25 J of energy over an approximate time interval of 1 microsecond. However, only a fraction of this energy from the capacitive discharge is loaded into the gas. A shock wave is subsequently formed as a result of the rapid energy addition, and propagates through the tube. A glow discharge (30 mA at 4.5 kV) is formed downstream, through which the shock propagates, and is created using a pair of cylindrical ring electrodes. Additional details are provided in ref.[2], as are detailed measurements of PAD signal characteristics and average shock speed measurements before the glow discharge, within the glow discharge, and downstream of the glow, for two different orientations of the electric field.

Among the many measurements reported in ref.[2], was the existence of a noticeable local minimum in the average shock speed downstream of that electrode closest to the shock-generating spark section upstream. These measurements have been carefully repeated using the technique described in ref.[2], and are shown here in Figs. 3 and 4. Figure 3 shows the average shock speed averaged over 3 shots within the glow discharge, downstream of the anode, which is the electrode closest to the shock-generating spark. The same data is shown in Fig. 4 for the case where the upstream electrode (with respect to the shock propagation direction) is the cathode. As can be seen from these figures, the local minimum in the average speed is present at all currents, irrespective of the direction of the electric field. It is likely therefore that this minimum in the average shock speed though counter to what would be expected due to heating from the discharge, is due to the presence of the electrode and the shock wave's encounter with it.

IIb. Shock tube with T-tube shock generating spark section

The shock tube described in ref.[2] has been fitted with a T-tube section upstream, which houses the spark discharge used to generate a shock wave. The rest of the shock tube, containing the ring electrodes for the DC glow discharge, is identical to that described in ref.[2]. A schematic of the apparatus is shown in Fig. 5. In order to verify that the T-tube shock generating spark section produces propagating shock waves similar to the earlier straight tube described in ref.[2] and briefly in Section IIA, some experiments were conducted in pure Argon at 30 Torr. As an illustration, the PAD signal downstream of the first electrode in the *absence* of a glow discharge in Ar at 30 Torr, is shown in Fig. 6, and is identical with the PAD signals obtained in the straight tube geometry. In this section, we report on preliminary temperature measurements in a CO/Ar gas mixture at a total pressure of 30 Torr and comprising 3.3% CO. The addition of CO serves two purposes. First, it enables a relatively quick means of obtaining an approximate gas rotational temperature since addition of CO to a discharge is well known to produce electronically excited C_2 which radiate as the Swan bands ($d^3\Pi_g \rightarrow a^3\Pi_u$, $\Delta v = 0$ sequence). Second, it benchmarks shock propagation behavior in the optically pumped discharge discussed in Section III, which is operated with the identical gas mixture.

Figure 7 shows the PAD signal at the same location between the electrodes as in Fig. 6, but with 3.3% CO/96.7% Ar at 30 Torr and in the absence of a glow discharge. Note that the PAD signals are virtually identical and sharp, despite the presence of the diatomic CO. Figure 8 shows the PAD signal at the same location as Figs. 6 and 7, but with the glow discharge on, operating at 4.5 kV and 30 mA in 3.3% CO/96.7% Ar at 30 Torr. There is a marked difference in the structure of the leading portion of the PAD signal with and without CO (for instance compare Fig. 8 with any of the PAD signals shown in an Argon plasma in refs.[1,2,4]). Without CO, a sharp rise in the PAD signal is usually observed as the shock front traverses the laser beam. However, as can be seen in Fig. 8, there is a gradual rise in the PAD signal in the presence of CO. This must <u>not</u> be taken to imply that the steepness of the shock front is lowered or that the shock is weakened, but that the deflection of the HeNe beam is altered by a change in the index of refraction of the medium. Other than a shallow shock front, a change in the index of refraction can be caused by the presence of electrons and molecular ions ahead of the shock front. Associative ionization processes such as $CO(v) + CO(w) \rightarrow (CO)_2^+ + e^-$ are known to occur in vibrationally excited CO [11] and the presence of CO in a discharge is known to produce copious amounts of vibrationally excited CO. The vibrationally excited CO is also partly responsible for production of C_2 in an electrical discharge. In addition to the dimer ion $(CO)_2^+$ it is quite likely that there are other cluster ions such as $CO^+ \bullet CO \bullet C_n$ (n=0,1,...,11) and CO^+ itself present[13]. That charged particles can diffuse ahead of the shock front is not new and has

1.4 Shock Propagation Through a Low-Pressure Glow Discharge in Argon

been considered previously in refs.[7,14]. In fact, presence of electrons in concentrations of 10^7 cm^{-3} has been detected as far as 1.5 m ahead of propagating shock fronts in Argon at Mach 8 and higher[14].

Presence of CO in the Argon discharge allows the gas temperature to be determined easily by monitoring the C_2 Swan band emission[15]. Figure 9 shows a sample spectrum of the C_2 Swan band emission along with a synthetic spectrum. Using this comparison with the synthetic spectrum, the gas temperature can be determined. Also, the intensities of the rotational lines in the measured spectrum can be used to form a Boltzmann plot as in ref.[15] with the slope yielding the gas temperature. Using these means, the axial variation of gas temperature in the CO/Ar glow discharge at 30 Torr has been determined and is shown in Fig. 10. Unfortunately, the uncertainty in this measurement is ± 200 K due to the poor resolution of the experimental spectrum. A more accurate determination of the temperature could be made from the overtone ($\Delta v=\pm 2$) emission from CO ($X^1\Sigma^+$), but the pyrex tube is opaque to this radiation. Nevertheless, it can be seen that the temperature in the positive column is quite uniform at 1000 K.

The C_2 Swan band emission has also been used to probe the magnitude of radial temperature gradients by using horizontal and vertical apertures, 5 cm. x 0.5 cm. Table I shows the measured temperatures in the middle of the glow discharge, and 2 cm. above and below the centerline.

Table I: Radial variation of gas temperatures measured in the CO/Ar glow discharge using the Swan band emission from C_2

Radial location of center of aperture, r (cm.)	Gas temperature, T (K)
-2	909 K ± 200 K
0	1009 K ± 200 K
+2	1030 K ± 200 K

The radial variation exhibited in Table I is not symmetric as would be expected in a cylindrical discharge, and appears to be non-parabolic. This departure from symmetry about the centerline may be due to the effect of free convection as suggested by the temperature at r = +2 cm. being greater than the temperature at r = -2 cm. The magnitude of the temperatures at r = +2 cm. and r = -2 cm. appear to be higher than anticipated and may be artificially high due to contributions from the emitting gas near the center of the tube. The outer wall of the tube is definitely hot to the touch, indicative of temperatures in excess of about 330 K. A point-wise measurement is needed for a more accurate determination of gas temperature.

III. Experiments in an Optically Pumped CO/Ar Plasma

The CO/Ar mixture used in the glow discharge discussed in the previous section can also be excited using a CO laser. Details of optical pumping using a CO laser are described elsewhere, and will only be briefly summarized here[9-12,15-17]. The lasing characteristics of the CO laser are described in ref.[17]. The laser lines are absorbed by low-lying vibrational levels (v=1 to v=9) of the CO molecules in the CO/Ar gas mixture. Approximately 7 Watts of the CO laser power is absorbed by resonant single-photon absorption, and the absorbed energy is re-distributed within the CO molecules so as to populate higher vibrational states. This process of anharmonic V-V (vibration-to-vibration) pumping is well known[9-12,15-17], and results in susbtantial dis-equilibrium between the vibrational modes and translational modes of the CO. As a result of V-V exchange collisions, states as high as $v \approx 40$ are populated and the resulting distribution of the population of vibrationally excited molecules is highly non-Boltzmann[17]. In addition, chemical reactions and energy transfer to low-lying electronic states occur. A key chemical reaction ($CO(v) + CO(w) \rightarrow C + CO_2$) results in the formation of C_2 just as in the glow discharge described in Section IIb. Another important reaction results in the production of electrons by an associative ionization process involving vibrationally excited CO[11]:

$$CO(v) + CO(w) \rightarrow \begin{cases} (CO)_2^+ + e^- \\ CO^+ + CO + e^- \end{cases}$$

provided $E(v)+E(w) \geq \varepsilon_i$, where ε_i is the ionization potential of CO. Formation of the dimer ion is favored because its ionization potential is about 1 eV lower than that for ionization of CO. Inevitably, some of the absorbed CO laser energy is transferred to the external modes by V-R (vibration-to-rotation) and V-T (vibration-to-translation) quenching collisions, and results in heating of the gas. The amount of heating and the level of ionization in the optically pumped CO/Ar gas mixture is influenced by gas flow, amount of absorbed laser energy, and the gas composition. It is important to point out that by adding an additional diluent such as He, the vibrational excitation of CO can be moderated. Thus,

the amount of heating as well as the ionization level in this optically pumped plasma can be controlled. In addition, this type of discharge is devoid of electrodes. The optically pumped discharge is therefore ideal for isolating thermal effects from any plasma effects. In this section, we present the preliminary results on the propagation of spark-generated shock waves through optically pumped discharges in CO/Ar mixtures.

The same gas mixture (3.3% CO/96.7% Ar) as in Section IIb, at a pressure of 30 Torr is used as the target gas. The CO laser described in ref.[16], lasing at 11 W, is focused into the tube containing the CO/Ar gas mixture. Approximately 7 W of the incident laser power is absorbed. A faint, but visible blue glow approximately 17 cm. long and 7 mm in diameter, is observed. A spark-generated shock is then launched into the optically pumped discharge and observed using the PAD technique. As the shock wave passes through this optically pumped discharge, the length of the visible blue glow diminishes and slowly recovers its original length of 17 cm. Figure 11 shows representative PAD signals for a weak shock wave ($M \approx 1.24$) before it enters the optically pumped discharge, inside the optically pumped plasma, and immediately downstream of the visible glow, respectively. The PAD signal within the optically pumped plasma bears a close resemblance to that observed in the CO/Ar glow discharge (Fig. 8). Note that there is a gradual rise in the PAD signal for both the CO/Ar optically pumped discharge as well as the CO/Ar glow discharge (Fig. 8).

The PAD technique has been used to measure the axial variation of the shock speed through the optically pumped discharge. Figure 12 shows this variation, and the trend is similar to that observed for shocks propagating through Ar glow discharges[2]. The quantitative differences in the shock speed profiles in the Ar glow discharge and CO/Ar optically pumped plasma are due to the presence of CO. The presence of CO in the Ar is expected to lower the electron and gas temperatures, and the results here are consistent with this expectation. The local maximum in the shock speed observed in ref.[2] for the glow discharge in Ar is also evident here for the CO/Ar optically pumped discharge.

As discussed earlier, vibrationally excited CO reacts to form atomic carbon, which subsequently recombines to form C_2. The visible Swan band emission from C_2 transmitted through the pyrex tube can be used to infer an approximate temperature, and is shown in Fig. 13 within the optically pumped CO/Ar discharge. Again, temperatures on the order of 1000 K are inferred, and these values are susceptible to rather high uncertainties as before, due to the low-resolution of the C_2 Swan emission spectra obtained. Nevertheless, the maximum temperature of 1000 K obtained for the present CO/Ar optically pumped discharge is not unreasonable, and is only slightly higher than temperatures obtained from more accurate emission measurements for CO/Ar mixtures at 100 Torr[12].

In summary, the optically pumped discharge is a plasma with zero net current flow. It contains electrons and molecular ions, as well as axial and radial temperature gradients similar to those found in glow discharges. In the optically pumped discharge, the production of charge carriers by associative ionization is balanced by losses due to diffusion to the walls and recombination. However, unlike the glow discharge, the gas temperature and electron concentration can be better controlled and varied by adjusting the gas flow rate and gas composition (CO/Ar/He)[11].

IV. Summary & Conclusion

The local minimum in shock speed upon entering the Ar glow discharge of ref.[2] has been closely examined and found to occur at all current levels, and regardless of polarity. In addition, shock propagation through a CO/Ar glow discharge plasma and optically pumped plasma have been examined in this paper. PAD signal characteristics for the CO/Ar glow discharge and optically pumped discharge appear to be similar, and approximate temperature measurements based on Swan band emission from C_2 indicate temperatures in the neighborhood of 1000 K $\pm$ 200 K. However, more accurate point-wise measurements need to be made to obtain temperature distributions as in ref.[3].

The experimentally observed trends regarding the axial dependence of shock speed can be explained on the basis of radial thermal gradients and wall shear[2,8]. If any electrostatic effects exist, they are clearly masked by the dominant thermal gradients.

The optically pumped plasma has been shown to be a good system for studying the propagation of shock waves through plasmas and especially for isolating effects of thermal gradients. Efforts are underway to make point-wise measurements of temperature in the optically pumped discharge, and to launch shocks into a Thomson discharge[11]. The Thomson discharge is an optically pumped discharge with electrodes around the laser-irradiated region to draw out the electrons produced by associative ionization[11]. This will

enable study of shock propagation in the presence of current flow where electron concentrations and thermal gradients can be controlled by varying the gas composition (CO/Ar/He). Finally, efforts are underway to examine the existence of electrostatic effects by introducing a sub-breakdown axial electric field downstream of the optically pumped discharge in various mixtures of CO/Ar/He.

Acknowledgements:

The authors acknowledge the assistance of Mr. W. C. Lee with experiments and helpful discussions with Prof. J. W. Rich. Many helpful discussions with Dr. B. Ganguly, Dr. P. Bletzinger, and Mr. A. Forlines of AFRL, and numerous discussions with Prof. R. Miles and Dr. S. Macheret of Princeton University, are also gratefully acknowledged. This work was supported by AFOSR grant F49620-99-1-0023 monitored by Dr. Steve Walker. Support was also provided in part by two Ohio Board of Regents Investment Fund Grants.

References:

[1] B. N. Ganguly, P. Bletzinger, and A. Garscadden, "Shock Wave Dispersion in Nonequilibrium Plasmas", **Phys. Lett. A 230**, p. 218, 1997. Also see B. N. Ganguly, and P. Bletzinger, "Acoustic Shock Wave Propagation in Non-equilibrium Nitrogen and Argon Plasmas", Proceedings of the Workshop on Weakly Ionized Gases, pp. HH-3 – HH-13, U.S. Air Force Academy, June 9 –13, 1997; and P. Bletzinger and B. N. Ganguly, "Local Acoustic Shock Velocity and Shock Structure Recovery Measurements in Glow Discharges", **Phys. Lett. A 258**, pp. 342-348, 1999.

[2] A. R. White, S. M. Aithal, and V. V. Subramaniam, "Experimental Studies of Spark-Generated Shock Waves", Paper AIAA-99-3670 presented at the AIAA 30th Plasmadynamics and Lasers Conference, Norfolk, Virginia, June 28 – July 1, 1999.

[3] A. P. Yalin, Y. Z. Ionikh, and R. B. Miles, "Temperature Measurements in Glow Discharges with Ultraviolet Filtered Rayleigh Scattering", Paper AIAA-99-3431 presented at the AIAA 30th Plasmadynamics and Lasers Conference, Norfolk, Virginia, June 28 – July 1, 1999.

[4] Y. Z. Ionikh, N. V. Chernysheva, A. V. Meshchanov, A. P. Yalin, and R. B. Miles, "Direct Evidence for Thermal Mechanism of Plasma Influence on Shock Wave Propagation", **Phys. Lett. A 259**, pp. 387-392, 1999.

[5] W. F. Bailey, and W. M. Hilbun, "Baseline of Thermal Effects on Shock Propagation in Glow Discharges", Proceedings of the Workshop on Weakly Ionized Gases, pp. GG3 – GG18, U.S. Air Force Academy, June 9 –13, 1997.

[6] S. O. Macheret, L. Martinelli, and R. B. Miles, "Shock Wave Propagation and Structure in Non-uniform Gases and Plasmas", paper AIAA 99-0598 presented at the 37th AIAA Aerospace Sciences Meeting and Exhibit, Reno, Nevada, January 11-14, 1999; Also see S. O. Macheret, R. Miles, and P. Efthimion, "Shock Propagation in Weakly Ionized Plasmas: Mechanisms and Key Problems", Proceedings of the Workshop on Weakly Ionized Gases, pp. X-11 – X-33, U.S. Air Force Academy, June 9 –13, 1997.

[7] I. Adamovich, V. V. Subramaniam, J. W. Rich, and S. O. Macheret, "Phenomenological Analysis of Shock Waves in Weakly Ionized Gases", **AIAA Journal**, Vol. 36, No. 5, pp. 816 – 823, May 1998.

[8] S. M. Aithal, and V. V. Subramaniam, "On the Characteristics of a Spark Generated Shock Wave", accepted for publication in **Phys. Fluids**.

[9] W. Urban, J. X. Lin, V. V. Subramaniam, M. Havenith, and J. W. Rich, "Treanor Pumping of CO Initiated by CO Laser Excitation," **Chemical Physics, 130**, pp. 389-399, 1989.

[10] C. E. Treanor, J. W. Rich, and R. G. Rehm, "Vibrational Relaxation of Anharmonic Oscillators with Exchange Dominated Collisions", **J. Chem. Phys. 48** (4), p. 1789, 1968.

[11] I. Adamovich, S. Saupe, M. J. Grassi, O. Schulz, S. Macheret, and J. W. Rich, "Vibrationally Stimulated Ionization of Carbon Monoxide in Optical Pumping Experiments", **Chem. Phys. 173**, pp. 491-504, 1993.

[12] E. Plonjes, P. Palm, A. P. Chernukho, I. V. Adamovich, and J. W. Rich, "Time-Resolved Fourier Transform Infrared Spectroscopy of Optically Pumped Carbon Monoxide", paper AIAA-99-3479 presented at the 30th Plasmadynamics and Lasers Conference, June 28-July 1, 1999, Norfolk, Virginia.

[13] Y. Kaufman, P. Avivi, F. Dothan, H. Keren, and J. Malinowitz, "Ion clusters in He-CO and Ar-CO glow discharges", **J. Chem. Phys.** 72(4), pp. 2606-2611, February 15, 1980.

[14] H. D. Weymann, "Electron diffusion ahead of Shock Waves in Argon", **Phys. Fluids**, Vol. 3, No. 4, pp. 545-548, July-August 1960.

[15] C. Flament, T. George, K. A. Meister, J. C. Tufts, J. W. Rich, V. V. Subramaniam, J. P. Martin, B. Piar, and M. Y. Perrin, "Nonequilibrium Vibrational Kinetics of Carbon Monoxide at High Translational Mode Temperatures", **Chemical Physics 163**, No. 2, pp. 241-262, 15 June 1992.

[16] I. V. Adamovich, M. Chidley, W. C. Lee, W. Lempert, P. Palm, E. Plonjes, and J. W. Rich, "Large-Scale Laser-Pumped Optical Discharges", paper AIAA-99-3722 presented at the 30th Plasmadynamics and Lasers Conference, June 28-July 1, 1999, Norfolk, Virginia.

[17] J. W. Rich, "Relaxation of Molecules Exchanging Vibrational Energy", Chap. 4 in *Gas Lasers, Applied Atomic Collision Physics*, Vol. 3, pp. 99-140, Academic Press, new York, 1982.

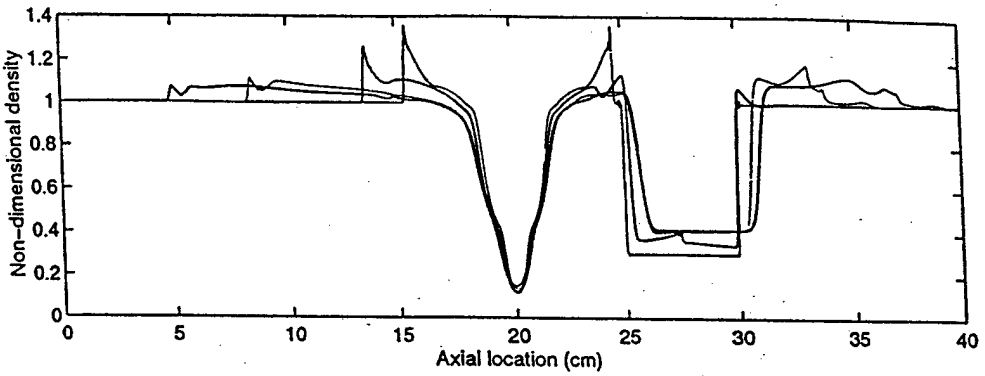

Fig. 1a: Calculated profiles of mass density along r = 0 non-dimensionalized by the undisturbed gas density, $\rho_0 = 0.0641$ kg/m^3, are shown here versus axial coordinate x, at several instants of time (100 μs, 150 μs, 300 μs, and 400 μs, respectively) after energy addition leads to formation of propagating shocks (from ref.[8]). The results from compressible Navier-Stokes simulations described in ref.[8] shown here are for the case of shock propagation in Argon initially at 30 Torr and 300 K. This case considers the realistic bounded viscous flow induced by a traveling shock wave in a 5 cm. diameter tube, where the rightward traveling wave encounters a heated region with an initial radial parabolic distribution of temperature (from 1000 K at the centerline to 300 K at the wall). This case considers the effects of both axial and radial thermal gradients as well as wall shear.

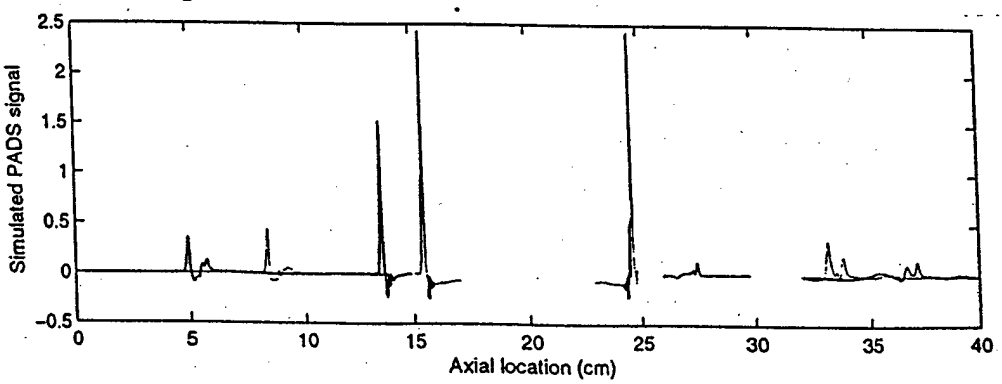

Fig. 1b: Simulated PAD signal obtained by integrating the axial derivative of density (corresponding to Fig. 1a) in the transverse, i.e. radial, direction (from ref.[8]).

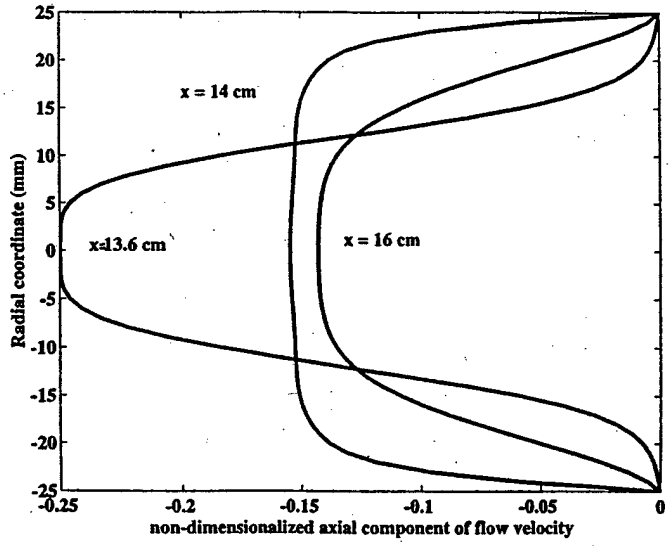

Fig. 2: Radial profiles of the axial component of flow velocity induced by passage of the shock calculated by the Navier-Stokes simulations in ref.[8], are shown here for the leftward moving wave, 150 μs after initiation of the shock wave, at three different axial locations behind the shock front. The location x = 13.6 cm refers to a location just behind the shock front, while x = 14 cm. and x = 16 cm. refer to locations further behind the shock front. The Mach number of this shock is ≈ 1.2, propagating into Ar at 30 Torr.

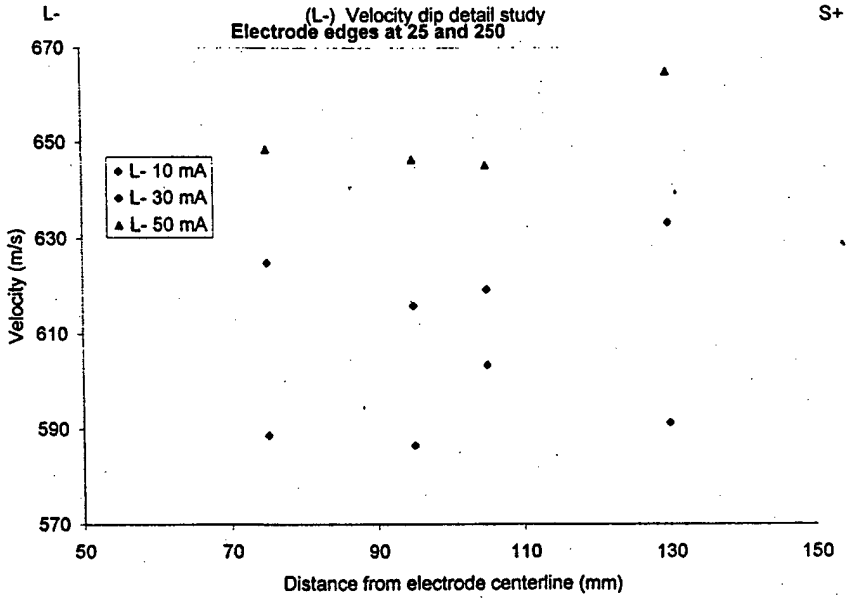

Fig. 3: Measured average shock propagation speeds versus distance inside the glow discharge plasma just downstream of the electrode nearest the spark gap, for various discharge currents. The electrode nearest the spark gap, is the cathode (L-) and the farthest electrode is the anode (S+).

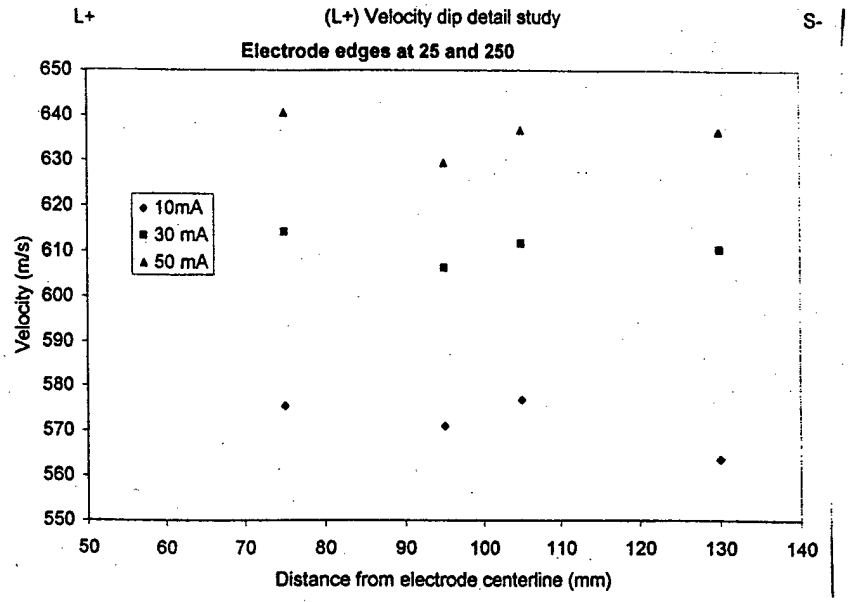

Fig. 4: Measured average shock propagation speeds versus distance inside the glow discharge plasma just downstream of the electrode nearest the spark gap, for various discharge currents. The electrode nearest the spark gap, is the anode (L+) and the farthest electrode is the cathode (S-).

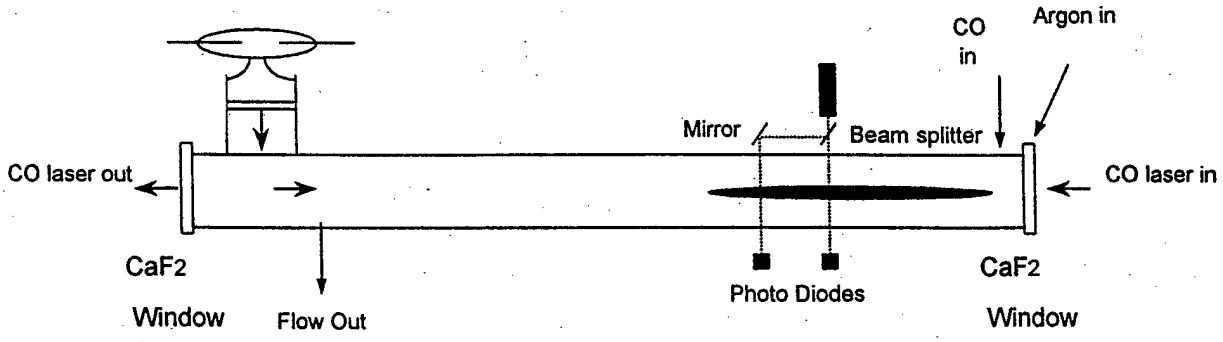

Fig. 5: Schematic of shock tube with T-tube shock generating spark section, also showing optical access for CO laser beam, and optically pumped discharge in a CO/Ar gas mixture.

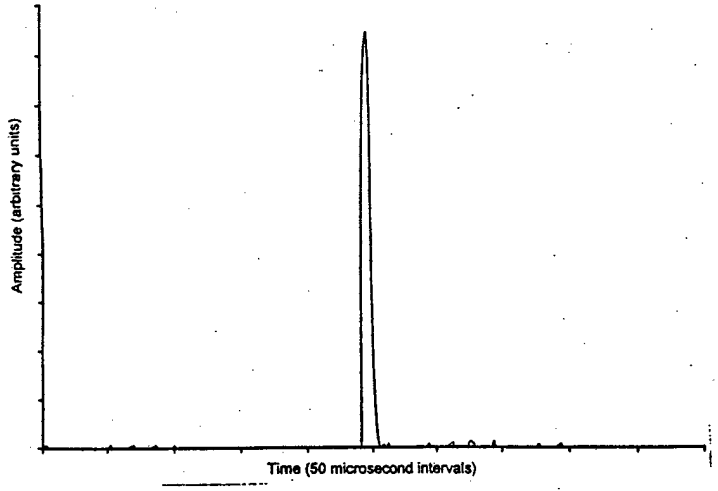

Fig. 6: PAD signal at a location between the electrodes for a shock propagating in pure Argon in the T-tube at 30 Torr, in the absence of a glow discharge.

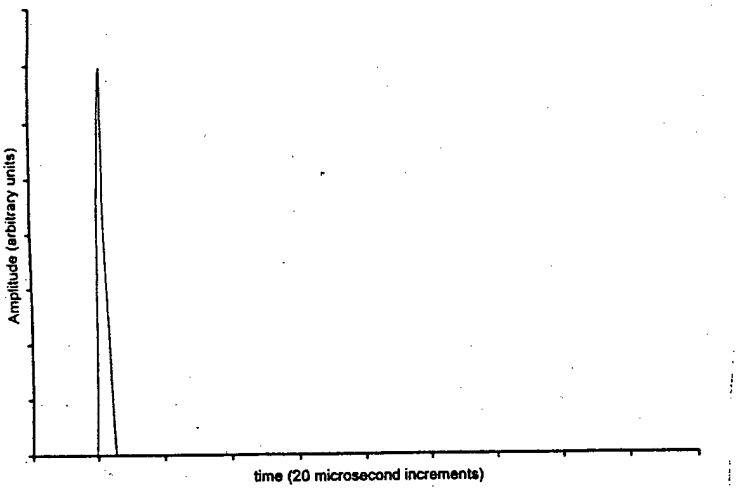

Fig. 7: PAD signal at a location between the electrodes for a shock propagating in 3.3 % CO/96.7 % Argon gas mixture at 30 Torr in the T-tube, in the absence of a glow discharge.

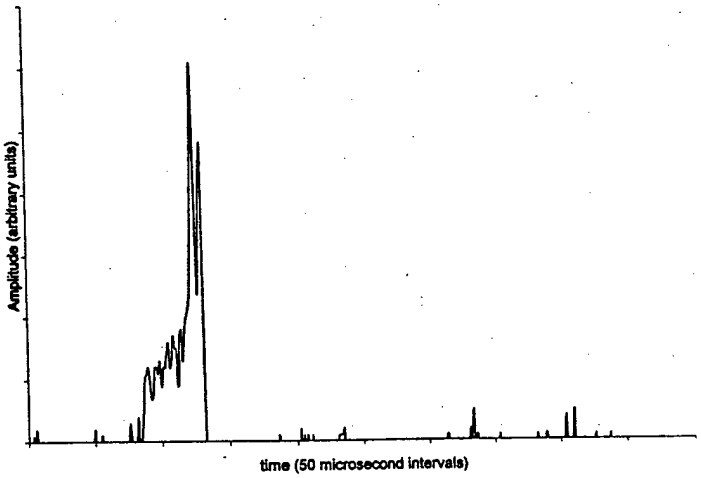

Fig. 8: Typical PAD signal at a location between electrodes for a shock propagating in 3.3 % CO/96.7 % Argon gas mixture at 30 Torr in the T-tube, with the glow discharge on.

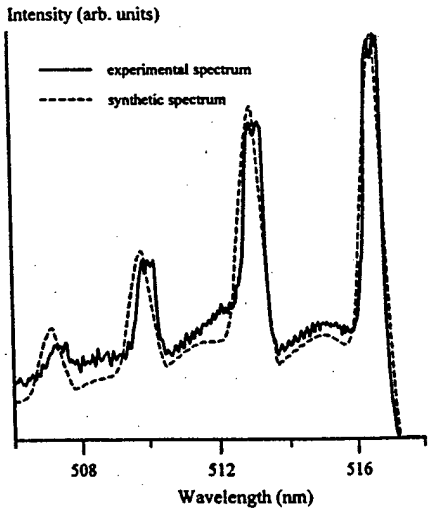

Fig. 9: Sample spectrum of the C_2 Swan band emission, as compared with a synthetic spectrum for the $\Delta v=0$ emission, for a 3.3% CO/96.7% Ar gas mixture at 30 Torr in the optically pumped discharge. Using the intensities in the measured spectrum, a Boltzmann plot can also be drawn as in ref.[15]. Since the measured spectrum is not as well resolved, both techniques (i.e. comparison with a synthetic spectrum and Boltzmann plot) yield an uncertainty of $\pm$ 200 K.

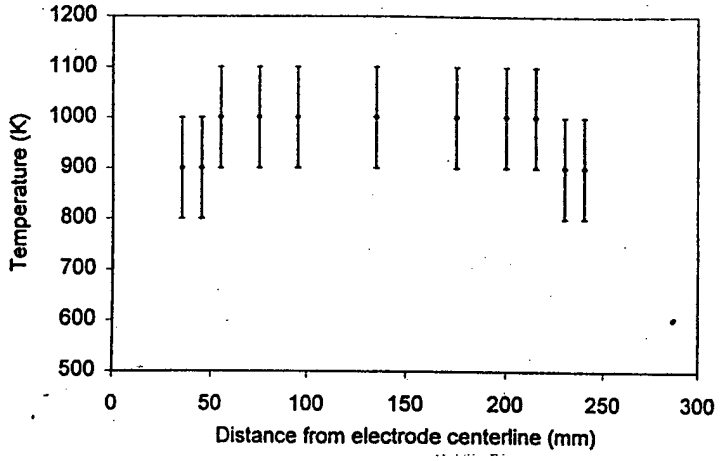

Fig. 10: Axial variation of temperature between the electrodes for a shock propagating in 3.3 % CO/96.7 % Argon gas mixture at 30 Torr in a T-tube, with the glow discharge on.

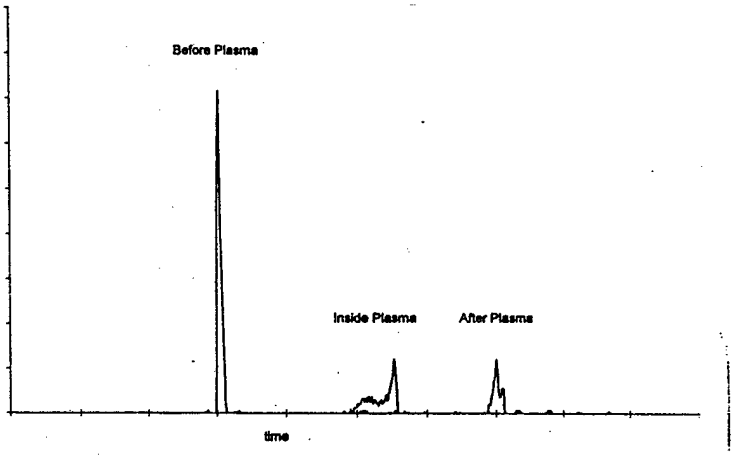

Fig. 11: Typical PAD signals in the T-tube for a shock propagating in 3.3 % CO/96.7 % Argon gas mixture at 30 Torr, before blue glow, inside blue glow, and downstream of blue glow, with an optically pumped discharge on.

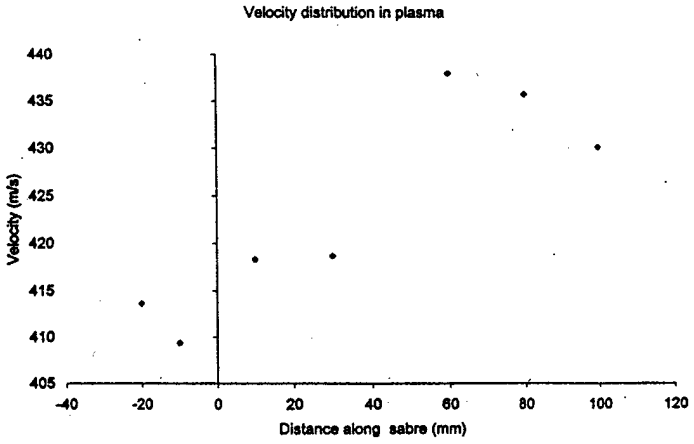

Fig. 12: Axial variation of shock speed in T-tube for a shock propagating in 3.3 % CO/96.7 % Argon gas mixture at 30, with an optically pumped discharge on.

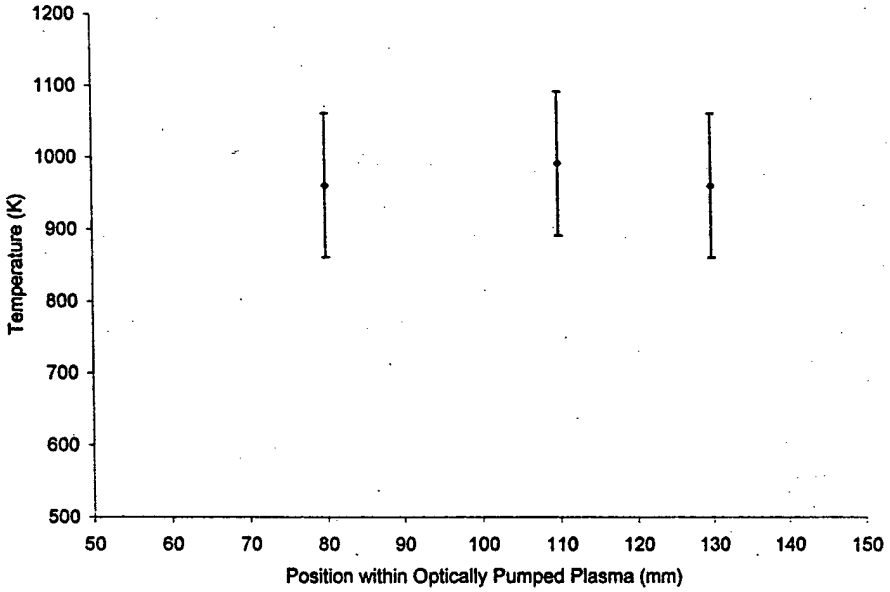

Fig. 13: Axial variation of temperature within the optically pumped discharge in the T-tube for a shock propagating in 3.3 % CO/96.7 % Argon gas mixture at 30 Torr, with the optically pumped discharge on.

JOURNAL OF THERMOPHYSICS AND HEAT TRANSFER
Vol. 15, No. 4, October–December 2001

Shock Propagation Through a Low-Pressure Glow Discharge in Argon

A. R. White* and V. V. Subramaniam†
The Ohio State University, Columbus, Ohio 43210

Experimental measurements recording spark-generated shock propagation characteristics within an argon glow discharge and in the afterglow region are reported here. Photoacoustic deflection is used to measure average shock speeds and to examine the shock wave recovery downstream of the glow discharge. Radial shock profiles at several axial locations are experimentally determined by measuring the arrival time at different radial locations. These measurements are found to be in qualitative agreement with predictions from numerical simulations that consider temperature gradients and viscous effects, but which do not account for any effects of the plasma on shock propagation.

Nomenclature

V_s = shock propagation velocity
x = axial distance along the shock tube
ε = energy loaded into the shock tube gas by the spark discharge
μ = gas viscosity
ρ = gas density

I. Introduction

THE structure and propagation of shock waves in gases has been a topic of much interest in this century, motivated primarily by aerospace applications. It has been the subject of several authoritative books.[1–4] Shock propagation in plasmas has also been studied with specific regard to reentry flows, interaction of the solar wind with the terrestrial magnetosphere, and magnetohydrodynamic applications. This research has also culminated in several authoritative texts.[5–9] Despite this abundance of information on shock wave propagation in ionized and nonionized gases, experiments conducted in Russia[10–16] and in the United States[17–19] have prompted further inquiry on this problem.[20–23] Experiments reported in Refs. 17–19 show apparent modification of shock structure within a glow discharge and report lengths on the order of the shock tube diameter, to recover the original shock structure downstream of the discharge. Analysis of this problem by numerical solution of the inviscid Euler equations[20–23] has shown that radial temperature gradients created by the glow discharge could explain the experimental observations reported in Refs.10–19.

In this paper, experimental results for the propagation of shock waves through weakly ionized argon are presented. The shock waves are generated using a capacitively discharged spark and subsequently launched into a low-pressure glow discharge in argon. The experimental apparatus is similar to that used in Refs.17–19 and is described therein. In addition, measurements of the average shock velocity and shock structure are provided at several axial locations along the length of the tube, and at several radial locations for given axial positions. Shock structure is inferred by photoacoustic deflection (PAD) measurements.[17–19] Measurements recording the effects of reversing the direction of the electric field on shock propagation velocity and photoacoustic signal characteristics are also discussed. An important focus of this paper is examination of the recovery of the photoacoustic signal downstream of the glow discharge, as a function of distance along the tube.

This paper is organized as follows. The experimental apparatus and procedure are briefly described in the following section. Section III describes the experimental measurements and plausible explanations for these results. A summary is provided in Sec. IV, along with the conclusions of this work.

II. Experimental Apparatus and Procedure

The experimental apparatus consists of a 5-cm-diam closed Pyrex® tube comprising a central glow discharge section. A Kolb tube[24] at one end houses the spark gap used to generate a shock wave. The spark gap consists of a pair of tungsten electrodes with a gap distance of 1 cm. The electrodes are cylindrical rods 0.3175 cm ($\frac{1}{8}$ in.) in diameter. The gas used in the measurements reported here is argon and is maintained at a pressure of 30 torr. Typically, a voltage of 10 kV is impressed across the spark gap, discharging approximately 25 J of energy over an approximate time interval of 1 μs. However, only a fraction of this energy from the capacitive discharge is loaded into the gas. A shock wave is subsequently formed as a result of the rapid energy addition and propagates through the tube. In the experiments involving a plasma, a glow discharge in 30 torr of argon is struck between the two electrodes located downstream of the spark gap. The electrodes in the glow discharge section are cylindrical, 2.5 cm in diameter, hollow, and concentric within the Pyrex shock tube, as can be seen in the schematic shown in Fig. 1. The argon gas is introduced via a rotameter and flows at 100 sccm (standard cubic centimeters per minute) in the direction counter to that of shock propagation as in Refs. 17–19. In Refs. 17–19, however, the flow was carefully controlled and introduced at a rate of 50 sccm using a mass flow controller. In an effort to reproduce one of the shock tube configurations of Refs. 17–19, the upstream electrode (i.e., nearest the spark gap) is longer, 5 cm in length, whereas the downstream electrode (i.e., farthest away from the spark gap) is shorter, 1.5 cm in length. The distance between the electrodes (edge to edge) in the glow discharge is 22.25 cm in the present work, and the corresponding distances in Refs. 17–19 were 19 and 20 cm. A visibly uniform glow discharge can be maintained in argon at 30 torr using this configuration, until the discharge current exceeds about 60 mA, after which point the discharge becomes filamentary. In the experiments reported here, the current in the glow discharge is varied from 0 to 50 mA, and the voltage is varied from 1.8 kV (for 10 mA) to 4.8 kV (for 50 mA). The discharge is operated for 15 min before shock waves are launched into the plasma, to ensure that any thermal gradients that exist would have attained steady state. This is especially important because the shock structure has been observed to be unchanged when the shock passes through immediately after the glow discharge is initiated.[25,26]

Received 17 November 2000; revision received 20 April 2001; accepted for publication 24 April 2001.

*Graduate Research Associate, Center for Advanced Plasma Engineering, Non-Equilibrium Thermodynamics Laboratories, Department of Mechanical Engineering.

†Professor, Center for Advanced Plasma Engineering, Non-Equilibrium Thermodynamics Laboratories, Department of Mechanical Engineering. Senior Member AIAA.

A Uniphase 1125 He–Ne laser (10 mW) is directed perpendicular to the axis of the shock tube, partially illuminating a Thor Laboratories PDA 155 high-speed amplified silicon detector on the other side of the tube, as shown in Fig. 1. The instant of spark initiation is relayed to the oscilloscope via a synchronization signal provided by the spark gap trigger. The oscilloscope is programmed with an appropriate delay after spark initiation to enable capture of the passing shock as it traverses the downstream location of the PAD detection system. The output of the detector is a voltage proportional to the intensity of the beam illuminating it. As the shock wave traverses across the laser beam, the gradient in density across the shock front gives rise to a variation in the index of refraction, causing the He–Ne beam to deflect. The resulting time-varying voltage is then recorded on a Tektronix digital oscilloscope (40 MHz). In the experiments reported here, a sampling rate of 5 MHz is used. The deflection of the beam is proportional to the axial density gradient integrated radially across the tube and results in a time-varying intensity recorded by the detector and which is output as a time-varying voltage. Therefore, a shock front would give rise to a PAD signal that appears as a sharp spike resembling a delta function. The same photoacoustic signal is used to measure the average velocity of the shock front. This is done by measuring the time of flight between two axial locations, 6.9 cm apart. In this instance, the He–Ne beam is passed through a beam splitter, one beam passing through the tube and illuminating a detector on the other side. The other beam is reflected off a mirror and then passed through the tube onto a second detector. Using the signal from the first detector as the trigger and prescribing a time delay then allows the shock wave arrival time to be determined at the second axial location. The travel time of the shock wave between the two locations is recorded, and because the distance between these locations is known, an average velocity can be calculated. The two split beams are separated by 6.9 cm due to physical limitations in the apparatus, which is coarser than the 2.59 cm separation used to measure the shock velocity in Refs. 17–19. The average shock velocity at a given point is, thus, measured by the time of flight between the split beams, 3.45 cm on either side of a point, in the present experiments. Variation of the average shock speed along the tube is determined by mounting the laser/detector assembly on an optical rail, which is then attached on a translation stage that traverses parallel to the shock tube. All measurements of the shock propagation speed within the glow discharge using the split beam were made with both beams within the glow region.

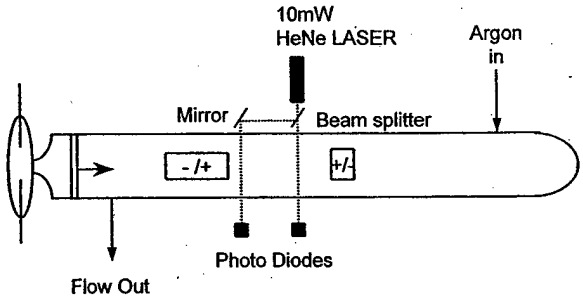

Fig. 1 Schematic of experimental apparatus.

In this paper, several experimental measurements are reported. Measurements of average shock speed are obtained at several axial locations. These are the regions before, within, and downstream of the glow discharge. These average velocity measurements are obtained for two discharge polarities, one where the applied electric field is in the same direction as shock propagation and the other in which the electric field is in the direction counter to that of shock propagation. Measurements of the average shock speed are also made for several values of the total current within the diffuse glow discharge: 0, 10, 30, and 50 mA. PAD signals are also obtained for these current levels and for both orientations of the applied electric field. In addition, shot-averaged shock arrival times are recorded for various radial locations at three axial positions to determine the shape of the shock front. These measurements are presented in the following section, along with an accompanying discussion of the results.

III. Experimental Results and Discussion

Shock propagation velocities along with the associated PAD signal characteristics are presented first. These results are obtained in the regions upstream of the glow discharge, within the glow discharge, and downstream of the glow discharge. The axial variation of the shock propagation speed is compared with theoretically expected trends for the viscous and inviscid cases. Recovery of the PAD signal after the shock exits the glow discharge is monitored. Finally, shot-averaged shock absolute arrival times are recorded radially for three axial locations upstream of and inside the glow discharge. These absolute arrival time measurements provide information regarding the shape of the shock front, to within shot-to-shot variation, and are compared with the numerical calculations presented in Ref. 27. These are compared with the PAD signal characteristics to infer the shape of the shock front.

Figure 2 shows a plot of the average shock propagation velocity as a function of position for the case where the longer (5-cm-long)

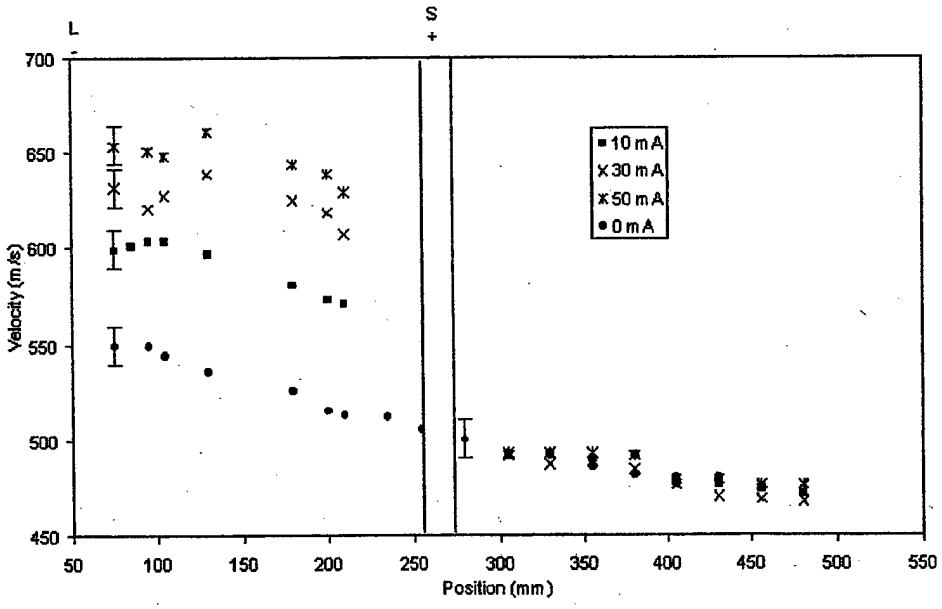

Fig. 2 Average shock propagation speeds measured vs distance along shock tube for various values of glow discharge current in $L-$ glow discharge configuration.

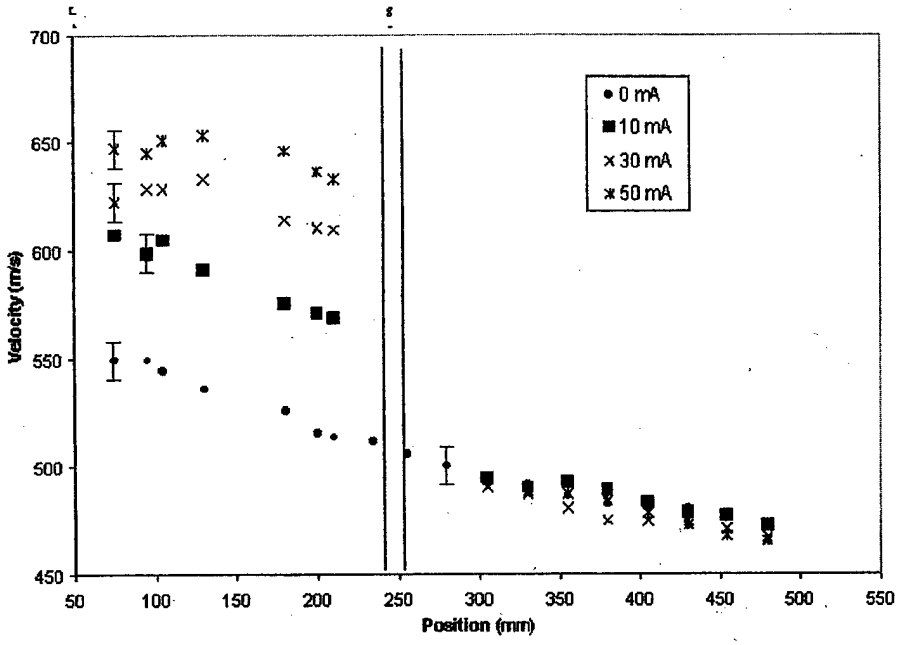

Fig. 3 Average shock propagation speeds measured vs distance along shock tube for various values of glow discharge current in $L+$ glow discharge configuration.

electrode located nearest to the spark gap is the cathode (denoted hereafter as $L-$) for different values of the total discharge current. In this case, the electric field is in the direction counter to that of shock propagation. Figure 3 shows the shock propagation speed vs axial position for the case where the longer electrode located nearest to the spark gap is the anode (denoted hereafter as $L+$) for different values of the total discharge current. Note from both Figs. 2 and 3 that, in the absence of the glow discharge, the shock propagation velocity decreases monotonically along the length of the shock tube. This is expected behavior and can be deduced from the following dimensional analysis.[3] The shock propagation speed in the inviscid case can be found by selecting the energy loaded into the gas by the spark discharge ε at the location $x = 0$, distance along the tube x, shock propagation velocity V_s, and density ρ as variables. If ε, x, and ρ are chosen as independent quantities, then the shock propagation speed can be expressed as

$$V_s \sim \sqrt{\varepsilon/\rho x^3} \tag{1}$$

Thus, in the case of inviscid expansion, the shock speed decreases monotonically as $x^{-3/2}$. For the viscous case, the set of variables includes ε, x, and V_s and is augmented by μ, the dynamic viscosity. If ε, x, and μ are chosen as the independent parameters, the shock speed is found to decrease as x^{-2}:

$$V_s \sim \varepsilon/\mu x^2 \tag{2}$$

The data in Figs. 2 and 3 in the absence of a glow discharge reveal a monotonic decrease in the shock propagation speed vs length along the tube. However, this decrease can be due to either the expansion itself or viscous effects. The experimental resolution is insufficient to distinguish between the $x^{-3/2}$ variation of Eq. (1) and the x^{-2} variation of Eq. (2). Hence, the effect of viscosity on shock propagation speed cannot be isolated from effects due to the expansion alone. This is important to bear in mind because viscous effects are expected to influence the PAD signal characteristics of weak shocks quite dramatically.[27,28] In contrast, for shocks of moderate strength considered here, the PAD signal characteristics in the absence of a discharge remain sharp and narrow all through the length of the tube.

Figures 2 and 3 also show shock propagation speeds vs length along the tube for various glow discharge currents, for the two orientations $L-$ and $L+$. In all cases, as mentioned in Sec. II, it was ensured that the rightmost of the two beams used to measure shock speed was within the glow discharge region. When the glow discharge is on, the shock speed exhibits a noticeable local maximum within the glow discharge section. Because the temperature within the glow discharge is uniform axially (see discussion later in this section), the shock speed should remain constant in the absence of viscous effects. However, the shock speeds in Figs. 2 and 3 exhibit a pronounced maximum in the middle of the glow region and, thus, cannot be explained by thermal effects alone. The maximum in the shock velocity, rather than a monotonic variation of the velocity in the glow discharge region, is due to the opposing influences of heating and wall shear. Ohmic heating within the discharge raises the gas temperature and, therefore, increases the shock velocity. On the other hand, wall shear becomes significant as the shock speed increases and ultimately serves to reduce the shock propagation speed. The effects of heating are evident in the observed increase in shock velocity as the current is raised. There is, however, a repeatable and noticeable local minimum in the shock velocity for the $L-$ case, near the cathode, for currents of 30 and 50 mA. More detailed experimental investigation suggests that the velocity dip is caused by the presence of the upstream electrode in the path of the shock wave.

On exiting the glow discharge section, the velocity of the shock can be seen to assume the same value as in the absence of the glow discharge, almost immediately. Figures 4 and 5 show PAD signals at several axial locations downstream of the glow discharge, for a representative discharge current of 10 mA and for the two orientations of electric field considered in this work. The same behavior is found for the higher currents (30 and 50 mA) as well. Evident in Figs. 4 and 5 is the recovery of the PAD signal to its delta-functionlike appearance on exiting the discharge. Typically, the PAD signal will increase in amplitude after the shock emerges from the glow discharge region, reach a maximum, and decline in amplitude thereafter. The recovery distance is defined here as the distance from the edge of the electrode at the end of the glow discharge to the axial location where the PAD signal recovers its delta-functionlike appearance. As can be seen from Figs. 4 and 5, there is a small but apparent dependence of the PAD signal recovery distance on the direction of the electric field. From Fig. 4, when the electric field is in the direction opposite to that of shock propagation, the recovery distance can be seen to be between 2.8 and 5.3 cm. In Fig. 5, when the electric field is aligned in the direction of shock propagation, the recovery distance is just beyond 5.3 cm, but very clearly before 7.8 cm. The recovery length is apparently longer when the electric field is in the direction of propagation of the shock, regardless of

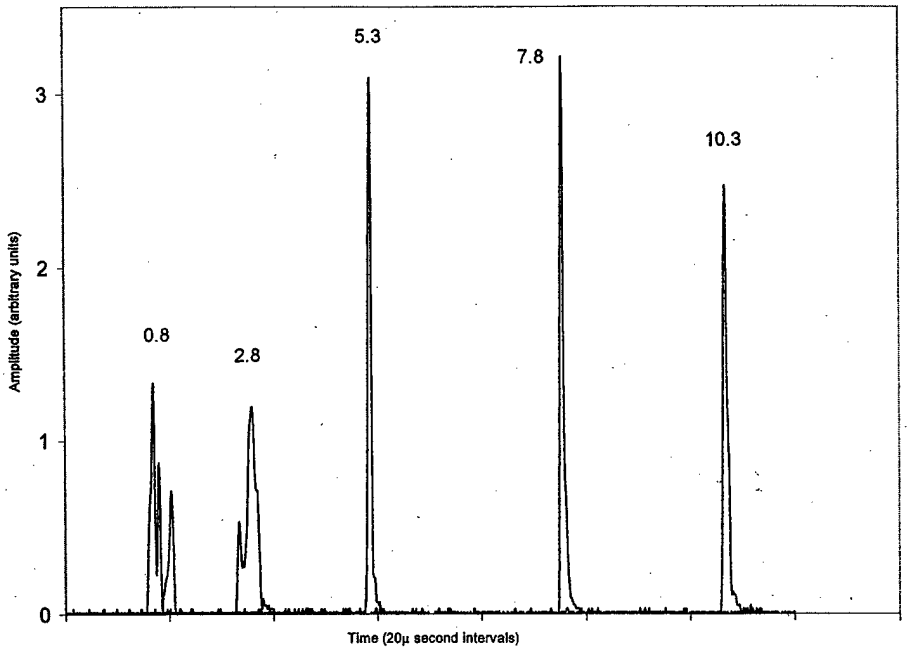

Fig. 4 Amplitude of PAD signal vs time, downstream of glow discharge, at various locations (indicated above PAD signals in centimeters ±0.5 cm) from trailing edge of anode for *L*− configuration for discharge current of 10 mA.

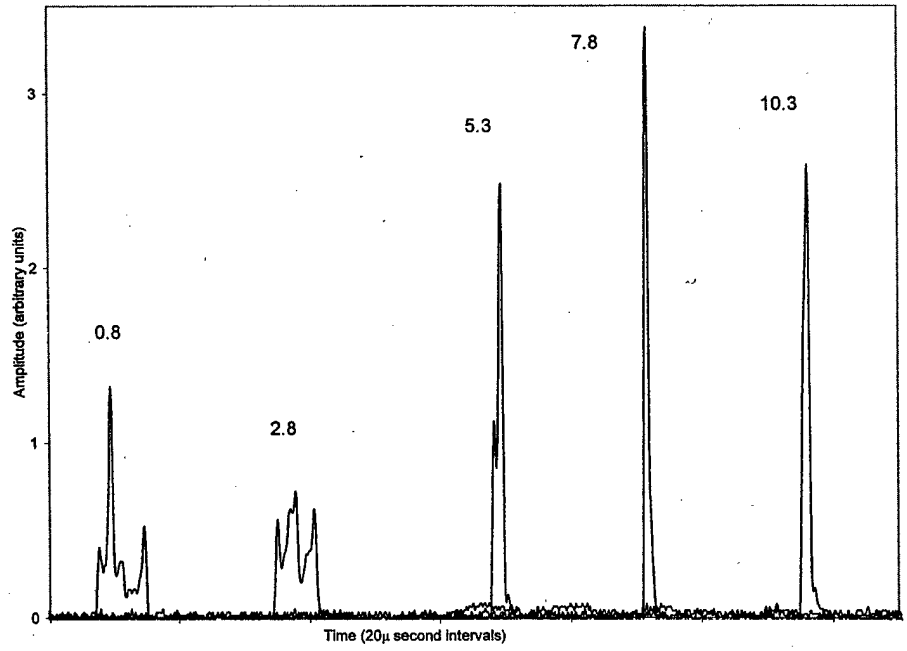

Fig. 5 Amplitude of PAD signal vs time, downstream of glow discharge, at various locations (indicated above PAD signals in centimeters ±0.5 cm) from trailing edge of cathode for *L*+ configuration for discharge current of 10 mA.

the magnitude of the discharge current. In the instance where the electric field is oriented in the direction of shock propagation, the cathode, which is expected to be the hotter of the two electrodes, is on the downstream side of the shock propagation direction. Thus, the observed increase in recovery length for this case may have its origin in thermal effects associated with the electrode rather than the properties of the plasma. Note that variations up to 0.5 cm were observed due to shot-to-shot variation in the experiments reported here, making a determination of the exact recovery length impossible. The recovery distances of several tube diameters or more, observed in the present experiments, are consistent with results from the numerical simulations reported in Ref. 27. To determine the temperature of the glow discharge, CO was added to the argon as a thermometric element. Although addition of CO changes the discharge characteristics, the shock structure as determined by PAD signal measurements was found to be unaffected. The mixture comprised 3.3% CO and balance argon, but maintained the total pressure at 30 torr and the flow rate at 100 sccm. When CO is added to a discharge, C_2 is produced in an electronically excited state. When the resulting rotationally resolved Swan band emission from the C_2 molecules is measured, it is possible to determine the rotational temperature of the gas (see Ref. 29). The translational temperature is equivalent to the rotational temperature because these two modes are in equilibrium at these pressures. By the use of 0.5-cm-wide

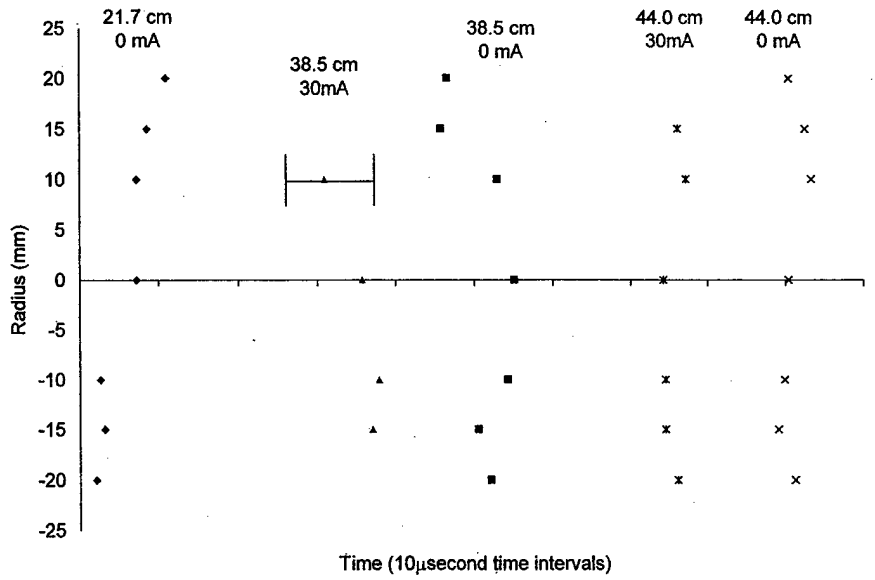

Fig. 6 Radial profile of passing shock front determined by measurement of absolute arrival time at axial locations upstream and within glow discharge; data for each axial location have been uniformly shifted by constant amounts [(21.7 cm, 0 mA) is shifted by −4 μs, (38.5 cm, 30 mA) is shifted by +14 μs, (38.5 cm, 0 mA) is shifted by +5 μs, (44 cm, 30 mA) is shifted by +35 μs, and (44 cm, 0 mA) is shifted by +20 μs to display radial profiles for different locations on the same figure].

apertures to view emission from a small region of the discharge, an average temperature distribution was inferred from the rotationally resolved Swan band spectra of C_2. This temperature represents an average value over the volume spanned by the cross section of the tube and the 0.5-cm width of the aperture. Measurements of the radial temperature distribution at several axial locations and of the axial temperature variation along the centerline were made for the $L-$ configuration. Only minute axial variation of the temperature (on the order of 10 K) was found. In the radial direction, temperatures were found to be 1009 K $\pm$ 200 K at the shock tube centerline, 1030 K $\pm$ 200 K at 2 cm above the centerline, and 909 K $\pm$ 200 K at 2 cm below the centerline. The temperatures determined using this method are within the same range as more detailed measurements undertaken by other groups.[25,26] The increase in shock propagation speed within the glow discharge region can, therefore, be attributed to the high temperatures associated with ohmic heating of the gas by the electrical discharge.

Thermal effects associated with the glow discharge plasma can explain acceleration of the shock as well as the splitting, spreading, and attenuation of the PAD signal. The high temperature within the glow discharge region serves to increase the local speed of sound and, thus, accelerates the shock wave. Moreover, because the pressure is constant, the density within the glow discharge region must be lower than that of the neutral gas outside the glow discharge. Therefore, the magnitude of the density gradient is also smaller within the glow discharge region, resulting in an attenuated PAD signal. In addition, there is a radial temperature gradient within the glow discharge region because the centerline has a high temperature (~1000 K) whereas the walls of the tube are relatively cool (<350 K). This causes the shock front to be curved near the wall, which in turn produces a split and spread PAD signal. Numerical simulations for both inviscid [20–23] and viscous cases [27] indicate that the shock does exhibit curvature in the presence of a radial thermal gradient and that this curvature causes splitting and spreading of the PAD signal comparable to that observed experimentally. Although this curvature is not pronounced (the near-wall regions of the shock front lag by ~5 mm from the centerline segment of the front, as will be discussed next) it is, nevertheless, important enough to influence the highly sensitive PAD technique.

To quantify shock curvature experimentally, measurements were made of the absolute arrival times for several radial locations at a given axial position. Because only one laser source and detector were used in the present experiments, the data at different radial locations correspond to different shots, although they are for the same parameters governing the spark discharge used for shock generation. These results are shown in Fig. 6 before the shock enters the glow discharge and within the glow discharge region. Note that although absolute arrival times (i.e., measured from the instant the spark is initiated) are used to detect the shock front, the data for each axial location have been uniformly shifted by different amounts to display all of the results in Fig. 6. Note from Fig. 6 that to within shot-to-shot variation, the near-wall portions of the front differ in arrival time from the centerline portion by less than 7.7 μs. However, because the uncertainty due to shot-to-shot variation is greater than 10 μs, we may conclude that there is negligible curvature of the shock front. Given the measured shock speed of 625 m/s, the lag in arrival time of 7.7 μs corresponds to an axial distance of less than 5 mm. Note, therefore, that the shock front is largely planar, at least over the measured region spanning 4 cm of the 5 cm diameter. In the numerical results reported in Ref. 27, lag distances of about 9 mm can be inferred based on the staggered density profiles for the case of a shock significantly weaker in strength compared to the present experiments. Consequently, smaller lag distances are expected as the strength of the shock increases. Note, therefore, from both the present experiments and the numerical results of Ref. 27, that most of the shock front is planar, with curvature confined to the near-wall regions. The PAD signal is sensitive even to such small curvatures and, therefore, displays a split signal when the curvature is increased in the presence of radial temperature gradients or because of wall shear.[28]

In summary, most of the trends observed in the experiments reported here can be explained in terms of classical effects due to thermal gradients and wall shear. A plasma produces ohmic heating of the gas and generates radial thermal gradients. Shock acceleration can be easily explained by the higher temperatures present in the glow discharge. The experiments of Refs. 25 and 26 offer conclusive evidence for this. The splitting and spreading of the PAD signal does not imply splitting and spreading of the shock front itself. Rather, this observation can be explained by curvature of the shock front in the near-wall regions of the shock tube, which can be induced either by radial thermal gradients[20–23,27] or by the presence of wall shear alone.[27,28] Moreover, the recovery of the shock speed and the PAD signal downstream of the plasma is consistent with results from numerical simulations of shocks traversing through regions of thermal gradients alone, that is, in the absence of a plasma. Therefore, no plasma effects need to be invoked to explain the shock propagation characteristics observed in these or other experiments.[10–19,25,26]

IV. Conclusions

Shock propagation through a glow discharge has been examined using the PAD technique described in Ref. 17. The effects reported in Refs. 17–19 have been reproduced for argon at a pressure of 30 torr. The shock propagation speed has been measured vs distance along the direction of propagation and is influenced by gas heating and wall shear effects. Detailed measurements of the PAD signal recovery indicate a dependence on the direction of the electric field, which in turn appears to be caused by thermal effects stemming from the presence of a hot electrode (the cathode). Splitting and spreading of the PAD signal observed when the shock passes through the glow discharge can be explained by the presence of radial thermal gradients and wall shear. Radial thermal gradients and wall shear are capable of introducing curvature to the shock front, especially in the near-wall regions. However, measurements of shock arrival time at various radial positions within the glow discharge and away from the wall indicate no change in shock structure or shock planarity (to within shot-to-shot variation). Shock curvature does influence the PAD signal due to the sensitivity of this measurement and because the recorded PAD signal is line of sight averaged. This explains why the PAD signal appears split and spread as the shock passes through the glow discharge, whereas shock arrival time measurements indicate the shock front to be, for the most part, planar. In conclusion, the basic characteristics of shock propagation within a glow discharge appear to be explainable in terms of the classical effects of thermal gradients and wall friction, with no recourse to any plasma effects. Although an electrostatic space charge layer does indeed exist near the shock front and travels along with it, there is no evidence that this space charge layer actually alters the structure of the shock wave in the primarily neutral gas.

Acknowledgments

This work was supported by U.S. Air Force Office of Scientific Research Grant F49620-99-1-0023, monitored by Steven Walker. Support was also provided for major equipment in part by two Ohio Board of Regents Investment Fund Grants. The authors gratefully acknowledge many helpful discussions with B. Ganguly, P. Bletzinger, and A. Forlines of the U.S. Air Force Research Laboratory and W. Bailey of the Air Force Institute of Technology.

References

[1]Courant, R., and Friedrichs, K. O., *Supersonic Flow and Shock Waves*, Springer-Verlag, New York, 1976.

[2]Shapiro, A. H., *Dynamics and Thermodynamics of Compressible Fluid Flow*, Vols. 1 and 2, Ronald, New York, 1953.

[3]Zel'dovich, Ya. B., and Raizer, Yu. P., *Physics of Shock Waves and High-Temperature Hydrodynamic Phenomena*, edited by W. D. Hayes and R. F. Probstein, Vols. 1 and 2, Academic International Press, New York, 1966.

[4]Liepmann, H. W., and Roshko, A., *Elements of Gasdynamics*, Wiley, New York, 1957.

[5]Hughes, W. F., and Young, F. J., *Electromagnetodynamics of Fluids*, Wiley, New York, 1966.

[6]Tidman, D. A., and Krall, N. A., *Shock Waves in Collisionless Plasmas*, Wiley-Interscience, New York, 1971.

[7]Clauser, C. H., (ed.), *Plasma Dynamics*, Addison Wesley Longman, Reading, MA, 1960.

[8]Sutton, G. W., and Sherman, A., *Engineering Magnetohydrodynamics*, McGraw–Hill, New York, 1965.

[9]Pai, S. I., *Dynamics of Fluids and Plasmas*, Academic International Press, New York, 1966.

[10]Klimov, A. I., Koblov, A. N., Mishin, G. I., Serov, Yu. L., and Yavor, I. P., "Shock Wave Propagation in a Glow Discharge," *Soviet Technical Physics Letters*, Vol. 8, No. 4, 1982, pp. 192–194.

[11]Klimov, A. I., Koblov, A. N., Mishin, G. I., Serov, Yu. L., Khodataev, K. V., and Yavor, I. P., "Shock Wave Propagation in a Decaying Plasma," *Soviet Technical Physics Letters*, Vol. 8, No. 5, 1982, pp. 240–241.

[12]Evytyukhin, N. V., Margolin, A. D., and Shmelev, V. M., "On the Nature of Shock Wave Acceleration in Glow Discharge Plasma," *Soviet Journal of Chemical Physics*, Vol. 3, No. 9, 1986, p. 2080.

[13]Voinovich, P. A., Ershov, A. P., Ponomareva, S. E., and Shibkov, V. M., "Propagation of Weak Shock Waves in Plasma of Longitudinal Flow Discharge in Air," *High Temperature*, Vol. 29, No. 3, 1991, p. 468.

[14]Babaeva, N., "On the Structure of Shock and Blast Waves in Nonequilibrium Plasma of Gas Discharge," *Russian Journal of Chemical Physics*, Vol. 12, 1993, p. 357.

[15]Babaeva, N., Mnatsakanyan, A., and Naidis, G., "Modeling of Shock Wave Propagation in a Gas Discharge Developing in Nitrogen," *High Temperature*, Vol. 31, No. 4, 1993, p. 820.

[16]Babaeva, N., and Nadis, G., "Simulation of Shock Wave Propagation in Gas Discharge Plasma Regions," *Proceedings of the Workshop: Perspectives of MHD and Plasma Technologies in Aerospace Applications*, 1999, p. 108.

[17]Ganguly, B. N., Bletzinger, P., and Garscadden, A., "Shock Wave Damping and Dispersion in Nonequilibrium Low Pressure Argon Plasmas," *Physics Letters A*, Vol. 230, June 1997, pp. 218–222.

[18]Bletzinger, P., and Ganguly, B. N., "Local Acoustic Shock Velocity and Shock Structure Recovery Measurements in Glow Discharges," *Physics Letters A*, Vol. 258, July 1999, pp. 342–348.

[19]Garscadden, A., Bletzinger, P., and Ganguly, B. N., "Acoustic Shock Interaction in a Positive Column Plasma," AIAA Paper 99-4973, Nov. 1999.

[20]Bailey, W. F., and Hilbun, W. M., "Baseline of Thermal Effects on Shock Propagation in Glow Discharges," *Proceedings of the 1st Weakly Ionized Gases Workshop*, U.S. Air Force Academy, CO, June 1997, pp. GG3–GG18.

[21]Macheret, S. O., and Miles, R., "Shock Propagation in Weakly Ionized Plasmas: Mechanisms and Key Problems," *Proceedings of the 1st Weakly Ionized Gases Workshop*, U.S. Air Force Academy, CO, June 1997, pp. X-11–X-33.

[22]Macheret, S. O., Martinelli, L., and Miles, R. B., "Shock Wave Propagation and Structure in Nonuniform Gases and Plasmas," AIAA Paper 99-0598, Jan. 1999.

[23]Adamovich, I., Subramaniam, V. V., Rich, J. W., and Macheret, S. O., "Phenomenological Analysis of Shock Waves in Weakly Ionized Gases," *AIAA Journal*, Vol. 36, No. 5, 1998, pp. 816–823.

[24]Kolb, A. C., "Production of High Energy Plasmas by Magnetically Driven Shock Waves," *Physical Review*, Vol. 107, No. 2, 1957, pp. 345–350.

[25]Ionikh, Y. Z., Chernysheva, N. V., Meschanov, A. V., Yalin, A. P., and Miles, R. B., "Direct Evidence for Thermal Mechanism of Plasma Influence on Shock Wave Propagation," *Physics Letters A*, Vol. 259, Aug. 1999, pp. 387–392.

[26]Ionikh, Y. Z., Chernysheva, N. V., Yalin, A. P., Macheret, S. O., Martinelli, L., and Miles, R. B., "Shock Propagation Through Glow Discharge Plasmas: Evidence of Thermal Mechanism of Shock Dispersion," AIAA Paper 2000-0714, Jan. 2000.

[27]Aithal, S. M., and Subramaniam, V. V., "On the Characteristics of a Spark Generated Shock Wave," *Physics of Fluids*, Vol. 12, No. 4, 2000, pp. 924–934.

[28]White, A. R., and Subramaniam, V. V., "Effect of Wall Shear on the Propagation of a Weak Spark-Generated Shock Wave in Argon," *Physics of Fluids*, Vol. 13, No. 8, 2001, pp. 2441–2444.

[29]Flament, C., George, T., Meister, K. A., Tufts, J. C., Rich, J. W., Subramaniam, V. V., Martin, J. P., Piar, B., and Perrin, M. Y., "Nonequilibrium Vibrational Kinetics of Carbon Monoxide at High Translational Mode Temperatures," *Chemical Physics*, Vol. 163, No. 2, 1992, pp. 241–262.

1.5 Experimental Studies of Spark Generated Shock Waves

AIAA – 99 - 3670

EXPERIMENTAL STUDIES OF SPARK GENERATED SHOCK WAVES

A. R. WHITE, S. M. AITHAL, AND V. V. SUBRAMANIAM
Center for Advanced Plasma Engineering
Non-Equilibrium Thermodynamics Laboratories
Department of Mechanical Engineering
The Ohio State University
Columbus, Ohio 43210

30th Plasmadynamics and Lasers Conference
28 June - 1 July, 1999 / Norfolk, VA

Abstract

Experimental measurements recording shock propagation characteristics within and downstream of a glow discharge are reported here. The apparatus and photo-acoustic deflection (PAD) measurement technique described in an earlier work (ref.[10]) are used to measure average shock velocities and examine the recovery of the PAD signal downstream of the glow discharge. Interpretation of the measurements is aided by numerical calculations obtained by solving the compressible Navier-Stokes equations for a shock wave generated in a cylindrical tube by rapid energy addition. Simulated PAD signals are obtained from calculated instantaneous profiles of the density. The numerical results show that wall shear plays at least as important a role in influencing the shock structure and the associated PAD signal, as do radial gradients in temperature. The latter have been proposed previously based upon numerical solutions of the inviscid Euler equations[11,12]. Experimental measurements of velocities and PAD signals show that most of the observed variations in shock structure can be understood in terms of influence of thermal gradients and wall shear. The measurements also show a small but noticeable effect of the orientation of the electric field on the average shock propagation velocity near the cathode, at certain values of the total current.

I. Introduction

The structure and propagation of shock waves in gases has been a topic of much interest in this century, motivated primarily by aerospace applications. It has been the subject of several authoritative books [1-4]. Shock propagation in plasmas has also been studied with specific regard to re-entry flows, interaction of the solar wind with the terrestrial magnetosphere, and magnetohydrodynamic (MHD) applications. This research has also culminated in several authoritative texts[5-7]. Despite this abundance of information on shock wave propagation in ionized and non-ionized gases, experiments conducted in Russia in the early 1980s[8, 9] and more recently in the United States[10] have prompted further inquiry on this problem[11-13]. Experiments reported in ref.[10] show apparent modification of shock structure within a glow discharge, and report lengths on the order of the shock tube diameter downstream of the discharge in order to recover the original shock structure. Analysis of this problem by numerical solution of the inviscid Euler equations [11,12] has shown that radial temperature gradients created by the glow discharge could explain the experimental observations reported in ref.[10].

In this paper, experimental results for some of the conditions reported in ref.[10] on the propagation of shock waves through weakly ionized Argon are presented, along with a numerical simulation of the propagation of a shock wave generated by rapid energy addition under the influence of wall shear. The shock waves are generated using a capacitively discharged spark, and subsequently launched into a low-pressure glow discharge in Argon. The experimental apparatus is similar to that used in ref.[10]. Passage of the shock at a given location is also monitored using the same photo-acoustic deflection technique described in ref.[10]. Experimental measurements of shock propagation velocity and characteristics of the photo-acoustic signal generated by the shock at various axial locations along the glow discharge tube are reported here. Measurements recording the effects of reversing the direction of the electric field on shock propagation velocity and photo-acoustic signal characteristics are also discussed. An important focus of this

paper is detailed examination of the recovery of the photo-acoustic signal downstream of the glow discharge, as a function of distance along the tube. These experimental measurements are guided by numerical simulations of shock propagation in a non-ionized gas obtained by solving the two-dimensional, compressible, Navier-Stokes equations in a cylindrical geometry. Viscous effects, especially with regard to wall shear are examined in these numerical calculations.

This paper is organized as follows. The experimental apparatus and procedure are briefly described in the following section, since they are very similar to those of ref.[10]. The interested reader is referred to ref.[10] for additional details. Results of numerical solutions of the compressible Navier-Stokes equations for weak shock waves generated by rapid energy addition (i.e. a simulated spark) in both a wall-bounded gas as well as in an unbounded gas are discussed in Section III. These calculations serve to provide a basis for examining shock propagation under the influence of viscous effects and wall shear alone, in the absence of any thermal gradients. This is a case that has not been previously examined[11-13]. Section IV describes experimental measurements aimed at reproducing the results reported in ref.[10], and plausible explanations for these results, guided by the numerical simulations presented in Section III, are given in Section V. A summary is provided in Section VI, along with the conclusions of this work.

II. Experimental Apparatus & Procedure

The experimental apparatus used in this work is nearly identical to that described in ref.[10]. It consists of a 5 cm. diameter closed pyrex tube comprising a central glow discharge section. A Kolb tube at one end houses the spark gap used to generate a shock wave. The spark gap consists of a pair of tungsten electrodes with a gap distance of 1 cm. The electrodes are cylindrical rods 0.3175 cm. (1/8 in.) in diameter. The gas used in the measurements reported here is Argon, and is maintained at a pressure of 30 Torr. Typically, a voltage of 10 kV is impressed across the spark gap, discharging approximately 25 J of energy over an approximate time interval of 1 microsecond. However, only a fraction of this energy from the capacitive discharge is loaded into the gas. A shock wave is subsequently formed as a result of the rapid energy addition, and propagates through the tube. In some of the experiments reported here, a glow discharge is struck in 30 Torr of Argon between the two electrodes located downstream of the spark gap. The electrodes in the glow discharge section are cylindrical, 2.5 cm. in diameter, hollow, and concentric within the pyrex shock tube as can be seen in Fig. 1. The Argon gas is introduced via a rotameter, slowly flowing at 100 sccm in a direction *counter* to that of shock propagation as in ref.[10]. In ref.[10] however, the flow was carefully controlled and introduced at a rate of 50 sccm using a mass flow controller. In an effort to reproduce one of the shock tube configurations of ref.[10], the upstream electrode (i.e. nearest the spark gap) is longer, 5 cm. in length, while the downstream electrode (i.e. farthest away from the spark gap) is shorter, and 1.5 cm. in length. The distance between the electrodes (edge to edge) in the glow discharge is 22.25 cm. in the present work, while the corresponding distances in ref.[10] were 19 cm. and 20 cm. A visibly uniform glow discharge can be maintained in Argon at 30 Torr using this configuration, provided the discharge current does not exceed about 60 mA after which point the discharge becomes

filamentary. In the experiments reported here, the current in the glow discharge is varied from 0 mA to 50 mA, and the voltage is varied from 1.8 kV (for 10 mA) to 4.8 kV (for 50 mA). Shock waves are launched into the glow discharge after it has been operating for 15 minutes, to ensure that any thermal gradients that exist would have attained steady state.

The spark gap serving as the trigger and a prescribed time delay are used together to detect the instant of time when the shock wave passes a given location. A Uniphase 1125 He-Ne laser (10 mW) is directed perpendicular to the axis of the shock tube, partially illuminating a Thor Laboratories PDA 155 high-speed amplified Silicon detector on the other side of the tube as shown in Fig. 1. The detector outputs a voltage proportional to the intensity of the beam illuminating it. As the shock wave traverses across the laser beam, the gradient in density across the shock front gives rise to a variation in the index of refraction, causing the He-Ne beam to deflect. The resulting time-varying voltage is then recorded on a Tektronix digital oscilloscope (40 MHz). In the experiments reported here, a sampling rate of 5 MHz is used. Since the deflection of the beam is proportional to the axial density gradient integrated across the tube, so is the resulting voltage time signature recorded by the detector. Therefore, a shock front would give rise to a photo-acoustic deflection (PAD) signal that appears as a sharp spike resembling a Delta function, as shown in Fig. 2. The same photo-acoustic signal is used to measure the average velocity of the shock front. This is done by measuring the time of flight between two axial locations, 6.9 cm. apart. In this instance, the He-Ne beam is passed through a beam splitter, one beam passing through the tube and illuminating a detector on the other side. The other beam is reflected off a mirror and then passed through the tube onto a second detector. Using the signal from the first detector as the trigger and prescribing a time delay then allows the shock wave to be detected at the second axial location. The travel time of the shock wave between the two locations is recorded, and since the distance between these locations is known, an average velocity can be calculated. The two split beams are separated by 6.9 cm. due to physical limitations in the apparatus, and this is coarser than the 2.59 cm. separation used to measure the shock velocity in ref.[10]. The average shock velocity at a given point is thus measured by the time of flight between the split beams, 3.45 cm. on either side of the point, in the present experiments. Variation of the shock velocity with position along the tube is enabled by mounting the laser/detector assembly on an optical rail, and mounting the rail on a translation stage.

In this paper, several experimental measurements are reported. Measurements of average shock velocity are obtained at several axial locations, before the glow discharge region, within the glow discharge region, and downstream of it. These average velocity measurements are obtained with two discharge polarities, one where the applied electric field is in the direction of shock propagation and the other in which the electric field is in the direction counter to that of shock propagation. Measurements of the average shock velocity are also made for several values of the total current within the diffuse glow discharge: 0 mA, 10 mA, 30 mA, and 50 mA. Photo-acoustic deflection signals are also obtained for these current levels and for both orientations of the applied electric field. Inference of the shock structure from these PAD signal measurements is not straightforward. Therefore, in order to aid interpretation of these PAD signals, we examine in the

following section, two-dimensional numerical solutions of the compressible Navier-Stokes equations for shock propagation in a neutral gas within a cylindrical tube, initiated by rapid energy addition.

III. Numerical Calculations of Shock Waves Initiated by Sudden Energy Release

In this section, we briefly present results of numerical calculations of a shock wave produced by sudden energy release. The interested reader is referred to ref.[14] for details of this calculation. In the experiments, a capacitive discharge in Argon at 30 Torr resulting in a spark, is used to generate a shock. This process begins with electrons being rapidly heated to tens of thousands of degrees Kelvin, within about a hundred nanoseconds. The electrons then heat the neutral atoms and ions over a time scale on the order of a microsecond. It is during this latter time period that the gas is rapidly heated and a shock wave is generated. The propagation of the shock wave in a neutral gas and associated motion and relaxation of the gas is determined by the compressible Navier-Stokes equations. The spark discharge can be modeled as an amount Q of power added to the gas per unit volume and per unit time. Then, $(\Delta t)Q$ represents the amount of power per unit volume added to the gas over the time interval (Δt). We consider here solutions to the compressible, two-dimensional, axi-symmetric Navier-Stokes equations in order to determine the characteristics of a shock wave generated by rapid energy addition. A value of $Q = 4.413 \times 10^{14}$ W/m^3/s over a duration of 1 microsecond, and within a cylindrical volume 5 cm. in diameter and 1 mm long, is used in the results of calculations presented here. This value of Q was chosen to produce a shock wave propagating at a Mach number on the order of 1.2 at a distance of about 20 cm. from the point of its initiation. Maintaining this Mach number for longer distances (as in the experiments) would require larger values of Q, which in turn would lead to larger gradients in the early portion of the transient. This imposes stringent constraints on the numerical solution, forcing small grids and time steps, which are unnecessarily limiting since we are primarily interested in the solution at much later instants of time. Therefore, in the interest of reducing the computational time and effort, a lower and more modest value is chosen for Q. It must be emphasized that this does not alter the conclusions drawn from the analysis since the magnitude of Q determines how far a shock wave can travel, while maintaining a sharp density gradient across its leading edge. We are specifically interested here in what happens in the presence of a bounding wall, and in the *absence* of thermal gradients. This is a case not previously considered in numerical solutions of the Euler equations for this problem[11,12].

Calculations are presented here for two specific cases. The first is the propagation of a shock wave in Argon initially at 30 Torr and 300 K. The effects of viscosity and wall friction are explored using two different boundary conditions. The first case with $\partial u/\partial r = 0$ and $\partial w/\partial r = 0$ applied at the wall of the tube, where u is the radial component of velocity and w is the axial component of velocity, examines viscous effects independently of wall friction (i.e. a bounding wall). The second case with the usual no-slip boundary conditions ($u = w = 0$ at the wall of the tube), represents real viscous flow in a tube including the effects of wall shear. Figure 3

shows the variation of density (non-dimensionalized by 0.0641 kg/m^3) with axial location at 100 μs, 200 μs, 300μs, and 400 μs after the rapid energy addition, for the first case where wall friction is absent. Note that the shape of the instantaneous density profile is essentially triangular with an expanding trailing portion, and with the leading edge being the shock front. The amplitude can be seen to decrease as the shock traverses down the tube, and is a necessary consequence of the expansion at the trailing edge of the structure. Figure 4 shows the axial profiles of the density gradient in the axial direction integrated across the tube diameter, which by virtue of being proportional to the PAD signal, is referred to here as the simulated PAD signal. As can be seen from Fig. 4, the simulated PAD signal resembles a Delta-function and therefore signifies that the density profile approximates a triangular waveform with a long tail. However, its amplitude can be seen to weaken due to spreading of the front as well as viscous effects. The decrease in amplitude of the simulated PAD signal is indicative of the density gradient in the axial direction becoming shallower as the shock wave propagates through the tube. Note that resolution would limit the ability to detect the trailing portion in an experiment. The variation of density shown in Fig. 3 is qualitatively similar to what would be predicted from a quasi one-dimensional calculation in the absence of wall friction, for comparable energy addition[14]. In the quasi 1-D solutions, the simulated PAD signal is found to decrease in amplitude but still resembles a Delta function since the wave front spreads out mainly in the trailing portion[14]. Figures 5 and 6 show the density profiles and simulated PAD signals for the realistic case of a shock propagating in a bounded tube (i.e. where no-slip boundary conditions are applied at the walls of the tube), at 100 μs, 150 μs, 200 μs, 300 μs, and 400 μs after the initial rapid energy addition, respectively. In this instance, it can be seen that the simulated PAD signal shows a split structure indicating non-monotonic variation of the density profile. It is important to point out that both cases considered here are ones where there are *no thermal gradients of any sort*. Splitting of the PAD signal is observed in the *absence* of thermal gradients and in the *absence* of a plasma. Splitting of the simulated PAD signal occurs because the part of the shock near the wall of the tube lags behind that part of the shock near the centerline. This can be clearly seen in Fig. 7, where axial variations of the instantaneous density are plotted at two different radial locations, one at the centerline and another midway between the centerline and the wall. It is important to point out that although the simulated PAD signals in Fig. 6 exhibit splitting, the shock front itself has not split. Indeed, the split structure of the simulated PAD signal can be caused by one of two distinct reasons. Either the shock front is curved or it is tilted out of the plane. It can be seen that the effect of the bounding wall is to retard the shock front due to the wall shear. These results from the numerical simulations suggest that wall friction can produce split PAD signals in a manner similar to those introduced by radial thermal gradients[11,12], provided the tube is long enough or if there is insufficient energy addition to the gas from the spark.

In summary, numerical simulations of a spark-generated shock wave reveal that wall friction is at least as important as thermal gradients in influencing PAD signal characteristics. For a given amount of initial energy loading into the gas, the PAD signal structure will show splitting and spreading

of peaks given a sufficiently long tube, even in the absence of thermal gradients. The same holds true for a tube of given length, where the energy loading by the spark into the gas may be low. Moreover, splitting and spreading of the PAD signal do not imply splitting and spreading of the shock. Such changes in the PAD signal do however indicate either curvature of the shock as noted in refs.[11-13] or tilting of the shock front away from the direction of propagation. With this understanding, we now proceed to examine experimental measurements of spark-generated shock propagation in Argon.

IV. Experimental Results & Discussion

In this section, we present PAD measurements of shock propagation characteristics in Argon at 30 Torr, within and outside of a glow discharge. The experimental apparatus and procedure have been described previously in Section II. Using the PAD technique of ref.[10], PAD signal structure is examined at various axial locations, for several values of the discharge total current. In addition, the effects of alignment of the applied electric field with respect to the shock propagation direction on velocity and PAD signal recovery are also explored.

Figure 8 shows a plot of the average shock velocity as a function of position for the case where the longer electrode located nearest to the spark gap is the cathode, for different values of the total discharge current. It can be seen that in the absence of the glow discharge, the shock velocity decreases monotonically as expected. When the glow discharge is on, the velocity is seen to exhibit a noticeable local maximum within the glow discharge section. The occurrence of a single maximum in the shock velocity in this region can be understood as the result of the opposing influences of heating and wall shear. Ohmic heating within the discharge raises the gas temperature and therefore increases the shock velocity. However, as the velocity increases, the wall shear tends to lower it since wall shear scales as the square of the velocity, as was discussed in the numerical simulations presented in Section III. The effects of heating are evident in the observed increase in shock velocity as the current is raised. There is however, a repeatable and noticeable local minimum in the shock velocity near the cathode for currents of 30 mA and 50 mA. Although this decrease in the shock velocity is small and within the band of experimental uncertainty, it is reproducible and not entirely consistent with the expected influence of thermal gradients and/or wall friction alone. It is also important to point out that this local minimum in the shock velocity within the discharge is independent of shot to shot variations. The origin of this local minimum is at present, unclear. It does appear to be inconsistent with expected behavior of shocks in the presence of thermal gradients and wall shear. Upon exiting the glow discharge section, the velocity of the shock can be seen to assume the same value as in the absence of the glow discharge, almost immediately. Figure 9 shows the shock velocity plotted versus total current within the glow discharge at two specific locations within the discharge. These are at an axial location of 9.5 cm (measured from the center of the electrode that is closest to the spark gap) or 7.0 cm from the edge of the electrode nearest the spark gap, and at 18 cm (i.e., 15.5 cm from the edge of the cathode and 6.75 cm from the edge of the anode). These trends are similar to those reported in the experiments of ref.[10]. It can be seen that the shock velocity varies non-linearly with the total current at both axial locations,

for this case where the electric field is directed opposite to the direction of shock propagation.

Figures 10 and 11 show corresponding variations of shock velocities for the case where the electrode closest to the spark gap is the anode. This is the case where the electric field is aligned in the direction of shock propagation. Some of the trends observed in Fig. 8 are also found in Fig. 10. Note that there is a noticeable local minimum near the anode, as there was near the cathode in Fig. 8. However, unlike Fig. 8, this local minimum is not repeatable. Figure 11 shows essentially the same non-linear trends as Fig. 9, when the shock velocity is plotted versus total discharge current. The gas temperature in the glow discharge is expected to scale as the square of the current and the shock velocity is expected to scale as the square root of temperature. Therefore, the velocity is expected to scale linearly with discharge current. The observed non-linear dependence of shock velocity on total current may be due to the fact that as the current and hence the temperature increase, the shock velocity increases. This in turn would increase the magnitude of the retarding force due to wall shear (which as stated earlier should scale as the velocity squared), and tend to limit the increasing shock velocity. This may explain the observed non-linear behavior evident in Figs. 9 and 11. However, the presence of a small local minimum in the average shock velocity downstream of the cathode within the glow discharge region is somewhat enigmatic.

Figures 12 through 17 show PAD signals at several axial locations downstream of the glow discharge, for discharge currents of 10 mA, 30 mA, and 50 mA respectively, and for the two orientations of electric field considered in this paper. Evident in these figures is the recovery of the PAD signal to its Delta function-like appearance. Typically, the PAD signal will increase in amplitude after the shock emerges from the glow discharge region, reach a maximum, and decline in amplitude thereafter. The recovery distance is defined here as the distance from the edge of the electrode at the end of the glow discharge, to the axial location where the PAD signal recovers its Delta function-like appearance. As can be seen from these figures, there is a small but noticeable dependence of the PAD signal recovery distance on the direction of the electric field. However, this may be attributed to shot to shot variations, since variations up to 0.5 cm were noted. From Fig. 12, the recovery distance can be seen to be $\geq$5.2(5) cm. and $\leq$7.7(5) cm. when the electric field is in the direction opposite to that of shock propagation, while from Fig. 13, the recovery distance is >5.2(5) cm. and $\leq$7.7(5) cm. when the electric field is aligned in the direction of shock propagation, for a total current of 10 mA. Similarly, for 30 mA, Fig. 14 shows a recovery length of $\geq$5.2(5) cm. and $\leq$7.7(5) cm., while Fig. 15 shows it to be >5.2(5) cm. and $\leq$7.7(5) cm. when the electric field is in the shock propagation direction. For 50 mA, when the electric field is opposite to the shock propagation direction, the recovery length from Fig. 16 is $\geq$5.2(5) cm. and $\leq$7.7(5) cm., while the recovery length is >5.2(5) cm. and $\leq$7.7(5) cm. (from Fig. 17) when the electric field is aligned in the direction of shock propagation. For all cases, the recovery length is noticeably longer when the electric field is in the direction of propagation of the shock. In this instance, the cathode, which is expected to be the hotter of the two electrodes is on the downstream side of the shock propagation direction so that the

longer recovery length may have its origin in thermal gradients.

In summary, most of the trends observed in the experiments reported here can be explained in terms of classical effects due to thermal gradients and wall shear. The only exception appears to be the local minimum in the average shock propagation speed near the cathode that was observed for the higher currents in the glow discharge. This decrease in velocity may have its origin in electrostatic interactions between the space charge layer across the shock front and the electrode-adjacent sheath. The presence of an electrostatic force is expected to influence shock structure in a manner analogous to the presence of wall friction considered in this work. The latter (wall friction) has been shown to alter the PAD signal structure. This raises the possibility of altering shock structure and shock propagation characteristics in the presence of ionization and externally applied electric fields. The possibility of mitigating the strength of propagating detonation shocks by application of electric fields is not new. It was first suggested by J. J. Thomson as early as 1910[15], but reportedly met with mixed success in experimental attempts to verify his idea[16,17]. As the shock traverses the electrode regions of the glow discharge, it encounters the sheath region near the cathode with its associated relatively high electric fields. The presence of fields of this magnitude (on the order of kV/cm) can influence the charge separation layer across the shock front, and in principle must affect the recovery of the propagating structure. A recent Direct Simulation Monte Carlo (DSMC) analysis reported in ref.[18], considers the effects of electrostatic forces interacting with the double layer caused by charge separation across the shock front on the propagating shock structure. This work shows that a steady state solution may not exist for an initially stationary shock wave subjected to a shock-centered force.

V. Summary & Conclusions

Shock propagation through a glow discharge has been examined using the PAD technique of ref.[10]. The effects reported in ref.[10] have been reproduced for Argon at a pressure of 30 Torr. A two-dimensional numerical calculation incorporating viscous effects, and simulating the propagation of a spark-generated shock in a cylindrical tube has also been conducted. The simulations reveal that wall shear can induce variations in the simulated PAD signal, similar to radial thermal gradients. The latter was proposed in earlier work to explain observed variations in the PAD signal[11-13]. Detailed measurements of shock velocity versus distance along the direction of propagation as well as recovery of the PAD signal downstream of the glow discharge have also been made. It appears as though the presence of thermal gradients and wall shear effects are capable of explaining most of the observed trends and observations. However, the average shock velocity exhibits some enigmatic characteristics. There is a local minimum in the average shock velocity near the cathode, within the glow discharge. Such a minimum is not observed near the anode. These effects may be due to electrostatic interaction between the shock and the cathode-adjacent sheath, or due to local temperature gradients. This can only be resolved by point-wise temperature measurements. On-going studies of shock propagation through optically pumped CO/Ar plasmas and gas mixtures would provide further insight into shock propagation in weakly ionized gases[19]. The role of thermal gradients and wall shear versus any electrostatic influences can then be isolated with the aid of such experiments.

Acknowledgements:

The authors gratefully acknowledge many helpful discussions with Dr. B. Ganguly, Dr. P. Bletzinger, and Mr. A. Forlines of AFRL and Prof. W. Bailey of AFIT. Numerous discussions with Prof. R. Miles and Dr. S. Macheret of Princeton University, and with Dr. I. Adamovich, Prof. W. Lempert, and Prof. J. W. Rich of The Ohio State University are also gratefully acknowledged. This work was supported by AFOSR grant F49620-99-1-0023 monitored by Dr. Steve Walker. Support was also provided in part by two Ohio Board of Regents Investment Fund Grants.

References:

[1] R. Courant, and K. O. Friedrichs, *Supersonic Flow and Shock Waves*, Springer-Verlag, 1976.

[2] A. H. Shapiro, *The Dynamics and Thermodynamics of Compressible Fluid Flow*, Vols. 1 & 2, The Ronald Press Company, 1953.

[3] Ya. B. Zel'dovich, and Yu. P. Raizer, *Physics of Shock Waves and High-Temperature Hydrodynamic Phenomena*, W. D. Hayes and R. F. Probstein (Eds.), Vols. I & II, Academic Press, 1966.

[4] H. W. Liepmann, and A. Roshko, *Elements of Gasdynamics*, John Wiley & Sons, 1957.

[5] W. F. Hughes, and F. J. Young, *The Electromagnetodynamics of Fluids*, John Wiley & Sons, 1966.

[6] D. A. Tidman, and N. A. Krall, *Shock Waves in Collisionless Plasmas*, Wiley Interscience, 1971.

[7] C. H. Clauser (Ed.), *Plasma Dynamics*, Addison-Wesley Publishing Company, Inc., 1960.

[8] G. W. Sutton, and A. Sherman, *Engineering Magnetohydrodynamics*, McGraw-Hill Book Company, 1965.

[9] S. I. Pai, *Dynamics of Fluids and Plasmas*, Academic Press, 1966.

[10] B. N. Ganguly, P. Bletzinger, and A. Garscadden, "Shock Wave Dispersion in Nonequilibrium Plasmas", **Phys. Lett. A 230**, p. 218, 1997. Also see B. N. Ganguly, and P. Bletzinger, "Acoustic Shock Wave Propagation in Non-equilibrium Nitrogen and Argon Plasmas", Proceedings of the Workshop on Weakly Ionized Gases, pp. HH-3 – HH-13, U.S. Air Force Academy, June 9 –13, 1997; and P. Bletzinger and B. N. Ganguly, "Local Acoustic Shock Velocity and Shock Structure Recovery Measurements in Glow Discharges", submitted to **Phys. Lett. A.** (under review).

[11] W. F. Bailey, and W. M. Hilbun, "Baseline of Thermal Effects on Shock Propagation in Glow Discharges", Proceedings of the Workshop on Weakly Ionized Gases, pp. GG3 – GG18, U.S. Air Force Academy, June 9 –13, 1997.

[12] S. O. Macheret, L. Martinelli, and R. B. Miles, "Shock Wave Propagation and Structure in Non-uniform Gases and Plasmas", paper AIAA 99-0598 presented at the 37th AIAA Aerospace Sciences Meeting and Exhibit, Reno, Nevada, January 11-14, 1999; See also S. O. Macheret, and R. Miles, "Shock Propagation in Weakly Ionized Plasmas: Mechanisms and Key Problems", Proceedings of the Workshop on Weakly Ionized Gases, pp. X-11 – X-33, U.S. Air Force Academy, June 9 –13, 1997.

[13] I. Adamovich, V. V. Subramaniam, J. W. Rich, and S. O. Macheret, "Phenomenological Analysis of Shock

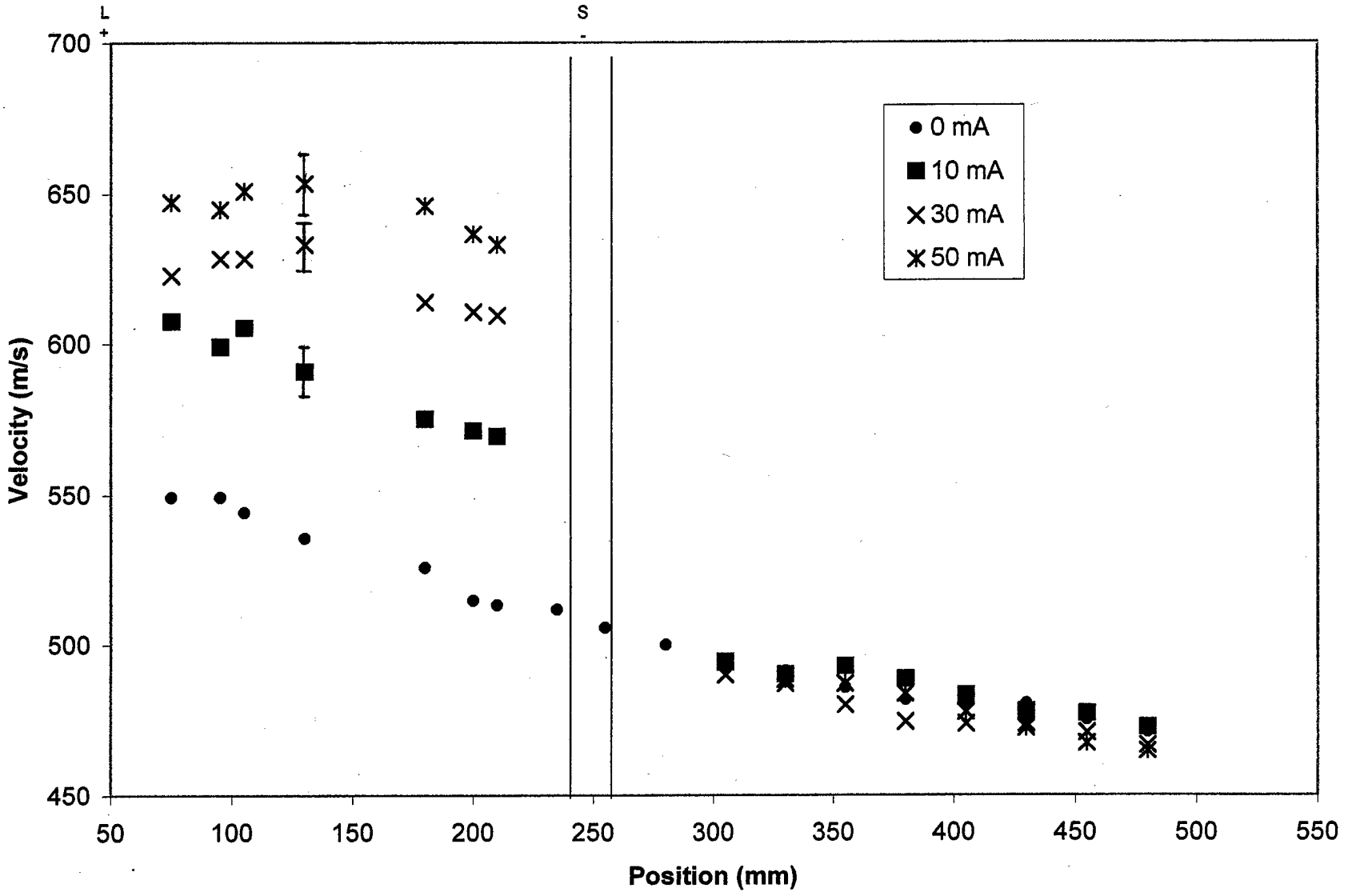

Figure 10: Measured shock propagation versus distance along the shock tube for various currents are shown here. The electrode nearest the spark gap is the anode (L+) and the farthest electrode is the cathode (S-) in this case.

Waves in Weakly Ionized Gases", **AIAA Journal**, Vol. 36, No. 5, pp. 816 – 823, May 1998.

[14] S. M. Aithal, and V. V. Subramaniam, "On the Characteristics of a Spark Generated Shock Wave", submitted to **Phys. Fluids** (under review).

[15] W. E. Garner, and S. W. Saunders, "Ionization in Gas Explosions", **Faraday Soc. Trans. 22**, pp. 281-288, 1926. See citation J. J. Thomson, B. A. Report on Gaseous Combustion, p. 501, 1910, therein.

[16] Dixon, Campbell, and Slater, **Proc. Roy. Soc. 90A**, p. 506, 1914.

[17] Malinowski, **J. Chim. Phys. 21**, p. 469, 1924.

[18] A. H. Auslender, and R. Rubinstein, "Shock Wave Propagation in a Gas far from Equilibrium", Proceedings of the 2nd Weakly Ionized Gases Workshop, pp. 119-126, Norfolk, Virginia, April 24-25, 1998.

[19] I. Adamovich, S. Saupe, M. J. Grassi, O. Schulz, S. Macheret, and J. W. Rich, "Vibrationally Stimulated Ionization of Carbon Monoxide in Optical Pumping Experiments", **Chem. Phys. 173**, pp. 491-504, 1993.

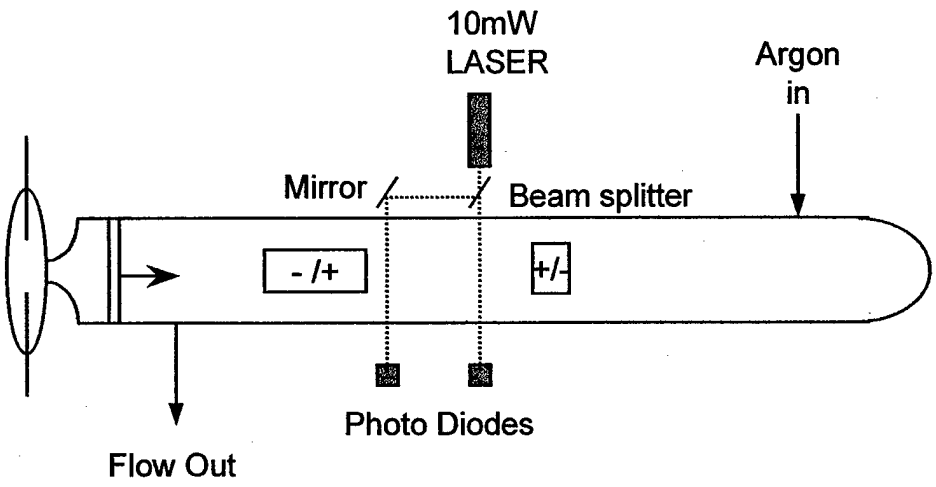

Fig. 1: Schematic of experimental apparatus

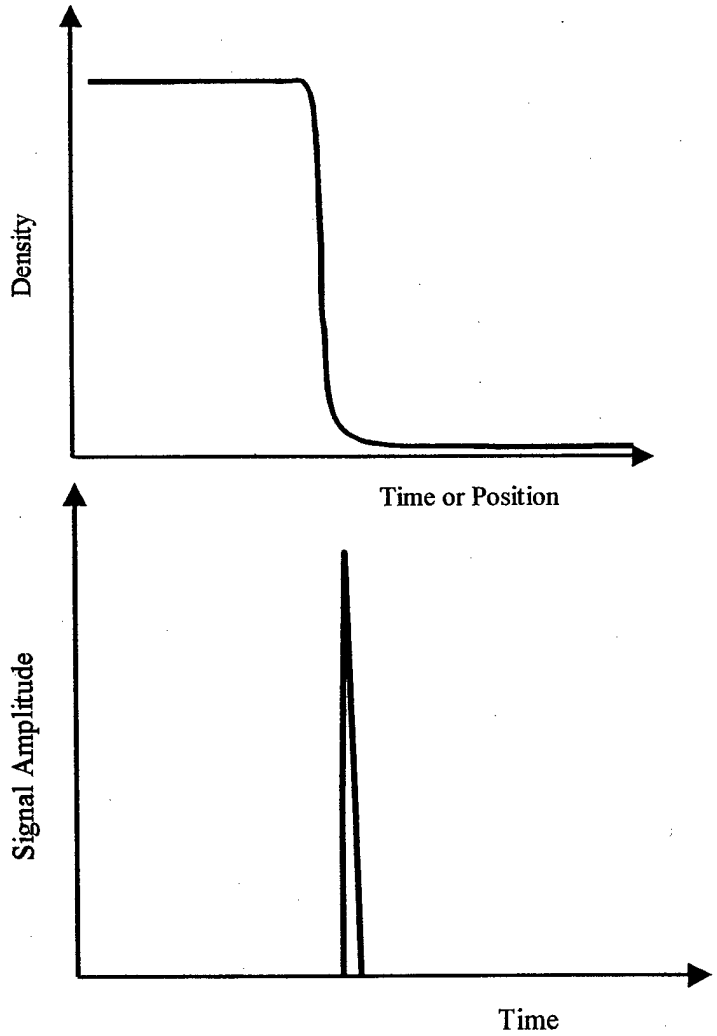

Fig. 2: Schematic of typical density profile and corresponding photo-acoustic deflection (PAD) signal. The PAD signal is proportional to the integral of the axial gradient of density over the radius of the tube.

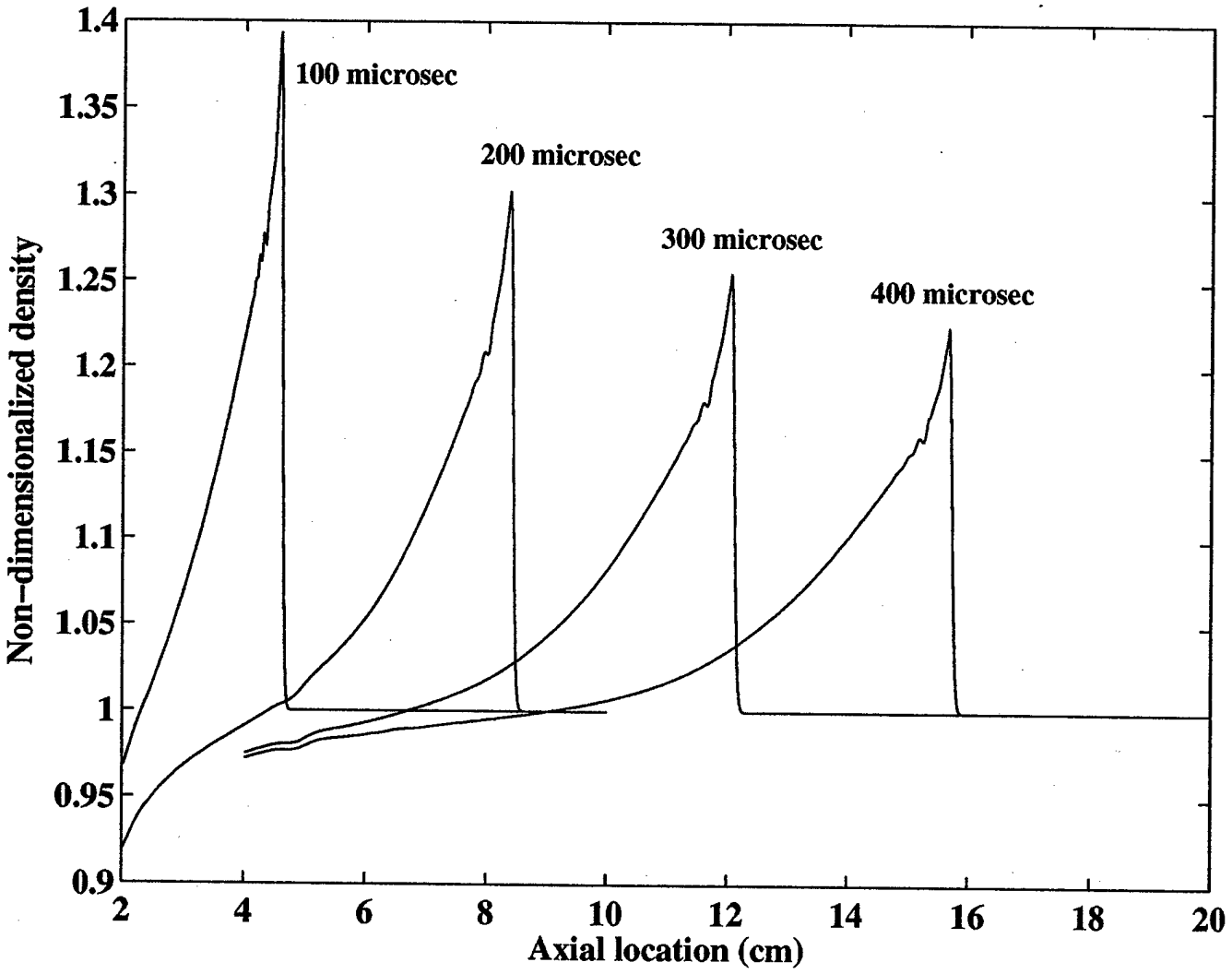

Fig. 3: Calculated profiles of density (non-dimensionalized by 0.0641 kg/m^3) are shown here at various instants of time after a rapid energy release at x = 0 cm. These results are obtained from numerical solutions of the 2-D, axi-symmetric, compressible, Navier-Stokes equations simulating the case of an unbounded cylindrical domain created by imposing slip boundary conditions at the wall. This case shows the propagation of a shock in a viscous fluid (Argon at 30 Torr), but without the influence of wall shear.

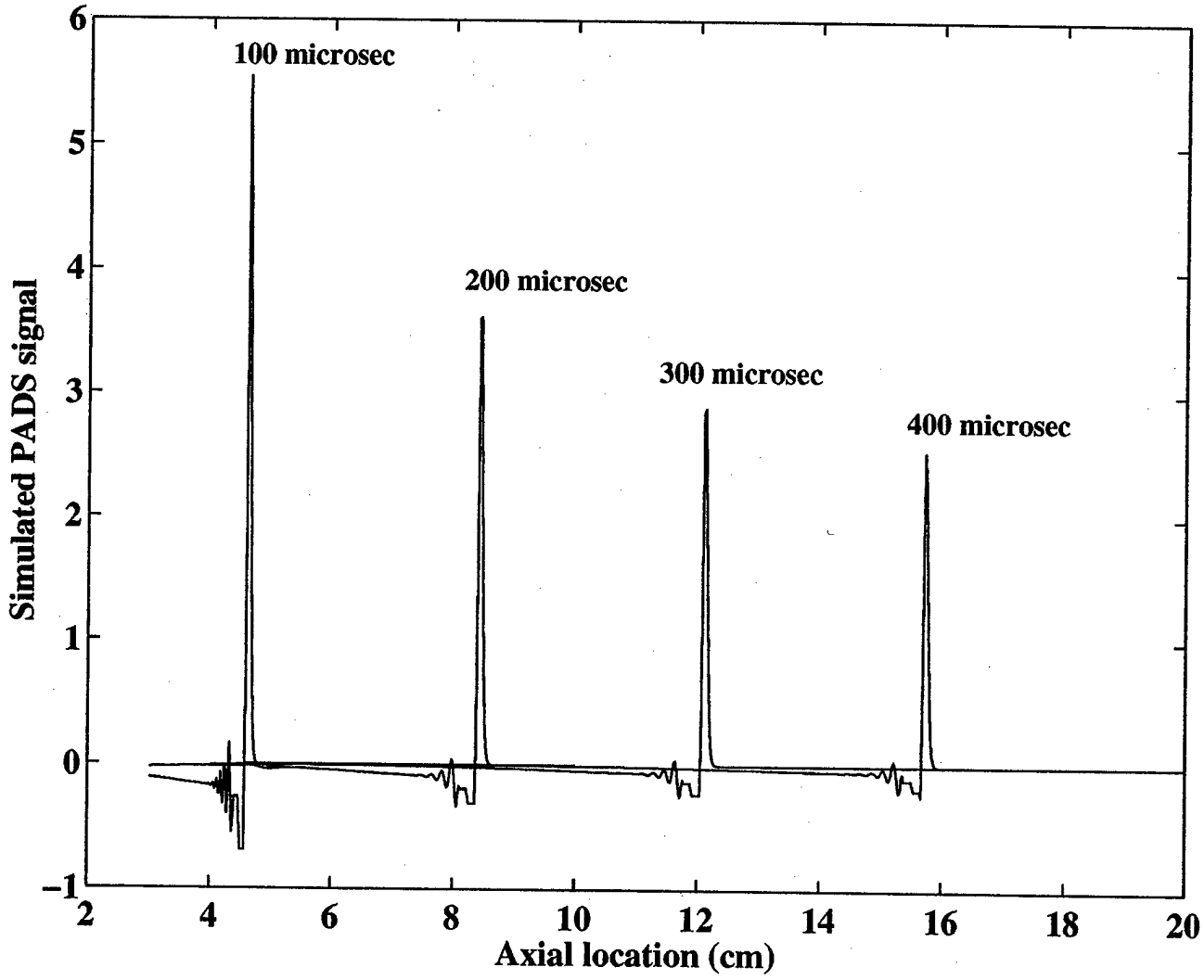

Fig. 4: The simulated PAD signal for the density profiles shown in Fig 3 are displayed here at various instants of time after a rapid energy release at x = 0 cm. These results are obtained by integrating the axial gradient of density across the diameter of the tube, for the case of an unbounded cylindrical domain. Although the horizontal axis is distance, similar profiles would be recorded in time by a detector located at a given point, observing the passing shock.

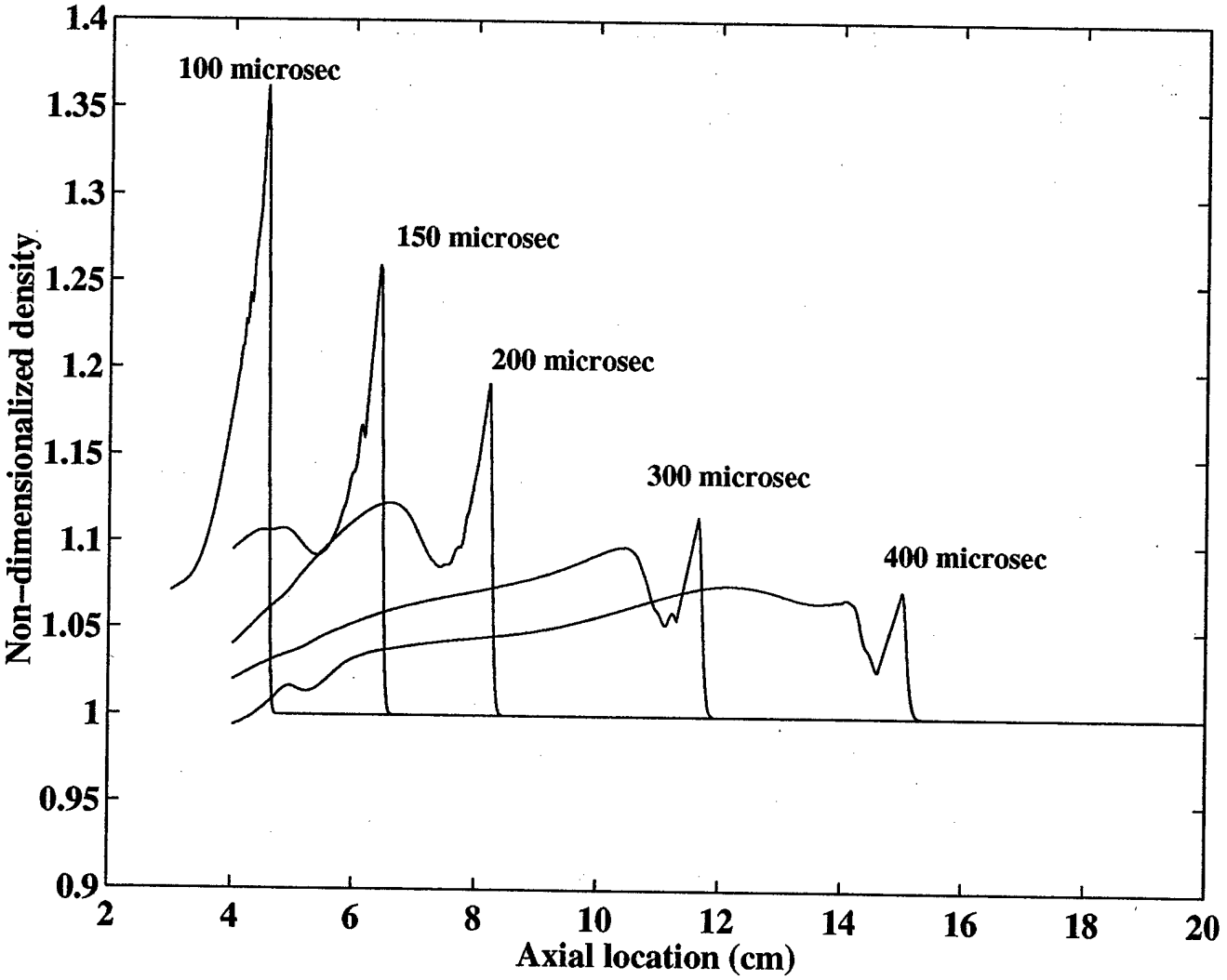

Fig. 5: Calculated profiles of density (non-dimensionalized by 0.0641 kg/m^3) are shown here at various instants of time after a rapid energy release at x = 0 cm. These results are obtained by numerically solving the 2-D, axi-symmetric, compressible, Navier-Stokes equations for the realistic case with no-slip boundary conditions at the wall. This case shows the propagation of a shock in a viscous fluid (Argon at 30 Torr), under the influence of wall shear.

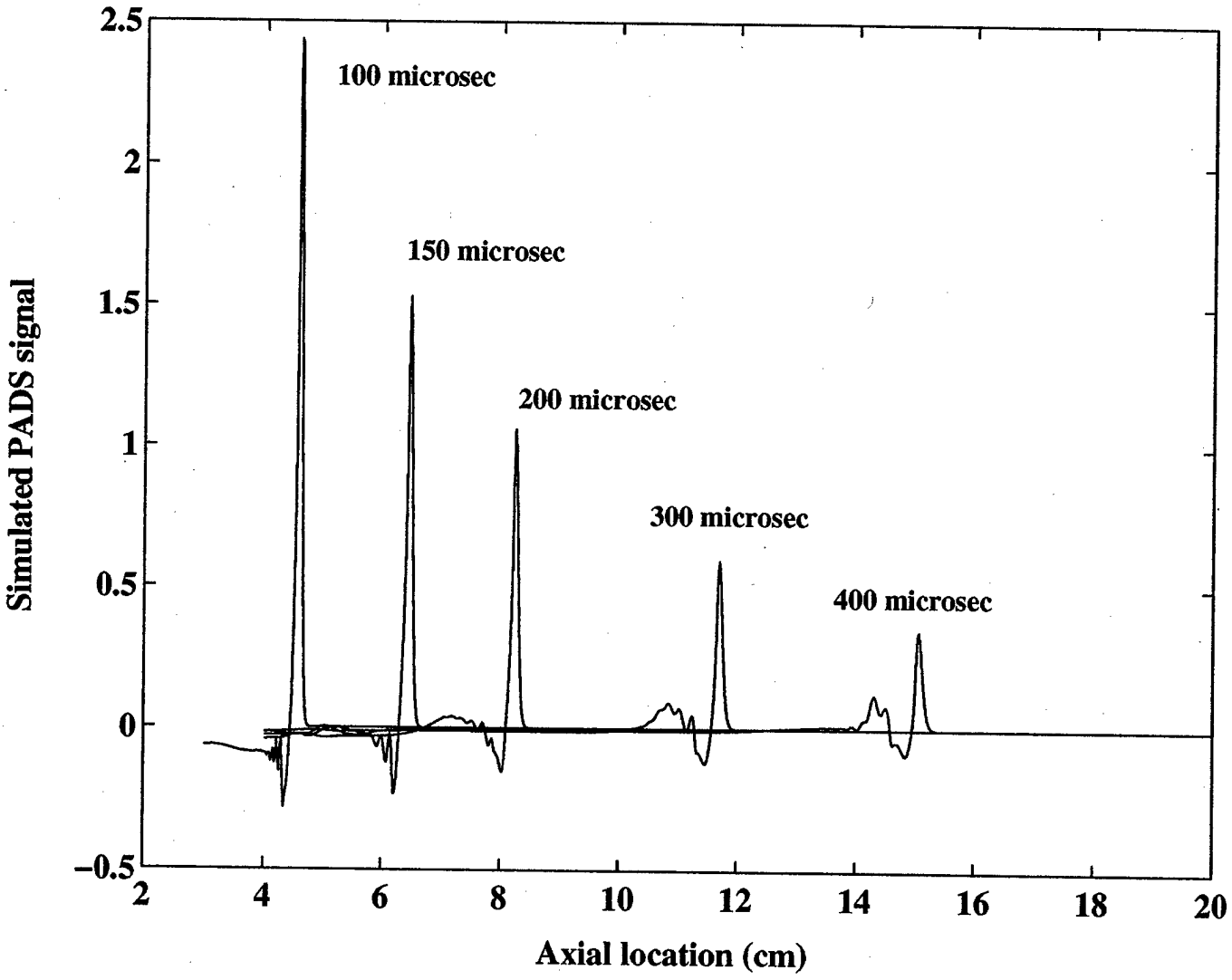

Fig. 6: The simulated PAD signal for the density profiles shown in Fig. 5 are displayed here at various instants of time after a rapid energy release at x = 0 cm. These results are obtained by employing the same procedure used in Fig. 4. This figure shows how the appearance of a PAD signal is modified when a shock propagates in a viscous fluid (Argon at 30 Torr), under the influence of wall shear.

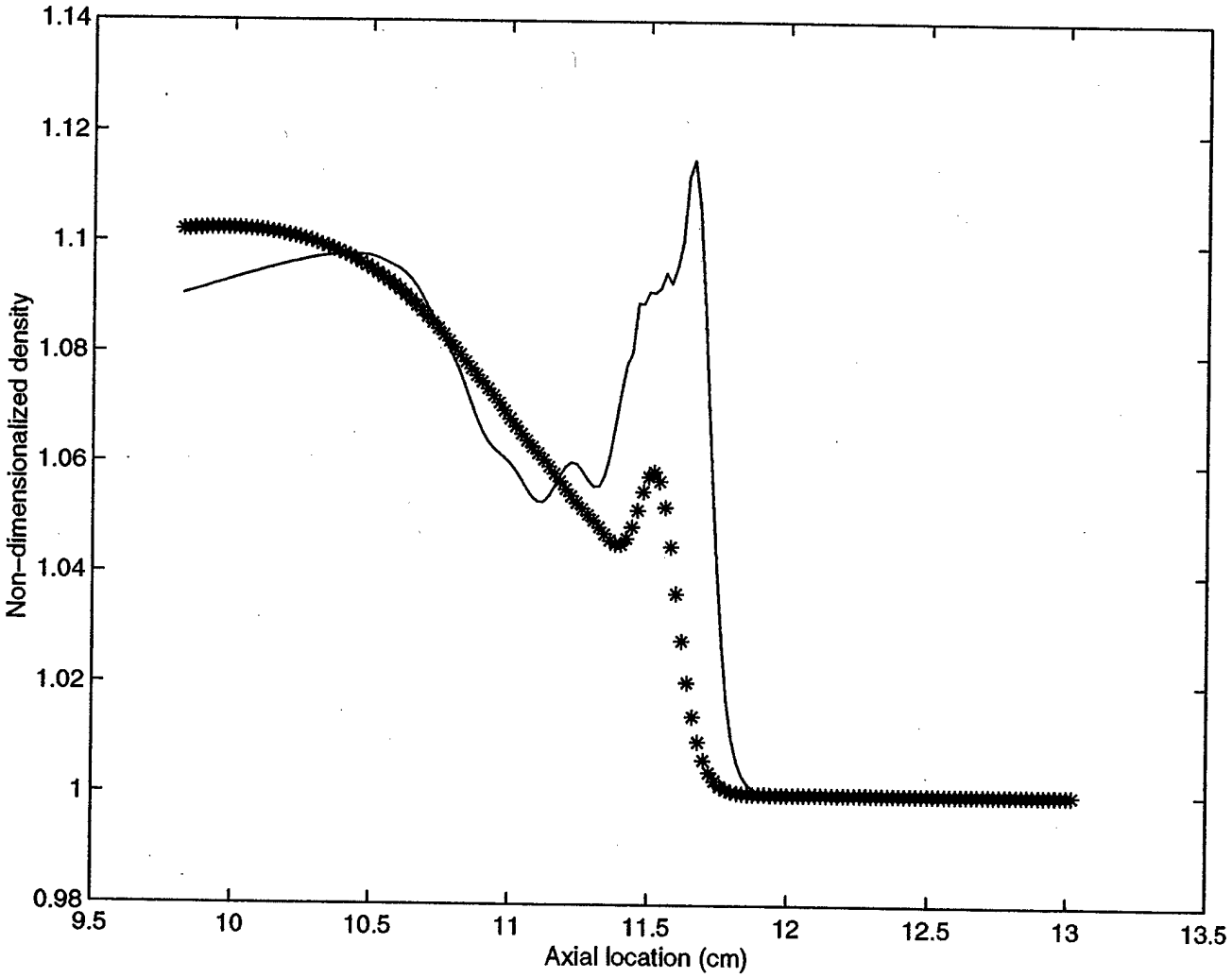

Fig. 7: Calculated profiles of density (normalized) are shown here 300 μs after rapid release of energy at x = 0 cm, at two different radial locations: r = 0, and r = 1.5 cm. It is this radial staggering of these density profiles that gives rise to apparent splitting in the PAD signal. This is the realistic case of a 5 cm. cylindrical tube containing Argon at 30 Torr, with no-slip conditions applied at the wall. Note that the portion of the wave nearest the wall is retarded relative to its counterpart at the centerline due to wall shear, and therefore lags behind in space (and in time). This gives the appearance of two or more split structures in the PAD signal.

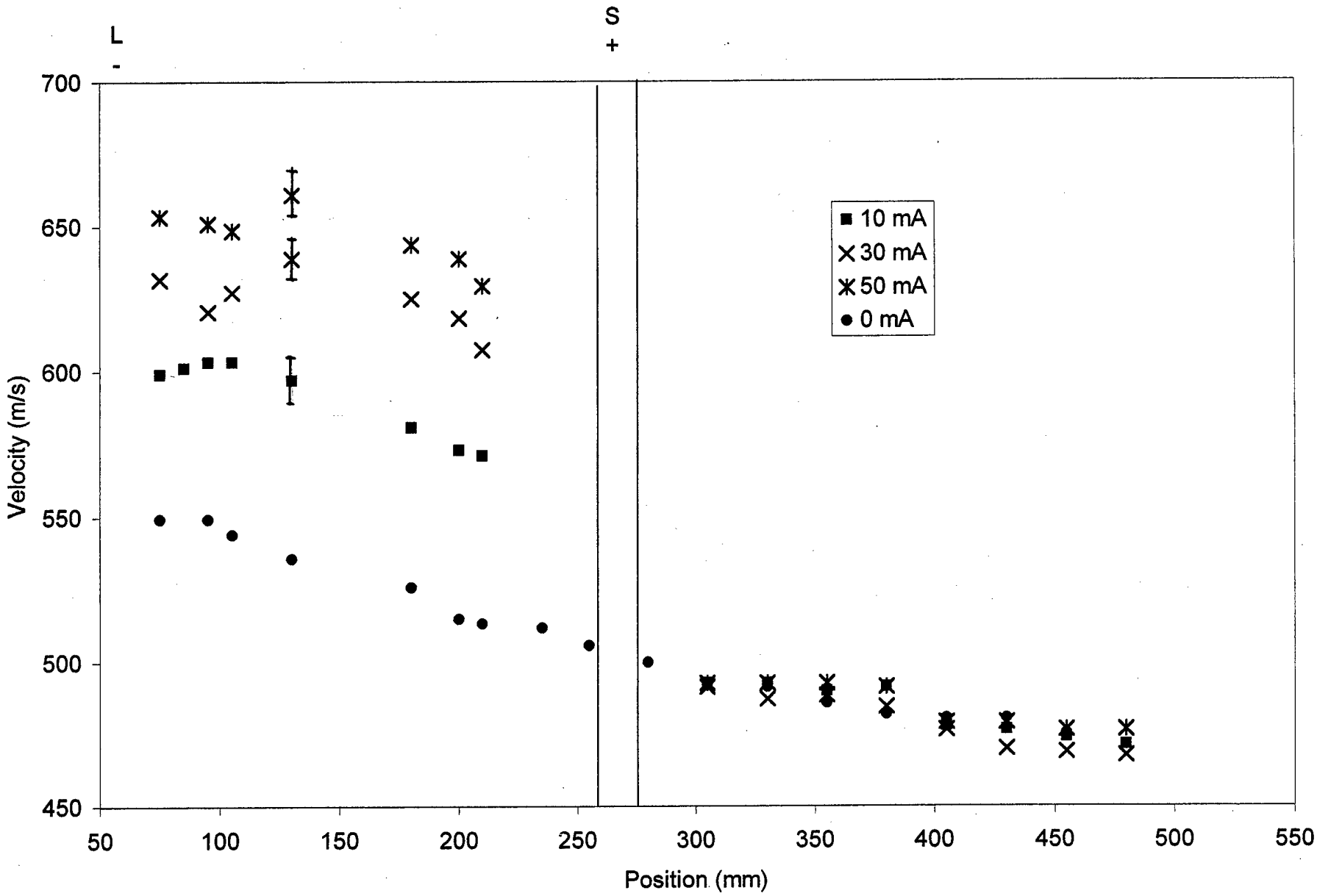

Figure 8: Measured shock propagation versus distance along the shock tube for various currents are shown here. The electrode nearest the spark gap is the cathode (L-) and the farthest electrode is the anode (S+) in this case.

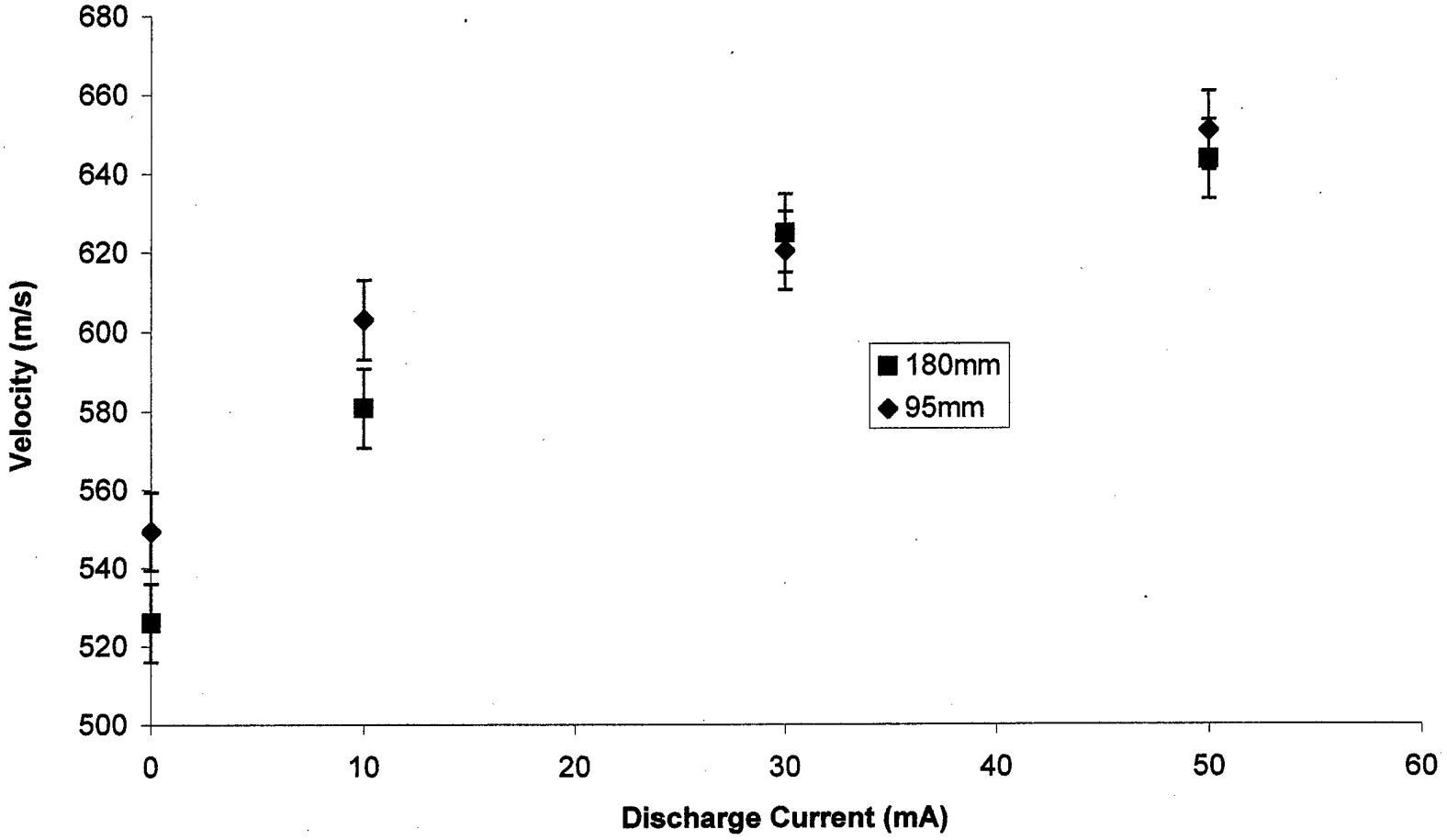

Figure 9: Variation of shock propagation velocity with current is shown at two specific locations (95mm and 180mm) from the edge of the cathode, which is the electrode nearest the spark gap.

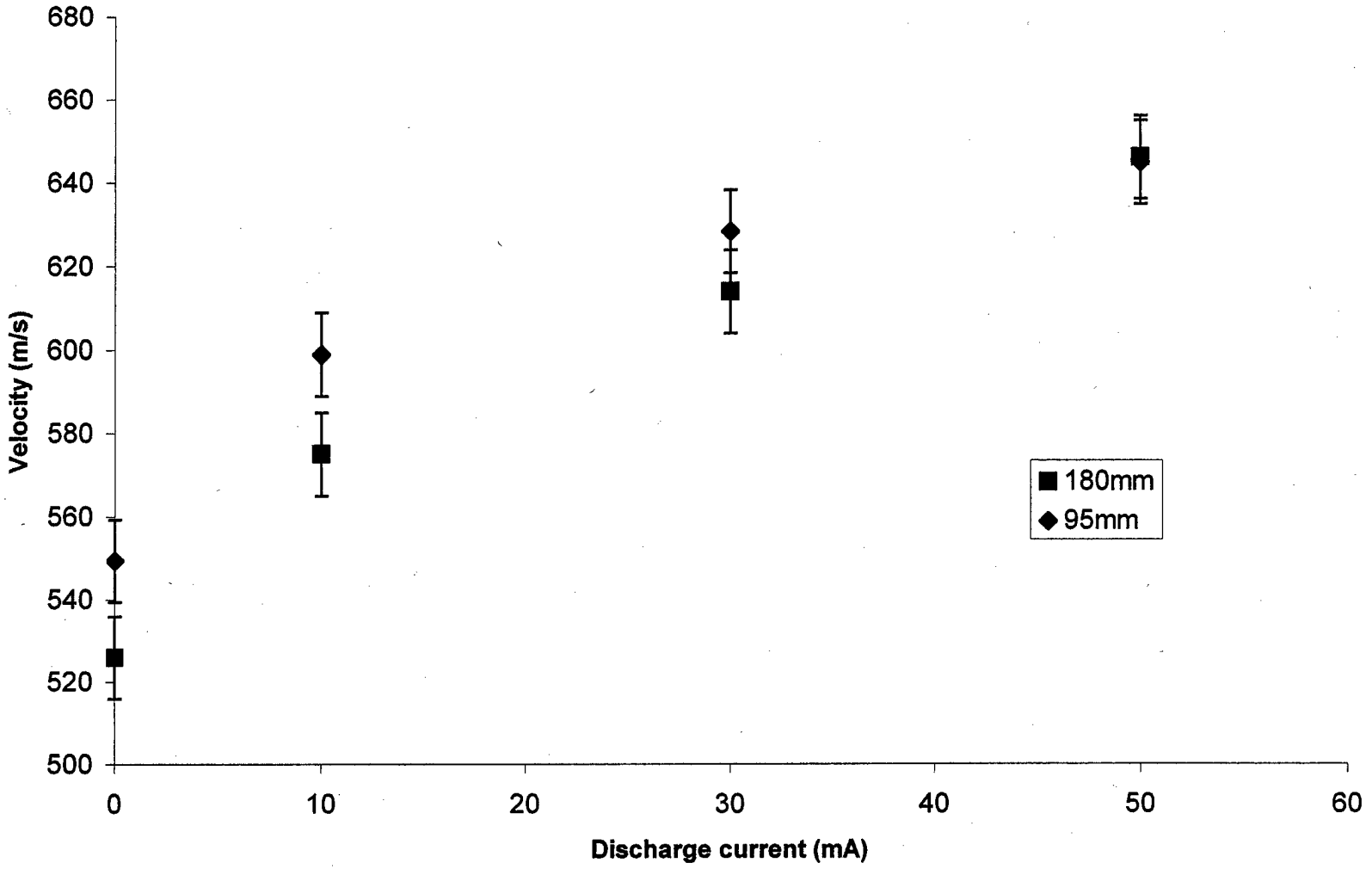

Figure 11: Variation of shock propagation velocity with current is shown at two specific locations (95mm and 180mm) from the edge of the anode, which is the electrode nearest the spark gap.

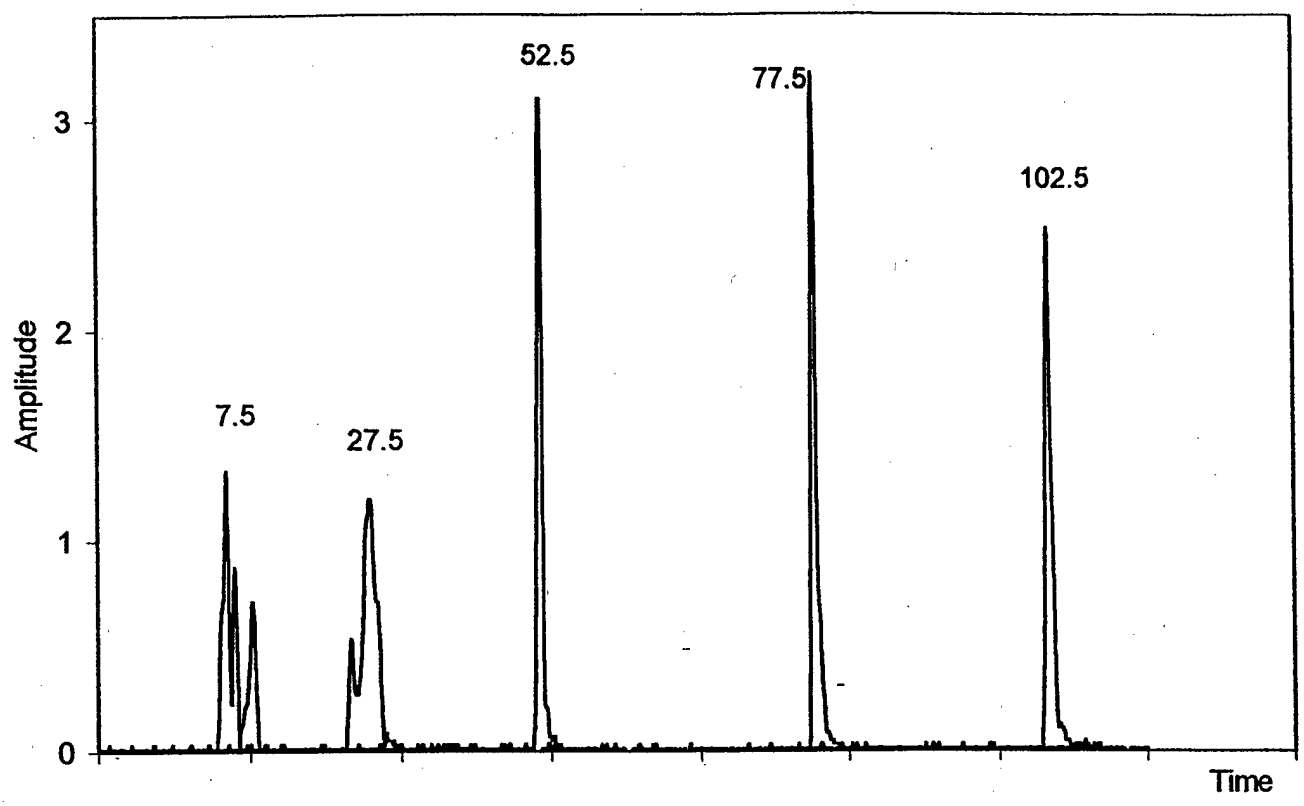

Fig. 12: The time signature of the amplitude of the photo-acoustic deflection signal is shown here at various locations (indicated in mm) downstream of the anode edge. The current in the glow discharge is 10mA for this case.

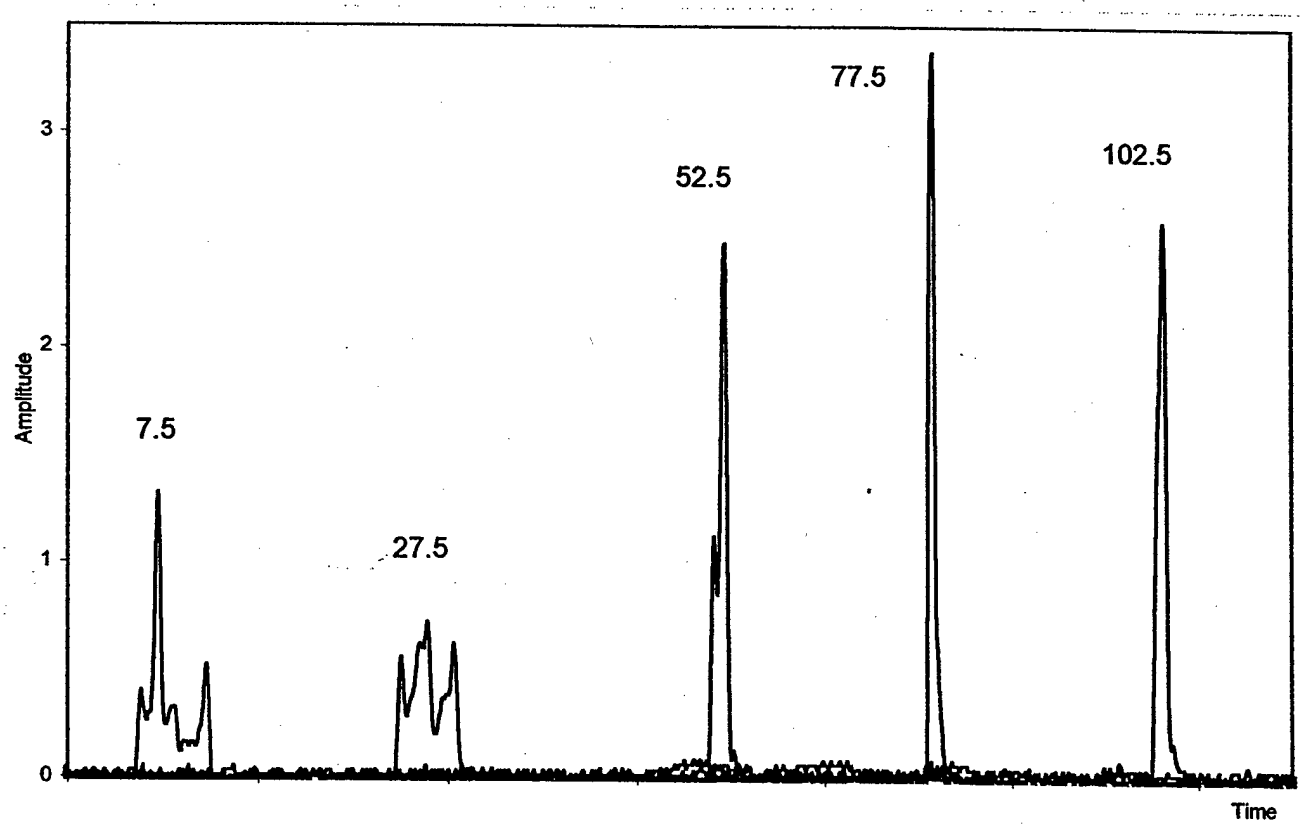

Fig. 13: The time signature of the amplitude of the photo-acoustic deflection signal is shown here at various locations (indicated in mm) downstream of the cathode edge. The current in the glow discharge is 10mA for this case.

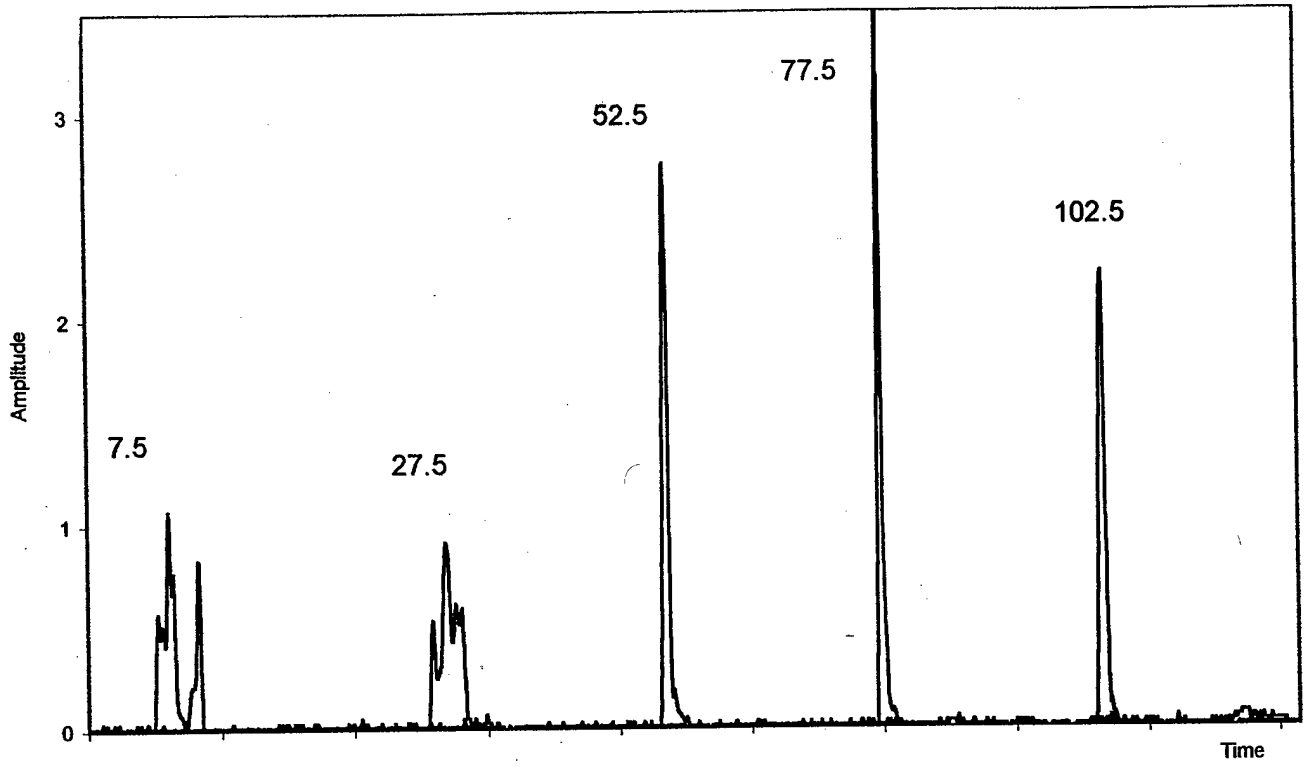

Fig. 14: The time signature of the amplitude of the photo-acoustic deflection signal is shown here at various locations (indicated in mm) downstream of the anode edge. The current in the glow discharge is 30mA for this case.

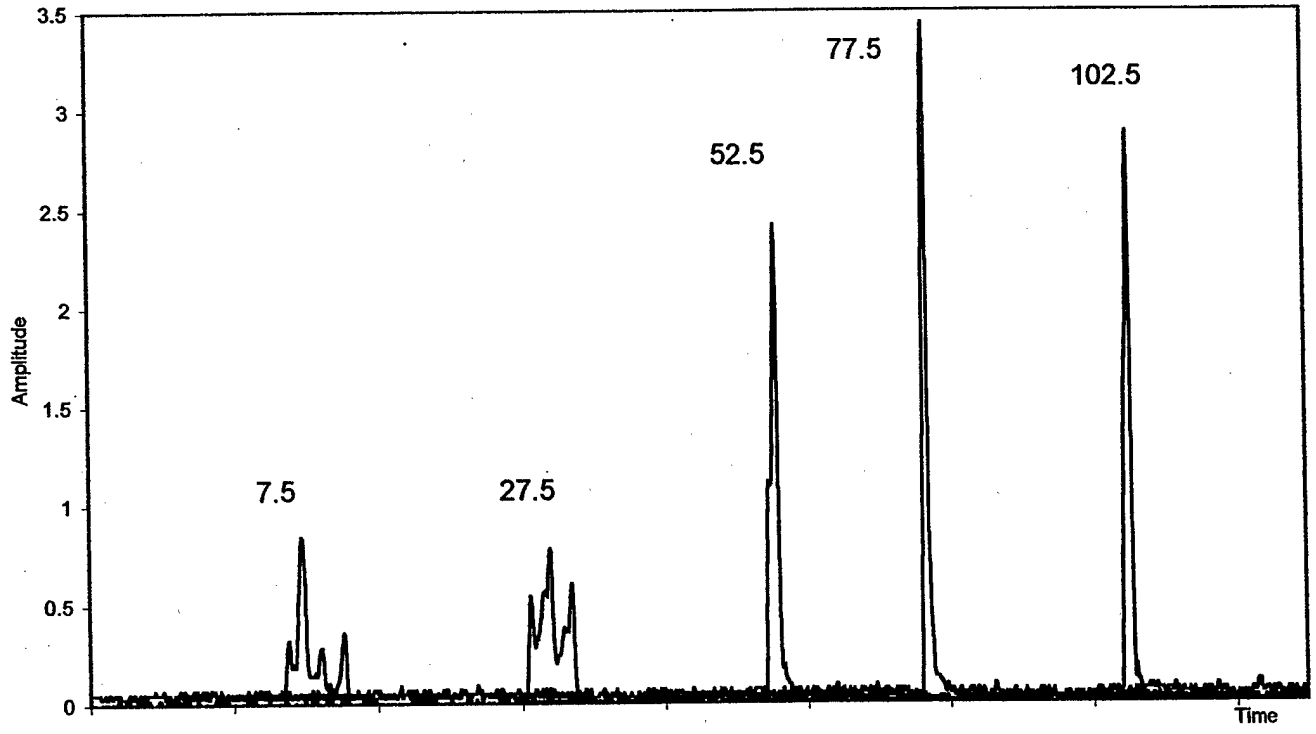

Fig. 15: The time signature of the amplitude of the photo-acoustic deflection signal is shown here at various locations (indicated in mm) downstream of the cathode edge. The current in the glow discharge is 30mA for this case.

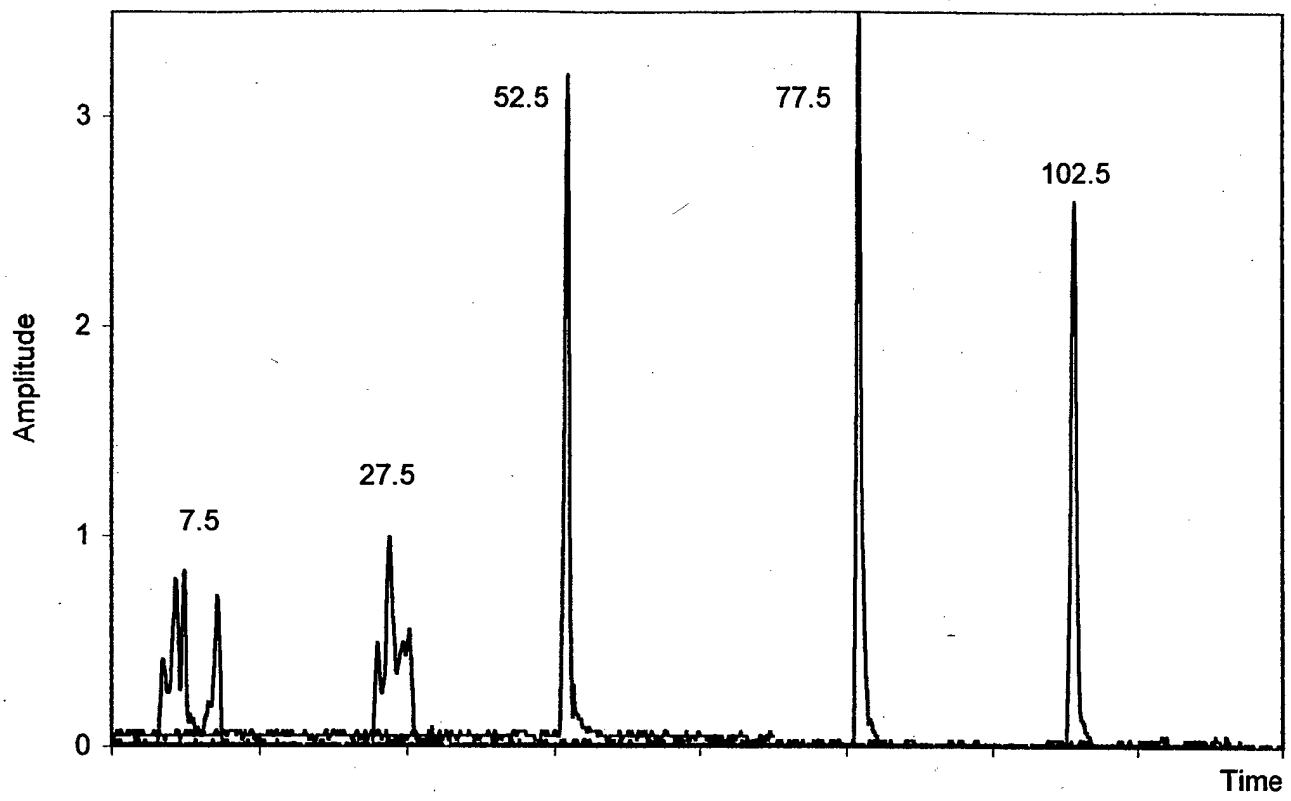

Fig. 16: The time signature of the amplitude of the photo-acoustic deflection signal is shown here at various locations (indicated in mm) downstream of the anode edge. The current in the glow discharge is 50mA for this case.

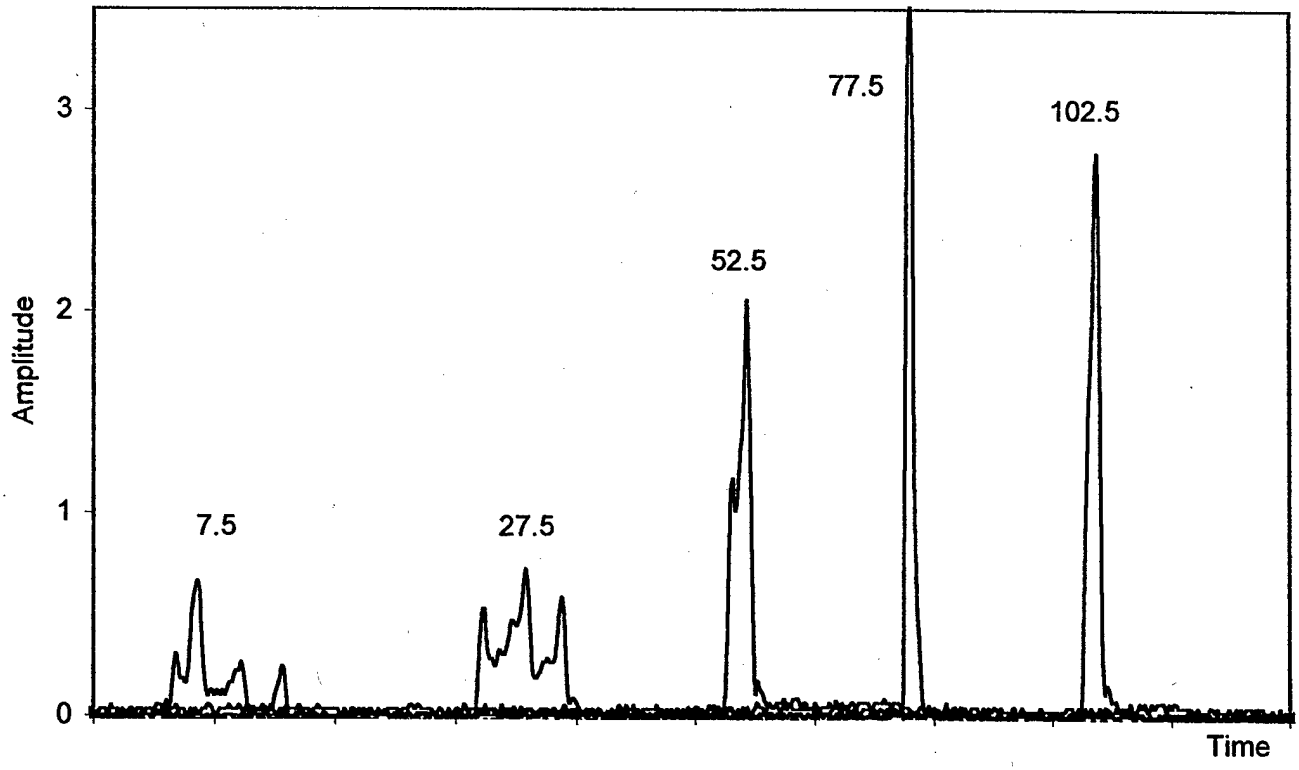

Fig. 17: The time signature of the amplitude of the photo-acoustic deflection signal is shown here at various locations (indicated in mm) downstream of the cathode edge. The current in the glow discharge is 50mA for this case.

1.6 Effect of Electron Density on Shock Wave Propagation in Optically Pumped Plasmas

AIAA 2001-3058

EFFECT OF ELECTRON DENSITY ON SHOCK WAVE PROPAGATION IN OPTICALLY PUMPED PLASMAS

Allen R. White, Peter Palm, Elke Plönjes, Vish V. Subramaniam, and Igor V. Adamovich

Nonequilibrium Thermodynamics Laboratories
Department of Mechanical Engineering
The Ohio State University, Columbus, OH 43210-1107

32nd AIAA Plasmadynamics and Lasers Conference and 4th Weakly Ionized Gases Workshop

11 - 14 June 2001 / Anaheim, CA

AIAA 2001-3058

EFFECT OF ELECTRON DENSITY ON SHOCK WAVE PROPAGATION IN OPTICALLY PUMPED PLASMAS[1]

Allen R. White[2], Peter Palm[3], Elke Plönjes[3], Vish V. Subramaniam[4], and Igor V. Adamovich[5]

Nonequilibrium Thermodynamics Laboratories
Department of Mechanical Engineering
The Ohio State University, Columbus, OH 43210-1107

Abstract

The paper discusses experimental studies of spark-generated shock wave propagation in CO-laser sustained optically pumped CO-Ar-O_2 plasmas. The rotational-translational temperature of the plasma is measured by Fourier transform infrared emission spectroscopy. The electron density in the plasma is determined by microwave attenuation. The line-of-sight density distribution across the propagating shock is detected by photo-acoustic deflection (PAD). The measurements show that adding of up to 0.1% of oxygen to the baseline optically pumped CO-Ar plasma increases the electron density and the ionization fraction by more than an order of magnitude (up to $n_e=0.9\cdot10^{10}$ cm^{-3} and $n_e/N=0.8\cdot10^{-8}$ cm^3/sec, respectively), while the gas temperature remains nearly constant, within 3-5%. Basically, this method allows varying the electron density in the plasma nearly independently of the gas temperature. The PAD measurements show considerable shock wave weakening and dispersion in the optically pumped plasma with a strong radial temperature gradient. However, varying the electron density at a nearly constant gas temperature does not produce any measurable effect on the gas density distribution across the shock. It is therefore concluded that the observed shock weakening is entirely due to the radial temperature gradient sustained by resonance absorption of the CO laser radiation near the centerline of the shock tube and is not affected by the presence of the charged species in the plasma.

1. Introduction

Shock wave propagation in weakly ionized glow discharge plasmas (with ionization fraction of $n_e/N\sim10^{-8}$-10^{-6}) has been extensively studied over the last 15 years, both in Russia [1-11] and in the U.S. [12-20]. A number of anomalous effects, such as shock acceleration, weakening, and dispersion, have been reported. These effects have been observed in discharges in various gases (air, N_2, Ar) at pressures up to P=30 Torr, and for Mach numbers M=1.5-4.5. They also persist

[2] Graduate Research Assistant
[3] Post-Doctoral Researcher
[4] Professor, Senior Member AIAA
[5] Associate Professor, Dept. of Aerospace Engineering and Aviation, Senior Member AIAA

for a long time after the discharge is off (up to ~1 ms). These results led to a suggestion that the anomalous shock wave behavior in nonequilibrium plasmas is primarily due to the effect of the speed of sound and the flow field modification by the charged species (e.g. ion-acoustic wave) [21] or by the metastable species [22-24] present in the plasma.

Recent experimental and modeling results suggest that these effects can in fact be explained by non-uniform gas heating in the discharge. Indeed, pulsed glow discharge / shock tube experiments [15] and supersonic plasma wind tunnel experiments [17-19] demonstrate that shock weakening and dispersion in glow discharge plasmas are no longer observed when the gas temperature gradients are reduced to a minimum (at about the same electron density). In addition, several computational fluid dynamics models predict acceleration, weakening, and dispersion of the shock wave propagating across axial and radial temperature gradients (without plasmas) [25-27], fairly consistent with the experiments. Finally, analysis of possible plasma-related mechanisms of the flow field modification (ion-acoustic waves, energy storage by metastable species, etc.) shows that both these phenomena have negligible effect on the shock wave propagation [28]. This occurs for two basic reasons: (i) the ionization fraction in these plasmas is far too low for the charged species, perturbed by the shock, to produce significant coupling with the neutral species flow field; and (ii) the amount of energy stored in the metastables is too low, or the metastable relaxation rate is too slow to affect the energy balance in the shock.

Although these recent results imply that shock dispersion and weakening in nonequilibrium plasmas is a purely thermal effect, they should not be regarded as entirely conclusive. Indeed, reduction of the temperature gradients in the plasma [15,17-19] also increases the flow number density and therefore decreases the ionization fraction, thereby reducing a possible effect of charged species on the shock propagation. On the other hand, varying the electron density in the plasma, *without* affecting the gas temperature distribution would allow distinguishing the effect of nonuniform Joule heating (i.e. temperature gradients) from the effect of charged species on the shock wave propagation. This would determine whether ionization contributed to acceleration, weakening, and dispersion of shock waves in glow discharge plasmas observed in previous experiments [1,2,12,13] or whether these effects are entirely due to radial and axial temperature gradients present in the plasma. Such uncoupling of the thermal and ionization effects constitutes the primary objective of the present experiment.

Since independent variation of the electron density and the gas temperature in glow discharge plasmas is rather problematic, we analyze shock wave propagation in strongly nonequilibrium optically pumped plasmas sustained by resonance absorption of CO laser radiation [29,30]. The gas pressure and temperature in these plasmas (P~100 torr, T~400-700 K) [30], as well as the electron density and electron temperature (n_e~10^{10}-10^{11} cm^{-3}, T_e~0.5 eV) [30,31] are similar to those achieved in glow discharges. In addition, our previous experiments [32,32] suggest that the electron density and the gas temperature in such plasmas can be varied independently. This makes optically pumped plasmas an ideal environment for studies of possible effects of ionization on the shock propagation.

2. Experimental

The schematic of the experimental setup is shown in Fig. 1. The experimental apparatus consists of a spark discharge shock wave generator (Kolb tube) attached to a Pyrex glass shock tube / optical absorption cell with a test section for diagnostics of both shock wave parameters and plasma parameters. The entire apparatus is mounted on a Newport optical bench supported by a Unistrut table. A shock wave is generated by a spark discharge in a T-shaped Pyrex glass Kolb tube containing two 1/8-inch diameter tungsten electrodes 2.5 cm apart. A 2.5-cm diameter opening in the Kolb tube, centered at the middle of the electrode gap, expands to the 5-cm diameter shock tube connected to the Kolb tube as shown in Fig. 1. The shock wave generated by the discharge propagates along the shock tube, which is 1 m long (see Fig. 1). The spark is initiated by a discharge of two 1 μF capacitors connected in parallel. The capacitors are charged by a Kaiser Systems 30 kV, 2.5 kW power supply. The spark is triggered by an EG&G TM-11A trigger module which applies a breakdown voltage to the electrodes. The trigger module also sends a synchronization signal to the digital oscilloscope to mark the spark initiation. The Kolb tube is surrounded by a copper mesh Faraday cage to prevent electromagnetic interference of the spark with the diagnostics equipment.

The line-of-sight averaged density gradient across the shock propagating along the tube, as well as the shock velocity, are determined by measuring the photo-acoustic deflection (PAD) of a He-Ne laser beam perpendicular to the tube axis (see Fig. 1). For this, a Uniphase 1125 Helium Neon (He-Ne) laser (λ=632.8 nm) with a beam diameter of 0.8 mm is used. The laser beam is split in two by a beam splitter and is directed onto two Thor Labs PDA 155 high-speed (50 MHz) amplified photodiode detectors (sensitive area of 1 mm^2) located 29.5 mm apart, as shown in Fig. 1. Both detectors are initially set slightly off the He-Ne laser beams such that the beams are deflected onto the detectors as the shock traverses across each beam, due to change in the refraction index. The amplitude of the resultant PAD signal is proportional to the deflection angle, which is in turn proportional to the line-of-sight averaged density gradient across the shock. The simultaneous use of two detectors allows measurements of the shock propagation velocity. The PAD signal from the detectors is acquired by a Tektronix TDA 360 digital oscilloscope at a sampling rate of 2 MHz (time resolution of 0.5 μsec). To acquire the PAD signal at the desired location, oscilloscope delay time relative to the synchronization signal from the TM-11A trigger (i.e. spark initiation) is adjusted. The entire PAD diagnostic system, including the He-Ne laser, the beamsplitter, the mirror, and the detectors is mounted on an optical rail, which can be moved along the shock tube, thus allowing measurements at different locations.

A c.w. CO laser beam enters the shock tube / optical absorption cell through a flange with a 2-inch diameter CaF_2 window at the end of the tube. The liquid nitrogen cooled CO laser [30] is designed in collaboration with the University of Bonn [34] and fabricated at Ohio State. It produces a substantial fraction of its power output on the $v = 2 \rightarrow 1$ fundamental band component in the infrared. In the present experiment, the laser is typically operated at 10-13 W c.w. broadband power on the lowest ten vibrational bands. The output on the lowest bands ($1 \rightarrow 0$ and $2 \rightarrow 1$) is necessary to start the absorption process in cold CO (initially at 300 K) in the absorption cell. The lower vibrational states of CO in the cell, $v \leq 10$, are populated by direct resonance absorption of the pump laser radiation in combination with rapid redistribution of population by vibration-vibration (V-V) exchange processes,

$$CO(v)+CO(w)\rightarrow CO(v+1)+CO(w-1),\quad v>w. \tag{1}$$

The V-V processes then continue to populate higher vibrational levels, up to v=40 [29,30], which are not directly coupled to the laser radiation. The large heat capacity of the Ar diluent, as well as conductive and convective cooling of the gas flow, enables sustaining fairly low translational/rotational mode temperatures in the cell (T=600-700 K). However, at steady-state conditions, the average vibrational mode energy of the CO corresponds to a few thousand degrees Kelvin [29,30]. Thus a strong disequipartition of energy can be maintained in the cell, characterized by very high vibrational mode energy and a low translational/rotational mode temperature. As shown in Fig. 1, the population of the vibrational states of CO in the cell is monitored using a Biorad FTS 175C Fourier transform infrared spectrometer (FTIR), which records spontaneous emission from the CO fundamental, first and second overtone bands through a CaF_2 window on the side of the cell. Figure 2 shows CO vibrational level populations inferred from these spectra. It can be seen that very high vibrational levels, up to v~40, are populated. Analysis of the rotationally resolved CO emission spectra also allowed inference of the translational/rotational temperature in the test section. The unfocused CO laser beam, ~7-8 mm diameter, can sustain a strongly nonequilibrium optically pumped gas region 5-15 cm long and up to ~1 cm diameter (see Figs. 3,4). These dimensions are estimated from the size of the visible blue glow of the C_2 Swan band radiation, which is strongly coupled with the high vibrational level populations of CO [35] (see Figs. 3,4). If the laser beam is focused, the visible plasma is reduced to about 3-4 mm. A cylindrical shape plastic purge flushed with argon (see Fig. 1) has been used to prevent strong CO laser radiation absorption by carbon monoxide in the cell near the beam entrance window, which would otherwise lead to soot deposit on the window and heat it up to high temperatures.

Ionization of highly excited CO molecules in the cell occurs by the associative ionization mechanism, in collisions of two highly vibrationally excited molecules when the sum of their vibrational energies exceeds the ionization potential [29,31-33],

$$\begin{gathered} CO(v)+CO(w)\rightarrow (CO)_2^+ + e^- , \\ E_v + E_w > E_{ion}. \end{gathered} \tag{2}$$

Our previous studies of ionization in CO-Ar optically pumped plasmas [31] showed that electron densities up to $n_e=3\cdot10^{11}$ cm^{-3} can be sustained at P=100 torr and CO laser power of 10-15 W.

The test section of the shock tube / optical absorption cell has a ½-inch gas inlet port through which the gas mixture (CO-Ar-O_2) enters the tube. An additional ½-inch inlet port in the end flange of the shock tube allows argon flow into the purge (see Fig. 1). By changing the purge length and varying the argon flow rate through the purge, the location of the optically pumped plasma in the tube can be controlled. The gas exit port is connected to a vacuum pump through a throttling valve, which controls the mass flow rate through the shock tube at ~100 sccm, which corresponds to a flow velocity of ~1 cm/sec at P~0.1 atm. With the pump valve closed, the shock tube assembly has a leak rate of about 0.1 torr/hr. To add controlled small amounts of oxygen to the baseline CO-Ar gas mixture in the absorption cell, O_2 was diluted in argon at 5% level. The

resultant O_2/Ar mixture has been added to the shock tube. The baseline pressure in the cell was P=70 torr, with the CO partial pressure of P_{CO}=3.5 torr. The O_2/Ar mixture partial pressure was varied in the range 0-3 torr. The reason for adding oxygen to the CO-Ar optically pumped plasma is that our previous experiments showed that small amounts of O_2 additive (~0.1%) strongly increase the electron density in the plasma (by a factor of 20-50) [32]. At the same time, previous temperature measurements in the optically pumped plasmas [33] showed that adding such small amounts of O_2 and NO did not result in significant gas temperature changes.

For the electron density measurements in the optically pumped plasma, the CaF_2 window flanges at the ends of the arms of the absorption cell (see Fig. 1) are replaced by a pair of flanges holding microwave waveguides, which are thus placed on both sides of the cylindrically shaped plasma. The electron density is determined from the relative attenuation of a 20 GHz microwave radiation across the plasma. The average electron density in the plasma is inferred from these measurements using the following relation [31],

$$n_e = \frac{m_e c \varepsilon_0}{e^2} \nu_{coll} \frac{\delta V}{V_{inc}} \frac{1}{d}, \qquad (3)$$

where ν_{coll} is the electron-neutral collision frequency, $\frac{\delta V}{V_{inc}} = \frac{V_{trans} - V_{inc}}{V_{inc}}$ is the relative attenuation factor in terms of the forward power detector voltage proportional to the incident and the transmitted microwave power, and d is the diameter of the ionized region produced by the unfocused laser beam. The microwave attenuation measurement apparatus is described in greater detail in our previous publication [32].

3. Results and Discussion

3.1 Temperature measurements

To verify that the CO-Ar gas mixture temperature in the test section of the shock tube / optical absorption cell is not affected by addition of small amounts of O_2, the rotational temperature in several optically pumped CO-Ar-O_2 gas mixtures has been measured by Fourier transform infrared emission spectroscopy at 0.25 cm^{-1} resolution, as discussed in Section 2. For these measurements, a shorter purge has been used so that the optically pumped plasma was centered in the region between the arms in the test section. Figures 5 and 6 show a typical rotationally resolved CO fundamental emission spectrum and the Boltzmann plots obtained from such spectra, respectively. The slope of the Boltzmann plot in the spectral region not affected by the self-absorption of the CO infrared radiation by the plasma (i.e. in the straight-line region in Fig. 6) gives the rotational temperature of the gas mixture. As one can see from Fig. 6, adding a small amount of O_2 (100 mtorr) to the baseline CO-Ar mixture at P=70 torr results in a translational-rotational temperature rise from T=630 K to T=665 K, or by about 5%. Table 1 shows the results of temperature measurements for various plasma and laser conditions, using both O_2 and NO as additives. One can see that adding small amounts of O_2 or NO (up to 0.1%) to the optically pumped CO-Ar mixtures results in a weak but consistent temperature increase by 3-5%. The

absolute error of these temperature measurements is ±10 K. Note these the emission spectroscopy measurements yield the gas temperature averaged along the line of sight over a region occupied by the vibrationally excited CO near the shock tube centerline (~1 cm diameter, see Figs. 3,4). For comparison, the gas temperature near the shock tube walls is much lower, only slightly exceeding the room temperature (the tube wall is warm to the touch). Therefore the optically pumped plasma creates a substantial radial temperature gradient in the shock tube. The insignificant effect of the O_2 additive on the gas mixture temperature is expected, since small amounts of oxygen can only weakly affect the CO vibrational energy balance. The observed temperature increase is mainly due to the faster CO vibrational relaxation rate by vibration-vibration and vibration-translation energy transfer in collisions with O_2 molecules [36]. Although the actual radial temperature distribution in these experiments is not measured, it is also very unlikely to be affected by the O_2 additive since the transport coefficients of the gas mixture are insensitive to such small changes in chemical composition.

Table 1. Temperature measurements in CO-Ar-O_2 and CO-Ar-NO mixtures

Laser	P_{CO}, torr	P_{Ar}, torr	P_{O2}, mtorr	P_{NO}, mtorr	T, K
Unfocused	3.5	70	0	-	630
Unfocused	3.5	70	50	-	644
Unfocused	3.5	70	100	-	665
Focused	3.0	100	0	-	607
Focused	3.0	100	75	-	627
Focused	3.0	100	-	0	611
Focused	3.0	100	-	100	640

3.2 Electron density measurements

Electron density in the optically pumped CO-Ar plasmas, with and without O_2 additive, has been measured using the microwave attenuation technique described in Section 2 (see also Ref. [32]). The electron-neutral collision frequency in a CO-Ar mixture at P=70 torr and T=650 K, $\nu_{coll}=7\cdot10^{10}$ cm^3/sec was obtained from the Boltzmann equation solution [31] using the experimental cross-sections of elastic and inelastic electron-molecule collision processes available in the literature. The results are summarized in Table 2. It can be seen that adding small amounts of oxygen to the baseline CO-Ar mixture results in a significant increase of the average electron density in the plasma (by more than an order of magnitude). This result is consistent with the previous electron density measurements in optically pumped CO-Ar and CO-N_2 plasmas with O_2 and NO additives recently conducted in our group [32]. Again, these measurements give the average electron density in the optically pumped region near the centerline of the shock tube, sustained by the unfocused CO laser beam (see Figs. 3,4). The accuracy of these measurements, ±25%, is primarily determined by the uncertainty of the diameter of the optically pumped plasma, d=8±2 mm (see Eq. (1)). Note that the previous measurements [32] also demonstrated that the observed electron density increase occurs in spite of the reduction of the electron production rate in the presence of oxygen or nitric oxide. Qualitative interpretation of this effect,

consistent with the previous measurements of ion composition in the CO-Ar-O_2 glow discharge plasmas [37], is that the oxygen additive results in replacing the rapidly recombining cluster ions of the general form $C_n(CO)_2^+$, n=1-12, which are the dominant ions in the CO-Ar plasmas [37], by the slowly recombining O_2^+ ions. With the O_2 additive present, the ionization fraction, $n_e=(0.6\text{-}0.8)\cdot10^{-8}$ cm^{-3}, is comparable with the ionization fraction in the previous experiments on shock wave propagation in glow discharge plasmas [12,13], where significant shock wave dispersion has been observed. Indeed, for the glow discharge current of I=30 mA, shock tube diameter of D=5 cm (current density of j=1.5 mA/cm^2), gas pressure of P=30 torr, and electric field of E=86 V/cm [12], the average electron density is $n_e=j/ew_{dr}=0.5\cdot10^{10}$ cm^{-3} and the ionization fraction is $n_e/N=1.0\cdot10^{-8}$. Here we assumed the average gas temperature at these conditions to be T~600 K and the electron drift velocity in argon $w_{dr}=2\cdot10^6$ cm/s at $E/N=2\cdot10^{-16}$ V·cm^2.

Table 2. Electron density measurements in CO-Ar-O_2 mixtures

P_{CO}, torr	P_{Ar}, torr	P_{O2}, mtorr	n_e, cm^{-3}	n_e/N
3.5	70	0	$0.61\cdot10^9$	$0.56\cdot10^{-9}$
3.5	70	50	$0.91\cdot10^{10}$	$0.85\cdot10^{-8}$
3.5	70	100	$0.65\cdot10^{10}$	$0.60\cdot10^{-8}$

Summarizing the results of the temperature and electron density measurements, we conclude that adding small amounts of O_2 to the optically pumped CO-Ar plasmas allows significant increase of the electron density in the plasma (by more than an order of magnitude) while keeping the gas temperature distribution nearly the same (within 3-5%). Therefore, comparison of the characteristics of shock waves propagating in the CO-Ar and in the CO-Ar-O_2 plasmas (in particular, density profile across the shock) would allow separation of the temperature gradient and the ionization effects on the shock dispersion. In other words, if any difference is observed between the density distributions across the shock in these two cases, it would be due to the electron density increase. On the other hand, absence of such difference would demonstrate that the shock dispersion is entirely due to the axial and radial temperature gradients in the optically pumped gas.

3.3 Shock dispersion measurements

The density distribution across the spark-generated shock waves propagating through the optically pumped plasmas has been measured in CO-Ar plasmas, with and without O_2 additive, using the PAD diagnostics described in Section 2. As discussed in Section 1, the primary objective of these measurements is to determine whether the electron density variation by adding oxygen to the plasma (at a nearly constant gas temperature) affects the shock dispersion in the plasma. First, we compared the PAD signals from the shock propagating through a cold non-ionized gas with the PAD signal from the shock propagating in the optically pumped CO-Ar plasma sustained by an unfocused CO laser beam at two different pressures, P=70 torr and P=130 torr (see Figs. 7,8). It can be seen that in both cases the shock in the plasma is considerably dispersed and weakened. Such weakening and spreading of the PAD signal has previously been attributed to curvature of the shock front [16,20]. The shock velocities in the

cold non-ionized gas are u_s=388±5 m/s and u_s=383±5 m/s at P=70 and 130 torr, respectively, which corresponds to the test section shock Mach number of M=1.2. The shock velocity in the optically pumped plasma at P=70 torr increased to u_s=434±7 m/s, while the shock velocity in the plasma at P=130 torr remained nearly the same as in the non-ionized gas, u_s=388±5 m/s. The shock propagation velocity in the plasma increases due to the higher temperature on the centerline of the shock tube (see Section 3.2). On the other hand, strong dispersion reduces the maximum density gradient (i.e. weakens the shock) and therefore reduces the shock propagation velocity. Therefore the shock speed in the plasma is controlled by these two competing mechanisms. The shot-to-shot shock velocity variation did not exceed 2%. At P=70 torr, the maximum density gradient in the shock propagating in the plasma decreased and the shock dispersion increased by up to a factor of 5, compared to the shock propagating in the cold non-ionized gas (see Fig. 7). At P=130 torr, the maximum density gradient in the shock propagating in the plasma decreased by up to a factor of 2.5, while the shock dispersion increased by up to a factor of 5, compared to the shock propagating in the cold non-ionized gas (see Fig. 8). In both cases, the signal from the PAD detector #2, located 29.5 mm downstream from detector #1 (see Fig. 1), shows that the shock propagating in the plasma becomes weaker and more dispersed compared to the signal from detector #1. These results are consistent with the previous experiments on the spark-generated shock wave propagation in the glow discharge plasmas [12].

To determine whether the observed shock weakening and dispersion are due to the non-uniform flow heating by the optically pumped plasma or due to the presence of electron and ions in the flow, we conducted a series of shock dispersion measurements in CO-Ar-O_2 mixtures. As discussed in Sections 3.1 and 3.2, adding up to 0.1% O_2 to the baseline CO-Ar mixture allows increase of electron density by more than an order of magnitude without changing the gas temperature. Figures 9, 10 show the PAD signals from shock waves propagating in the optically pumped CO-Ar plasmas and CO-Ar-O_2 plasmas (with 50 mtorr oxygen), at P=70 and 130 torr. One can see that in both cases the density gradient distributions across the shocks are nearly identical. Increasing the oxygen partial pressure up to 100 mtorr also did not produce any detectable change in the PAD signals.

Repeating the same measurements in the plasma sustained by a focused laser beam produced essentially the same results. Under no conditions did the increase of electron density by adding the oxygen additive produce any detectable effect on the density distribution across the shock. This negative result is consistent and repeatable and is not affected by the shot-to-shot variation. In other words, these results suggest that the electron density variation does not have any detectable effect on the density distribution across the shock wave. Therefore we conclude that the shock weakening and dispersion previously observed in nonequilibrium glow discharge plasmas [12,13] are both entirely due to the non-uniform flow heating by the plasma.

4. Summary

The paper discusses experimental studies of spark-generated shock wave propagation in CO-laser sustained optically pumped CO-Ar-O_2 plasmas. The rotational-translational temperature in the plasma is measured by Fourier transform infrared emission spectroscopy. The electron density in the plasma is determined by microwave attenuation. The density distribution across

the shock is determined by photo-acoustic deflection (PAD). The measurements show that addition of up to 0.1% of oxygen to the baseline optically pumped CO-Ar plasmas increases the electron density and the ionization fraction by more than an order of magnitude, while the gas temperature remains nearly constant, within 3-5%. This method allows varying the electron density in the plasmas nearly independently of temperature. The PAD measurements show considerable shock wave weakening and dispersion in the optically pumped plasma with a strong radial temperature gradient. However, varying the electron density at nearly constant gas temperature does not produce any measurable effect on the gas density distribution across the shock. We therefore conclude that the observed shock weakening is entirely due to the radial temperature gradient sustained by resonance absorption of the CO laser radiation near the centerline of the shock tube and it is not affected by the presence of the charged species in the plasma.

5. Acknowledgements

Support from the Air Force Office of Scientific Research (AFOSR Grant No. 49620-99-1-0023), as well as partial support from the Ohio Board of Regents Investment Fund is gratefully acknowledged. We would also like to thank Prof. J. William Rich, Dr. B. Ganguly, and Dr. P. Bletzinger for numerous useful discussions.

6. References

1. Klimov, A.I., Koblov, A.N., Mishin, G.I., Yu.L. Serov, and I.P. Yavor, "Shock Wave Propagation in a Glow Discharge", Soviet Technical Physics Letters, vol. 8, No. 4, 1982, pp. 192-194
2. A.I. Klimov, A.N. Koblov, G.I. Mishin, Yu.L. Serov, K.V. Khodataev, and I.P. Yavor, "Shock Wave Propagation in a Decaying Plasma", Soviet Technical Physics Letters, vol. 8, No. 5, 1982, pp. 240-241
3. I.V. Basargin and G.I. Mishin, "Probe Studies of Shock Waves in the Plasma of a Transverse Glow Discharge", Soviet Technical Physics Letters, vol. 11, No. 11, 1985, pp. 535-538
4. V.A. Gorshkov, A.I. Klimov, G.I. Mishin, A.B.Fedotov, and I.P. Yavor, "Behavior of Electron Density in a Weakly Ionized Nonequilibrium Plasma with a Propagating Shock Wave", Soviet Physics - Technical Physics, vol. 32, No. 10, 1987, pp. 1138-1141
5. A.P. Ershov, S.V. Klishin, A.A. Kuzovnikov, S.E. Ponomareva, and Yu.P. Pyt'ev, "Application of the Reduction Method to the Microwave Interferometry of Shock Waves in Weakly Ionized Plasma", Soviet Physics - Techical Physics, vol. 34, No. 8, 1989, p. 936-937
6. I.V. Basargin and G.I. Mishin, "Precursor of Shock Wave in Glow-Discharge Plasma", Soviet Technical Physics Letters, vol. 15, No. 4, 1989, p. 311-313
7. S.A. Bystrov, I.S. Zaslonko, Yu.K. Mukoseev, and F.V. Shugaev, "Precursor Ahead of a Shock Front in an RF Discharge Plasma", Soviet Physics - Doklady, vol. 35, No. 1, 1990, pp. 39-40
8. G.I. Mishin, Yu.L. Serov, and I.P. Yavor, "Flow Around a Sphere Moving Supersonically in a Glow Discharge Plasma", Soviet Technical Physics Letters, vol. 17, No. 6, 1991, pp. 413-416

9. G.I. Mishin, A.I. Klimov, and A.Yu. Gridin, "Measurements of the Pressure and Density in Shock Waves in a Gas Discharge Plasma", Soviet Technical Physics Letters, vol. 17, No. 8, 1992, pp. 602-604
10. A.Yu. Gridin, A.I. Klimov, and K.V. Khodataev, "Propagation of Shock Waves in a Nonuniform Transverse Pulsed Discharge", High Temperature, vol. 32, No. 4, 1994, pp. 454-457
11. A.P. Bedin and G.I. Mishin, "Ballistic Studies of the Aerodynamic Drag on a Sphere in Ionized Air", Technical Physics Letters, vol. 21, 1995, pp. 5-7
12. B.N. Ganguly, P. Bletzinger, and A. Grascadden, "Shock Wave Dispersion in Nonequilibrium Plasmas", Physics Letters A, vol. 230, No. 3-4, 1997, pp. 218-222
13. P. Bletzinger and B.N. Ganguly, "Local Acoustic Shock Velocity and Shock Structure Recovery Measurements in Glow Discharges", Physics Letters A, vol. 258, No. 4-6, 1999, pp. 342-348
14. H. Lowry, M. Smith, P. Sherrouse, J. Felderman, J. Drakes, M. Bauer, D. Pruitt, and D. Keefer, "Ballistic Range Tests in Weakly Ionized Argon", AIAA Paper 99-4822, AIAA 30th Plasmadynamics and Lasers Conference, Norfolk, VA, June 28-July 1, 1999
15. Yu.Z. Ionikh, N.V. Chernysheva, A.V. Meshchanov, A.P. Yalin, and R.B. Miles, "Direct Evidence for Thermal Mechanism of Plasma Influence on Shock Wave Propagation", Physics Letters A, vol. 259, 1999, pp. 387-392
16. A. R. White, S. M. Aithal, and V. V. Subramaniam, "Experimental Studies of Spark Generated Shock Waves", paper AIAA 99-3670 presented at the 30th AIAA Plasmadynamics and Lasers Conference, Norfolk, Virginia, June 28-July 1, 1999
17. Yano. R., Contini, V., Ploenjes, E., Palm, P., Merriman, S., Aithal, S., Adamovich, I., Lempert. W., Subramaniam. V., and Rich, J.W., "Supersonic Nonequilibrium Plasma Wind Tunnel Measurements of Shock Modification and Flow Visualization", AIAA Journal, vol. 38, No. 10, 2000, pp. 1879-1888
18. I.V. Adamovich, S. Merriman, E. Ploenjes, and P. Palm, "Shock Wave Control by Nonequilibrium Plasmas in Cold Supersonic Gas Flows", Paper 00-2327, presented at special session on high-speed flow control, AIAA Fluids 2000 Conference, Denver, CO, June 19-22, 2000; accepted for publication in AIAA Journal, 2001
19. R. Meyer, P. Palm, E. Plönjes, J. W. Rich, and I.V. Adamovich "The Effect of Nonequilibrium RF Discharge Plasma on a Shock Wave on a Cone in a M=2.5 Flow", AIAA Paper 2001-3059, presented at 32th AIAA Plasmadynamics and Lasers Conference, Anaheim, CA, June 11-14, 2001
20. A. R. White and V. V. Subramaniam, "Shock Propagation through a Low Pressure Glow Discharge in Argon", accepted for publication in J. Thermophysics & Heat Transfer, 2001
21. R.F. Avramenko, A.A. Rukhadze, and S.F. Teselkin, "Structure of a Shock Wave in a Weakyly Ionized Nonisothermal Plasma", Soviet Physics - ZhETP Letters, vol. 34, No. 9, pp. 463-466, 1981
22. G.V. Vstovskii and G.I. Kozlov, "Propagation of Weak Shock Waves in a Vibrationally Excited Gas", Sov. Tech. Phys., vol.31, No. 8, pp. 911-914, 1986
23. V. Soloviev, V. Krivtsov, A. Konchakov, and N. D. Malmuth, "Mechanisms of Shock Wave Dispersion and Attenuation in Weakly Ionized Cold Discharge Plasmas", AIAA Paper 99-4908, AIAA 30th Plasmadynamics and Lasers Conference, Norfolk, VA, June 28-July 1, 1999

24. V. Bychkov, and N. Malmuth, "Shock Wave Structure in Nonequilibrium Ar Discharge Plasma", AIAA Paper 99-4938, AIAA 30th Plasmadynamics and Lasers Conference, Norfolk, VA, June 28-July 1, 1999
25. W.F. Bailey and W.M. Hilbun, "Baseline of Thermal Effects on Shock Propagation in Glow Discharges", Proceedings of Workshop on Weakly Ionized Gases, pp. GG3-GG18, U.S. Air Force Academy, June 9-13, 1997
26. Y.Z. Ionikh, N.V. Chernysheva, A.P. Yalin, S.O. Macheret, L. Martinelli, and R.B. Miles", "Shock Wave Propagation Through Glow Discharge Plasmas - Evidence of Thermal Mechanism of Shock Dispersion", AIAA Paper 2000-0714, 38th AIAA Aerospace Sciences Meeting and Exhibit, Reno, NV, January 10-13, 2000
27. S. Aithal and V.V. Subramaniam, "On the Characteristics of a Spark Generated Shock Wave", Physics of Fluids, vol. 12, 2000, pp. 924-934
28. I.V. Adamovich, V.V. Subramaniam, J.W. Rich, and S.O. Macheret, "Phenomenological Analysis of Shock Wave Propagation in Weakly Ionized Plasmas", AIAA Journal, vol. 36, No.5, 1998, pp. 816-822
29. I. Adamovich, S. Saupe, M.J. Grassi, O. Shulz, S. Macheret and J.W. Rich, "Vibrationally Stimulated Ionization of Carbon Monoxide in Optical Pumping Experiments", Chemical Physics, vol. 173, 1993, pp. 491-504
30. E. Ploenjes, P. Palm, A.P. Chernukho, I.V. Adamovich, and J.W. Rich, "Time-Resolved Fourier Transform Infrared Spectroscopy of Optically Pumped Carbon Monoxide", Chemical Physics, vol. 256, pp. 315-331, 2000
31. I.V. Adamovich and J.W. Rich, "The Effect of Superelastic Electron-Molecule Collisions on the Vibrational Energy Distribution Function", Journal of Physics D: Applied Physics, vol. 30, No. 12, 1997, pp. 1741-1745
32. P. Palm, E. Plönjes, M. Buoni, V.V. Subramaniam, and I.V. Adamovich, "Electron Density and Recombination Rate Measurements in CO-Seeded Optically Pumped Plasmas", accepted for publication in Journal of Applied Physics, 2001
33. E. Ploenjes, P. Palm, I.V. Adamovich, and J.W. Rich, "Ionization Measurements in Optically Pumped Discharges", Journal of Physics D: Applied Physics, vol. 33, No. 16, 2000, pp. 2049-2056
34. S. Büscher, O. Schulz, A. Dax, H. Kath, W. Urban, "Improvement of the Performance of CW CO Lasers by Using Externally Ribbed Wall Cooled Discharge Tubes", Applied Physics B Lasers and Optics, vol. 64, No. 3, 1997, pp. 307 - 309
35. H.L. Wallaart, B. Piar, M.Y. Perrin, and J.P. Martin, Chem. Phys., Vol. 196, 1995, p. 149
36. E. Ploenjes, P. Palm, W. Lee, M. D. Chidley, I.V. Adamovich, W.R. Lempert, and J. William Rich, "Vibrational Energy Storage in High-Pressure Mixtures of Diatomic Molecules", Chemical Physics, vol. 260, 2000, pp. 353-366
37. Y. Kaufman, P. Avivi, F.Dothan, H. Keren, J. Malinowitz, J. Chem. Phys., Vol. 72, 1980, p. 2606

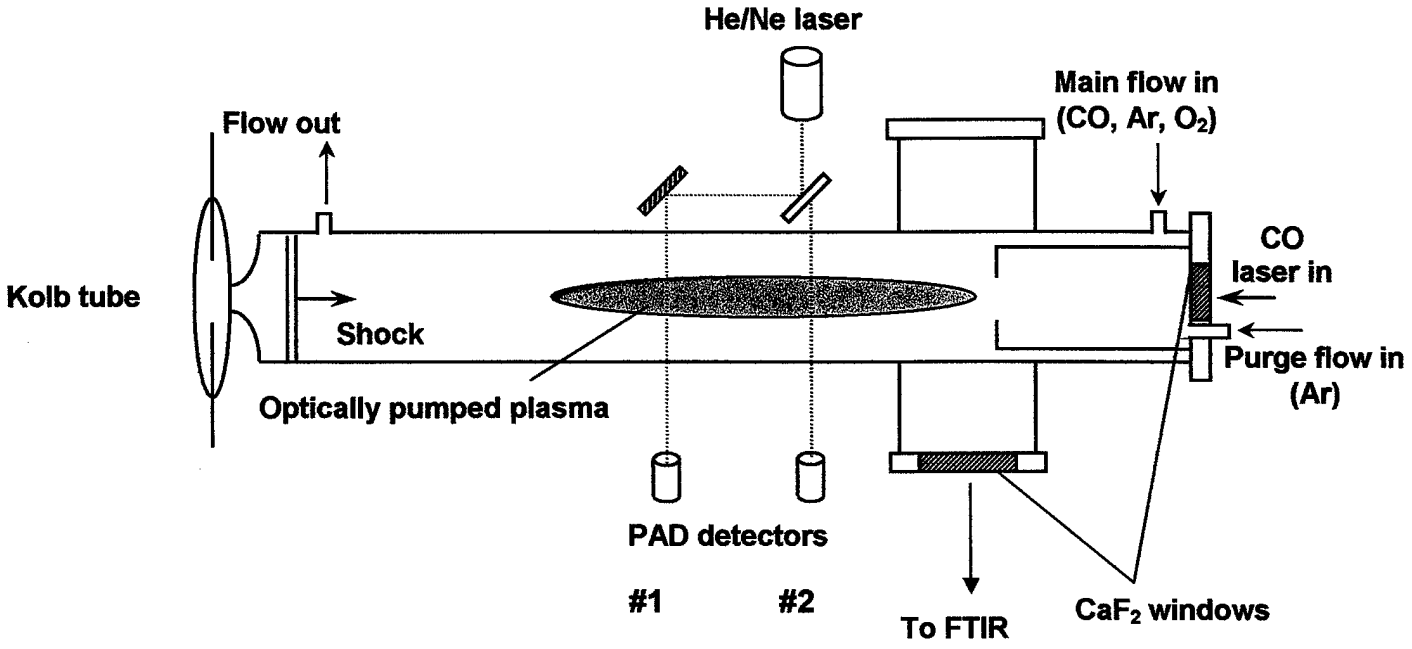

Figure 1. Schematic of the experimental apparatus

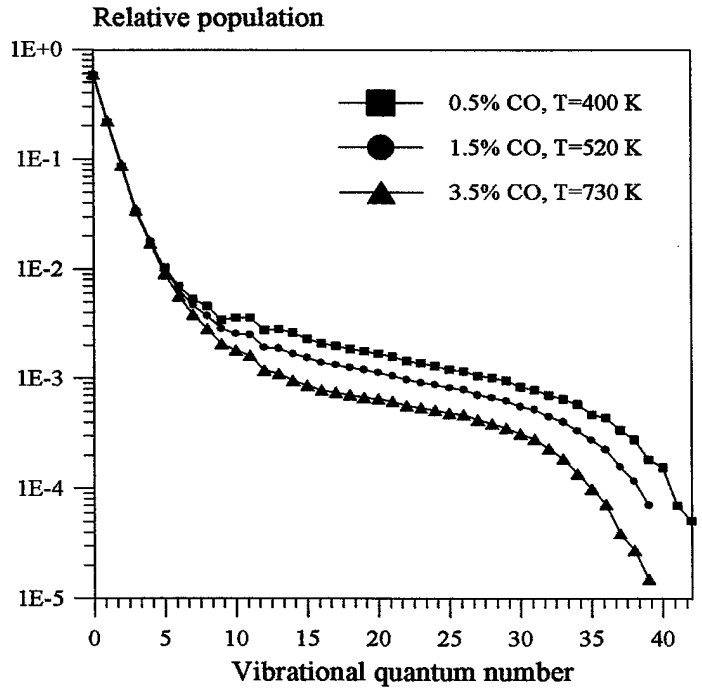

Figure 2. Vibrational distribution functions of CO in different CO/Ar mixtures. P=100 Torr, CO laser power is 10 W.

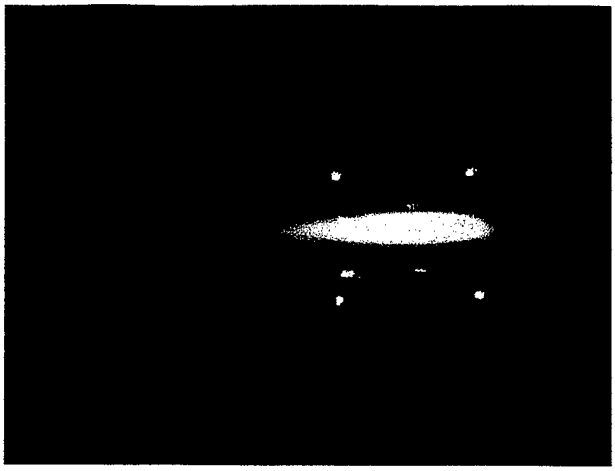

Figure 3. Photograph of the optically pumped CO-Ar plasma at P=70 torr

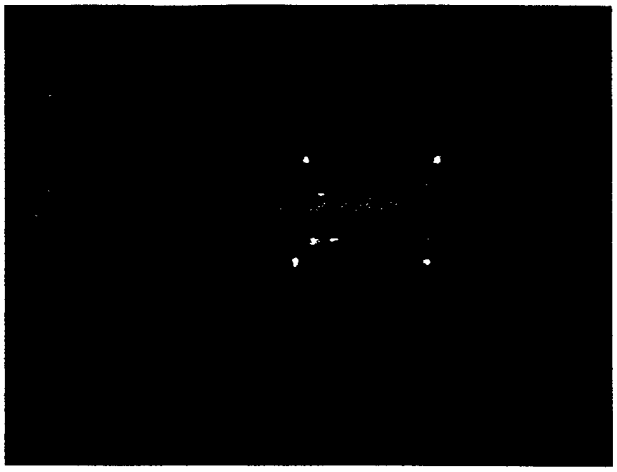

Figure 4. Photograph of the optically pumped CO-Ar plasma at P=130 torr

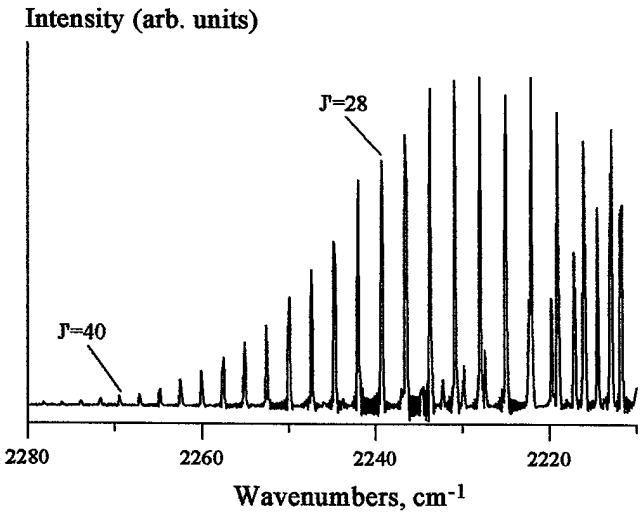

Figure 5. Typical rotationally resolved CO fundamental emission spectrum in a CO-Ar optically pumped plasma at P=70 torr.

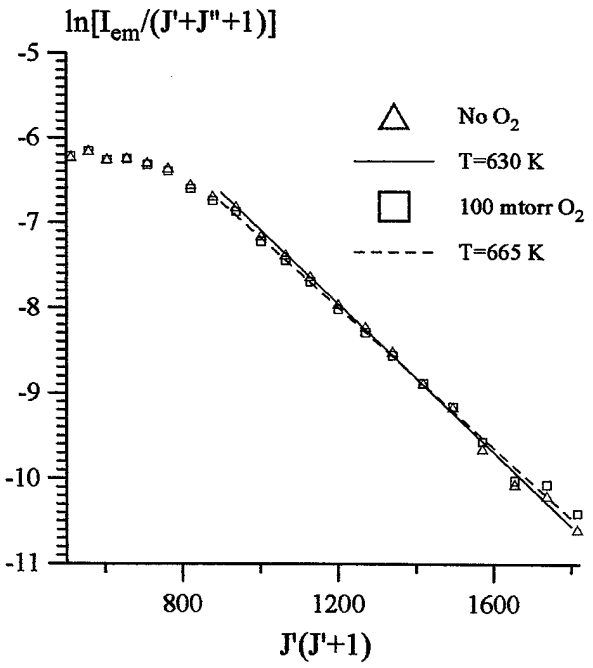

Figure 6. Boltzmann plots used for the rotational-translational temperature inference in CO-Ar and CO-Ar-O_2 optically pumped plasmas at P=70 torr.

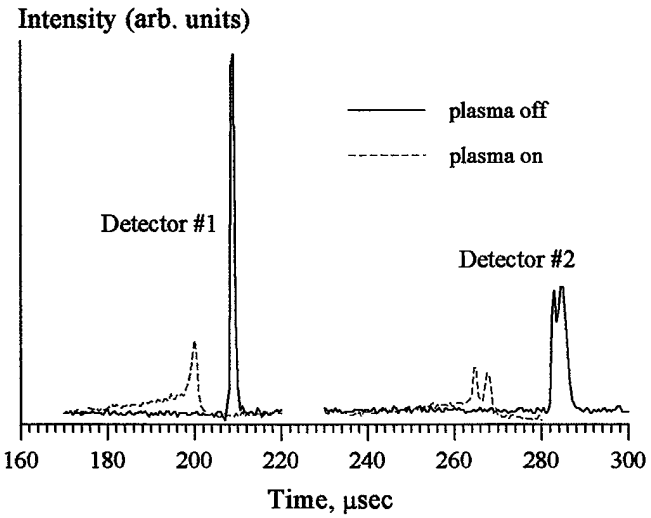

Figure 7. PAD signals (density gradient distributions) in a cold CO-Ar mixture and in a CO-Ar optically pumped plasma at P=70 torr.

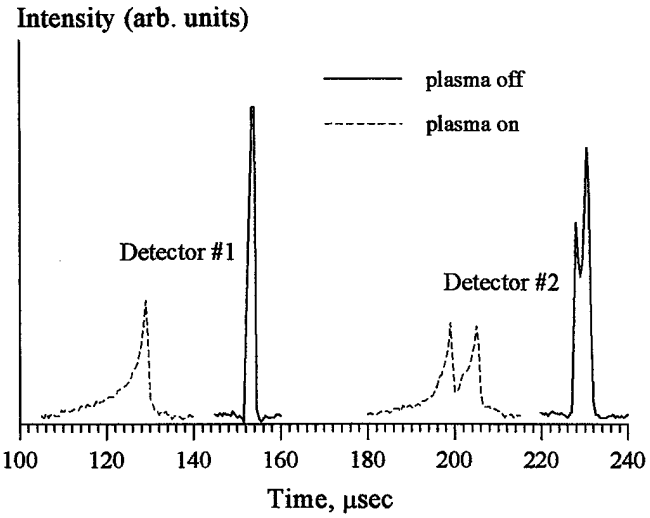

Figure 8. PAD signals (density gradient distributions) in a cold CO-Ar mixture and in a CO-Ar optically pumped plasma at P=130 torr.

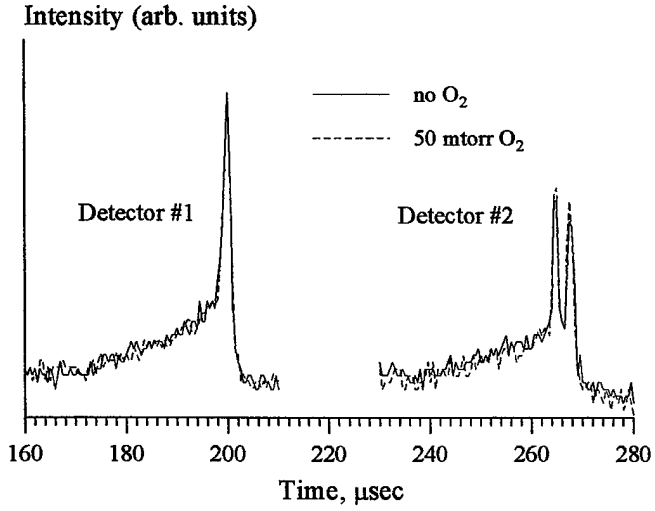

Figure 9. PAD signals in CO-Ar and in CO-Ar-O_2 optically pumped plasma at P=70 torr.

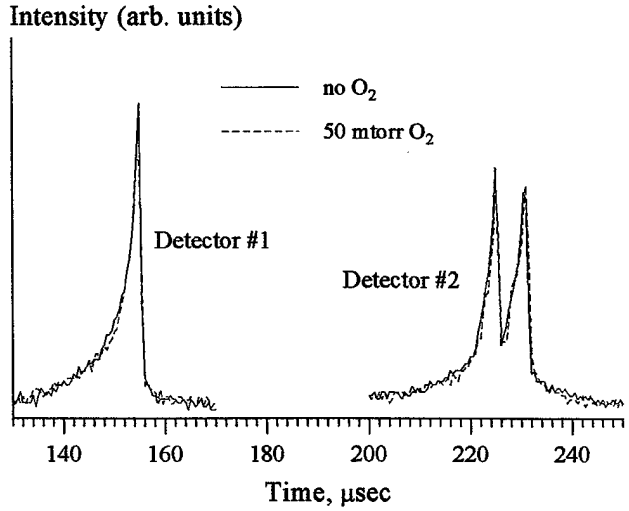

Figure 10. PAD signals in CO-Ar and in CO-Ar-O_2 optically pumped plasma at P=130 torr.

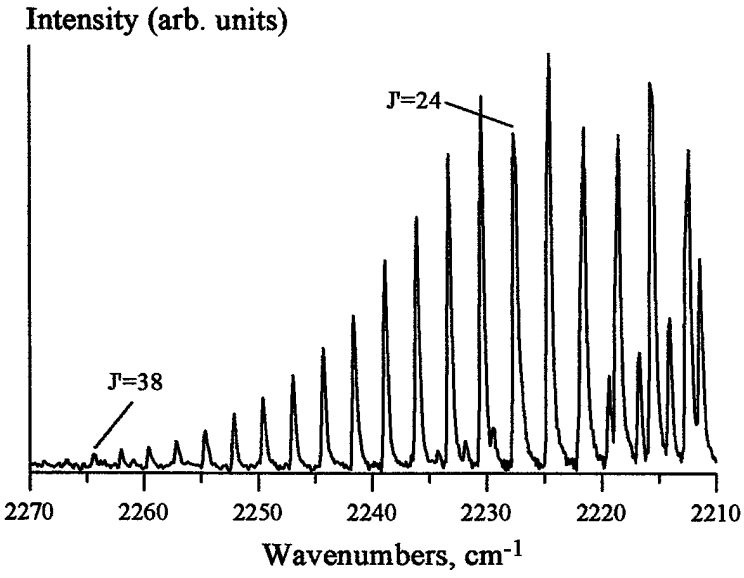
Intensity (arb. units)
J'=24
J'=38
2270
2260
2250
2240
2230
2220
2210
Wavenumbers, cm-1

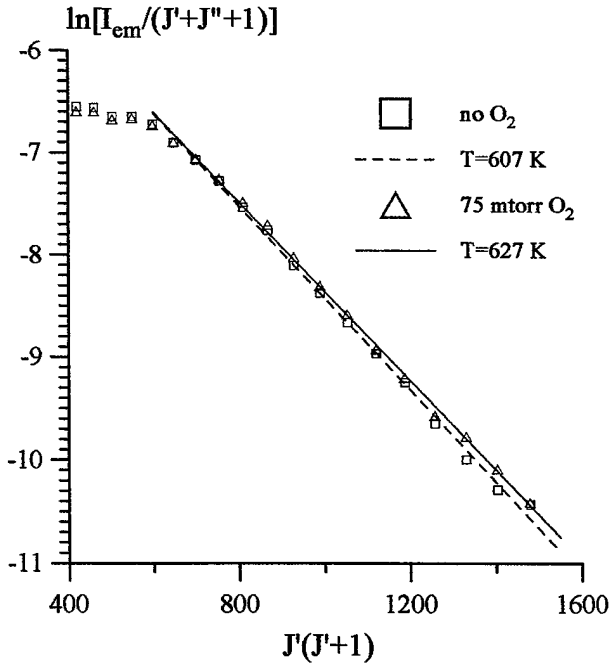
ln[Iem/(J'+J"+1)]
-6
-7
-8
-9
-10
-11
400
800
1200
1600
J'(J'+1)
no O2
T=607 K
75 mtorr O2
T=627 K

2. Two and Three Dimensional Steady Shocks

Studies in Supersonic Nonequilibrium Plasma Wind Tunnels

2.1 Experimental Characterization of Shock Dispersions in Weakly Ionized Nonequilibrium Plasmas

AIAA 99-3671

EXPERIMENTAL CHARACTERIZATION OF SHOCK DISPERSIONS IN WEAKLY IONIZED NONEQUILIBRIUM PLASMAS

R. Yano, V. Contini, P. Palm, S. Merriman, S. Aithal,
I. Adamovich, W. Lempert, V. Subramaniam, and J. W. Rich

Nonequilibrium Thermodynamics Laboratory
Dept. of Mechanical Engineering
The Ohio State University, Columbus, OH 43220-1107

30rd Plasmadynamics and Lasers Conference
28 June - 1 July, 1999 / Norfolk, VA

AIAA 99-3671

EXPERIMENTAL CHARACTERIZATION OF SHOCK DISPERSIONS IN WEAKLY IONIZED NONEQUILIBRIUM PLASMAS[1]

R. Yano[2], V. Contini[2], P. Palm[3], S. Merriman[2], S. Aithal[4],
I. Adamovich[5], W. Lempert[6], V. Subramaniam[6], and J. W. Rich[7]

Nonequilibrium Thermodynamics Laboratory
Dept. of Mechanical Engineering
The Ohio State University, Columbus, OH 43220-1107

Abstract

Experiments have been conducted to investigate possible shock weakening in a weakly ionized supersonic gas flows. A supersonic flowing afterglow wind tunnel was used. The tunnel produces a highly nonequilibrium flows with low gas kinetic temperatures. The tunnel operating characteristics are described. Steady supersonic flows are maintained for tens of seconds to complete steady state, depending on plenum pressure. Attached shock structure on the nose of 30° wedges with and without ionization in a M=3 flow was studied. No significant influence of ionization on the shock strength was seen. Ionization fractions (n_e~10^{10} cm^{-3}, n_e/N~10^{-8}), however, were at the lower end of the range in which shock modifications have previously been reported. Further studies will focus on flows with higher electron densities and over a range of Mach numbers.

---

[2] Graduate Research Assistant
[3] Visiting Scholar from Institute für Angewandte Physik, University of Bonn, Germany
[4] Post-Doctoral Researcher
[5] Research Scientist, Senior Member AIAA
[6] Associate Professor, Senior Member AIAA
[7] Ralph W. Kurtz Professor, Associate Fellow AIAA

1. Introduction

Shock wave propagation in weakly ionized plasmas (ratio of electron to gas density, or "ionization fraction", $n_e/N \sim 10^{-8}$-10^{-6}) has been extensively studied for the last 15 years, mostly in Russia [1-11], and recently in the U.S. [12,13]. The following anomalous effects have been observed: (i) shock acceleration; (ii) non-monotonic variation of flow parameters behind the shock front; (iii) shock weakening; and (iv) shock wave splitting and spreading. These effects have been observed in discharges in various gases (air, CO_2, Ar) at pressures of 3-30 Torr, and for Mach numbers M~1.5-4.5. They also persist for a long time after the discharge is off (~1 ms in air [2,9]).

As is well known, shock wave acceleration can be qualitatively explained by gas heating in the discharge and/or by energy relaxation of the species excited in a discharge. A number of one-dimensional models have been proposed that predict acceleration of the shock traveling in a vibrationally excited gas (e.g. moist nitrogen), or across a temperature gradient [14-16]. Energy relaxation models also predict non-monotonic variation of flow parameters behind shocks in molecular gas plasmas. However, they fail to explain why these effects occur in monatomic gases such as argon, where much less energy is stored in the internal degrees of freedom. Further, none of the existing models explain effects (iii) and (iv), that is, anomalous shock absorption and dispersion. In the experiments at P=10-30 Torr, the shock is observed to split into a series of two or more individual shocks at ionization fractions as low as $n_e/N \sim 10^{-8}$ (see Fig. 1, [12]). These individual shocks become separated by tens of millimeters at $n_e/N \sim 10^{-6}$ (see Fig. 2, [9]).

At the present time, no consistent theoretical model has been advanced which explains all of the features of these various experiments. If the level of plasma heating and the magnitude of thermal gradients are as small in these experiments as reported, the plasma shock strength reduction is a strikingly unexplained result. Global gas dynamic analysis by the OSU group [17] indicates that transport of energy of the order of 100 W/cm^2 across the shock wave would be required to achieve the reported levels of shock wave dispersion. There is no process yet identified supplying this flux for any of the different gas species used in the experiments.

A major complexity with previous experiments on these anomalous shock weakening and dispersion effects has been that the experiments use short-duration test facilities. These experiments are in two general classes, each of which have been repeated in the U.S. [12,13]. In the first class, a shock wave is propagated into a previously ionized, non-flowing (or very slowly flowing) gas [12]. This is essentially a shock tube experiment in which the test gases have been pre-ionized, usually by some type of steady state electric discharge. In the second class, a model (usually, a small sphere) is projected at supersonic velocities into, again, a previously ionized, non-flowing gas [13]. This is essentially a ballistic range experiment in which the test gases have again been pre-ionized by a steady-state electric discharge. In both classes of experiment, the test duration is of the order of milliseconds, and the shock structure must be observed "on the fly", during a short period as the structure passes the measurement stations.

A second, more remediable complexity is the control and measurement of the thermodynamic parameters of the test plasma. Ideally, the preionized test plasma should be of uniform properties throughout the spatial and temporal domain of the experiments. It is desirable to have uniform gas temperature (or uniform energy distribution), uniform

gas pressure, uniform species concentration, and uniform electron temperature and density throughout the test region, and these should remain constant except as perturbed by the passing shock structure. These are difficult test conditions to achieve in any real electric discharge in gases. In principle, such conditions are most easily achievable in a purely thermal plasma, in which the test gas is heated to a uniformly high temperature at which the ionization level desired is merely the equilibrium Saha ionization fraction. However, without exception, all the experiments for which shock weakening is reported occur in a nonequilibrium plasma, for which the ionization level is considerably above that provided by equilibrium ionization. It even more difficult to guarantee uniform properties in such plasmas, and in the absence of equilibrium, it becomes mandatory to investigate the distribution of energy. Improved control and measurement of plasma properties in the test gas is needed.

The experiments conducted in the program reported here represent an effort to address and circumvent the complexities noted in previous experiments. The present experiments are conducted in a new, unique, steady-state supersonic flow facility, with well-characterized, near uniform, nonequilibrium plasma properties.

2. Experimental Facility

The facility being used here is a recently-developed, small-scale, nonequilibrium plasma wind tunnel. As noted above, operation is effectively steady-state, in contrast to the shock tube and ballistic range studies which have been the most common type of previous laboratory investigations. This wind tunnel is the high-pressure-discharge/supersonic-flowing-afterglow apparatus of Fig. 3. The figure shows an overall schematic (approximately 1/2 full size) of the entire system. Flow direction is indicated by the arrows. The upstream "discharge" section, labeled on the figure, is an aerodynamically-stabilized, self-sustained glow discharge, developed and patented by one of the OSU group and co-workers under a USAF contract for use in gas laser systems [18-20]. With this simple system, it is possible to generate diffuse, stable glow discharges in pure molecular gases (N_2, etc.) to pressures of at least 2/3 atm. (500 Torr), or in mixtures of these gases with He, which improves thermal transport in the positive column, to pressures of at least 6 atm. The discharge section is contained by a quartz tube of rectangular cross-section. True glow discharge conditions exist at the exit of the discharge, which forms the throat of the downstream supersonic nozzle. This throat, again of rectangular cross-section, is made in a 1/8 " copper flange, which also forms the downstream electrode of the discharge. Conditions of the gases at the throat exhibit the marked thermal disequilibrium characteristic of the positive column of a molecular glow discharge; the heavy species temperature (the translational/rotational mode temperature) is cold (~300 K for an uncooled discharge tube), the energy in the vibrational mode is high (0.1 to 0.2 eV per diatomic molecule), the electron density is $\sim 10^{10} cm^{-3}$, and the average electron energy is in the 1.0 eV range.

Downstream of the discharge section is the supersonic nozzle, as shown. This is a two-dimensional expansion, the planform (expansion plane) being shown. The nozzle is made of transparent acrylic plastic, which allows optical access to the expansion. The nozzle is aerodynamically contoured to provide boundary layer relief and uniform supersonic flow in the test section at a supersonic Mach number in the M = 3 range, for

the tests reported here. However, fabrication and use of a range of nozzles with varying expansion ratios and test section lengths is straightforward and rapid. The system is connected, through a simple channel diffuser, to a ballast tank pumped by a several hundred cfm vacuum pump. Run durations for the M = 3 case of approximately one minute are attained; longer run times can be achieved at higher operating pressures, where diffuser recovery increases.

A critical feature of the nozzle operation is that, for the test gases used, electron-ion recombination is sufficiently slow that the ionization fraction does not significantly decrease in the expansion into the test section of the tunnel. As a specific example, we take the case of a pure N_2 flow, expanding from a plenum (discharge) pressure of 0.6 atm. The entirely dominant electron removal mechanism in the downstream nozzle afterglow will be dissociative recombination of nitrogen, with a rate not exceeding $\sim 10^{-7}$ cm^3/sec for unexcited nitrogen [21]. In this case of a pure N_2 flow, the recombination length is ~4 cm. The total streamwise length in which the ionization fraction does not significantly change ($n_e(x)/n_e(0) \geq 1/e$) is expected to be longer than this due to the decreasing flow density (by about a factor of 4 at M=2). Inhibition of recombination by vibrational and electronic excitation also extends this length. Addition of He is expected to greatly increase the effective recombination length (up to an order of magnitude) for the following reasons:

(i) the dominant helium ion in the medium and high pressure plasmas is He_2^+ due to the fast ion conversion process $He^+ + He + M \rightarrow He_2^+ + M$; the lifetime of He^+ ion with respect to the conversion is ~1 μsec at P=100 torr [21];

(ii) dissociative recombination is still the dominant recombination mechanism in weakly ionized inert gas plasmas; the recombination rate for He_2^+ is $\sim 10^{-8}$ cm^3/sec (an order of magnitude smaller than for N_2^+ [21]).

Note that the high level of vibrational excitation existing at the nozzle entrance persists throughout the nozzle length, for flows in pure N_2. The vibrational relaxation time of pure N_2 at room temperature is of the order of a second at atmospheric pressure; at the reduced pressures and temperatures in the expansion, these times are even longer [22]. The nitrogen vibrational mode energy content is essentially frozen at the throat values. In order to vary the N_2 vibrational energy content, He can be added in the discharge; the system can be run stably even with several atmospheres of added He. By this means, it will be possible to quench N_2 vibrationally excited metastables entirely in the expansion, if desired. Regardless of the ratio of He to the diatomics, the free electron energies are controlled by the close coupling of the electrons with the N_2 vibrational mode. Detailed modelling and predictive studies of such flows have been the subject of very recent work by the OSU group [23] Results of modeling calculations for the tunnel conditions of the present tests are presented in Appendix I.

Summarizing, the system is, in effect, a small supersonic wind tunnel, but with a critical difference. An electric discharge forms the high pressure plenum for an, otherwise, conventional supersonic nozzle expansion section. However, this is *not* an arc-heated tunnel. The electric discharge is a diffuse, glow discharge, achieving an extreme non-thermal (nonequilibrium) gas state in the tunnel plenum. This state is characterized by high energy content in internal molecular energy modes, principally the vibrational mode of the nitrogen gas, and a quite low rotational/translational mode temperature. On the other hand, the average energy of the free electrons is rather high, of O[1 eV]; if the

electron gas were in equilibrium, this would correspond to an electron temperature of O[10^4 K]. Although the electrical power into the discharge is rather high, ~ 500 W per cm^3 of discharge volume, greater than 90% of this input electrical power goes into the vibrational mode of the test gases. In contrast to an electric arc, very little of the power goes directly to gas heating. Indeed, the walls of the tunnel are made of transparent acrylic plastic ("Lucite"). We are using the type of diffuse glow discharge commonly used to excite infrared molecular lasers, such as the well-known N_2/CO_2 and CO lasers. Usually, however, such glow discharge operation is maintained at small fractions of atmospheric pressure. Here, the aerodynamic stabilization technique employed inhibits glow-to-arc transition in the discharge, and permits stable glow discharge operation at atmospheric pressures. Operation at such relatively high plenum pressures creates a supersonic flow, of reasonable quality, in the test section of the tunnel. As we will show, the flow in the test section is typically ~ 75% inviscid core. We produce a uniform, supersonic gas flow, with a weak level of ionization, with low translational/rotational mode temperatures. Test section pressures are of the order of 10 Torr. This is quite close to the environments for which anomalous shock weakening effects are reported in [1-13]. We note, however, that the previous experiments cover a rather wide range of conditions, and, in many of the results, all details of the plasma parameters were not measured or were incompletely reported. In the present facility, the plasma/gas parameters are well characterized and controlled.

For the shock dispersion/weakening studies reported here, a wedge is inserted into the supersonic ionized flow as shown in Fig. 3. With this system, the effects of nonequilibrium plasmas on the structure and stability of the resultant oblique shock, attached to the nose of the wedge, can be studied in detail, in a steady and well-controlled plasma environment. The basic plan of the experiments is to measure the angle of the oblique shock attached to the wedge, under both discharge-on and discharge-off conditions. It has been reported that the effect of the plasma is to weaken the shock. This gives an effect on the shock angle similar to raising the gas temperature, i.e., the apparent Mach number of the shock is reduced. Fig. 4 shows a standard shock polar for a diatomic gas (ratio of specific heats, γ, = 1.4). Note that for a 30° total angle wedge (15° flow deflection angle), a reduction in the apparent shock Mach number from M = 3 to M = 2 would create a change in the shock wave angle of more than 15°. Changes of this magnitude, between the plama-off and the plasma-on conditions, would be readily detectable in the present system.

3. Diagnostics

Diagnostic measurements are fairly straightforward, due principally to the steady-state nature of the experiment.

3.1 Static Pressure Measurements

Pressure is measured at a variety of locations in the tunnel using static wall taps connected to capacitance manometers (MKS "Baratron"). Fig. 5 shows the location of the pressure measurement taps on one of the most throughly instrumented nozzles used in the present experiments. As shown, pressure is measured at the following locations:

a) In the delivery line to the discharge, upstream of the gas injector for the discharge. For optimum operation of the aerodynamically stabilized discharge, the flow through the injector, into the discharge, should be choked. For this, the pressure upstream of the injector should be approximately double the discharge pressure. For this reason, the delivery line pressure was usually measured for all runs.

b) Discharge pressure. This was measured by a wall tap on the upstream face of the discharge section, and, again, was measured for all runs.

c) Static pressure along the nozzle, in the test section, and at the diffuser entrance. As shown, pressure is measured at three axial locations along the nozzle expansion, in the test section, and at the entrance to the diffuser. In addition to all these axial measurements, at the end of the nozzle, two additional taps measured the transverse pressure distribution.

Not all of these measurement stations were used for all of the experiments, as some of the pressure taps interfered with electron density measurements, with flow visualization studies, or with schlieren measurements of the shock angle. In addition, the tap in the middle of the test section is blocked by the model (the wedge) during shock angle measurements. However, the ease of fabrication of the plastic flow channels allows several test sections, of identical contours, to be used, with the number of taps varying depending on the other measurements planned. The experimental protocol is to fully characterize the flow pressure distribution using a channel with all the taps as shown in Fig. 5. In subsequent tests, pressure is always measured upstream of the injector, in the discharge, and at one location in the flow channel. These are sufficient to establish that the subsequent tests are replicating the static pressure conditions of the more complete measurement series.

3.2. Discharge Voltage and Current.

The discharge is powered by a regulated, current-limited, 50kV/50mA d.c. supply (Del Corp. Model No. RHVS 50-2500). The discharge power circuit is ballasted by 400 KΩ resistance in series with the discharge load. Voltage and current are read from the meters in the power supply.

3.3 Electron Density

For the measurement of electron density in the supersonic afterglow, the nozzle is equipped with with pairs of transverse strip electrodes, placed flush in the nozzle walls. These electrodes are in effect probes, which can be used to infer the electron density in non-self-sustained discharges, such as the present flowing afterglow. The theory of such probes (Thomson discharges [24]) is given a previous paper from the Nonequilibrium Thermodynamics Laboratory, where their use for associative ionization studies was reported [25]. Using this technique, the electrons can be almost completely removed from the flow by applied small d.c. potentials across the electrodes. As shown in [25], the

electron concentration can be inferred from the measured current and saturation voltage. With this technique, it is also possible to vary the electron concentration in the test section without changing any of the plenum discharge parameters.

3.4. Shock Angle

A conventional schlieren system is used to visualize the oblique shocks attached to the nose of the wedge model. A schematic of the system is shown in Fig. 6. Shock pictures are recorded with a framing camera as shown on the schematic. With this system, quite good shock visualization is obtained for runs in air or nitrogen with plenum pressures in the range 0.6 atm $< P_o <$ 1.0 atm. Fig. 7 shows a typical schlieren picture of the shock pattern on a 30° total angle wedge in the tunnel, operating at M = 3.0 and P_0 = 2/3 atm of pure N_2.

3.5. Flow Visualization

The discharge section is made of quartz glass, and the nozzle, the test section, and the diffuser are made of acrylic plastic. The walls of the entire tunnel are therefore transparent, except for where there is some blocking by electrodes or pressure tap fittings. This transparency, combined with the large energy storage and subsequent light emission by the internal modes of nitrogen in the flow, provides a unique flow visualization. The long radiative lifetime of the nitrogen metastables creates a fluorescence that persists throughout the length of the flow channel. This is displayed in the photograph of Fig. 8, which shows the tunnel in operation in nitrogen. The nozzle, test section, and diffuser are filled with the nitrogen afterglow, arising primarily from the well-known 1st Positive nitrogen bands. The radiating N_2 electronic states are primarily the N_2 B $^3\Pi$. The actual fraction of flow enthalpy lost through this radiation is quite small; most of the flow internal energy is essentially frozen in the vibrational mode. As can be seen from Fig. 8, radiation is more intense from the slower, higher density flow regions in the discharge and upstream in the nozzle throat, and is relatively uniform from the steady inviscid core flow in the test section and diffuser sections. Regions of flow separation and stagnation, in which molecular internal energy is quenched, do not fluoresce.

4. Test Results

4.1. Gas Dynamic Performance

Extensive gas dynamic tests were conducted to determine the extent and duration of the supersonic test flows that could be achieved in the tunnel. All tests to-date have been conducted in a nozzle with the planform dimensions shown in Fig. 5. As shown in the figure, the channel is essentially two-dimensional, of rectangular cross-section. However, the top and bottom surfaces of the channel diverge slightly, to allow for boundary layer displacement; this feature is shown on the side view on Fig. 5. The initial gas dynamic tests were performed with the top and bottom channel separation varying from 0.3 cm at the throat to 1.0 cm at the diffuser exit, as dimensioned in the figure. The tunnel was operated with dry air or nitrogen, expanded from P_0 = 1 atm. plenum conditions, with the electric discharge turned off. For these conditions, steady flows of

approximately 1 minute duration were maintained. The static pressures, P_i, measured during such a test are recorded on Fig. 5, next to the correspondingly numbered (i) measurement tap. Shown immediately below the pressure reading is the effective Mach number of the flow at that tap location, inferred from the measured pressure ratio P_0/P_i and the standard isentropic relation:

$$P_0/P_i = [1 + (\gamma-1)M^2/2]^{\gamma/(\gamma-1)}$$

It can be seen that the flow accelerates to M = 3.8 at the entrance to the test section. Flow is supersonic and reasonably constant across most of the channel at this location. As indicated by the transverse pressure readings at taps 3 and 5, flow is slightly slower nearer the walls, at the beginning of the actual boundary layer. At the diffuser entrance, there is already a separation shock pattern decelerating the flow, and the pressure begins to rise (tap 6). The most downstream measurement, at tap 7, near the diffuser outlet, gives an indication of the very moderate recovery afforded by the simple diffuser geometry for such a relatively low density expansion. The pressure at the diffuser exit is P_7 = 23.3 Torr, giving a recovery factor of only P_7/P_0 = .03. When the pressure in the dump tank, downstream of the diffuser, is allowed to rise to values exceeding P_7, a separation shock pattern moves up the diffuser into the test section, eventually ending the supersonic flow. This behavior is shown in Fig. 9, which plots the static pressure at the entrance to the test section, P_4, as a function of time during a run when the ballast tank pump was valved off, and the back pressure allowed to rise as the tank filled. It can be seen that, after starting, a steady, M = 3.8 supersonic flow corresponding to P_4 = 6.2 Torr is maintained for almost 60 seconds. After this, pressure rises continously at this station. This rise is created by an oblique-shock separation pattern, originating on the tunnel walls, moving up into the nozzle, and rapidly decreasing the extent of the inviscid supersonic core.

The planar (2-D) nozzle expansion contours were designed for M = 3 supersonic operation in the test section. The tests reviewed above, showing an M = 3.8 test section Mach number, indicate that the divergence of the top and bottom sections, as shown in Fig. 5, is an over-correction for boundary layer growth. The higher-than-design Mach number is created by some expansion of the core flow in the vertical direction. Accordingly, subsequent tests in the program were conducted with the nozzle top and bottom divergence slightly modified from that shown in the figure. In all subsequent tests, dimensions and contour are the same as shown in Fig. 5, with the single exception that the height of the channel at the diffuser exit was 0.65 cm, rather than the 1.02 cm value shown. With this modification, static pressure at the test section corresponded to M = 3 operation; overall operation and relative pressure distribution was otherwise similar to that observed previously.

The measured gas dynamic performance of the tunnel is strikingly confirmed by model calculations for a nitrogen flow, performed using the OSU compressible two-dimensional Navier-Stokes code. The calculations have been made for nitrogen with stagnation parameters P_0=1 atm and T_0=300 K. The nozzle contour and dimensions used in the calculations are those of Fig. 5. Some of the results of the model calculation are shown in Figures 10-12. Figures 10 and 11 show the centerline Mach number distribution

and the flow velocity profile at the end of the nozzle expansion (in front of the wedge placed in the test section). One can see that the flow in the test section reaches M=3, which is in good agreement with the Mach number values determined by the static pressure measurements and by subsequent, schlieren, oblique shock angle measurements (section 4.4 below). Also, about 80% of the flow is the inviscid core (Fig. 11). This is in quite reasonable agreement with the transverse pressure measurements made in the tunnel.The boundary layer is relatively large in the low density tunnel, but most of the test flow is essentially inviscid. Figure 12 shows the Mach number contour plot and the oblique shock attached to the model in the test section. Again, these correspond well with schlieren (sect. 4.4) and flow visualization (sect. 4.5) measurements.

4.2 Electric Discharge Performance

The electric discharge section is small, its walls formed by a contoured quartz tube of rectangular cross section, with dimensions approximately 1 x 1 cm at the (larger) upstream end. The effective length, from the upstream injector/anode end to the downstream nozzle-throat/cathode end, is 2 cm. Details of the design and operational characteristics of discharge tubes of this type are given in [18 - 20]. Basically, the aerodynamic stabilization technique involves injecting the entire gas flow into the discharge through small slots on the top and bottom walls of the discharge tube. Small copper strips flush with the slot edges form the anode. Flow through the slots is choked, so that gas velocity past the anode is sonic, and gas density is relatively high. Immediately after the slot, the gases expand (subsonicly) into the discharge tube, and flow through the discharge at lower velocities. This design insures a high speed, relatively dense, gas flow across the face of the anode. This flow is transverse to the current direction. Incipient arc filaments, regions of higher temperature and lower density which could coalesce into arc breakdown, are convectively dissipated by this transverse flow. This technique, combined with current limiters in the power supply, inhibits arc formation and subsequent glow-to-arc contraction in the discharge. It becomes possible to run a diffuse glow discharge at very high pressures. While conventional glow discharge tubes in pure molecular nitrogen will collapse into an arc at pressures of a few tens of Torr, the present device will maintain a true glow at pressures of an atmosphere.

The above features are observed when operating the discharge. With pure N_2 in the tube, at pressures of 2/3 atm, a substantial voltage (~30 kV) must be applied across the electrodes to strike the discharge. When this voltage is applied, however, essentially all of the discharge section is filled with the positive column of the glow. The glow is uniform, with uniform emission intensity. Current can be increased to 20 mA and this stable, uniform discharge can still be maintained. At this level, the applied voltage is 34 kV, and the input power to the discharge is 680 W. This is a power loading into the discharge tube of ~500 W/cm^3. If current is increased beyond the 20 mA level, incipient arc filaments are observed, forming and extinguishing. Persistence in increasing the current to even slightly higher levels results in contraction of the discharge into a single, narrow, very bright, true arc. The device is not generally run to this limit (at least, not

intentionally!), since the action of the arc, specifically the gas heating and the rapid erosion of the electrodes, can cause severe damage.

The kinetics, the extreme nonequilibrium distribution of internal energy, and the electron physics of such a glow are very well-known and understood. Calculations for the coupled electron energy distribution and the vibrational states have been existing since the development of electrically excited molecular gas lasers. Fig. 13 shows the standard result for such a discharge as given by Raizer [21]; the OSU modeling code is essentially identical. What is plotted is the fraction of the discharge input power going into the various modes of the flowing gas, as functions of E/N, the ratio of the applied d.c. electric field in the discharge to the total gas number density. The E/N operating point for the experimental conditions described in the preceding paragraph is indicated on the figure (E/N = 4.3 x 10^{-16} V cm^2). It can be seen that at this E/N, > 95 % of the input electrical power is going into the vibrational mode of the N_2. The very small remaining fraction of the input power goes into creating ionization, rotational/translational heating, and electronic state excitation. Indeed, the electron density created in the discharge is rather small. The electron density is inferred with fair accuracy from the measured discharge voltage, current, and pressure. The electric field, E, is determined as the ratio of the applied voltage to the electrode separation. Since gas translational mode heating is negligible, gas number density, N, is determined from the measured discharge pressure and the ideal gas law for 300 °K gas. For this E/N operating point, the electron drift velocity, v_d, is known from these standard modeling calculations to be ~ 5 x 10^6 cm/sec. With the drift velocity known, and with the measured current, I, electron density, n_e, is inferred from the usual relation:

$$n_e = I / eAv_d,$$

where e is the electron charge and A is the discharge cross-sectional area. For the conditions stated above, this gives $n_e \approx 6 \times 10^{10}$ cm^{-3}, and the ionization fraction, n_e/N, is 4 x 10^{-9}. This electron density is typical for glow discharges; the rather low ionization fraction reflects the unusually high operating pressure of the electric discharge.

4.3 Electron Density

As described in Sect. 3.3, transverse wall electrodes were placed in the supersonic nozzle. A small regulated d.c. power supply (photomultiplier supply) was used to bias these electrodes, and the voltage-current characteristic of these probes was measured. Fig. 14 shows a typical voltage-current characteristic from a probe located at the M = 3 station at the beginning of the test section. For these tests, plenum gases were again 2/3 atm of N_2, with, in this case, some added He (~1/3 atm). Note that, as is typical of electrostatic probes, current (18 μA) can be drawn at zero applied voltage; negative bias can be applied to null out this current and thereby determine the plasma potential. Notice that the current increases slowly with increasing bias, and almost saturates near 300 - 400 V. In this (near-saturation) region, most of the free electrons are being drawn by the probe electrodes, and local electron density can be inferred from this saturation voltage and corresponding current, using the Thomson discharge theory [25]. The electron density

inferred from these probe measurements is reasonable consistent with the upstream n_e values inferred at the plenum, and with the known recombination rates for the N_2 plasma. For the pure N_2 flows, with $P_0 = 2/3$ atm, $n_e = 2 \times 10^9$ cm^{-3} in the M = 3 test section, and $n_e/N = 2 \times 10^{-9}$ at that location.

The near-saturation voltage, ~ 350 V, is well below breakdown for the gas density and electrode separation at this point in the nozzle. When the plenum discharge in turned off, no current is drawn through the probe at this voltage nor at any lower bias. To draw current through the probe electrodes without the flow between them preionized by the upstream plenum discharge, much higher voltages must be applied, creating breakdown. However, if this is done, the resultant discharge is a very unstable, spatially inhomogeneous transverse affair, giving primarily local arcs through the boundary layer. However, if, for the case with the plenum discharge on, the voltage on the probe is increased beyond the near-saturation region, a much different behavior is seen. With voltages beyond the near-saturation region, the current begins to rise rapidly (Fig. 14). Fig. 15 shows the extended voltage characteristic, with the applied voltage extending to almost 2 kV across the small channel height (0.5 cm). At the higher voltages here, we are well beyond breakdown E/N for an unionized gas. However, we appear to be driving a quite uniform transverse discharge across an M=3 flow channel. At these high voltages and transverse currents, we clearly appear to have discharge ignition, but with a uniform transverse current distribution in the channel. Visual observation shows an increasing local luminosity between the probe electrodes, evenly distributed across the inviscid core flow in the channel, but not extending into the boundary layer regions near the walls. This luminosity increases with the current. Only beyond the highest values recorded, 0.14 mA at 1.9 kV, did transverse arc filaments began to appear. The voltages were not increased much beyond this point.

4.4 Shock Angle and Shock Dispersion Tests

For study of the possible shock dispersion/weakening by the ionization of the supersonic flow, a 30^0 total angle wedge was placed in the test section. The wedge extends from the top to the bottom wall of the flow channel, i.e., this reasonably approximates a two-dimension flow. The leading edge of the wedge is 0.3 cm downstream of the end of the nozzle section, i.e., 0.3 cm downstream of position 4 in Fig. 5. The wedge extends for 2 cm in the downstream direction, forming an isosceles triangular planform with apex pointing upstream. The schlieren system described in Sect. 3.4 is used to visualize the oblique shock attached to the leading edge of the wedge. Fig. 7 shows a typical schlieren image of the shock, again for the $P_0 = 2/3$ atm of pure N_2, M = 3 test conditions. The wedge planform and the quite straight oblique shock on either side of the nose can be seen. The total shock angle, of approximately 65^0, implies a flow Mach number of 3.1, which is entire consistent with the measured pressure ratio at the test station, as well as with the predictions of the Navier-Stokes modeling code.

With this model, and for these flow conditions, an extensive series of test runs were performed to investigate the possible weakening or dispersion of the shock by the

effect of ionization in the test flow. The test procedure for these runs was to initiate the flow in the tunnel, confirm steady state conditions by static pressure measurements, and to record the shock schlieren picture over several seconds and several frames, with the electric discharge in the plenum off. After this, at several seconds into the run, the plenum electric discharge was struck, with voltage and current set to pre-selected values. The tunnel operation was continued for several more seconds and the shock schlieren pictures were again recorded for several frames. Finally, in the same run, the discharge was turned off, and the shock schlieren pictures again recorded for several frames. During the entire run, the pressures were monitored to insure that steady supersonic flow was being maintained throughout the test duration, and that back pressure did not exceed recovery values. Basically, then, a test run consisted of several measurements of shock position for a "plasma off" flow, followed by several measurements with "plasma on", followed by several more measurements with, again, "plasma off".

In no runs was any substantial break-up or dispersion of the oblique shock observed. In order to determine if there was any overall change in the shock strength between plama-on and plasma-off conditions, the shock angle was measured for every frame in each test run. Measurement was by the operator placing cursor lines along the shock front on the computerized schlieren picture, and recording the angle as given from the computer. Table 1 is a summary of the data for four such test runs, two for plenum electric discharge currents of 15.7 mA, and two for higher input powers, with plenum electric discharge currents of 20 mA. Each of the shock angle measurements reported in Table 1 represent an average of many data frames. It can be seen that the accuracy with which the shock angle can be measured for these conditions is $\pm 3^0$, with the average shock angle being near 66^0. In addition to the average shock angle measured in the runs, Table 1 also records the Mach number and the temperature ratio, T/T_0, corresponding to the measured shock angle. Static pressure at the entrance to the test section was measured during all of these runs. For these, P = 11.0 Torr, giving $P/P_0 = .022$, implying a test section Mach number M = 3.1, in excellent agreement with the shock angle measurement, as noted above.

With the strongly nonequilibrium nature of the flow, there is no single static temperature characterizing the local (static) flow enthalpy. However, in these continuum flows, the translational and rotational molecular modes are equilibrated, and there is a unique temperature characterizing the energy in these modes. This translational/rotational temperature is what is denoted without further qualification as gas temperature, or static temperature, T, throughout this report. Stagnation temperature, T_0, is defined conventionally: it represents the total temperature that the flow gases would achieve if the gas were to be decelerated to zero velocity, and all modes - translation, rotation, vibration, electronic, were to be brought into thermal equilibrium. Since the total energy input from the discharge into the flow gases is measured, as are the flow velocities, the total (stagnation) flow enthalpy is known, and T_0 is unambiguously inferred. For the higher discharge power loading runs of Table 1, where 680 W were added to the flow, $T_0=500^0$K.

Table 1. Plasma Shock Angle Measurements

Test	Discharge Conditions	Flow Conditions	Average Shock Angle	Mach Number	T/To
1	Plasma Current: 15.7 mA	Plasma Off	64.65° $^{+2.02°}_{-2.70°}$	2.989	0.3588
	Plasma Power: 529.4 W	Plasma On	67.43° $^{+2.82°}_{-2.75°}$	2.816	0.3866
	Pressure: 0.667 Atm N_2	Plasma Off	65.55° $^{+2.35°}_{-2.49°}$	2.930	0.3681
2	Plasma Current: 15.7 mA	Plasma Off	62.99° $^{+2.44°}_{-2.52°}$	3.105	0.3414
	Plasma Power: 529.4 W	Plasma On	67.77° $^{+4.88°}_{-4.03°}$	2.797	0.3899
	Pressure: 0.667 Atm N_2	Plasma Off	63.94° $^{+2.63°}_{-3.57°}$	3.037	0.3515
3	Plasma Current: 20.0 mA	Plasma Off	62.91° $^{+1.38°}_{-1.67°}$	3.111	0.3406
	Plasma Power: 680.0 W	Plasma On	67.91° $^{+2.65°}_{-2.65°}$	2.789	0.3913
	Pressure: 0.667 Atm N_2	Plasma Off	65.23° $^{+2.04°}_{-1.18°}$	2.950	0.3648
4	Plasma Current: 20.0 mA	Plasma Off	65.33° $^{+3.29°}_{-3.72°}$	2.944	0.3658
	Plasma Power: 680.0 W	Plasma On	66.03° $^{+2.61°}_{-3.15°}$	2.900	0.3729
	Pressure: 0.667 Atm N_2	Plasma Off	64.81° $^{+1.91°}_{-2.75°}$	2.978	0.3605

The static temperature has not been directly measured in the experiments to date. However, the energy distribution in the discharge and plenum is well-characterized, as discussed previously. Using the measured flow and plasma data, the OSU nonequilibrium gas dynamic flow modeling codes have been run for the test conditions. The details of these calculations are given in Appendix I. As shown there, there is very little loss of energy from the vibrational mode in the supersonic expansion, and therefore negligible rise in the static temperature due to such internal energy transfer. This effect causes static temperature increase in the test section core flow by less than 5 ^{0}K, even for the most extreme power loading conditions. As shown in Table 2 in this Appendix, the test section static temperature for all these runs is low, T = 100 ^{0}K.

The data of Table 1 do not seem to show a significant detectable shock movement between the plasma-on and plasma-off conditions. While some of the data seem to show a slight weakening of the shock (larger shock angles) with the plasma on, the change is well within the scatter of the data. More recent runs, with better schlieren imaging than the data used in Table 1, also support this conclusion. No significant shock movement is seen for these run conditions. In addition to the use of operator-positioned cursors to measure the shock angle, "plasma-on" images have been computer-differenced with the corresponding "plasma-off" images for the same run. Again, no significant change in shock strength can be detected.

We conclude that for these test conditions, at least, any change in shock angle due to ionization in the flow is less than 3^0. As shown in the table, the corresponding change in the apparent Mach number is less than 0.3, i.e., a Mach number change of less than 10% at the M = 3 test conditions. Such change is well below the weakening effects reported in some of the literature; but any greater change would have been readily detectable by the present experiments.

4.5 Flow Visualization in Supersonic Flowing Afterglow

Color photographs of the supersonic flowing afterglow are an especially effective means of displaying the key features of these extremely nonequilibrium flows. Fig. 16 shows a photograph of the nozzle with the plasma on and the 30^0 wedge model in place. One can see the luminous boundary layers on the nozzle and model walls, dark flow separation regions in the nozzle and in the wake of the wedge, and even the oblique shock attached to the model. The striations visible in the expansion show that the electric field from the discharge penetrates into the afterglow, where steep density and electron temperature gradients result in the ionization instability causing striations. Note that the luminous regions in striations follow the equal Mach number lines (see Fig. 12), and therefore the equal density lines. We conclude that the flowing afterglow technique allows accurate flow visualization, including shocks, boundary layers, and recirculating flow regions. This method might be especially important in the low-density expansion flows where other visualization methods become less efficient.

5. Conclusions

The experiment has been designed to minimize temperature rise by dissipative processes in the test flow. The test flow is the very nearly isentropic core of the nozzle expansion, with a negligible rise in flow heating due to vibrational relaxation. The tunnel boundary layer does not extend into the test flow of the model. Any higher heating in the tunnel flow is confined to these boundary layers, where the temperature could rise to stagnation values (500 K). While such a boundary layer heating effect could conceivably increase the boundary layer thickness and decrease the isentropic core expansion, estimates suggest this effect, also, will be small. In actuality, no significant effective Mach number reduction has been observed under even the highest enthalpy loading conditions.

The results obtained, to-date, do not show any significant effect of free electrons/electric discharge on shock weakening or attenuation. Inasmuch as the present experiment has been carefully designed to eliminate any significant heating or local thermal gradient effects on the shock, these results may have especial import. However, it is important to note that the experiments to-date have been run at somewhat lower electron densities than those apparently used in other experiments giving a positive effect. Also, the strongest effects are principally claimed in the range $1 < M < 2$, substantially below the $M = 3$ values of the present tests. It is crucial to note that the present experimental approach can almost immediately be used to provide data in these test ranges. The present results demonstrate that the test and measurement techniques used here will provide easy, relatively artifact-free data in these ranges. Measurement conditions at the lower Mach numbers will be at higher electron and gas densities, greatly facilitating the experiments. The following extensions of the present studies should be pursued:

1. Tests in an $M = 2$, and $M = 1.5$ flow. Such flows will automatically have higher electron number density than the present experiments.

2. Tests in which a fast relaxant, such as small amounts of O_2, are added in the discharge. This will produce nonisentropic temperature increases, and effective shock weakening of a sufficient magnitude to be easily observable should be obtained.

3. Tests with a blunt-nose model, such as a half-circular nose, replacing the 30^0 wedge used here. The bow shock created in this flow will be quite strong close to the stagnation point, and schlieren visualization will be of good quality. Perhaps weakening effects, similar to those reported in [13], may be observed for this significantly different flow geometry.

4. Tests using the control of the electron parameters afforded by the probe electrodes in the tunnel walls. Rather than turning the main discharge on and off, we can remove a large fraction of the free electrons by applying small voltages to the probe, as we have shown. Thus, the electron density can be varied without significantly affecting the flow enthalpy. Beyond this, the effects of increasing the electron energy by running the probe

voltages into the ignition regime should be studied in detail. Will such increases eventually cause shock weakening? The results of running the transverse discharge into the arc transition regime should be examined; we can deliberately create local heating effects.

5. Finally, the utility of the present facility for studies of a wide variety of nonequilibrium fluid and plasma phenomena should be explored. More extensive diagnostics can, of course, be incorporated. Temperature measurements can be made using the N_2 plasma emission to resolve the rotational structure of these electronic bands, using the OSU optical multichannel analyser. Both temperature and vibrational energy content can be determined by adding an infra-active trace species, such as CO, to the flow gases, and using Fourier Transform Infrared Spectroscopy to resolved vibrational state emission bands. Both of these techniques are well-developed in the Nonequilibrium Thermodynamics Laboratory. An example of a broader study that should be made in the system is the power loading of a supersonic flow with the transverse wall electrode system. It has already been shown here that the present technique creates a stable, diffuse discharge with current path transverse to an $M = 3$ flow.

6. Acknowledgements

The support of MSE Technologies, Inc., under a NASA prime, is gratefully acknowledged. The support of the Director of Defense Research and Engineering (DDR&E) Air Plasma Ramparts MURI Program, managed by AFOSR for the construction of the supersonic flowing afterglow apparatus is gratefully acknowledged. The able assistance of Matthew Chidley is thankfully acknowledged. We wish to thank Dr. Jean-Luc Cambier for helpful advice and direction during the course of the program. We wish also to thank Mr. Richard Bergman, Dr. Daniel Kelley, Profs. Harvey Lam and Richard Miles, and Dr. Sergey Macheret for helpful consultation and advice.

7. References

1. A.I. Klimov, A.N. Koblov, G.I. Mishin, Yu.L. Serov, and I.P. Yavor, Sov. Tech. Phys. Lett, vol. 8, p. 192, 1982
2. A.I. Klimov, A.N. Koblov, G.I. Mishin, Yu.L. Serov, K.V. Khodataev, and I.P. Yavor, Sov. Tech. Phys. Lett, vol. 8, p. 240, 1982
3. I.V. Basargin and G.I. Mishin, Sov. Tech. Phys. Lett., vol. 11, p. 535, 1985
4. V.A. Gorshkov, A.I. Klimov, G.I. Mishin, A.B.Fedotov, and I.P. Yavor, Sov. Phys. Tech. Phys., vol. 32, 1987, p. 1138
5. A.P. Ershov, S.V. Klishin, A.A. Kuzovnikov, S.E. Ponomareva, and Yu.P. Pyt'ev, Sov. Tech. Phys., vol. 34, p. 936, 1989
6. I.V. Basargin and G.I. Mishin, Sov. Tech. Phys. Lett., vol. 15, p. 311, 1989
7. S.A. Bystrov, I.S. Zaslonko, Yu.K. Mukoseev, and F.V. Shugaev, Sov. Phys. Dokl., vol. 35, p. 39, 1990
8. G.I.Mishin, Yu.L.Serov, and I.P. Yavor, Sov. Tech. Phys. Lett., vol. 17, p. 413, 1991
9. G.I. Mishin, A.I. Klimov, and A.Yu. Gridin, Sov. Tech. Phys. Lett., vol. 17, p. 602, 1992

10. A.Yu. Gridin, A.I. Klimov, and K.V. Khodataev, High Temp., vol. 32, p. 486, 1994
11. A.P. Bedin and G.I. Mishin, Tech. Phys. Lett., vol. 21, p. 5, 1995
12. B.N. Ganguli and P. Bletzinger, AIAA Paper 96-4607, November 1996
13. Lowry, H., Blanks, J., Stepanek, C., Smith, M., Crosswy, L., Sherrouse, P., Felderman, J. and Wood, B., "Characterization of the Shock Structure of a Spherical Projectile in Weakly Ionized Air Through Ballistic Range Test Techniques", 2nd Weakly Ionized Gas Workshop, Norfolk, VA, April 24-25, 1998
14. G.V. Vstovskii and G.I. Kozlov, Sov. Tech. Phys., vol.31, 1986, p.911
15. A.Kh. Mnatsakanyan, G.V. Naidis, and S.V. Rumyantsev, in "Shock Waves and Tubes", p. 201, Proc. 16th Intl. Symp. on Shock Tubes and Waves, Aachen, July 1987
16. S.A. Bystrov, V.I. Ivanov, and F.V. Shugaev, Sov. J. Plasma Phys., vol. 15, p. 324, 1989
17. Adamovich, I.V., Subramaniam, V.V., Rich, J. W., and Macheret, S.O., AIAA J., vol. 36, p.816, 1998
18. W. Rich, R.C. Bergman, and J.A. Lordi, AIAA J., vol. 13, p. 95, 1975
19. W. Rich, R.C. Bergman, and J.A. Lordi, "Carbon Monoxide Laser Systems", Technical Report AFAL-TR-78-37, CALSPAN Corp., Buffalo, New York, April 1978;
20. R.C. Bergman, "Gaseous Discharge Stabilized Apparatus and Method", U.S. Patent 4,132,961, Jan. 2, 1979
21. Raizer, Y.P., "Gas Discharge Physics", Springer-Verlag, Berlin, 1991
22. Yarley, J.T., "Introduction to Molecular Energy Transfer", Academic Press, NY, 1980
23 Adamovich, I.V., Rich, J.W., and Nelson. G.L., AIAA J. vol. 36, p. 590, 1998
24. Thomson, J.J., and Thomson, G.P., "Conduction of Electricity through Gases", Vol. 1, Cambridge Univ. Press, Cambridge, 1928
25. Adamovich, I., Saupe, S., Grassi, M.J., Shulz. O., Macheret, S., and Rich, J.W., Chem. Phys. vol. 173, p. 491, 1993

Appendix I. One-Dimensional Nonequilibrium Flow Calculations

To estimate the effect of the gas flow heating due to relaxation of energy stored in vibrational degrees of freedom of nitrogen, we used quasi-one-dimensional nonequilibrium flow modeling calculations. The code used solves coupled one-dimensional gas dynamics equations and master equation for the populations of vibrational levels of molecules. The kinetic model incorporates processes of vibrational excitation of molecules by electron impact in the electric discharge section, as well as V-T and V-V energy transfer processes that are primarily responsible for the flow heating in the supersonic afterflow. The objective of these calculations was to determine whether the flow heating by vibrational relaxation is enough to cause substantial changes in the test section Mach number and therefore in the oblique shock angle.

The calculations have been performed for nitrogen at stagnation pressure of P_0=500 torr and stagnation temperature of T_0=300 K. The nozzle throat cross sectional

area was $A^*=0.21$ cm^2, with the area ratio $A/A^*=5.2$ and the length of the supersonic section L=10 cm.

Table 2 shows that for discharge power used in the experiments the flow heating in the inviscid core is negligibly small (static temperature in the test section increases by only about 1-5 K). This occurs due to the slow rate of vibrational energy relaxation in V-V processes and short residence time. However, heating might well be a major factor in the boundary layer where the flow is near stagnation and therefore has enough time to vibrationally relax. Indeed, for typical experimental conditions the stagnation temperature increase due to power loading by the discharge is about 200 K.

Table 2

Discharge power, W	**Test section static temperature**	**Test section Mach number**	**Test section vibrational temperature**	**Test section stagnation temperature**
0	98	3.24	300	300
120	98	3.24	1000	335
767*	99	3.23	2000	522
1628	103	3.21	3000	772

* Close to the experimentally measured value of 700 W

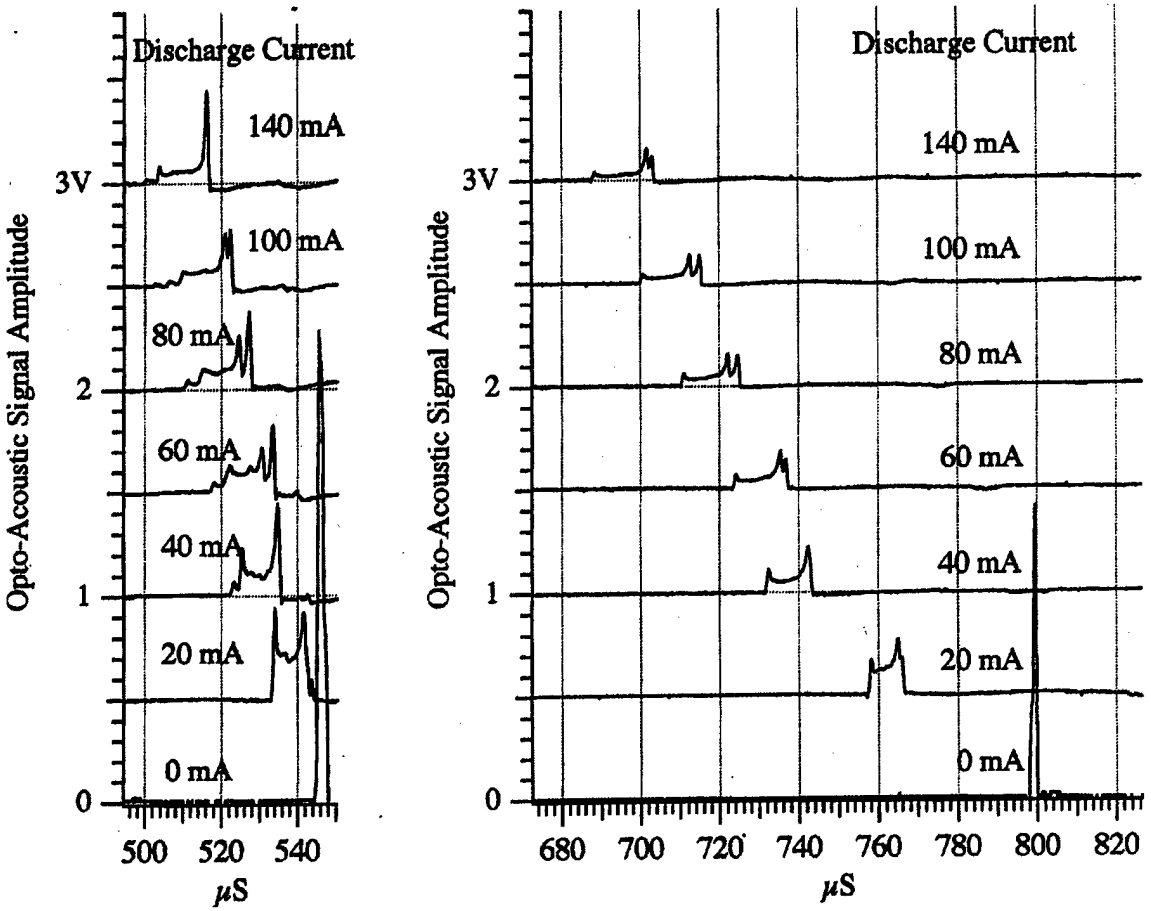

Figure 1. Optoacoustic signal from a shock wave (density gradient) in a 30 Torr axial glow discharge in argon (M~1.7). The discharge tube diameter is 5 cm [12].

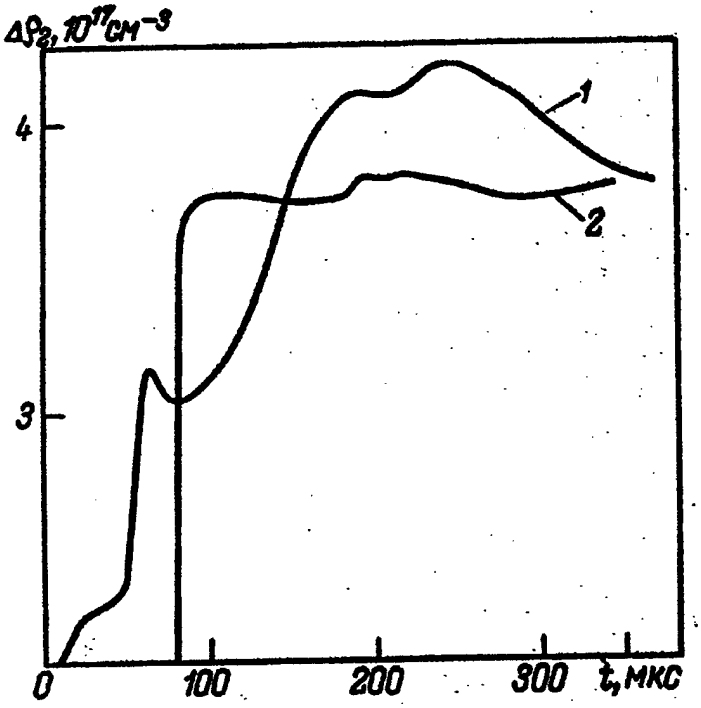

Figure 2. Density profile across the plasma shock in transverse glow discharge in air (T~350 K, P=12 Torr, initial shock velocity v_s=500 m/s, j_{tr}=30 mA/cm^2; 1, in plasma; 2, without plasma) [9].

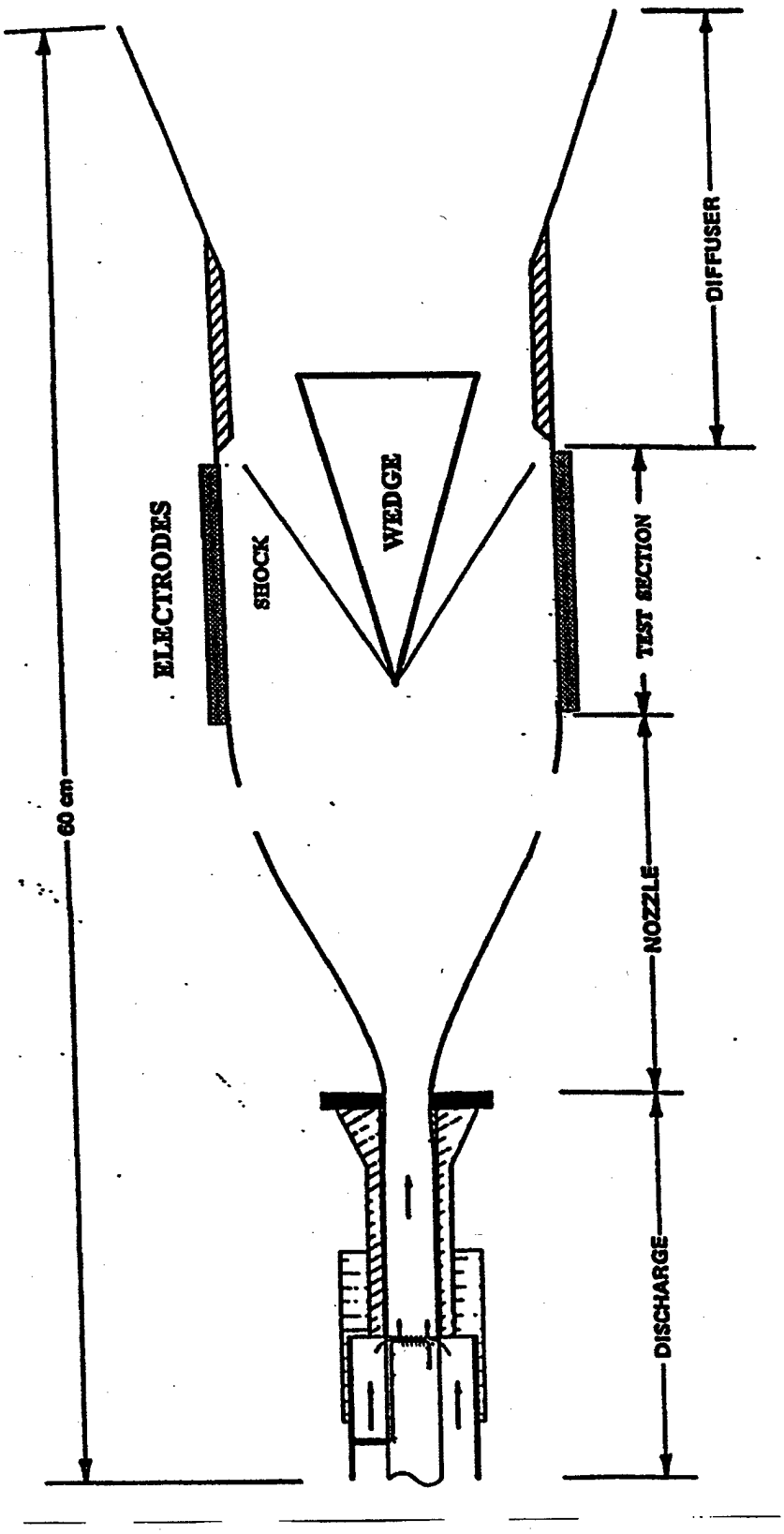

Figure 3. Schematic of wind tunnel experiment.

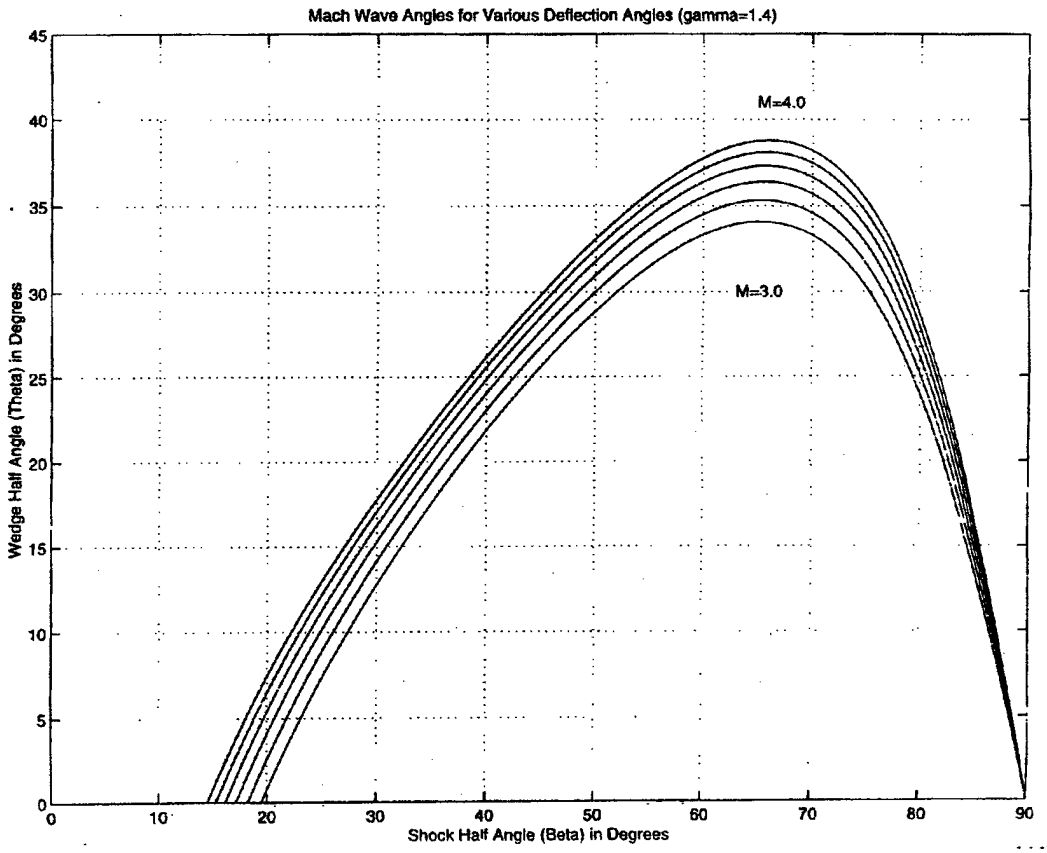

Figure 4. Shock polar for N_2.

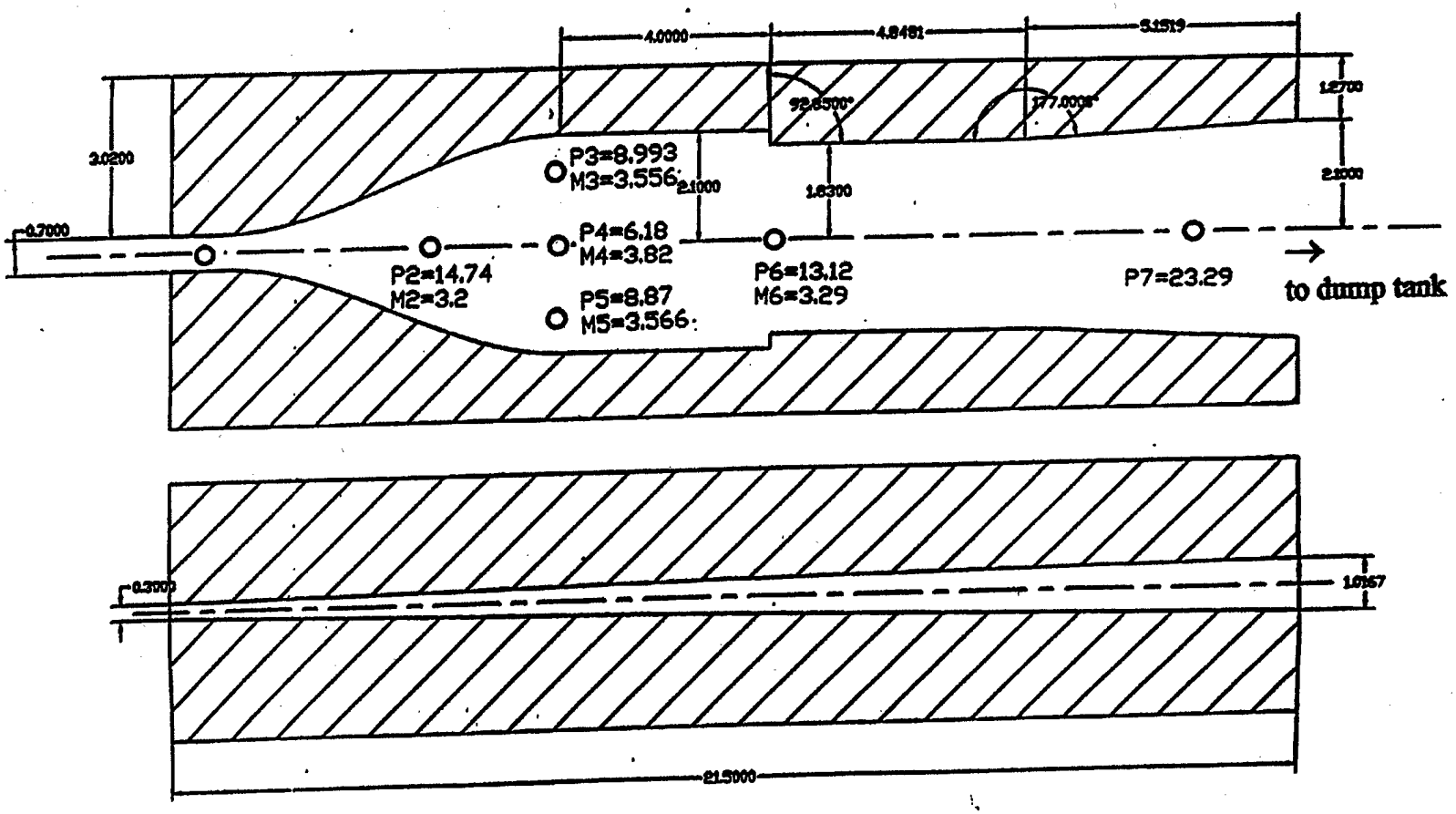

Figure 5. Flow channel layout with pressure taps.

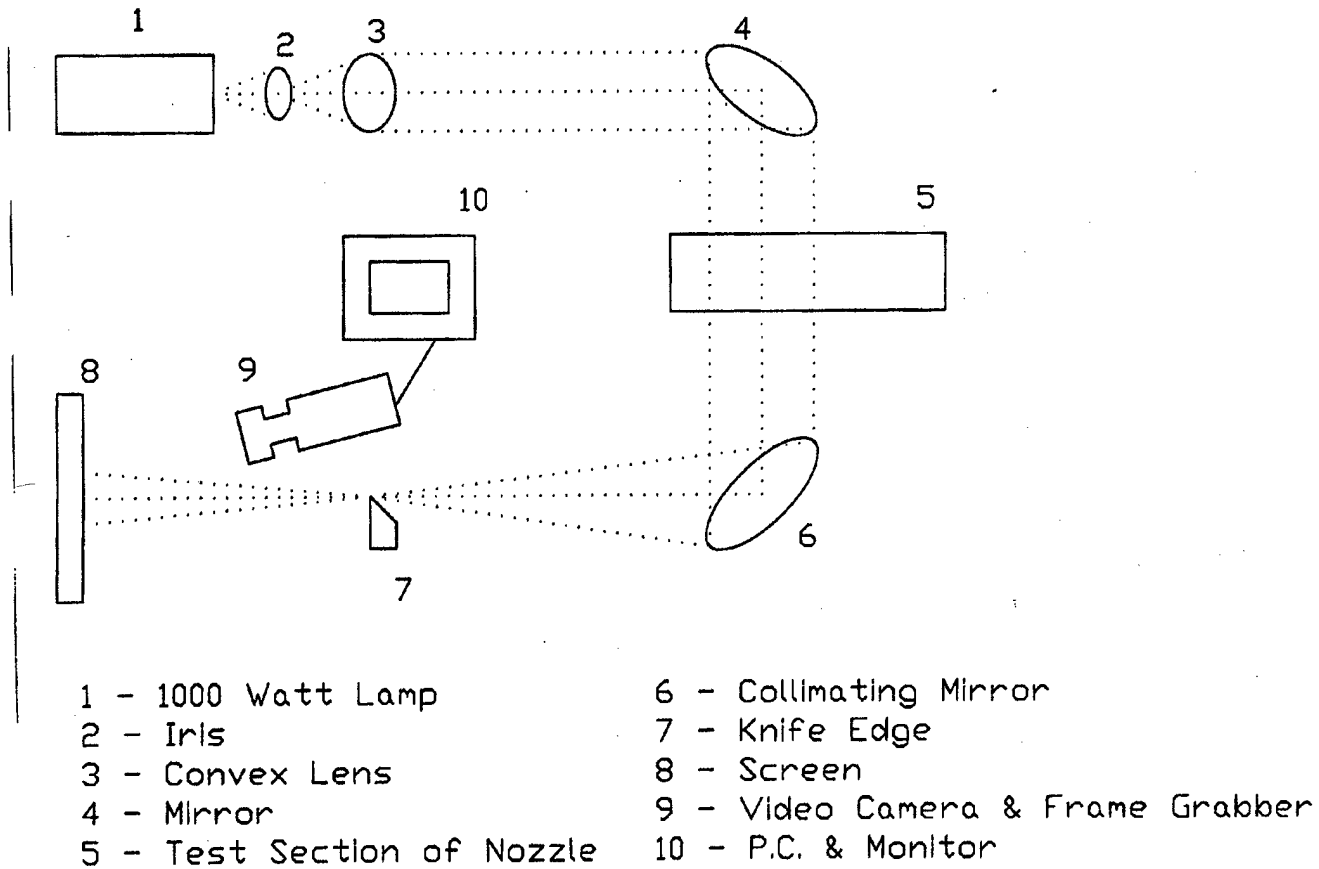

Figure 6. Schieren system schematic.

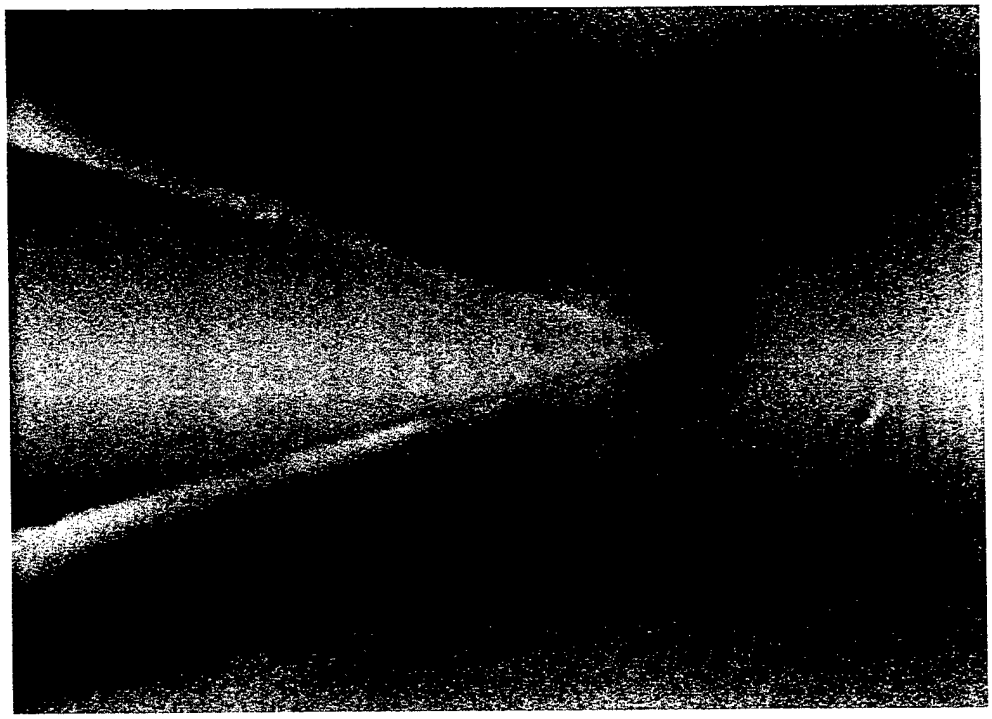

Figure 7. Typical schlieren image of oblique shocks

Figure 8. Wind tunnel in operation (photograph).

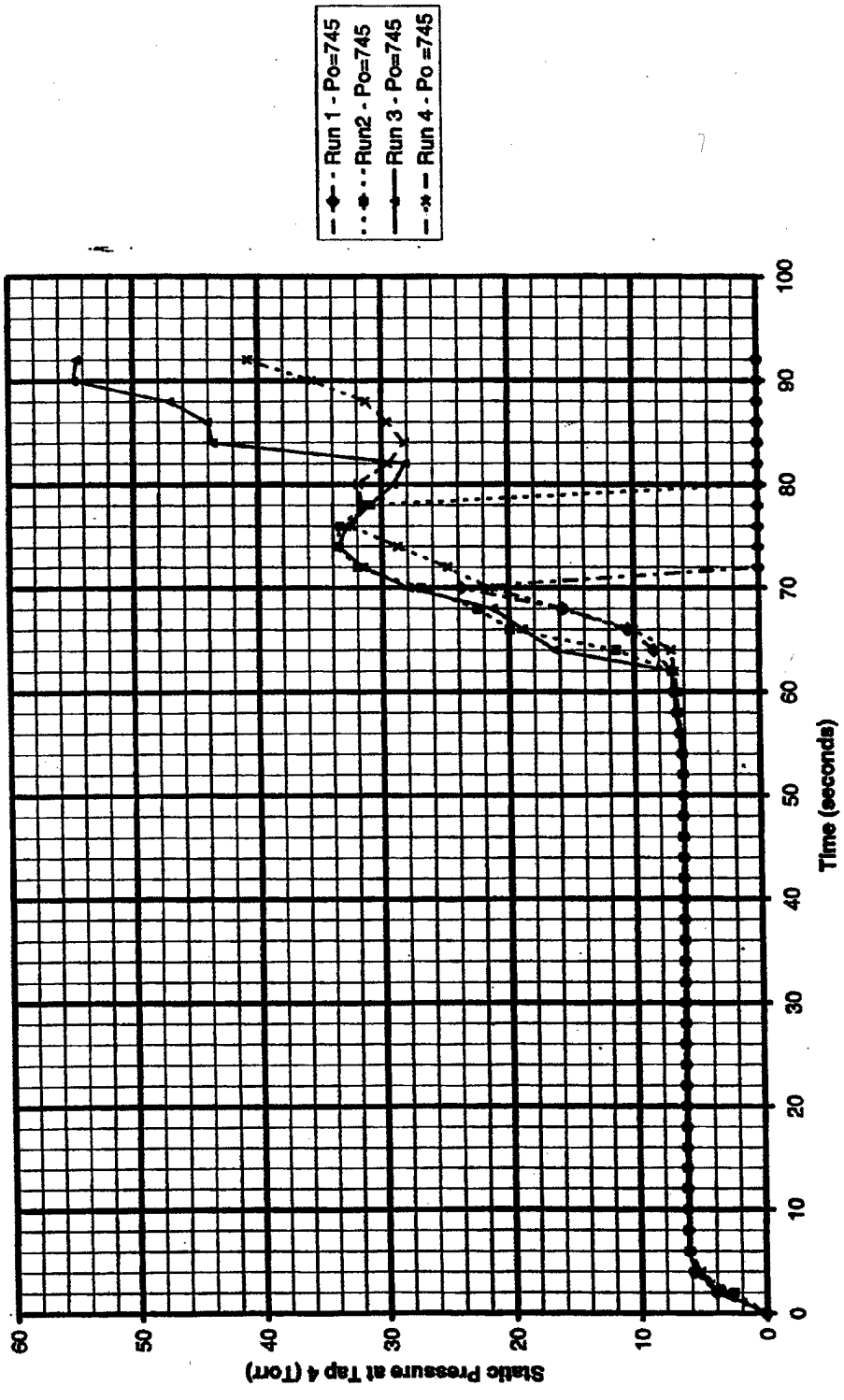

Figure 9. Test section static pressure as a function of time.

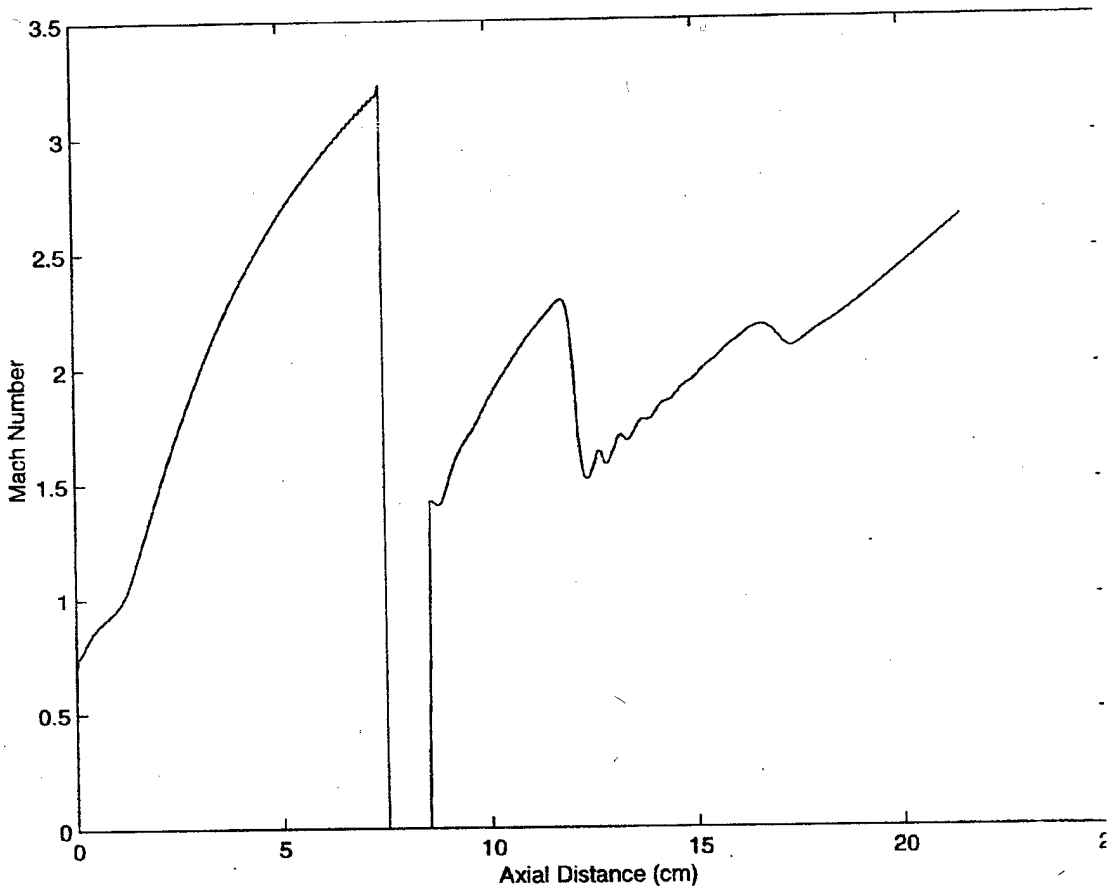

Figure 10. Centerline Mach number profile.

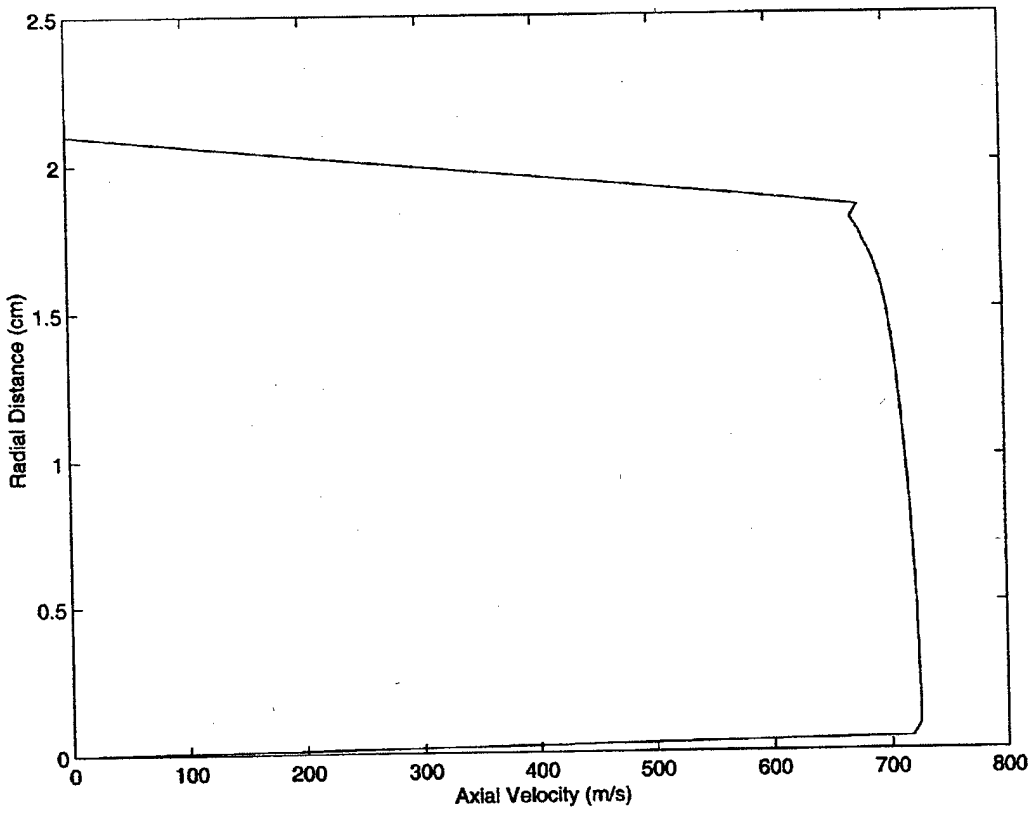

Figure 11. Radial profile of axila velocity at wedge nose location.

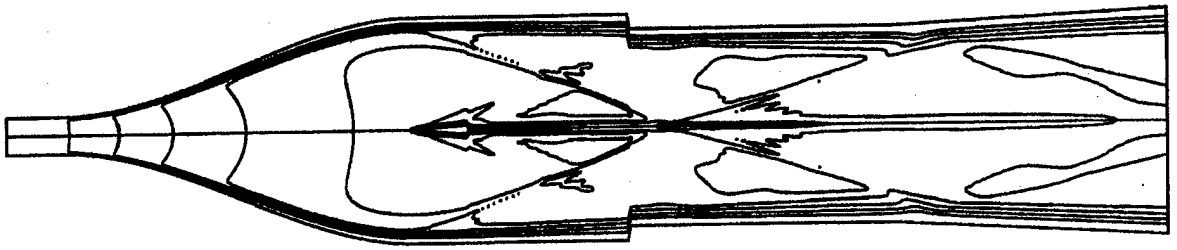

0.350E+01

0.300E+01

0.250E+01

0.200E+01

0.150E+01

0.100E+01

Figure 12. Mach number contour plot.

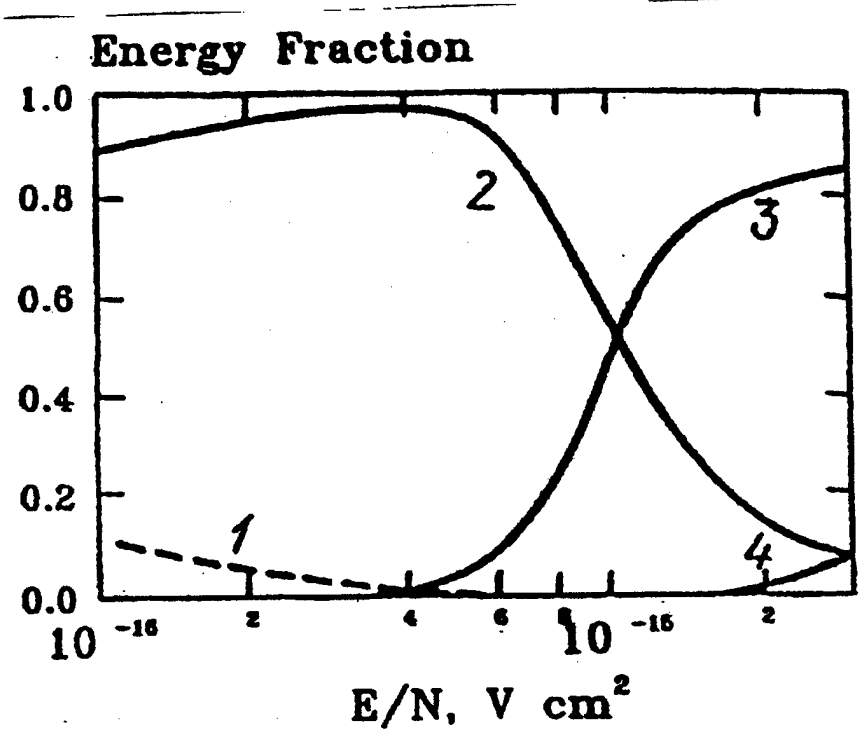

N_2 glow discharge, fraction of energy transferred by electrons to (1) rotation, (2) vibration, (3) electronic excitation, and (4) ionization.

Figure 13. Electron energy balance in nitrogen glow discharge [21].

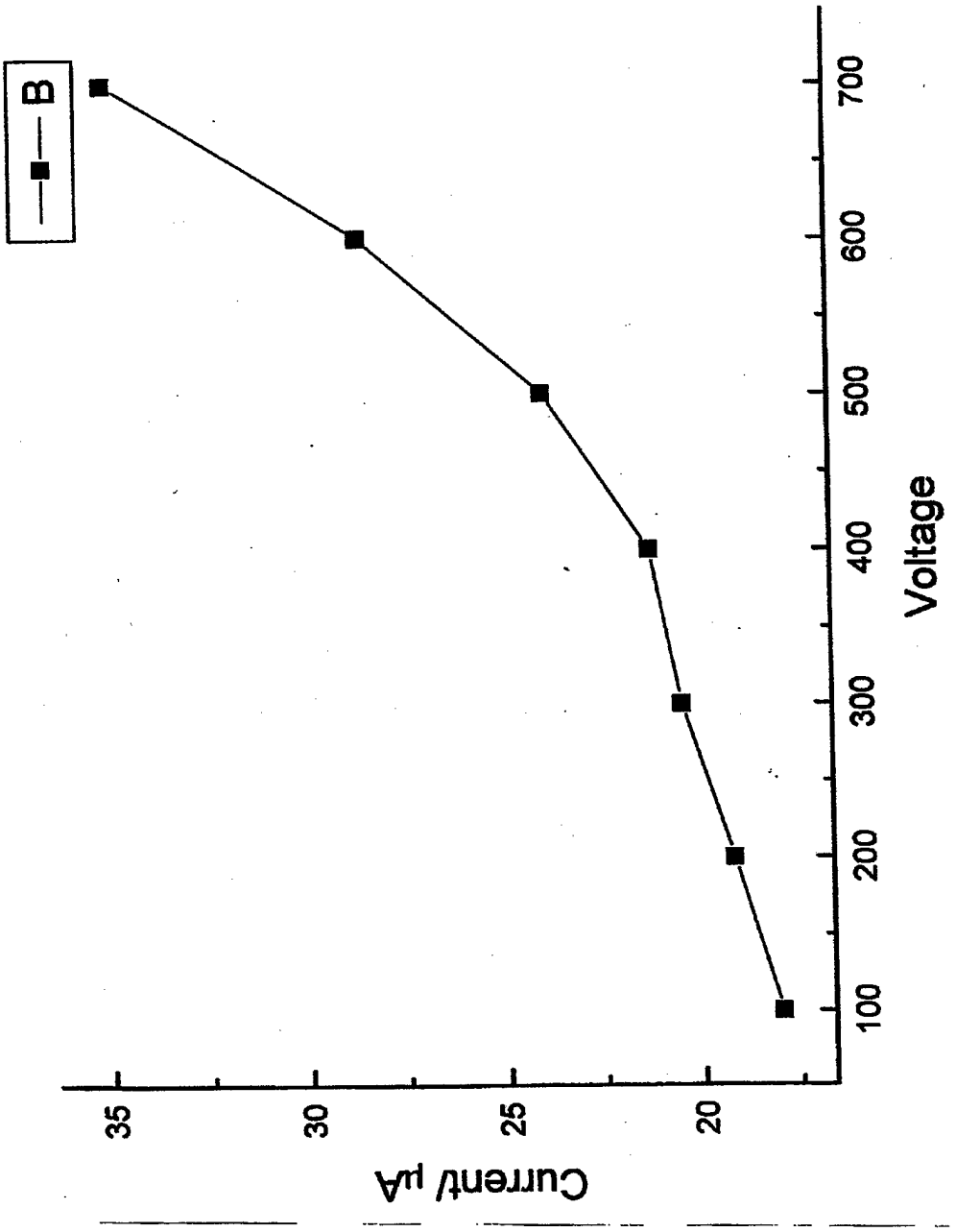

Figure 14. Probe voltage-current characteristic (Thomson discharge regime).

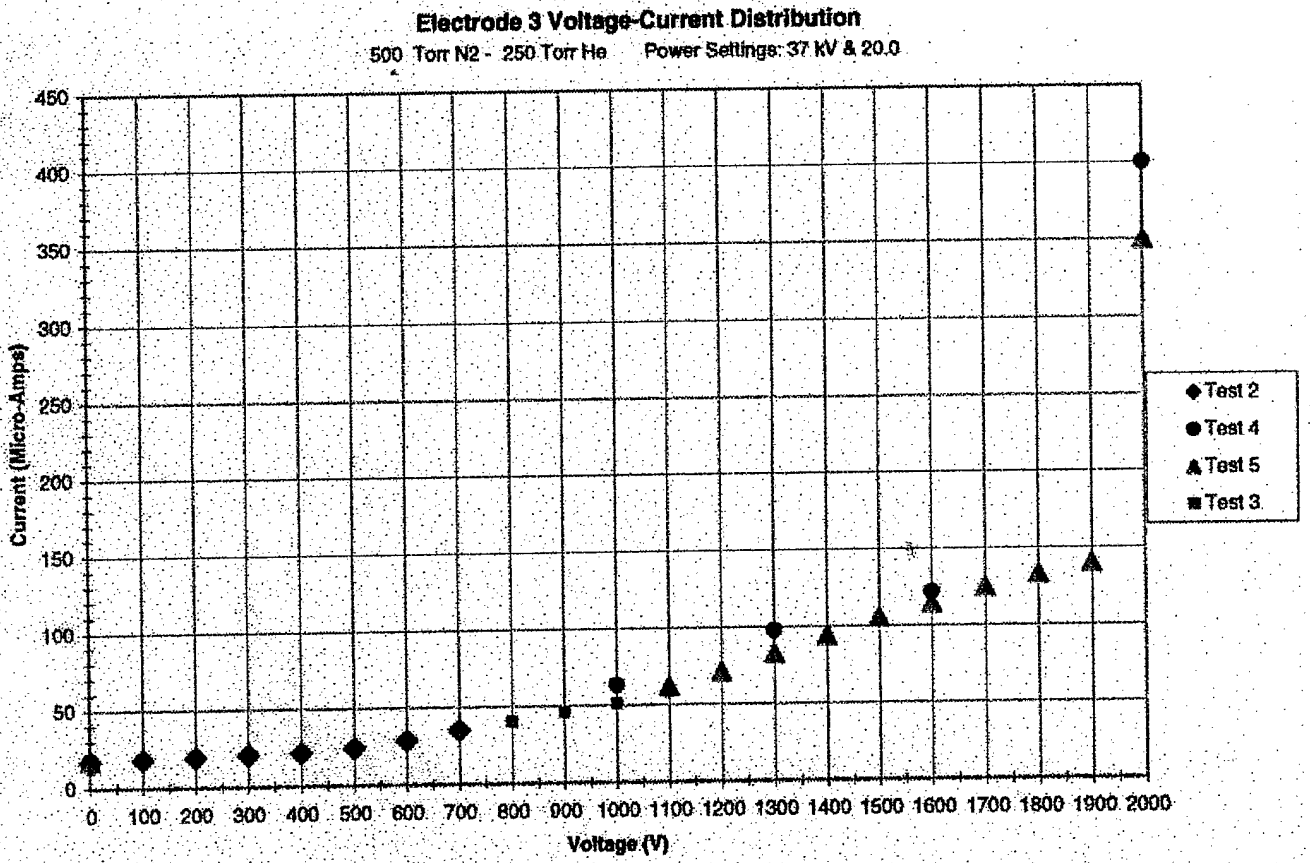

Figure 15. Probe voltage-current characteristic (self-ignited regime).

Figure 16. Wind tunnel operation with wedge model (photograph).

2.2 Studies of Oblique Shock Waves in Weakly Ionized Nonequilibrium Plasmas

AIAA 99-4823

STUDIES OF OBLIQUE SHOCK WAVES IN WEAKLY IONIZED NONEQUILIBRIUM PLASMAS

Samuel Merriman, Igor Adamovich, and J. William Rich

Nonequilibrium Thermodynamics Labordtory
Dept. of Mechanical Engineering
The Ohio State University, Columbus, OH 43220-1107

AIAA 9th International Space Planes and Hypersonic Systems and Technologies Conference and 3rd Weakly Ionized Gases Workshop
1 - 5 November, 1999 / Norfolk, VA

AIAA 99-4823

STUDIES OF OBLIQUE SHOCK WAVES IN WEAKLY IONIZED NONEQUILIBRIUM PLASMAS

Samuel Merriman[1], Igor V. Adamovich[2], and J. William Rich[3]

Nonequilibrium Thermodynamics Laboratory
Dept. of Mechanical Engineering
The Ohio State University, Columbus, OH 43220-1107

Abstract

The paper discusses experimental studies of possible shock dispersion in weakly ionized supersonic gas flows. In these experiments, a supersonic flowing afterglow wind tunnel, which produces highly nonequilibrium plasma flows with low gas kinetic temperatures at M=2-4, is used. Supersonic flows are maintained at complete steady state. The flow is ionized by the high-pressure aerodynamically stabilized DC discharge in the tunnel plenum. Attached oblique shock structure on the nose of a 40° wedge with and without ionization in a M=2 flow was studied. No effect ct of ionization on the shock angle was observed. Ionization fraction in the test section (n_e~10^9 cm^{-3}, n_e/N~10^{-9}), however, was at the lower end of the range in which shock modifications have previously been reported. To increase the electron density in the supersonic test section, additional ionization by a transverse RF discharge was used. Preliminary results show that a stable diffuse RF discharge with ionization fraction of n_e/N~10^{-7} (n_e~10^{11} cm^{-3}) can be sustained in the test section at M=2-3. Supersonic flow visualization in these plasmas allows straightforward and reliable diagnostics of possible shock modification.

1. Introduction

Shock wave propagation in weakly ionized plasmas (with ionization fraction n_e/N~10^{-8}-10^{-6}) has been extensively studied for the last 15 years (e.g. see [1-5] and references therein). The following anomalous effects have been observed: (i) shock acceleration; (ii) non-monotonic variation of flow parameters behind the shock front; (iii) shock weakening; and (iv) shock wave splitting and spreading. These effects have been observed in discharges in various gases (air, CO_2, Ar) at pressures of 3-30 Torr, and for Mach numbers M~1.5-4.5. They also persist for a long time after the discharge is off.

At the present time, no consistent theoretical model has been able to interpret the results of these experiments on the basis of nonequilibrium plasma effects alone. On the other hand, it appears that some of these results can be explained by the nonuniform heating of the plasma flow. A major complexity with the previous experiments on the anomalous shock weakening and dispersion is that the short-duration test facilities (shock tubes and ballistic ranges) have been used. A second complexity is the control of the thermodynamic parameters of the test plasma. Ideally, it is desirable to have uniform gas temperature, pressure, species concentrations, and electron density throughout the test region, and these parameters should remain constant except as perturbed by the passing shock structure.

The present study represents an effort to address and circumvent these complexities. The present experiments are conducted in a new, unique, steady-state supersonic flow facility, with well-characterized, near uniform, nonequilibrium plasma properties.

2. Experimental Facility

The facility used in the present study is a recently developed, small-scale, nonequilibrium plasma wind tunnel. In contrast to the shock tube and ballistic range studies, it operates at steady state. This wind tunnel is the high-pressure-discharge/supersonic-flowing-afterglow apparatus of Fig. 1. The design and

[1] Undergraduate Research Assistant
[2] Research Scientist, Senior Member AIAA
[3] Ralph W. Kurtz Professor, Associate Fellow AIAA

operation of the wind tunnel has been described in greater detail in [6]. Briefly, the aerodynamically stabilized DC diffuse glow discharge in the tunnel plenum can be sustained at high pressures, up to 500 torr in nitrogen, or up to 6 atm in helium. This is *not* an arc-heated tunnel. Although the electrical power into the discharge is rather high, up to 500 W/cm^3 in N_2, more than 90% of the input power goes into the vibrational mode of nitrogen. In contrast to an electric arc, very little of the power goes directly to gas heating. Therefore, conditions of the gases at the throat exhibit the extreme thermal disequilibrium of the positive column of a glow discharge; the translational/rotational mode temperature is low (~300 K for an uncooled discharge tube), the energy in the vibrational mode is high (0.1 to 0.2 eV per diatomic molecule), the electron density is ~10^{10}cm^{-3}, and the average electron energy is in the 1.0 eV range.

Downstream of the discharge section is a two-dimensional plane supersonic nozzle, as shown. The nozzle is made of transparent acrylic plastic, which allows optical access to the expansion. Fabrication and use of a range of nozzles with varying expansion ratios and test section lengths is straightforward and rapid. The system is connected, through a simple channel diffuser, to a ballast tank pumped by a several hundred cfm vacuum pump. Operation at relatively high plenum pressures creates a supersonic flow, of reasonable quality (~75% inviscid core), in the test section of the tunnel [6]. At M=2, run durations of at least a few minutes are attained. An important feature of the nozzle operation is that the electron-ion recombination is sufficiently slow, so that the ionization fraction (n_e/N~10^{-9}) remains nearly constant in the expansion into the test section of the tunnel [6]. Also, high level of vibrational excitation existing at the nozzle entrance persists throughout the nozzle length, for flows in pure N_2. The vibrational temperature of nitrogen is essentially frozen at the throat values.

For the shock dispersion/weakening studies reported here, a wedge is inserted into the supersonic ionized flow as shown in Fig. 1. With this system, the effect of nonequilibrium plasmas on the structure and stability of the resultant oblique shock, attached to the nose of the wedge, can be studied in detail, in a steady and well-controlled plasma environment. The objective of the experiments is to measure the angle of the oblique shock attached to the wedge, under both discharge-on and discharge-off conditions. It has been reported that the effect of the plasma is to weaken the shock. This should produce an effect of the apparent reduction of the shock Mach number. For a 40° total angle wedge, a shock Mach number reduction from M = 3 to M = 2 would create a change in the shock wave angle of more than 15°. Changes of this magnitude would be readily detectable in the present system.

Since the previous experiments in the M=3 supersonic flowing afterglow sustained by the DC discharge in plenum [6] did not show any measurable shock attenuation, the main objective of the present study is to increase the electron density in the test section. To achieve this, a transverse RF discharge sustained between the strip electrodes embedded in the top and bottom nozzle walls, as shown in Fig.1, is used. It is well known that relatively low current RF discharges are more stable than DC discharges [7], since the former do not have high electric field sheaths. Indeed, the experiments with DC voltage applied to the test section electrodes showed that the discharge is very unstable and readily transforms into an arc. On the other hand, applying RF electric field to the electrodes, in the frequency range ν=15-60 MHz allowed sustaining a stable, diffuse, and uniform transverse discharge.

In the present experiments, with the auxiliary DC discharge on, RF voltage was applied to the test section electrodes located a few millimeters upstream of the model (1 cm long 40° copper wedge, see Fig. 1). The DC discharge provided pre-ionization of the flow upstream of the test section. The RF power supply consisted of a 50 W broadband (15-512 MHz) amplifier, Mini Circuits LZY-1, driven by a HP 33120A function generator at 15 MHz or Mini Circuits voltage controlled oscillator ZOS-75 between 30 and 60 MHz. The RF circuit impedance was matched using an MFJ-949E tuner. The applied RF voltage was varied in the range 0-300 V peak-to-peak.

3. Results and Discussion

In the first series of experiments in a M=2 nozzle, ionization in the flow was created by a DC glow discharge in the nozzle plenum. With the DC discharge off, a conventional schlieren system [6] was used to visualize the oblique shocks attached to the nose of the wedge model (see Fig. 2). The wedge

planform and the quite straight oblique shock on either side of the nose can be seen. The total shock angle is approximately 102^0, which indicates the Mach number of M=2.1. With the DC discharge on, the plasma flow visualization technique [8] was used to measure the shock angle. Our previous experiments with supersonic flowing afterglow demonstrated that the use of the schlieren system is not necessary for shock visualization. During these experiments, the nozzle, test section, and diffuser are filled with the bright visible emission, arising primarily from the well-known orange-red first positive bands, $B^3\Pi_g \rightarrow A^3\Sigma_u^+$, in nitrogen and from the blue lines of helium [8]. This emission makes all features of the supersonic flow, including shocks, boundary layers, and wakes, clearly visible. Fig. 3 shows a black and white photograph of the M=2 nitrogen plasma flow around the 40° wedge model in the test section. This photograph is taken by a high resolution monochrome COHU-4910 camera. One can see that, in addition to the primary oblique shocks, Fig. 3 also displays a pair of fainter secondary oblique shocks produced by the supersonic flow reflection off the luminous boundary layer growing on the wedge walls, boundary layers extending downstream of the wedge, and the wake behind it. Note that all these spectacular features can be easily observed in real time simply by looking at the wind tunnel during its operation. The total shock angle with the plasma on, $\theta=102^0$ (see Fig. 3), is in excellent agreement with the schlieren measurements with the plasma off (see Fig. 2). In other words, no measurable effect of the plasma on the shock angle is seen. This result is consistent with our previous measurements in a M=3 plasma wind tunnel.

Most previous plasma shock experiments have been made at higher ionization fractions than attained in an afterglow sustained by a DC discharge only ($n_e \geq 10^{-8}$ vs. $n_e \sim 10^{-9}$ in the present experiments). Therefore, in the second series of experiments we attempted to increase the electron density in the test section by using a transverse RF discharge. The supersonic flow in the test section flow was still preionized by the aerodynamically stabilized DC discharge, which made initiation of the RF discharge much easier. In helium flows, after the RF discharge was initiated, the DC voltage could be turned off, while the RF discharge, now completely self-sustained, remained on. Fig. 4 shows the photographs of the RF discharge in helium at plenum pressure P_0=1 atm (test section Mach number M=3, static pressure P_{static}=24 torr), with and without an auxiliary DC discharge. One can see that RF discharge produces a bright afterglow extending a few cm downstream of the RF-powered electrodes. The RMS conduction current of the RF discharge (i.e. the difference between the current measured with and without RF plasma on) is I_{cond}=12 mA at the applied RMS voltage of U=300 V, which gives the electron density $n_e \sim 10^{11}$ cm^{-3} and ionization fraction $n_e/N \sim 10^{-7}$. These conditions are comparable with the discharge parameters of the previous plasma shock studies.

Fig. 5 shows the RF discharge sustained in the mixture of helium and nitrogen at plenum pressure P_0=1 atm and 4% of N_2 in the mixture, in the same M=3 nozzle. In this case, the RF discharge cannot be sustained after the DC preionization is turned off. Moreover, if the N_2 fraction in the mixture is increased, initiation of the RF discharge occurs at an increasingly higher RF input power. This type of the discharge behavior is expected; it occurs because of the higher electron energy losses in the inelastic collisions with N_2 molecules (mainly resulting in vibrational excitation by electron impact). With the current power supply, we could initiate and sustain the RF discharge with up to 20% of N_2 in the mixture. Initiation of the discharge in pure nitrogen would require a more powerful RF amplifier or power supply. At all experimental conditions described above, the RF discharge was always diffuse, stable, did not produce any arc filaments, and was not blown off by the incident flow. Similar results have been obtained in a M=2 nozzle. Estimates of the RF power coupled to the plasma (3-5 W) show that the heating of the flow in the test section does not exceed ΔT=1-2 K.

Sustaining the RF discharge in the gas mixture with high percentage of nitrogen is critical for the flow visualization technique used in the present study. Although most flowfield structures, such as boundary layers, wakes, and separation regions are clearly visible both in nitrogen and in helium afterglows [8], we were able to observe the well-defined hairline oblique shocks only in pure nitrogen or in the mixtures with a few percent of helium. We believe this to be due to a more dispersed shock structure in the flows with large amounts of helium. These preliminary results suggest that the use of the

flowfield visualization in stable transverse RF discharges sustained in the cold, uniform, supersonic plasma flows would finally determine whether the shock dispersion in nonequilibrium plasmas is due to anomalous plasma effects or due to the nonuniform heating of the flow.

4. Summary

Experimental studies of possible shock dispersion in weakly ionized supersonic gas flows are reported. In these experiments, a supersonic flowing afterglow wind tunnel, which produces highly nonequilibrium plasma flows with low gas kinetic temperatures at M=2-4, is used. Supersonic flows are maintained at complete steady state. The flow is ionized using high-pressure aerodynamically stabilized DC discharge in the tunnel plenum. Attached oblique shock structure on the nose of a 40° wedge with and without ionization in a M=2 flow was studied. No effect of ionization on the shock angle was observed. Ionization fraction in the test section (n_e~10^9 cm^{-3}, n_e/N~10^{-9}), however, was at the lower end of the range in which shock modifications have previously been reported. To increase the electron density in the supersonic test section, additional ionization by a transverse RF discharge was used. Preliminary results show that a stable diffuse RF discharge with ionization fraction of n_e/N~10^{-7} (n_e~10^{11} cm^{-3}) can be sustained in the test section at M=2-3. Supersonic flow visualization in these plasmas allows straightforward and reliable diagnostics of possible shock modification. Further experiments with transverse RF discharges sustained in supersonic nitrogen flows are expected to determine whether the anomalous shock dispersion is indeed produced in cold, uniform supersonic plasma flows.

5. Acknowledgements

The support of MSE Technologies, Inc., under a NASA prime, and Air Force Office of Scientific Research is gratefully acknowledged. We would also like to express our sincere gratitude to Dr. Peter Palm and Dr. Scott Harris for numerous useful suggestions.

6. References

1. Klimov, A.I., Koblov, A.N., Mishin, G.I., Yu.L. Serov, and I.P. Yavor, Sov. Tech. Phys. Lett, vol. 8, p. 192, 1982
2. Basargin, I.V., and Mishin, G.I., Sov. Tech. Phys. Lett., vol. 11, p. 535, 1985
3. Mishin, G.I., Klimov, A.I., and Gridin, A.Yu., Sov. Tech. Phys. Lett., vol. 17, p. 602, 1992
4. Ganguli, B.N., and Bletzinger, P., AIAA Paper 96-4607, November 1996
5. Lowry, H., Blanks, J., Stepanek, C., Smith, M., Crosswy, L., Sherrouse, P., Felderman, J. and Wood, B., "Characterization of the Shock Structure of a Spherical Projectile in Weakly Ionized Air Through Ballistic Range Test Techniques", 2nd Weakly Ionized Gas Workshop, Norfolk, VA, April 1998
6. Yano. R., Contini, V., Palm, P., Merriman, S., Aithal, S., Adamovich, I., Lempert. W., Subramaniam. V., and Rich, J.W., "Experimental Characterization of Shock Dispersions in Weakly Ionized Nonequilibrium Plasmas", AIAA Paper 99-3671, 30th Plasmadynamics and Lasers Conference, Norfolk, VA, June 1999
7. Raizer, Yu.P., Shneider, M.N., and Yatsenko, N.A., "Radio-Frequency Capacitive Discharges", CRC Press, Boca Raton, 1995
8. Yano. R., Contini, V., Ploenjes, E., Palm, P., Merriman, S., Aithal, S., Adamovich, I., Lempert. W., Subramaniam. V., and Rich, J.W., "Flow Visualization In A Supersonic Nonequilibrium Plasma Wind Tunnel", AIAA Paper 99-3725, 30th Plasmadynamics and Lasers Conference, Norfolk, VA, June 1999

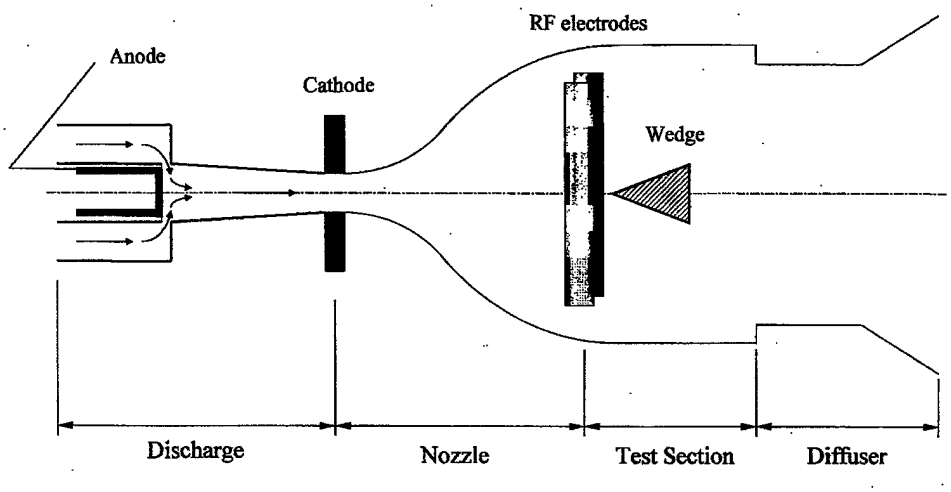

Figure 1. Schematic of the wind tunnel experiment

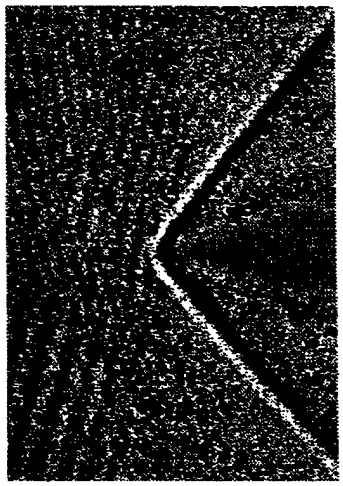

Figure 2. Schlieren image of an oblique shock in a M=2 flow around a 40^0 wedge (plasma off)

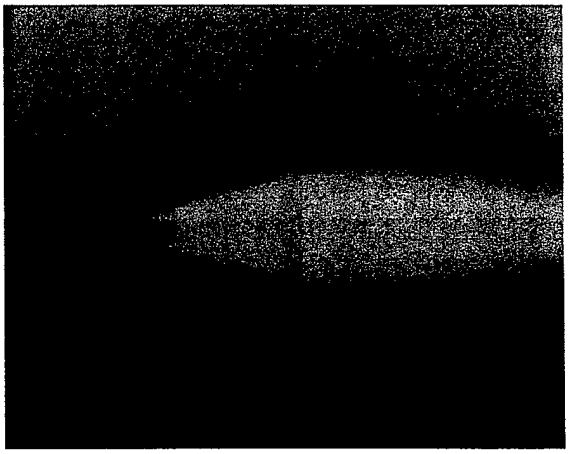

Figure 3. Photograph (*not schlieren!*) of a flowfield in a M=2 flow around a 40^0 wedge (plasma on)

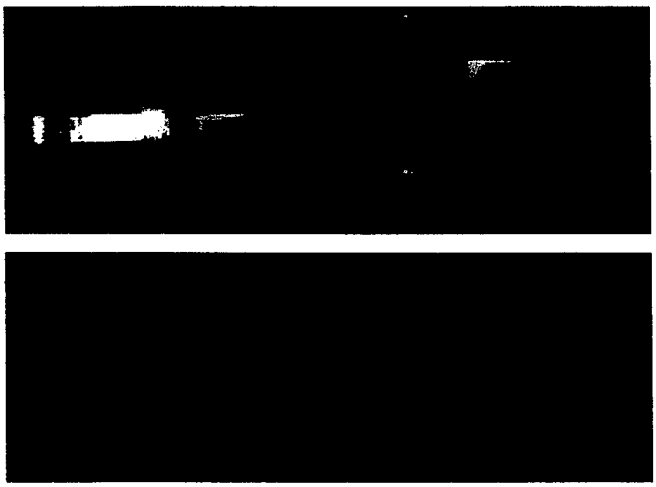

Figure 4. Transverse RF discharge in the supersonic helium flow. P_0=1 tam, T_0=300 K, M=3. (a) both DC (preionization) and RF (main) discharges are on; (b) only RF discharge is on

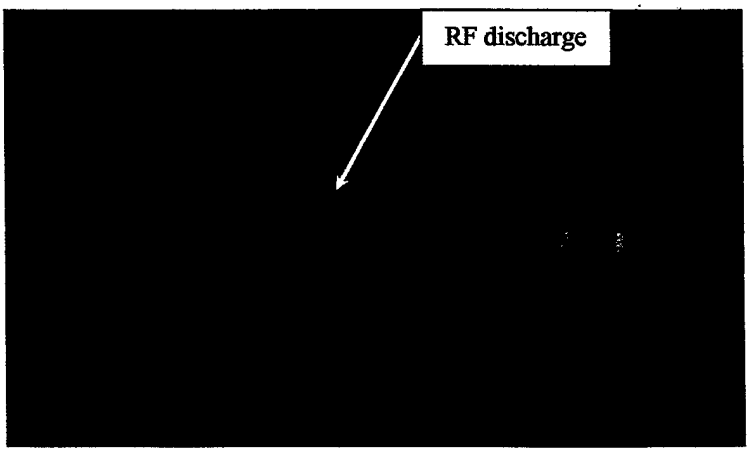

Figure 5. Transverse RF discharge in the preionized supersonic N_2-He flow. P_0=1 tam, T_0=300 K, M=3, 4% of N_2 in the mixture. Both DC (preionization) RF (main) discharges are on

2.3 Studies of Conical Shock Wave Modification by Nonequilibrium RF Discharge Plasma

AIAA-2001-0347

STUDIES OF CONICAL SHOCKWAVE MODIFICATION BY NONEQUILIBRIUM RF DISCHARGE PLASMA

Samuel Merriman, Adam Christian, Rodney Meyer, Peter Palm,
and Igor V. Adamovich

Nonequilibrium Thermodynamics Laboratory
Dept. of Mechanical Engineering
The Ohio State University, Columbus, OH 43220-1107

39st AIAA Aerospace Sciences Meeting and Exhibit
8-11 January 2001 / Reno, NV

AIAA 2001-0347

STUDIES OF CONICAL SHOCK WAVE MODIFICATION BY NONEQUILIBRIUM RF DISCHARGE PLASMA[1]

Samuel Merriman[2], Adam Christian[2], Rodney Meyer[2], Peter Palm[3], and Igor V. Adamovich[4]

Nonequilibrium Thermodynamics Laboratory
Dept. of Mechanical Engineering
The Ohio State University, Columbus, OH 43220-1107

Abstract

The paper discusses preliminary results of an on-going experimental study of shock modification in a supersonic flow of nonequilibrium plasma over a cone. The experiments are conducted at a nonequilibrium plasma supersonic wind tunnel. Recent experiments at Ohio State using a supersonic plasma flow over a quasi-two-dimensional wedge showed that an oblique shock can be considerably weakened by the transverse RF discharge plasma. The previously observed shock weakening, however, has been found consistent with the temperature rise in the boundary layers heated by the discharge. In the present study, an attempt is made to reduce the boundary layer effects by placing an entire cone into a supersonic inviscid core flow. Preliminary results using a relatively low-power RF discharge did not show any measurable shock weakening. Additional measurements at higher RF discharge powers are suggested.

1. Introduction

Shock wave propagation in weakly ionized plasmas (with ionization fraction $n_e/N \sim 10^{-8}$-10^{-6}) has been extensively studied for the last 15 years (e.g. see [1-5] and references therein). The following anomalous effects have been reported: (i) shock acceleration; (ii) non-monotonic variation of flow parameters behind the shock front; (iii) shock weakening; and (iv) shock wave splitting and spreading. These effects have been observed in discharges in various gases (air, CO_2, Ar) at pressures of 3-30 Torr, and for Mach numbers M~1.5-4.5. They also persist for a long time after the discharge is turned off.

At the present time, no consistent theoretical model has been able to interpret the results of these studies on the basis of nonequilibrium plasma effects [6]. On the other hand, recent experiments in a pulsed glow discharge [7], as well as modeling calculations [8], suggest that most of these results can in fact be explained by the nonuniform heating of the gas flow in the discharge. A major complexity with most of the previous experiments on the anomalous shock weakening and dispersion in nonequilibrium plasmas is that short-duration test facilities (shock tubes and ballistic ranges) have been used. A second complexity is the control of the test plasma parameters. Ideally, it is desirable to have uniform gas temperature, pressure, species concentrations, and electron density throughout the test region, and these parameters should remain constant in time. Finally, in the majority of the previous experiments the weakly ionized plasma has been produced in a stagnant or very slowly moving gas, while most practical applications of shock wave control by plasmas require sustaining ionization in a supersonic flow. These requirements define a need for an experimental study conducted in a steady-state supersonic flow of stable, uniform, and well characterized nonequilibrium plasma.

Such an experiment using a nonequilibrium plasma supersonic wind tunnel has been recently developed at Ohio State [9,10]. In this experiment, an oblique shock attached to a wedge located in a supersonic flow of cold nonequilibrium N_2-He plasma was monitored using high-pressure plasma flow visualization. The plasma was produced by an aerodynamically stabilized diffuse DC glow discharge [9]

[2] Undergraduate Research Assistant
[3] Post-Doctoral Researcher
[4] Visiting Assistant Professor, Senior Member AIAA

sustained in the tunnel plenum and by a transverse RF discharge [10] sustained in the supersonic test section. The experiments showed considerable shock angle increase with the RF discharge turned on, i.e. shock weakening. With the RF discharge on, the shock angle increased from its baseline value of $\alpha=99^0$ to $\alpha=113^0$, which corresponds to an apparent Mach number reduction from M=2.0 to M=1.8. However, both the observed shock weakening and its subsequent recovery after the RF discharge was turned off occurred on a long time scale, over a few seconds. For comparison, the supersonic flow residence time in the test section is of the order of 10 μsec. In addition, the observed Mach number reduction was found to be consistent with the temperature increase in the boundary layers on the test section walls, adjacent to the transverse RF discharge electrodes. These observations suggest that the observed shock weakening is likely to be due to thermal effects, in particular, oblique shock interaction with the heated boundary layers.

The present paper presents preliminary results of an on-going experimental study where we attempt to reduce the boundary layer effects on the shock. The main objective of this on-going work is to determine whether the shock weakening by plasmas reported in previous studies at Ohio State and elsewhere is indeed due to thermal effects.

2. Experimental Facility

The facility used in the present study is an upgrade of a recently developed, small-scale, steady-state nonequilibrium plasma wind tunnel [9,10]. The design and operation of the wind tunnel has been described in greater detail in [9,10]. Briefly, the supersonic flow of nonequilibrium plasma in the wind tunnel is produced by an aerodynamically stabilized diffuse DC glow discharge [9] sustained in the tunnel plenum and by a transverse RF discharge [10] sustained in the supersonic test section. Both discharges can be sustained at quite high plenum and test section pressures, up to $P_0=2/3$ atm and $P_{test}=0.1$ atm, respectively, in nitrogen. Operation at relatively high plenum pressures creates a supersonic flow of reasonable quality (~75% inviscid core), in the test section of the tunnel [9]. At M=2, run durations of at least a few minutes are attained [10]. This is *not* an arc-heated tunnel. Although the electrical power into the discharges is rather high, up to 500 W DC and 200 W RF in pure N_2, more than 90% of the input power goes into the vibrational and electronic energy modes of nitrogen [11]. In contrast to an electric arc, very little of the power goes directly to gas heating. Therefore, conditions of the gases in the test section exhibit the extreme thermal disequilibrium of the positive column of a glow discharge; the translational/rotational mode temperature is low (~100-200 K), the energy in the vibrational mode is high (0.1 to 0.2 eV per diatomic molecule), the electron density is $n_e \sim 10^{10}$-10^{11} cm^{-3}, and the average electron energy is in the 1.0 eV range.

Downstream of the plenum / DC discharge section is a 9 cm long, rectangular cross section supersonic nozzle, shown in Figure 1. The nozzle is made of transparent acrylic plastic, with a CaF_2 window, which provides optical access to the test section. Fabrication and use of a range of nozzles with varying expansion ratios and test section lengths is straightforward and rapid. The nozzle is connected, through a simple step diffuser, to a ballast tank pumped by a several hundred cfm vacuum pump. To reduce the effect of the side wall boundary layers on the supersonic inviscid core flow, the side walls of the nozzle are diverging at a constant angle of 5.5^0. This also allows accommodation of a small plastic cone model in the test section. The nozzle throat and exit dimensions are 17 mm x 3 mm and 29 mm x 20 mm, respectively. During the wind tunnel operation, static pressure in the test section is monitored using two pressure taps in the top nozzle wall, one between the RF electrodes and the other approximately halfway between the electrodes and the diffuser (see Fig. 1). The diameter of the pressure taps is about 0.2 mm.

In the present experiment, DC discharge in the nozzle plenum is used only for the supersonic plasma flow visualization [9,10]. Our previous experiments [9] showed that turning the DC discharge on and off does not produce a detectable effect of the shock angle. On the other hand, RF discharge is primarily used to produce ionization in the supersonic test section. The RF discharge is sustained between 17 mm long, 4 mm wide strip copper electrodes embedded in the nozzle side walls, as shown in Fig.1. Both RF electrodes are covered with flush mounted layers of 1 mm thick Pyrex glass to prevent

secondary electron emission which would result in the discharge collapse into an arc. The electrodes do not extend wall to wall, since this would produce considerable discharge and temperature nonuniformity in the boundary layers because of the long flow residence time there. The RF voltage was applied to the electrodes using a 13.56 MHz, 600 W ACG-6B RF power supply and a 3 kW MFJ-949E tuner was used for RF circuit impedance matching. Typically, the reflected RF power did not exceed 5% of the forward power. This allowed sustaining a stable, diffuse, and uniform transverse discharge in air, nitrogen, and N_2-He mixtures. Initiating and sustaining of the RF discharge did not require flow pre-ionization by the DC discharge upstream. The RMS RF voltage and current can be varied in the range 0.8-1.75 kV and 80-280 mA. The estimated test section electron density at these conditions is $n_e \sim 10^{11}$ cm^{-3}, which is about two orders of magnitude higher than produced by the DC discharge [9]. At these conditions, ionization fraction in the test section is $n_e/N \sim 10^{-7}$.

For the shock modification studies reported here, an 8 mm long, 39^0 full angle plastic cone is inserted into the supersonic ionized flow 10 mm downstream of the RF electrodes, as shown in Fig. 1. The model is glued to a metal pin embedded in a thin plastic brace located in the diffuser. The distance between the test section side walls at the model location exceeds the model base diameter by about a factor of 2.2. The model occupies about 6% of the test section cross sectional area. With this system, the effect of the nonequilibrium plasmas on the strength of the resultant shock attached to the nose of the wedge can be studied in detail, in a steady and well-controlled plasma environment. The objective of the experiments is to measure the oblique shock angle, under both plasma on and plasma off conditions. Previously it has been reported that the effect of the plasma is to weaken the shock. This should produce an apparent reduction of the shock Mach number and therefore increase the shock angle. Flow images visualized by plasma were taken using a high-resolution monochrome camera COHU-4910.

3. Results and Discussion

The presents experiments have been conducted in air, nitrogen, and a 70% N_2 - 30% He gas mixture at the plenum pressure of P_0=250 torr. The main reason for adding helium to the gas mixture was to lower the voltage required for sustaining the DC discharge (U=20 kV in a 70% N_2 – 30% He mixture vs. U=25-30 kV in pure nitrogen). The transverse RF discharge was equally diffuse and stable in all gases and gas mixtures used.

Figure 2 shows the results of the test section pressure measurements during the wind tunnel operation with both DC and RF discharges turned off. One can see that the static pressure remains stable and nearly constant (within 5%) for about 30 seconds. Turning the DC discharge on had almost no effect of the test section pressure, while turning the RF discharge on resulted only in a slight pressure increase (within 1-3% depending on the RF power).

As in our previous experiments [9], with the DC and/or RF discharge on, the nozzle and the test section are filled with bright visible emission, arising primarily from the well-known second positive bands of nitrogen, $C^3\Pi_u \rightarrow B^3\Sigma_g$ [9,10]. This emission allowed straightforward supersonic plasma flow and shock visualization [9,10]. As a crude first-order approximation, neglecting kinetic processes of population and decay of electronically excited radiating species, we can assume that the observed emission intensity (i.e. the radiation species concentration) is simply proportional to the local number density. The rationale for this assumption is the fact that the excited electronic level populations of N_2 are strongly coupled with the ground state vibrational populations of nitrogen which relax extremely slowly. For example, the vibration-translation (V-T) relaxation time of N_2 by He at the conditions of the present experiment is of the order of seconds [12], while the flow residence time in the test section is of the order of tens of microseconds.

Figure 3 shows inverted B&W photographs of a supersonic N_2-He flow over a wedge in a quasi-two-dimensional plane nozzle [10] and a supersonic N_2-He flow over a cone in the nozzle shown in Fig. 1. Both flows are visualized by a 230 W DC discharge and are shown in scale. Comparison of these two images shows significant qualitative differences. Indeed, the supersonic flow field over the wedge appears to be quite complicated. First, one can see that the visible oblique shock attached to the wedge nose extends only over about 1/4 of the wedge length. Second, there appears to be a fainter secondary shock

formed about halfway along the wedge. Finally, there are two distinct bright features formed near the wedge surface, which look similar to boundary layers. On the other hand, the supersonic flow over the cone appears to be much less complicated. The entire region behind the shock is filled with bright, nearly uniform visible emission, with no apparent bright or dark structures (see Fig. 3). This observation is consistent with our assumption regarding the correlation between the emission intensity and the local number density. Indeed, in the absence of the shock perturbation by the nozzle walls the number density of the flow behind the conical shock is expected to be uniform. The conical shock front looks somewhat less distinct compared to the oblique shock front (see Fig. 3), since in the former case we are looking at a three dimensional object which is not entirely in focus.

This qualitative analysis suggests that the flow over a wedge in the quasi-two-dimensional plane nozzle studied in our previous experiment [9,10] is strongly perturbed by the nozzle side walls, which were only 4-5 mm apart. In the wedge flow shown in Fig. 3, the oblique shock angle of $\alpha=100^{\circ}$ indicates a test section Mach number of M=2.0. In the cone flow, the shock angle is $\alpha=69^{\circ}$, which corresponds to a Mach number of M=2.3.

Unlike in our previous experiments [10], turning the RF discharge on and off during the wind tunnel operation did not result in a measurable shock angle increase. In these measurements, the 230 W DC discharge was on all the time to provide plasma flow visualization and enable shock angle measurements with the RF discharge off. The maximum RF discharge power applied was 100 W, which is only half the maximum RF power used in our previous experiments in a quasi-two-dimensional plane nozzle [10]. At attempt to further increase the RF power resulted in discharge arcing through a small gap between the plastic nozzle wall and the glass layer covering both RF electrodes (see Fig. 1). This occurred due to insufficient glass layer / copper electrode overlap. Figure 4 shows two flow images of a 70% N_2 - 30% He flow over a cone with the RF discharge on and off. One can see that in both cases the flow behind the shock looks fairly uniform. Figure 5 also shows two supersonic flow images (for wedge and cone flows), each composed of two separate frames, with the RF discharge on and off. For both flows, the two frames have been differentiated using a Scion Image software package to highlight the location of the shock front and then added together. In the wedge flow taken from Ref. [10], one can clearly see two shock fronts with distinctly different angles, the larger angle corresponding to the frame with the RF discharge on. However, there appears to be no measurable shock weakening in the cone flow. The two possible reasons for these are (i) lower RF power (100 W) compared to the previous wedge flow experiment (200 W), and (ii) absence of the inviscid core flow interaction with the side wall boundary layers heated by the RF discharge. Additional measurements at the higher RF power, comparable to the power used in the quasi-two-dimensional flow experiment are required to determine the reason for the absence of shock weakening in the supersonic plasma flow over a cone.

4. Summary

The paper discusses preliminary results of an on-going experimental study of shock modification in a supersonic flow of nonequilibrium plasma over a cone. The experiments are conducted at a nonequilibrium plasma supersonic wind tunnel. Previous experiments at Ohio State using a supersonic plasma flow over a quasi-two-dimensional wedge showed that an oblique shock can be considerably weakened by the transverse RF discharge plasma. The previously observed shock weakening, however, has been found consistent with the temperature rise in the boundary layers heated by the discharge. In the present study, an attempt is made to reduce the boundary layer effects by placing an entire cone into a supersonic inviscid core flow. Preliminary results using a relatively low-power RF discharge did not show any measurable shock weakening. Additional measurements at higher RF discharge powers are suggested.

5. Acknowledgements

The support of the Air Force Office of Scientific Research is gratefully acknowledged.

6. References

1. Klimov, A.I., Koblov, A.N., Mishin, G.I., Yu.L. Serov, and I.P. Yavor, Sov. Tech. Phys. Lett, vol. 8, p. 192, 1982
2. Basargin, I.V., and Mishin, G.I., Sov. Tech. Phys. Lett., vol. 11, p. 535, 1985
3. Mishin, G.I., Klimov, A.I., and Gridin, A.Yu., Sov. Tech. Phys. Lett., vol. 17, p. 602, 1992
4. Ganguly, B.N., and Bletzinger, P., "Shock Wave Damping and Dispersion in Nonequilibrium Low Pressure Argon Plasmas", Phys. Lett. A230, p. 218, 1997
5. Lowry, H., Blanks, J., Stepanek, C., Smith, M., Crosswy, L., Sherrouse, P., Felderman, J. and Wood, B., "Characterization of the Shock Structure of a Spherical Projectile in Weakly Ionized Air Through Ballistic Range Test Techniques", 2nd Weakly Ionized Gas Workshop, Norfolk, VA, April 1998
6. I.V. Adamovich, V.V. Subramaniam, J.W. Rich, and S.O. Macheret, "Phenomenological Analysis of Shock Wave Propagation in Weakly Ionized Plasmas", AIAA Journal, vol. 36, No.5, p. 816, 1998
7. Ionikh, Yu.Z., Chernysheva, N.V., Yalin, A.P., Macheret, S.O., Martinelli,L., and Miles, R.B., "Shock Wave Propagation Through Glow Discharge Plasmas: Evidence of Thermal Mechanism of Shock Dispersion," AIAA Paper 2000-0714
8. Macheret, S.O., Martinelli, L., and Miles, R.B., "Shock Wave Propagation and Structure in Non-Uniform Gases and Plasmas", AIAA Paper 99-0598
9. Yano. R., Contini, V., Ploenjes, E., Palm, P., Merriman, S., Aithal, S., Adamovich, I., Lempert. W., Subramaniam. V., and Rich, J.W., "Measurements of Shock Modification and Flow Visualization In A Supersonic Nonequilibrium Plasma Wind Tunnel", accepted for publication in AIAA Journal, 2000
10. S. Merriman, E. Ploenjes, P. Palm, and I.V. Adamovich, "Shock Wave Control by Nonequilibrium Plasmas in Cold Supersonic Gas Flows", Paper 00-2327, presented at special session on high-speed flow control, AIAA Fluids 2000 Conference, Denver, CO, June 19-22, 2000
11. Raizer, Yu.P., "Gas Discharge Physics", Springer, Berlin, 1991
12. M.M. Maricq, E.A. Gregory, C.T. Wickham-Jones, D.J. Cartwright, and C.J.S.M. Simpson, Chemical Physics, Vol. 75, 1983, p. 347

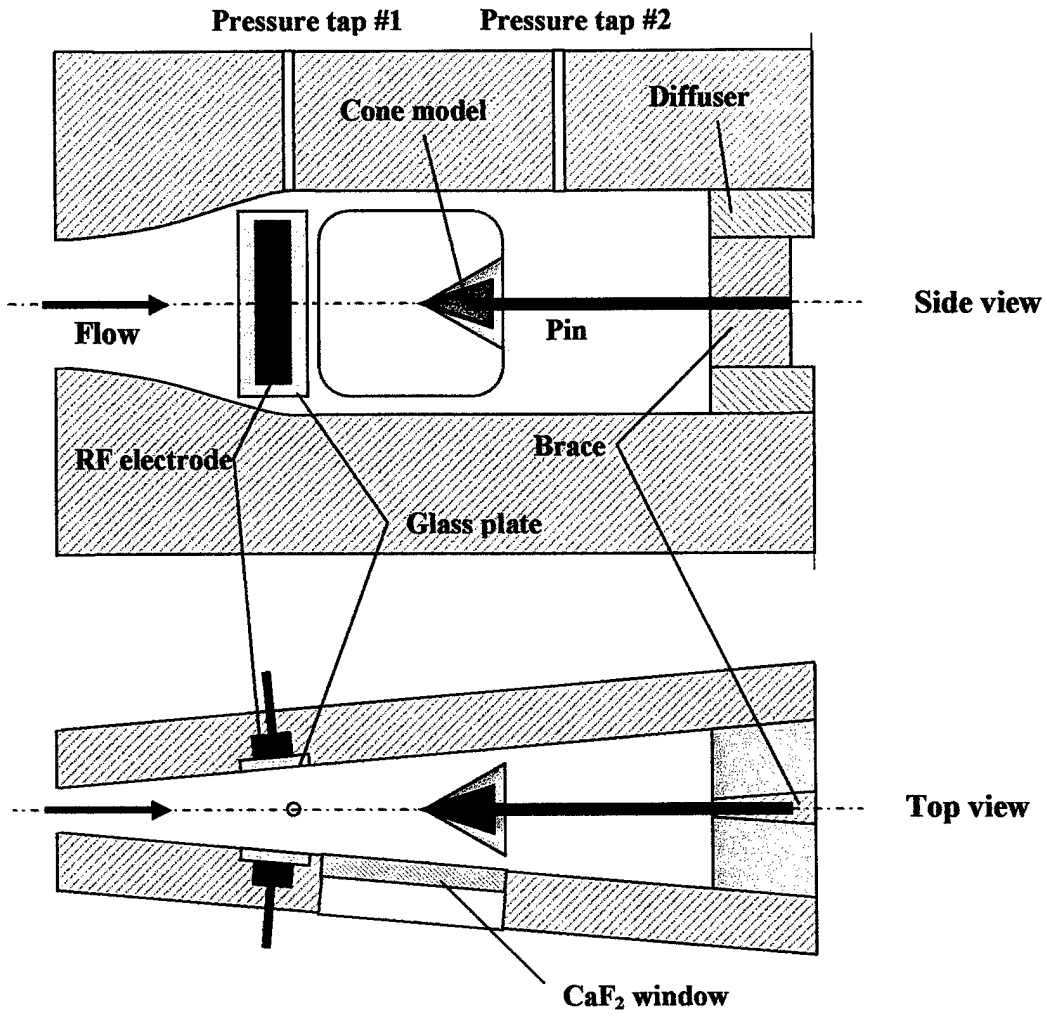

Figure 1. Schematic of the supersonic RF discharge / test section

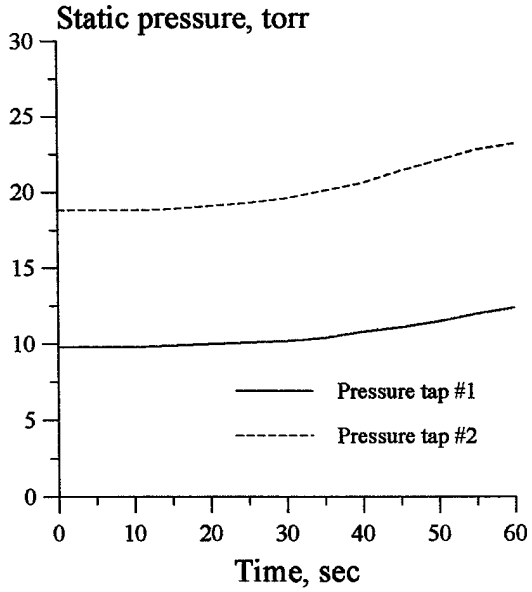

Figure 2. Results of test section static pressure measurements. Air at P_0=250 torr

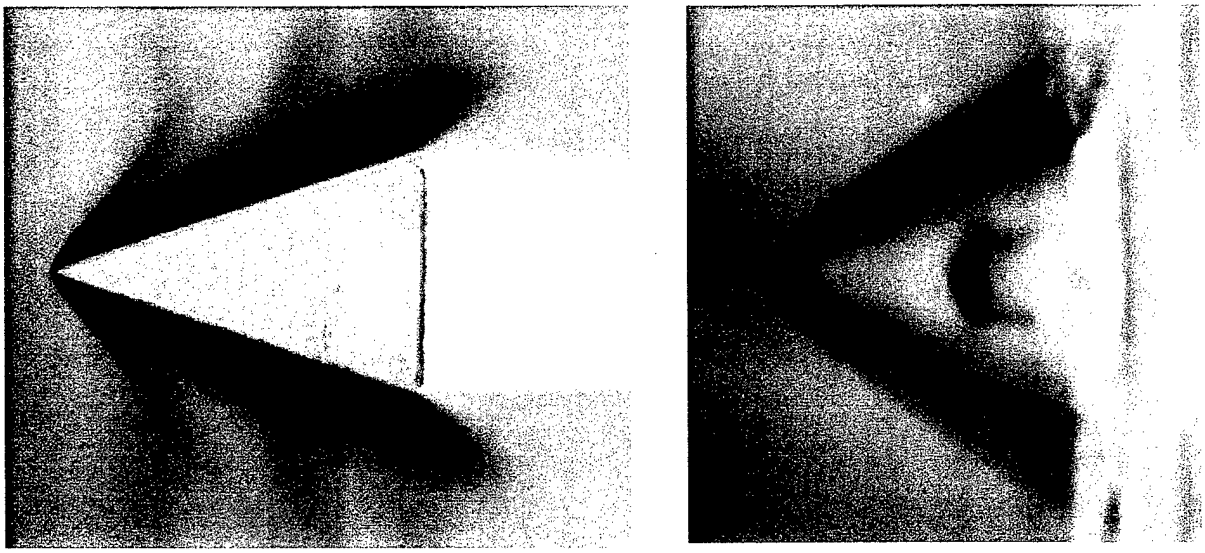

Figure 3. Photographs of the supersonic flows visualized by the plasma generated by a DC discharge in the nozzle plenum at P_0=250 torr.
Left: 50% N_2 – 50% He flow over a 35^0 wedge [10]. The shock angle is 100^0 (M=2.0).
Right: 70% N_2 – 30% He flow over a 39^0 cone. The shock angle is 69^0 (M=2.3).

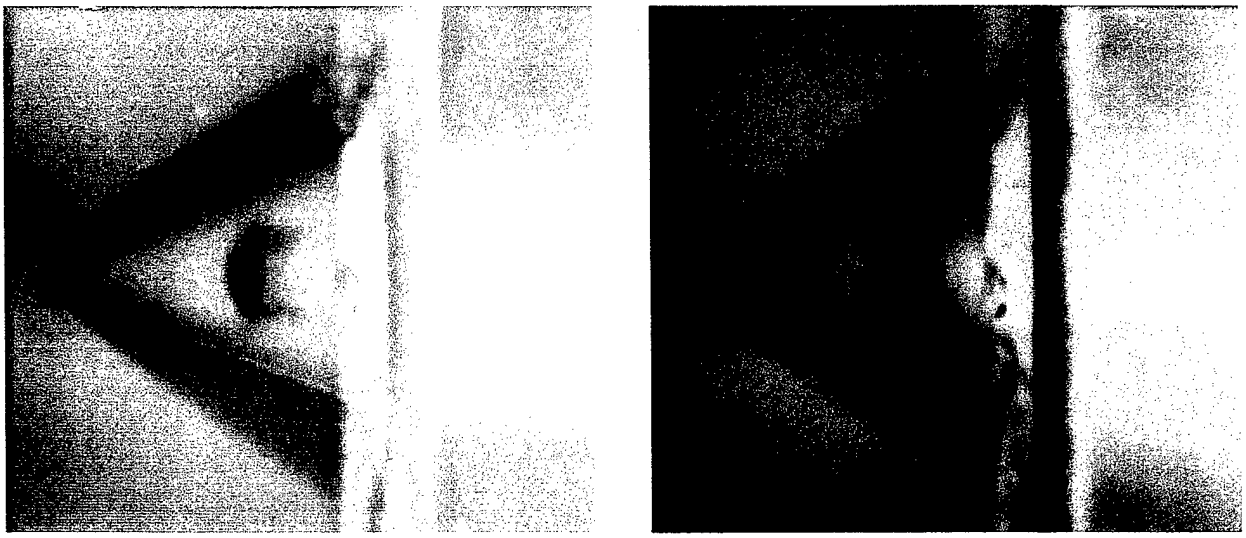

Figure 4. Photographs of the supersonic flow over a cone visualized by the plasma generated by a DC and an RF discharges in a 70% N_2 – 30% He flow at P_0=250 torr
Left: only the 230 W DC discharge is on.
Right: both the 230 W DC and the 100 W RF discharge are on.

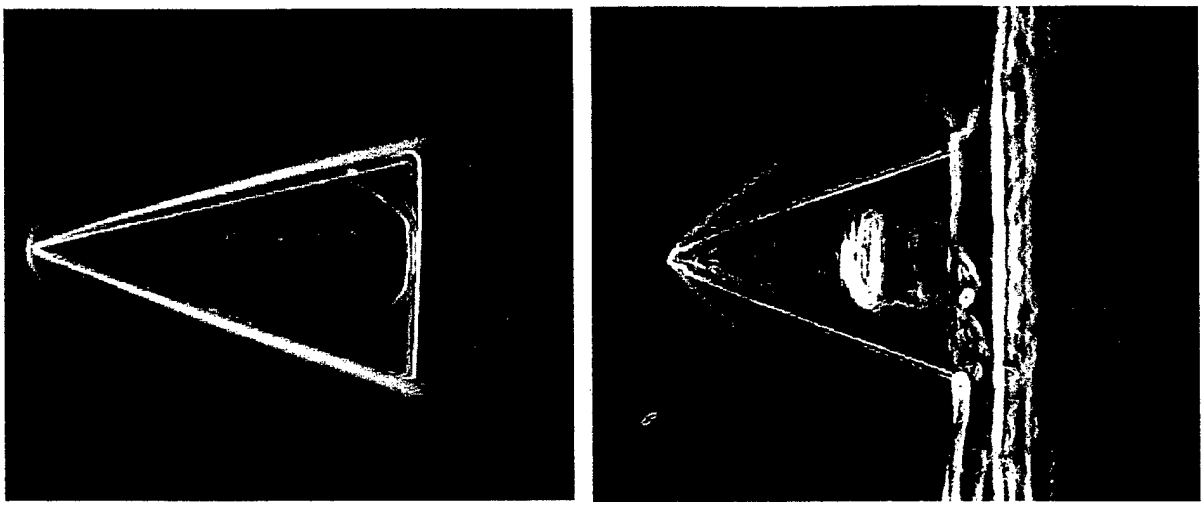

Figure 5. Shock weakening by the plasma. Two flow images with RF discharge off and RF discharge on are differentiated to highlight the shock front location and then added together.
Left: 50% N_2 – 50% He flow over a 35^0 wedge [10]. The larger angle shock (117°) corresponds to the "RF on" frame, and the smaller angle shock (105°) corresponds to the "RF off" frame.
Right: 70% N_2 – 30% He flow over a 39^0 cone. The shock angles for both the "RF on" and "RF off" frames are 69^0.

2.4 Shock Wave Control by Nonequilibrium Plasma in Cold Supersonic Flows

AIAA 2000-2327

SHOCKWAVE CONTROL BY NONEQUILIBRIUM PLASMAS IN COLD SUPERSONIC GAS FLOWS

Samuel Merriman, Elke Ploenjes, Peter Palm,
and Igor V. Adamovich

Nonequilibrium Thermodynamics Laboratory
Dept. of Mechanical Engineering
The Ohio State University, Columbus, OH 43220-1107

Fluids 2000
19 - 22 June 2000 / Denver, CO

AIAA 2000-2327

SHOCK WAVE CONTROL BY NONEQUILIBRIUM PLASMAS IN COLD SUPERSONIC GAS FLOWS[1]

Samuel Merriman[2], Elke Ploenjes[3], Peter Palm[4], and Igor V. Adamovich[5]

Nonequilibrium Thermodynamics Laboratory
Dept. of Mechanical Engineering
The Ohio State University, Columbus, OH 43220-1107

Abstract

The paper discusses experimental studies of shock modification in weakly ionized supersonic gas flows. In these experiments, a supersonic nonequilibrium plasma wind tunnel, which produces a highly nonequilibrium plasma flow with the low gas kinetic temperature at M=2, is used. Supersonic flow is maintained at complete steady state. The flow is ionized by a high-pressure aerodynamically stabilized DC discharge in the tunnel plenum and by a transverse RF discharge in the supersonic test section. The DC discharge is primarily used for the supersonic flow visualization, while the RF discharge provides high electron density in the supersonic test section. High-pressure flow visualization produced by the plasma makes all features of the supersonic flow, including shocks, boundary layers, expansion waves, and wakes, clearly visible. Attached oblique shock structure on the nose of a 35° wedge with and without RF ionization in a M=2 flow is studied in various nitrogen-helium mixtures. It is found that the use of the RF discharge increases the shock angle by 14°, from 99° to 113°, which corresponds to Mach number reduction from M=2.0 to M=1.8. Time-dependent measurements of the oblique shock angle show that the time for the shock weakening by the RF plasma, as well as the shock recovery time after the plasma is turned off, is of the order of seconds. Since the flow residence time in the test section is of the order of ten microseconds, this result suggests a purely thermal mechanism of shock weakening due to heating of the boundary layers and the nozzle walls by the RF discharge. Gas flow temperature measurements in the test section using infrared emission spectroscopy, with carbon monoxide as a thermometric element, are consistent with the observed shock angle change. This shows that shock weakening by the plasma is a purely thermal effect. The results demonstrate the feasibility of both sustaining uniform ionization in cold supersonic nitrogen and air flows and the use of nonequilibrium plasmas for supersonic flow control. This opens a possibility for the use of transverse stable RF discharges for MHD energy extraction and/or acceleration of supersonic air flows.

1. Introduction

Shock wave propagation in weakly ionized plasmas (with ionization fraction $n_e/N \sim 10^{-8}$-10^{-6}) has been extensively studied for the last 15 years (e.g. see [1-5] and references therein). The following anomalous effects have been observed: (i) shock acceleration; (ii) non-monotonic variation of flow parameters behind the shock front; (iii) shock weakening; and (iv) shock wave splitting and spreading. These effects have been observed in discharges in various gases (air, CO_2, Ar) at pressures of 3-30 Torr, and for Mach numbers M~1.5-4.5. They also persist for a long time after the discharge is off.

At the present time, no consistent theoretical model has been able to interpret the results of these studies on the basis of nonequilibrium plasma effects alone [6]. On the other hand, recent experiments in a steady-state glow discharge using spatially resolved gas temperature measurements by filtered Rayleigh

---

[2] Undergraduate Research Assistant
[3] Post-Doctoral Researcher
[4] Post-Doctoral Researcher
[5] Visiting Assistant Professor, Senior Member AIAA

scattering [7] and in pulsed glow discharge [7], as well as modeling calculations [8], suggest that most of these results can be explained by the nonuniform heating of the gas flow in the discharge. A major complexity with the previous experiments on the anomalous shock weakening and dispersion in nonequilibrium plasmas is that short-duration test facilities (shock tubes and ballistic ranges) have been used. A second complexity is the control of the test plasma parameters. Ideally, it is desirable to have uniform gas temperature, pressure, species concentrations, and electron density throughout the test region, and these parameters should remain constant in time. Finally, in the previous experiments the weakly ionized plasma has been produced in a stagnant or very slowly moving gas, while most practical applications of shock wave control by plasmas require sustaining ionization in a supersonic flow.

The present study represents an effort to address and circumvent these complexities. The present experiments are conducted in a new, unique, steady-state supersonic flow facility, with well-characterized, near uniform, nonequilibrium plasma properties. This facility allows simultaneous measurements of the flow field parameters (such as temperature and pressure), electric discharge parameters (current and voltage), as well as complete supersonic flow visualization. The main objective of the present work is to study the feasibility of the supersonic flow modification and control by nonequilibrium plasmas and to determine whether the shock weakening by plasmas reported in previous studies is indeed due to thermal effects.

2. Experimental Facility

The facility used in the present study is a recently developed, small-scale, nonequilibrium plasma wind tunnel [9]. In contrast to the shock tube and ballistic range studies, it operates at steady state. The schematic of the wind tunnel is shown in Fig. 1. The design and operation of the wind tunnel has been described in greater detail in [9]. Briefly, an aerodynamically stabilized DC diffuse glow discharge in the tunnel plenum can be sustained at high pressures, up to 2/3 atm in nitrogen, or up to 6 atm in helium. This is *not* an arc-heated tunnel. Although the electrical power into the discharge is rather high, up to 500 W in pure N_2, more than 90% of the input power goes into the vibrational mode of nitrogen [10]. In contrast to an electric arc, very little of the power goes directly to gas heating. Therefore, conditions of the gases at the throat exhibit the extreme thermal disequilibrium of the positive column of a glow discharge; the translational/rotational mode temperature is low (~300 K for an uncooled discharge tube), the energy in the vibrational mode is high (0.1 to 0.2 eV per diatomic molecule), the electron density is $n_e \sim 10^{10} cm^{-3}$, and the average electron energy is in the 1.0 eV range.

Downstream of the discharge section is a two-dimensional plane supersonic nozzle, as shown. The nozzle has a high aspect ratio of about 7.5:1, so that in the test section the nozzle width is 3 cm while the distance between the top and bottom nozzle walls is 4 mm. The top and bottom walls of the nozzle are slightly diverging to provide boundary layer relief in the third dimension. The nozzle is made of transparent acrylic plastic, with glass and CaF_2 windows, which allow optical access to the test section. Fabrication and use of a range of nozzles with varying expansion ratios and test section lengths is straightforward and rapid. The system is connected, through a simple channel diffuser, to a ballast tank pumped by a several hundred cfm vacuum pump. Operation at relatively high plenum pressures creates a supersonic flow, of reasonable quality (~75% inviscid core), in the test section of the tunnel [9]. At M=2, run durations of at least a few minutes are attained. An important feature of the nozzle operation is that high level of vibrational excitation existing at the nozzle entrance persists throughout the nozzle length. The vibrational temperature of nitrogen is essentially frozen at the throat values. Also, the electron-ion recombination in the expansion into the test section of the tunnel is sufficiently slow, so that the ionization fraction produced in the DC discharge in plenum ($n_e/N \sim 10^{-9}$) remains nearly constant [9].

Our previous experiments in the M=3 supersonic flowing afterglow with ionization sustained by the DC discharge in plenum [9] did not show any measurable shock modification by the plasma. One possible reason for that was the low ionization fraction in the test section, $n_e/N \sim 10^{-9}$. In previous shock tube and ballistic range experiments which demonstrated considerable shock dispersion and weakening [1-5] the ionization fraction was in the range 10^{-8}-10^{-6}. In the present study, the electron density in the test section is considerably increased by using a transverse RF discharge. It is well known that RF discharges

with dielectric-covered electrodes are considerably more stable than DC discharges [10]. The main reason for this is that this type of RF discharge does not form unstable high electric field cathode layers where ionization is sustained by secondary electron emission [11]. This prevents formation of cathode spots with the normal current density [10] and therefore allows considerable increase of the electrode surface area and the volume occupied by a uniform discharge. In the present experiment, the RF discharge is sustained between 17 mm long, 4 mm wide strip electrodes embedded in the top and bottom nozzle walls, as shown in Fig.1. Both RF electrodes are covered with layers of 1-2 mm thick Pyrex glass to prevent secondary electron emission which results in the discharge collapse into an arc. The electrodes do not extend wall to wall, which would produce considerable discharge and temperature nonuniformity in the boundary layers because of the long flow residence time there. The RF voltage was applied to the electrodes using a 13.56 MHz, 600 W ACG-6B RF power supply and a 3 kW MFJ-949E tuner was used for RF circuit impedance matching. Typically, the reflected RF power did not exceed 5-10% of the forward power. This allowed sustaining a stable, diffuse, and uniform transverse discharge in pure nitrogen, in N_2-He mixtures, and in air. Note that initiating and sustaining of the RF discharge did not require flow pre-ionization by the DC discharge upstream. The RMS RF voltage and current were varied in the range 0.8-1.75 kV and 80-280 mA. The estimated test section electron density at these conditions is up to $n_e=(2\text{-}3)\cdot 10^{11}$ cm^{-3} (i.e. two orders of magnitude higher than produced by the DC discharge), which gives an ionization fraction of $n_e/N\sim 10^{-7}$.

For the shock control studies reported here, an 8 mm long 35° plastic wedge is inserted into the supersonic ionized flow a few millimeters downstream of the RF electrodes, as shown in Fig. 1. With this system, the effect of the nonequilibrium plasmas on the strength of the resultant oblique shock attached to the nose of the wedge can be studied in detail, in a steady and well-controlled plasma environment. The objective of the experiments is to measure the oblique shock angle, under both plasma on and plasma off conditions. Previously it has been reported that the effect of the plasma is to weaken the shock. This should produce an apparent reduction of the shock Mach number and therefore increase the oblique shock angle. Unlike our previous work [9] where the shock angle was measured using a schlieren system, in the present experiments the high-pressure supersonic plasma flow visualization technique [9] is used for shock angle measurements. Since our previous experiments showed that the aerodynamically stabilized DC discharge sustained in the nozzle plenum did not produce any detectable shock angle change, in the present study this discharge is primarily used for the flow visualization. Flow images were taken using a high-resolution monochrome COHU-4910 camera and a SONY digital video camera. On the other hand, the transverse RF discharge sustained in the test section is mainly used to produce high electron densities comparable with those obtained in previous plasma shock experiments [1-5], to study the feasibility of shock weakening by the plasma.

To determine whether the shock modification by the plasma is thermal, i.e. produced by Joule heating of the incident supersonic flow by the discharge, the flow temperature in the test section is measured using infrared emission spectroscopy. For this, a small amount of infrared active gas (2-4% of carbon monoxide) is added to the gas mixture. The rotational temperature of the flow is inferred from high-resolution CO infrared emission spectra taken with a Bruker Fourier transform infrared (FTIR) IFS-66 spectrometer. Each temperature measurement took about 30 seconds. Because of the relatively high flow density (about 1/10 of the atmospheric density), the rotational and translational mode temperatures are in equilibrium.

3. Results and Discussion

Most experiments have been conducted in various N_2-He gas mixtures at the same plenum pressure of P_0=250 torr. The amount of nitrogen in the gas mixture was varied from 10% to 100%. The main reason for adding helium to the gas mixture was to lower the voltage required for sustaining the DC discharge (U=8-12 kV in a 30% N_2 – 70% He mixture vs. U=20-25 kV in pure nitrogen), as well as to lower the power needed to sustain the RF discharge. However, both DC and RF discharges were equally diffuse and stable both in N_2-He mixtures and in pure nitrogen.

With the DC and/or RF discharge on, the nozzle, test section, and diffuser are filled with bright visible emission, arising primarily from the well-known second positive bands of nitrogen, $C^3\Pi_u \rightarrow B^3\Sigma_g$, and from the blue lines of helium [9]. Figure 2 shows typical color images of the flow field around a 35° wedge in the test section in a 50% N_2 – 50% He mixture, with only the DC discharge on and both DC and RF discharges on. One can see that the visible emission makes all features of the supersonic flow, including shocks, boundary layers, expansion waves, and wakes, clearly visible. Detailed interpretation of the flow visualization mechanism is beyond the scope of the present paper; a brief discussion of the possible kinetic mechanisms involved can be found in [9]. In addition to the primary oblique shocks, Fig. 2 also displays a pair of fainter secondary oblique shocks produced by the supersonic flow reflection off the boundary layer growing on the wedge walls, luminous boundary layers, centered expansion waves where the supersonic flow turns a corner, and the dark wake behind the wedge. All these features can be observed in real time simply by looking at the wind tunnel during its operation. Note that a slight curvature of the primary oblique shock near the nose of the wedge is due to a slight gap between the wedge and one of the nozzle walls, rather than the incident plasma flow nonuniformity. Indeed, Fig. 3 shows a high-resolution monochrome image of the test section flow field in the same gas mixture but in a different nozzle with a much better fit between the wedge and the walls. One can see that in this case the oblique shock is nearly perfectly straight. The shock angle of $\alpha=100°$ indicates a test section Mach number of M=1.96. In all experiments discussed in the present paper the DC discharge section used to produce a supersonic flowing afterglow is the same.

Turning the RF discharge on and off during the wind tunnel operation resulted in a considerable shock angle increase. The DC discharge was on all the time to provide plasma flow visualization and enable shock angle measurements with the RF discharge off. Figure 4 shows two high-resolution monochrome flow images in a 30% N_2 - 70% He mixture with the RF discharge on and off. In this experiment, the DC discharge voltage and current were 11 kV and 11 mA, respectively, so the total DC power added to the flow is about 70 W (with about 50 W dissipated on a 400 KΩ ballast resistor). The RF discharge RMS voltage and RMS current were 1100 V and 180 mA, respectively, so the total RF power was about 200 W. The electron density in the RF discharge, estimated from the RF current, is $n_e \cong 2 \cdot 10^{11}$ cm^{-3}, and the ionization fraction is $n_e/N \sim 10^{-7}$. From Fig. 4 one can see that the shock angle increases from $\alpha=99°$ to $\alpha=113°$, which corresponds to a flow Mach number reduction from M=2.0 to M=1.8. Figure 5 also shows a flow image composed of two separate frames, with the RF discharge on and off. Both frames have been differentiated using a Scion Image software package to highlight the location of the shock front and then added together. From Fig. 5, one can clearly see two shock fronts with distinctly different angles, the larger angle corresponding to the frame with the RF discharge on.

Using a COHU monochrome camera, we took a series of still flow frames during the run. The frames were taken at a frequency of approximately 1 frame/second. The objective was to look at the time-dependent behavior of the oblique shock with the RF discharge turned on and off. Figure 6 shows the oblique shock angle as a function of the frame number (i.e. time). One can see that after the RF discharge is turned on, the shock angle slowly (on the order of a few seconds) increases and reaches the near steady state. After the RF discharge is off, the reverse process (i.e. shock angle recovery to its initial value) also takes a few seconds. Note that the flow residence time in the test section is of the order of ten microseconds. During these experiments, both DC and RF voltage and current remained nearly constant in time.

The slow shock angle increase and recovery suggest a purely thermal mechanism, i.e. the heating of the boundary layer in the third dimension (along the line of sight) and the nozzle walls near the RF discharge electrodes, which may well take a few seconds. The observed Mach number reduction is consistent with a flow temperature increase by $\Delta T=24$ K (this number is obtained for a one-dimensional Rayleigh flow at M=2 with $\gamma=1.55$). In the present experiments, we never observed the anomalous shock behavior previously reported by several groups [1-5] (such as shock dispersion, shock splitting, and "precursor" formation in front of the shock). The shock front is always clearly defined, and no visible splitting occurs (e.g. see Figs. 4,5). We believe that these previously reported effects are most likely to be

due to nonuniform heating of the flow by the discharge, which in the present experiment is reduced to a minimum.

To determine whether the observed shock weakening is indeed a purely thermal effect, we measured the flow temperature in the test section, with only the DC discharge on, with only the RF discharge on, and with both discharges on, using infrared emission spectroscopy. For the temperature measurements, 10 torr of CO was added to the baseline 75 torr N_2 / 175 torr He mixture. The temperature was measured downstream of the RF electrodes but upstream of the wedge model, halfway between the nozzle axis and the wall. The FTIR signal was collected from a region of about 1 mm^2 area, while the rest of the nozzle was masked off. However, the resultant CO fundamental emission spectrum is integrated along the line of sight in the third dimension across the nozzle, which includes the boundary layers near the top and the bottom nozzle walls.

Figure 7 shows two typical CO fundamental emission spectra (R-branch of the $1\rightarrow0$ band) taken with only the DC discharge on and with only the RF discharge on. The DC discharge voltage and current were 19.6 kV and 24.0 mA, respectively, with about 230 W power added to the flow. The RF RMS voltage and current were 1.6 kV and 120 mA, with the total RF power of about 200 W. Note that the measured CO $1\rightarrow0$ emission intensity in the DC discharge afterglow exceeds the emission intensity in the RF discharge afterglow by about a factor of five (see Fig. 7). Also, the CO spectrum in the RF discharge afterglow has a very weak $2\rightarrow1$ band (a second series of rotational lines below 2170 cm^{-1}, see Fig. 7). This shows that the CO vibrational temperature in the RF discharge is considerably lower than in the DC discharge. In other words, in the RF discharge a much smaller fraction of the input power goes into vibrational excitation, while more power goes into excitation of more rapidly relaxing electronic states of N_2 and He and ultimately into gas heating. This is consistent with the estimated reduced electric field values, $(E/N)_{DC}\cong5\cdot10^{-16}$ V·cm^2 and $(E/N)_{DC}\cong10\cdot10^{-16}$ V·cm^2. Thus, the transverse RF discharge is expected to heat the gas flow more efficiently than the DC discharge.

Figure 8 shows Boltzmann plots obtained from two CO emission spectra, one with 230 W DC added to the flow, and the other with 230 W DC and 200 W RF coupled to the flow. One can see that in both cases the flow is optically thin for the CO emission since there is no significant self-absorption among the low rotational levels. The best fit to the data obtained using the rotational maxima between $J'=1$ and $J'=12$ corresponds to the translational-rotational temperatures of T=190 K and 221 K for these two cases. However, the best fit to the rotational maxima from $J'=13$ and $J'=19$ gives the temperatures of T=200 and 271 K, respectively. This result most likely indicates a temperature nonuniformity across the line of sight, with the lower temperature in the inviscid core and the higher recovery temperature in the boundary layer.

Figure 9 shows the flow temperature as a function of the RF discharge power added to the flow. At each value of the RF power, the temperature was measured both with the 230 W DC discharge on and off. One can see that when 200 W RF power is added to the flow, the temperature inferred from the low rotational level populations ($J'=1$-12) increases by only $\Delta T=15$ K, while the temperature inferred from the high rotational levels populations ($J'=12$-19) rises by $\Delta T=50$ K. The temperature inferred from all available data ($J'=1$-19) increases by $\Delta T=35$ K This can be interpreted as preferential heating of the boundary layers by the RF discharge. This temperature increase is consistent with the one-dimensional estimate of the temperature rise needed to explain the observed shock angle change by the flow heating, $\Delta T=24$ K. Thus, the temperature measurements, in addition with the extremely slow shock weakening and recovery (see Fig. 6) suggest that the shock control by the plasma is a purely thermal effect.

The emission spectroscopy measurements also explain why the use of 200 W RF power results in a substantial shock weakening, while adding 500 W of DC power to the flow does not produce any detectable effect on the shock angle [9]. Basically, it occurs because in the transverse RF discharge a larger fraction of the electric field power goes to gas heating, which preferentially occurs in the boundary layers.

An additional run was conducted in a 10% N_2 / 90% He mixture. In flows with large fraction of helium, the oblique attached shock becomes strongly curved and closely resembles a bow shock. With

both 30 W DC discharge and 100 W RF discharge turned on, the shock stand-off distance increased by about 0.1 mm (see Fig. 10).

In the last series of experiments, the nonequilibrium plasma wind tunnel facility was operated in atmospheric air. Room air entered the nozzle plenum at the pressure P_0=250 torr through a valve opened in the gas line upstream and the transverse RF discharge was initiated in the supersonic test section. As in all previous runs in N_2-He mixtures and in nitrogen, the discharge in air was diffuse and stable, with no sign of arc filaments (see Fig. 11). The only significant difference from the N_2-He runs was that the visible afterglow in air was nearly absent due to very rapid relaxation of radiating electronically excited molecules, which did not allow straightforward plasma flow visualization. For this reason, no plasma shock weakening measurements in air have been performed. However, such measurements can be easily made on the present facility using a conventional schlieren system available in our group. These experiments showed that uniform and stable plasma with the electron density of $n_e=(2\text{-}3)\cdot 10^{11}$ cm^{-3} can be sustained in supersonic air flows using a transverse RF discharge. Both electron density and ionization efficiency are expected to be considerably increased by replacing the sine wave RF voltage by a series of very short high-voltage pulses, such as been done in high-power CO lasers [12]. This would allow operation at a very low duty cycle and would therefore greatly improve the discharge stability and the plasma power budget [12], thereby opening a possibility of the use of transverse high-frequency pulsed discharges for MHD energy extraction and/or acceleration of supersonic air flows [13,14]. The high voltage, high repetition rate pulsed power supply for this application is currently being developed at Ohio State.

4. Summary

A unique supersonic nonequilibrium plasma wind tunnel, which produces a highly nonequilibrium plasma flow with low gas kinetic temperatures at M=2, is used for studies of shock modification by nonequilibrium plasmas. Supersonic flow is maintained at complete steady state. The flow is ionized by a high-pressure aerodynamically stabilized DC discharge in the tunnel plenum and by a transverse RF discharge in the supersonic test section. The DC discharge is primarily used for the supersonic flow visualization, while the RF discharge provides high electron density for shock modification in the supersonic test section. High-pressure flow visualization produced by the plasma makes all features of the supersonic flow, including shocks, boundary layers, expansion waves, and wakes, clearly visible. Attached oblique shock structure on the nose of a 30° wedge with and without RF ionization in a M=2 flow is studied in various nitrogen-helium mixtures. It is found that the use of the RF discharge increases the shock angle by 14°, from 99° to 113°, which corresponds to Mach number reduction from M=2.0 to M=1.8. Time-dependent measurements of the oblique shock angle show that the time for the shock weakening by the plasma, as well as the shock recovery time after the plasma is turned off, is of the order of seconds. Since the flow residence time in the test section is of the order of ten microseconds, this result suggests a purely thermal mechanism of shock weakening due to heating of the boundary layers and the nozzle walls by the discharge. Gas flow temperature measurements in the test section using infrared emission spectroscopy, with carbon monoxide as a thermometric element, are consistent with the observed shock angle change. This also shows that shock weakening by the plasma is a purely thermal effect. The results demonstrate feasibility of both sustaining uniform ionization, with electron density up to $n_e=(2\text{-}3)\cdot 10^{11}$ cm^{-3} in supersonic nitrogen and air flows and the use of nonequilibrium plasmas for supersonic flow control. This opens a possibility for the use of transverse stable RF discharges for nonequilibrium MHD energy extraction and/or acceleration of supersonic air flows.

5. Acknowledgements

The support of MSE Technologies, Inc., under a NASA prime, and Air Force Office of Scientific Research is gratefully acknowledged. Partial support from the Ohio Board of Regents Investment Fund is gratefully acknowledged. We would also like to express our sincere gratitude to Prof. Frank DeLucia and Dr. Scott Harris for useful suggestions, and to Prof. Mo Samimy for lending us a digital color camera.

6. References

1. Klimov, A.I., Koblov, A.N., Mishin, G.I., Yu.L. Serov, and I.P. Yavor, Sov. Tech. Phys. Lett, vol. 8, p. 192, 1982
2. Basargin, I.V., and Mishin, G.I., Sov. Tech. Phys. Lett., vol. 11, p. 535, 1985
3. Mishin, G.I., Klimov, A.I., and Gridin, A.Yu., Sov. Tech. Phys. Lett., vol. 17, p. 602, 1992
4. Ganguly, B.N., and Bletzinger, P., "Shock Wave Damping and Dispersion in Nonequilibrium Low Pressure Argon Plasmas", Phys. Lett. A230, p. 218, 1997
5. Lowry, H., Blanks, J., Stepanek, C., Smith, M., Crosswy, L., Sherrouse, P., Felderman, J. and Wood, B., "Characterization of the Shock Structure of a Spherical Projectile in Weakly Ionized Air Through Ballistic Range Test Techniques", 2nd Weakly Ionized Gas Workshop, Norfolk, VA, April 1998
6. I.V. Adamovich, V.V. Subramaniam, J.W. Rich, and S.O. Macheret, "Phenomenological Analysis of Shock Wave Propagation in Weakly Ionized Plasmas", AIAA Journal, vol. 36, No.5, p. 816, 1998
7. Ionikh, Yu.Z., Chernysheva, N.V., Yalin, A.P., Macheret, S.O., Martinelli,L., and Miles, R.B., "Shock Wave Propagation Through Glow Discharge Plasmas: Evidence of Thermal Mechanism of Shock Dispersion," AIAA Paper 2000-0714
8. Macheret, S.O., Martinelli, L., and Miles, R.B., "Shock Wave Propagation and Structure in Non-Uniform Gases and Plasmas", AIAA Paper 99-0598
9. Yano. R., Contini, V., Ploenjes, E., Palm, P., Merriman, S., Aithal, S., Adamovich, I., Lempert. W., Subramaniam. V., and Rich, J.W., "Measurements of Shock Modification and Flow Visualization In A Supersonic Nonequilibrium Plasma Wind Tunnel", accepted for publication in AIAA Journal, 2000
10. Raizer, Yu.P., "Gas Discharge Physics", Springer, Berlin, 1991
11. Raizer, Yu.P., Shneider, M.N., and Yatsenko, N.A., "Radio-Frequency Capacitive Discharges", CRC Press, Boca Raton, 1995
12. Generalov, N.A., V.P. Zimakov, V.D. Kosynkin, Yu.P. Raizer, and D.I. Roitenburg, Technical Physics Letters, vol. 1, p. 431, 1975
13. Macheret, S.O., Shneider, M.N., Miles, R.B., Lipinski, R.L., and Nelson, G.L., "MHD Acceleration of Supersonic Air Flows Using Electron Beam Enhanced Conductivity", AIAA Paper 98-2922, 29th Plasmadynamics and Lasers Conference, Albuquerque, NM, June 1998
14. Macheret, S.O., Shneider, M.N., and Miles, R.B., "MHD Power Extraction from Cold Hypersonic Air Flow with External Ionizers", AIAA Paper 99-4800

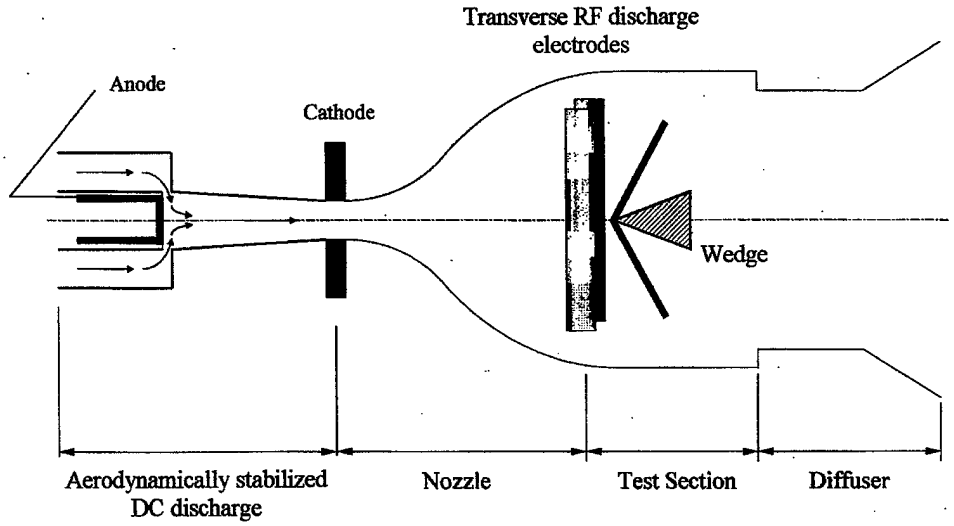

Figure 1. Schematic of the wind tunnel experiment

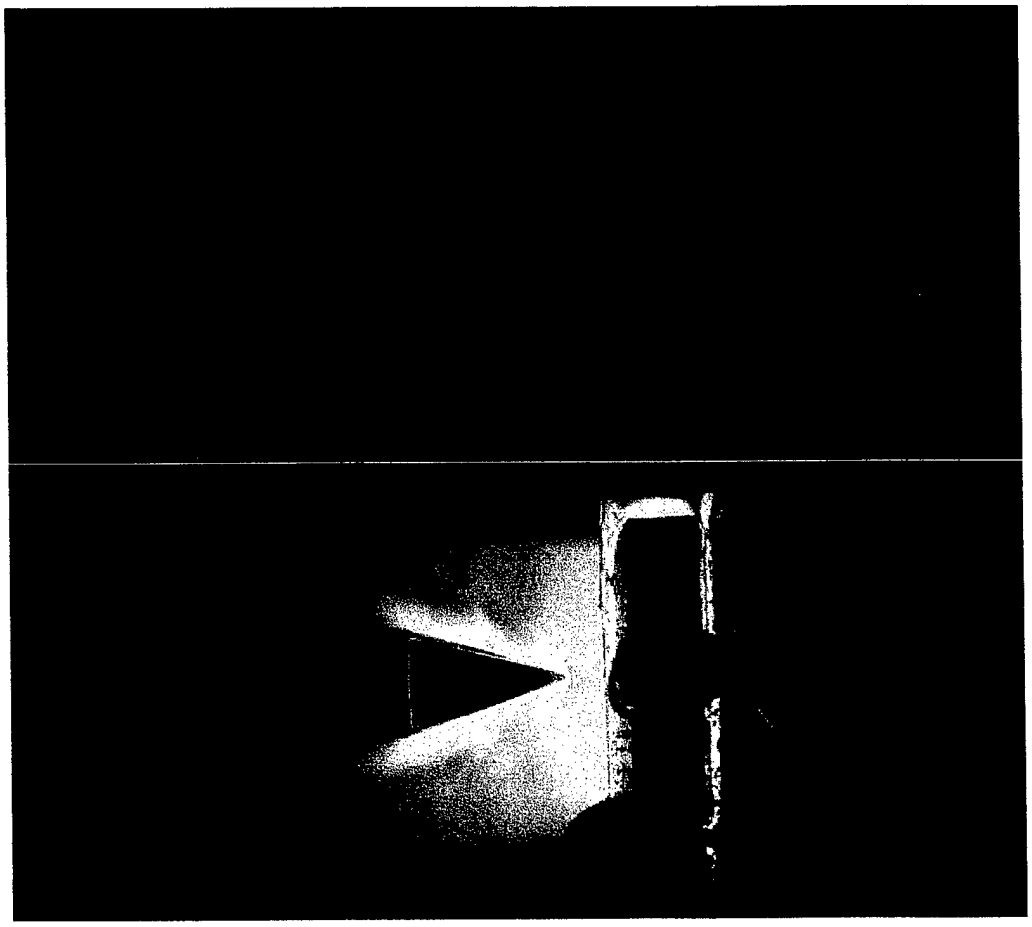

Figure 2. Plasma flow visualization in a 50% N_2 – 50% He mixture. Top, only DC discharge is on; bottom, both DC and RF discharges are on.

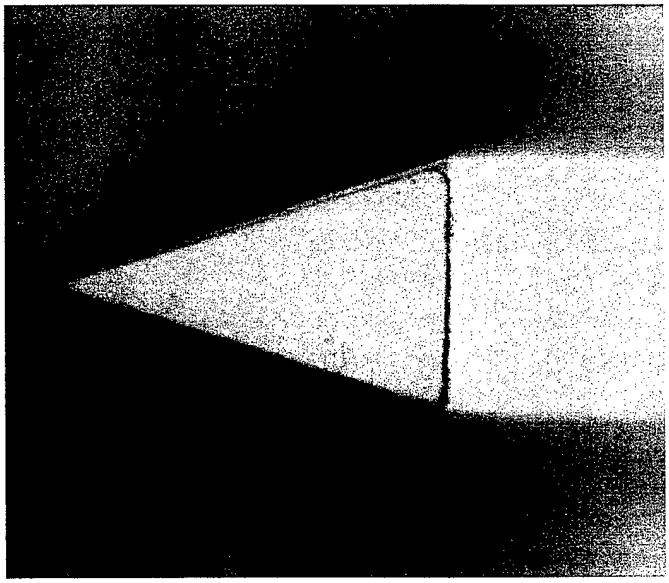

Figure 3. Plasma flow visualization in a 50% N_2 – 50% He mixture. Only DC discharge is on. The wedge full angle is 35^0, the shock full angle is 100^0, which indicates the Mach number of M=1.96

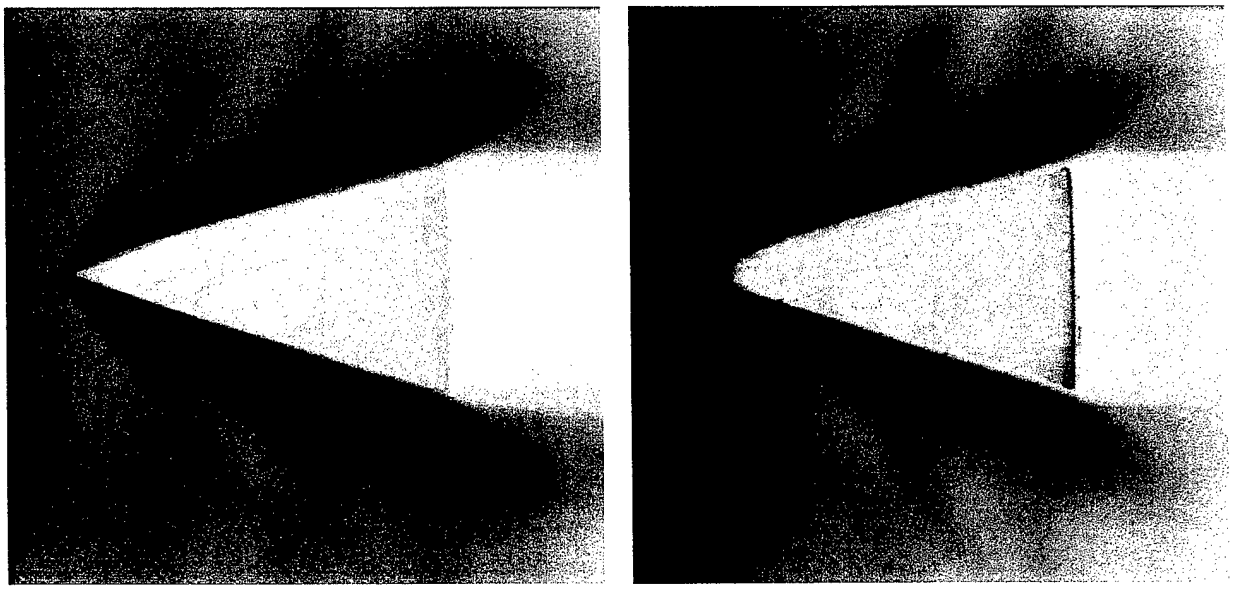

Figure 4. Shock weakening by the plasma in a 30% N_2- 70% He mixture. Left, only DC discharge on (α=99°); right, both DC and RF discharges are on (α=113°).

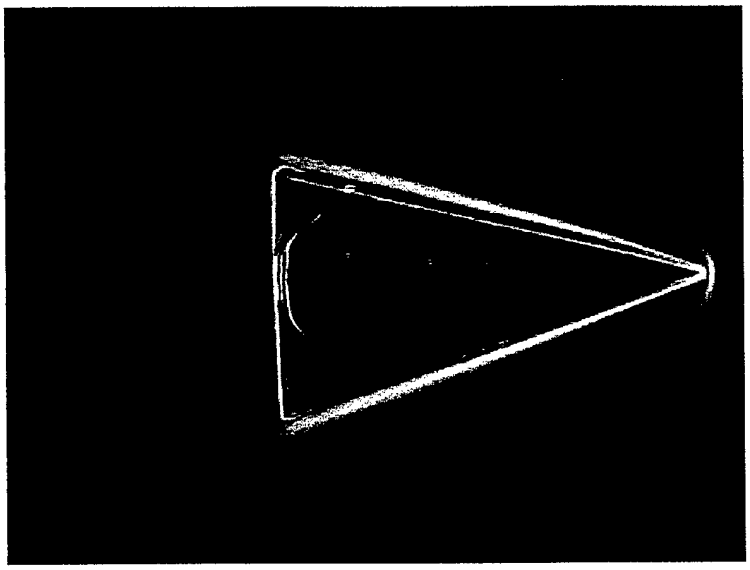

Figure 5. Shock weakening by the plasma in a 30% N_2 – 70% He mixture. Two flow images with RF discharge off and RF discharge on are differentiated to highlight the shock front location and then added together. The larger angle shock (117°) corresponds to the "RF on" frame, and the smaller angle shock (105°) corresponds to the "RF off" frame

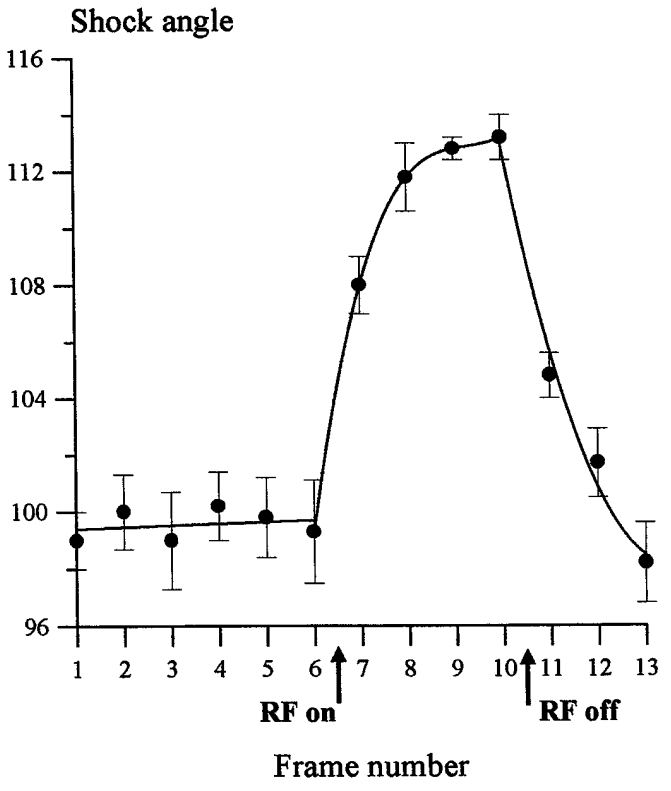

Figure 6. Oblique shock angle as a function of a frame number (i.e. time) in a 30% N_2 – 70% He mixture.

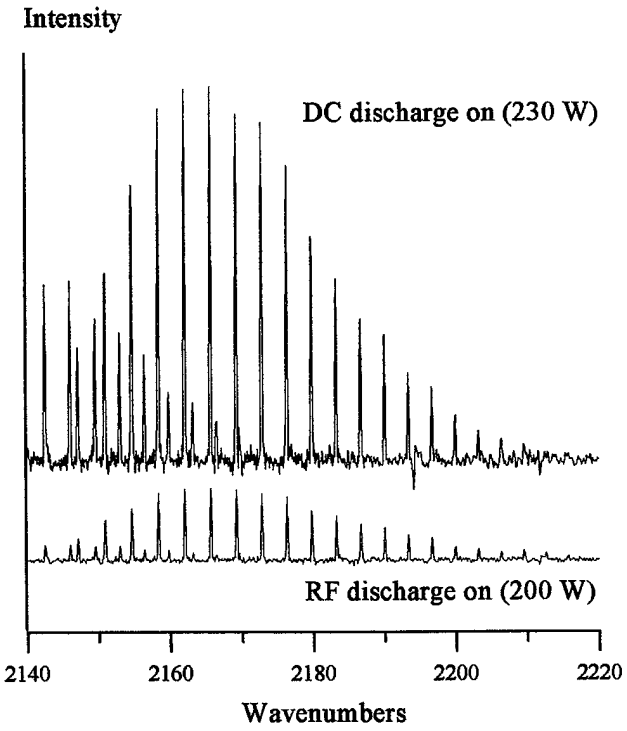

Figure 7. Typical test section R-branch 1→0 CO emission spectra in a 75 torr N_2 / 175 torr He / 10 torr CO mixture.

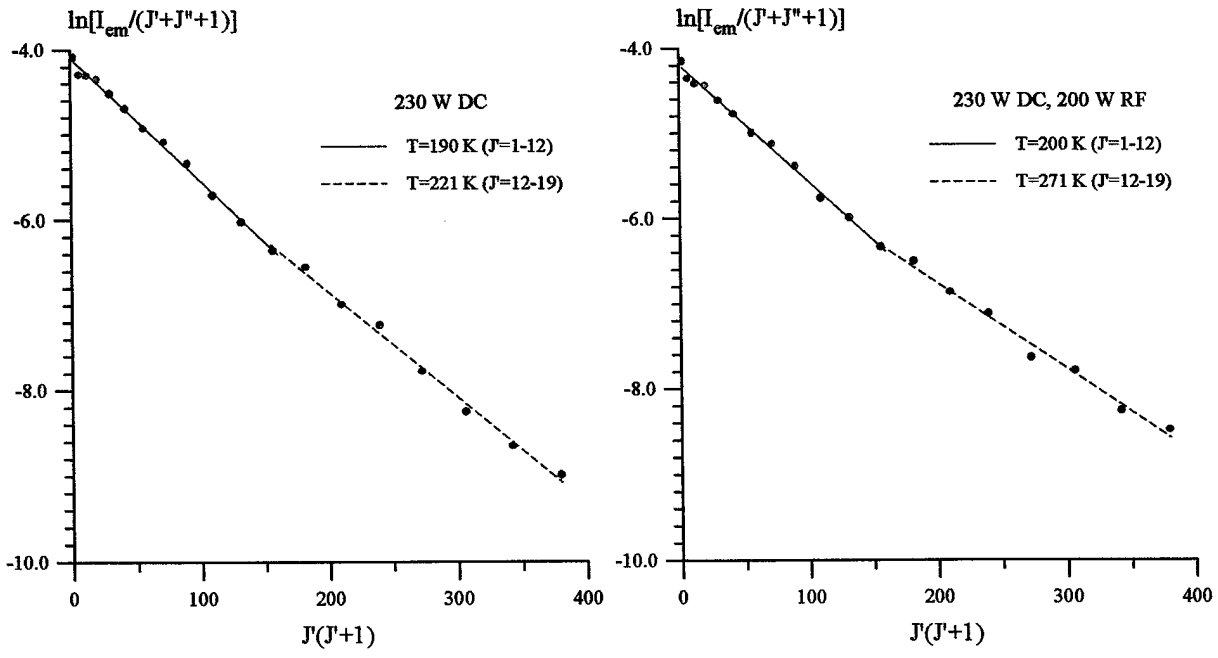

Figure 8. Botzmann plots of the CO emission spectra in a 75 torr N_2 / 175 torr He / 10 torr CO mixture. (a) only DC discharge is on, (b) both DC and RF discharges are on

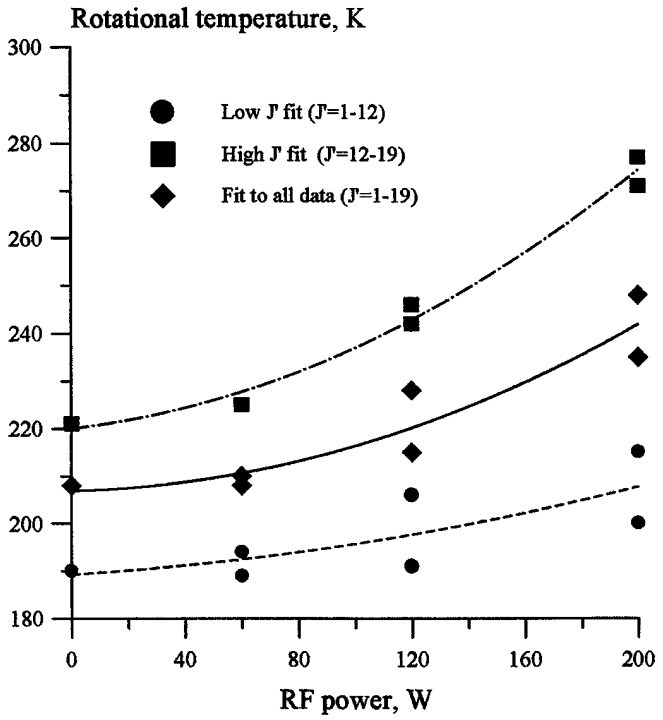

Figure 9. Test section temperature in a 75 torr N_2 / 175 torr He / 10 torr CO mixture as a function of the RF discharge power. At each value of RF power, the temperature is measured both with the 230 W DC discharge on and off.

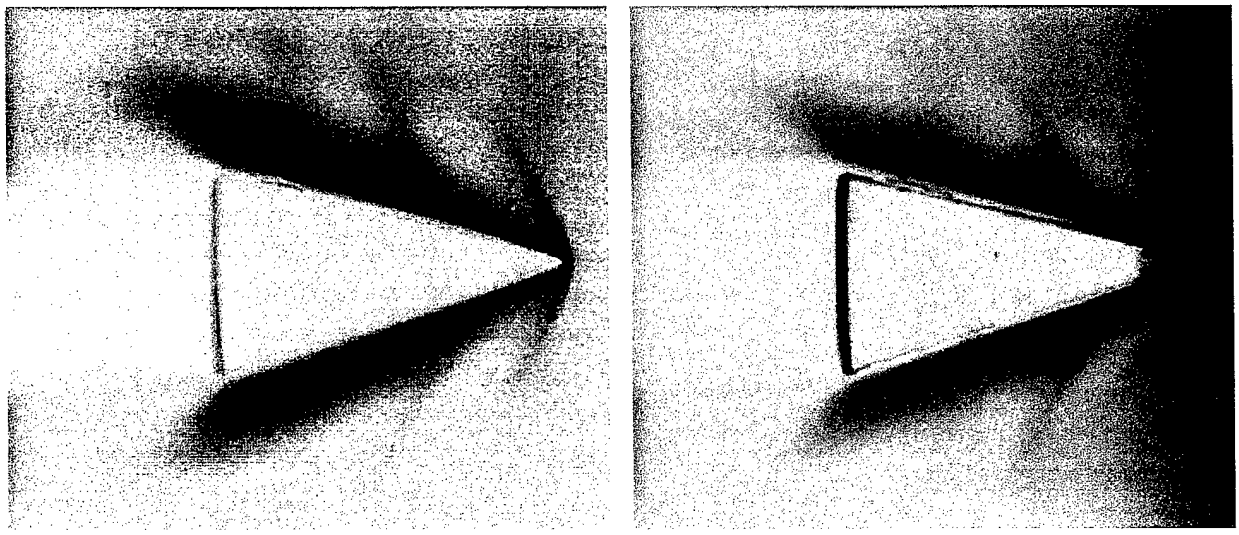

Figure 10. Oblique shock and bow shock in a 10% N_2 / 90% He mixture. Left, RF discharge off; right, RF discharge on. Shock stand-off distance increase is 0.1 mm

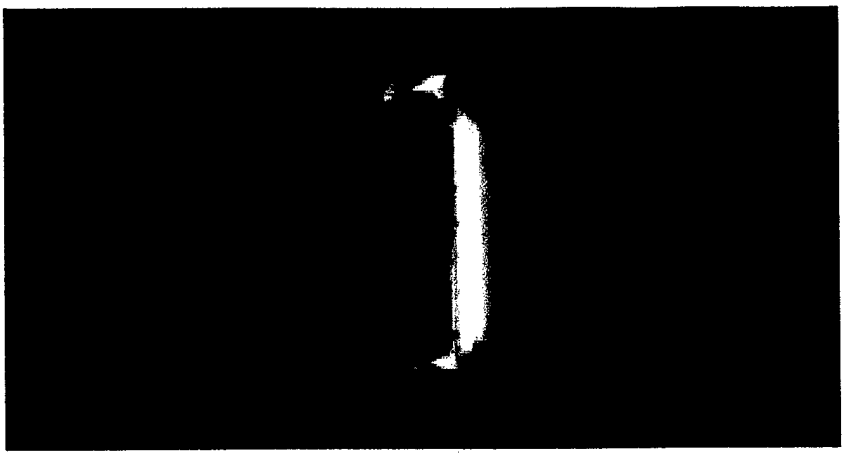

Figure 11. Transverse RF discharge in atmospheric air. P_0=250 torr

2.5 The Effect of a Nonequilibrium RF Discharge Plasma on a Conical Shock Wave in a M = 2.5 Flow

AIAA 2001-3059

THE EFFECT OF A NONEQUILIBRIUM RF DISCHARGE PLASMA ON A CONICAL SHOCK WAVE IN A M=2.5 FLOW

Rodney Meyer, Peter Palm, Elke Plönjes, J. William Rich,
and Igor V. Adamovich

Nonequilibrium Thermodynamics Laboratory
Department of Mechanical Engineering
The Ohio State University, Columbus, OH 43210-1107

32nd AIAA Plasmadynamics and Lasers Conference and 4th Weakly Ionized Gases Workshop

11 - 14 June 2001 / Anaheim, CA

AIAA 2001-3059

THE EFFECT OF A NONEQUILIBRIUM RF DISCHARGE PLASMA ON A CONICAL SHOCK WAVE IN A M=2.5 FLOW[1]

Rodney Meyer[2], Peter Palm[3], Elke Plönjes[3], J. William Rich[4], and Igor V. Adamovich[5]

Nonequilibrium Thermodynamics Laboratory
Department of Mechanical Engineering
The Ohio State University, Columbus, OH 43220-1107

Abstract

The paper discusses results of an experimental study of shock modification in a M=2.5 supersonic flow of nonequilibrium plasma over a cone. The experiments are conducted at a nonequilibrium plasma supersonic wind tunnel. Recent experiments at Ohio State using supersonic plasma flow over a quasi-two-dimensional wedge showed that an oblique shock can be considerably weakened by a transverse RF discharge plasma. The previously observed shock weakening, however, has been found consistent with a temperature rise in the boundary layers heated by the discharge. In the present study, the boundary layer effects are reduced by placing an entire cone model into a supersonic inviscid core flow. Electron density in the supersonic plasma flow in the test section is measured using microwave attenuation. The ionization fraction in the discharge is in the same range as in the previous plasma shock experiments, up to $n_e/N=(1.2\text{-}3.0)\cdot 10^{-7}$. The results do not show any measurable shock weakening. This strongly suggests that the previously observed shock weakening and dispersion in nonequilibrium plasmas are entirely due to thermal effects.

1. Introduction

Shock wave propagation in weakly ionized glow discharge plasmas (with ionization fraction of $n_e/N\sim 10^{-8}\text{-}10^{-6}$) has been extensively studied over the last 15 years, both in Russia [1-11] and in the U.S. [12-20]. A number of anomalous effects, such as shock acceleration, weakening, and dispersion, have been reported. These effects have been observed in discharges in various gases (air, N_2, Ar) at pressures up to P=30 Torr, and for Mach numbers M=1.5-4.5. They also persist for a long time after the discharge is off (up to ~1 ms). These results led to a suggestion that the anomalous shock wave behavior in nonequilibrium plasmas is primarily due to the effect of the speed of sound and the flow field modification by the charged species (e.g. ion-acoustic wave) [21] or by the metastable species [22-24] present in the plasma.

---

[2] Undergraduate Research Assistant
[3] Post-Doctoral Researcher
[4] Ralph W. Kurtz Professor of Mechanical Engineering, Associate Fellow AIAA
[5] Associate Professor, Dept. of Aerospace Engineering and Aviation, Senior Member AIAA

Recent experimental and modeling results suggest that these effects can in fact be explained by non-uniform gas heating in the discharge. Indeed, pulsed glow discharge / shock tube experiments [15] demonstrate that shock weakening and dispersion in glow discharge plasmas are no longer observed when the gas temperature gradients are reduced to a minimum. In addition, several computational fluid dynamics models predict acceleration, weakening, and dispersion of the shock wave propagating across axial and radial temperature gradients (without plasmas) [25-27], fairly consistent with the experiments. Finally, analysis of possible plasma-related mechanisms of the flow field modification (ion-acoustic waves, energy storage by metastable species, etc.) shows that both these phenomena have negligible effect on the shock wave propagation [28]. This occurs for two basic reasons: (i) the ionization fraction in these plasmas is far too low for the charged species, perturbed by the shock, to produce significant coupling with the neutral species flow field; and (ii) the amount of energy stored in the metastables is too low, or the metastable relaxation rate is too slow to affect the energy balance in the shock.

Recently, experimental studies of shock modification have been conducted at Ohio State using a nonequilibrium plasma supersonic wind tunnel [17-19]. In this experiment, an oblique shock attached to a wedge located in a supersonic flow of a cold, nonequilibrium N_2-He plasma was monitored using high-pressure plasma flow visualization. The plasma was produced by an aerodynamically stabilized diffuse DC glow discharge [17] sustained in the tunnel plenum and by a transverse RF discharge [18] sustained in the supersonic test section. The advantage of this experiment is that a stationary shock is observed in a steady state plasma flow with well-characterized parameters. In addition, in this experiment the ionization is sustained in a cold supersonic flow without producing considerable gas heating. In other words, the thermal and ionization effects are uncoupled. Such an experiment can determine whether ionization contributed to acceleration, weakening, and dispersion of shock waves in glow discharge plasmas observed in previous experiments [1,2,12,13] or whether these effects are entirely due to radial and axial temperature gradients present in the plasma.

Our previous measurements [18] showed considerable shock angle increase with the RF discharge turned on, i.e. shock weakening. With the RF discharge on, the shock angle increased from its baseline value of $\alpha=99^0$ to $\alpha'=113^0$, which corresponds to an apparent Mach number reduction from M=2.06 to M=1.88. However, both the observed shock weakening and its subsequent recovery after the RF discharge was turned off occurred on a long time scale, over a few seconds. For comparison, the supersonic flow residence time in the test section is of the order of 50 μsec. In addition, the observed Mach number reduction was found to be consistent with the temperature increase in the boundary layers on the test section walls, adjacent to the transverse RF discharge electrodes. These observations suggest that the observed shock weakening is likely to be due to thermal effects, in particular, oblique shock interaction with the heated boundary layers.

The present paper discusses the results of a follow-on experimental study where the boundary layer effects on the shock are reduced. The main objective of this work is to determine whether the shock weakening by plasmas reported in previous studies at Ohio State and elsewhere is indeed due to thermal effects.

2. Experimental Facility

The facility used in the present study is a modification of a recently developed, small-scale, steady-state nonequilibrium plasma wind tunnel [17-19]. The design and operation of the wind tunnel has been described in greater detail in Refs. [17,18]. Briefly, the supersonic flow of nonequilibrium plasma in the wind tunnel is produced by an aerodynamically stabilized diffuse DC glow discharge [17] sustained in the tunnel plenum and by a transverse RF discharge [18] sustained in the supersonic test section. Both discharges can be sustained at quite high plenum and test section pressures, up to P_0=2/3 atm and P_{test}=0.1 atm, respectively, in nitrogen and air. Operation at relatively high plenum pressures creates a supersonic flow of reasonable quality (~75% inviscid core), in the test section of the tunnel [17]. At M=2, run durations of at least a few minutes are attained [18]. This is *not* an arc-heated tunnel. Although the electrical power into the discharges can be rather high, up to 500 W DC and 300 W RF in pure N_2, up to about 90% of the input power goes into the vibrational and electronic energy modes of nitrogen [29]. In contrast to an electric arc, very little of the power goes directly to gas heating. Therefore, conditions of the gases in the test section exhibit the extreme thermal disequilibrium of the positive column of a glow discharge; the translational/rotational mode temperature is low (~100-200 K), the energy in the vibrational mode is high (0.1 to 0.2 eV per diatomic molecule), the electron density is $n_e \sim 10^{11}$ cm^{-3}, and the average electron energy is in the 1.0 eV range.

Downstream of the plenum / DC discharge section is a 9 cm long, rectangular cross section supersonic nozzle, shown in Figure 1. The nozzle is made of transparent acrylic plastic, with a CaF_2 window, which provides optical access to the test section. Fabrication and use of a range of nozzles with varying expansion ratios and test section lengths is straightforward and rapid. The nozzle is connected, through a simple step diffuser, to a ballast tank pumped by a several hundred cfm vacuum pump. To reduce the effect of the side wall boundary layers on the supersonic inviscid core flow, the side walls of the nozzle are diverging at a constant angle of 5.5^0. This also allows accommodation of a small plastic cone model in the test section. The nozzle throat and exit dimensions are 17 mm x 3 mm and 29 mm x 20 mm, respectively. During the wind tunnel operation, static pressure in the test section is monitored using two pressure taps in the top nozzle wall, one between the RF electrodes and the other approximately halfway between the electrodes and the diffuser (see Fig. 1). The diameter of the pressure taps is about 0.2 mm.

In the present experiment, the DC discharge in the nozzle plenum is used only for the supersonic plasma flow visualization [17,18]. Our previous experiments [17] showed that turning the DC discharge on and off does not produce a detectable effect of the shock angle. On the other hand, the RF discharge is primarily used to produce ionization in the supersonic test section. The RF discharge is sustained between 17 mm long, 4 mm wide strip copper electrodes embedded in the nozzle side walls, as shown in Fig. 1. Both RF electrodes are placed inside the C-shaped rectangular quartz channels, as shown in Fig. 1, to prevent secondary electron emission which would result in the discharge collapse into an arc. The thickness of the quartz layers between the electrodes and the flow is 1 mm. The electrodes do not extend wall to wall (see Fig. 1), since this would produce considerable discharge and temperature nonuniformity in the boundary layers because of the long flow residence time there. The RF voltage was applied to the electrodes

using a 13.56 MHz, 600 W ACG-6B RF power supply and a 3 kW MFJ-949E tuner was used for RF circuit impedance matching. Typically, the reflected RF power did not exceed 3-5% of the forward power. This allowed sustaining a stable, diffuse, and uniform transverse discharge in air, nitrogen, and N_2-He mixtures. Initiating and sustaining of the RF discharge did not require flow pre-ionization by the DC discharge upstream.

For the electron density measurements in the test section, two rectangular microwave waveguides, 2 cm x 1 cm across, are placed on both sides of the nozzle immediately downstream of the RF electrodes. The electron density in the plasma is determined from the relative attenuation of a 10 GHz microwave radiation across the plasma. The average electron density in the plasma is inferred from these measurements using the following relation [30],

$$n_e = \frac{m_e c \varepsilon_0}{e^2} \nu_{coll} \frac{\delta V}{V_{inc}} \frac{1}{d}, \qquad (1)$$

where ν_{coll} is the electron-neutral collision frequency, $\frac{\delta V}{V_{inc}} = \frac{V_{trans} - V_{inc}}{V_{inc}}$ is the relative attenuation factor in terms of the forward power detector voltage proportional to the incident and the transmitted microwave power, and d=7.5 mm is the average distance between the internal nozzle walls in the test section (i.e. at the location of the waveguides). The microwave attenuation measurement apparatus is described in greater detail in our previous publication [30].

For the shock modification studies reported here, an 8 mm long, 40^0 full angle plastic cone is inserted into the supersonic ionized flow 5 mm downstream of the RF electrodes, as shown in Fig. 1. The model is glued to a metal sting embedded in a thin plastic brace located in the diffuser. The distance between the test section side walls at the model location exceeds the model base diameter by about a factor of 2.2. The model occupies about 6% of the test section cross sectional area. With this system, the effect of the nonequilibrium plasmas on the strength of the resultant shock attached to the nose of the wedge can be studied in detail, in a steady and well-controlled plasma environment. The objective of the experiments is to measure the oblique shock angle, under both plasma on and plasma off conditions. Previously it has been reported that the effect of the plasma is to weaken the shock. This should produce an apparent reduction of the shock Mach number and therefore increase the shock angle. Flow images visualized by plasma were taken using a high-resolution monochrome camera COHU-4910.

3. Results and Discussion

The presents experiments have been conducted in pure nitrogen as well as in two different N_2 - He gas mixtures, 70% N_2 - 30% He and 30% N_2 - 70% He at the same plenum pressure of P_0=250 torr. At these conditions, the mass flow rate through the nozzle is from 4.3 g/s in a 70% He mixture to 5.1 g/s in nitrogen. Both the axial DC and the transverse RF discharges were equally diffuse and stable in all gas mixtures used. The results of the DC and the RF current and voltage measurements at these conditions are summarized in Table 1. It can be seen that a sizable fraction of the DC power generated by the power supply is dissipated in the ballast resistor (from

25% in nitrogen up to 60% in a 30% N_2 - 70% He mixture). The reduced electric field in the aerodynamically stabilized DC discharge, determined from the measured DC voltage, plenum pressure, and the interelectrode distance varied in the range $(E/N)_{DC}=(4\text{-}6)\cdot10^{-16}$ V·cm^2. At these conditions, up to 90% of the input electrical power goes to vibrational excitation of N_2 by electron impact rather than to direct gas heating [29]. This limits the maximum temperature rise in the DC discharge to only a few degrees. Indeed, for a nitrogen flow with a mass flow rate of 5.1 g/sec and the DC discharge power of 290 W, the temperature rise can be estimated as $\Delta T\sim5$ K. Due to the very slow rate of N_2 vibrational relaxation at these temperatures [31], its contribution to the gas heating in the supersonic expansion flow is negligible.

The estimated reduced electric field based on the measured RMS RF voltage and the distance between the RF electrodes of ~10 mm, is significantly higher, $(E/N)_{RF}=(10\text{-}20)\cdot10^{-16}$ V·cm^2. This estimate does not take into account the voltage drops across the quartz layers covering the electrodes as well as across the plasma sheaths. The measured RMS RF current varies from 72 mA to 184 mA which gives the current density in the transverse RF discharge of j=100-270 mA/cm^2. Although at these conditions a much smaller fraction of the input power goes to vibrational excitation [29], the temperature rise in the RF discharge remains rather modest. Our previous measurements [18] show that the temperature rise in the inviscid core of a M=2 30% N_2 – 70% He flow excited by a 200 W RF discharge is only $\Delta T=15$ K.

Table 1. DC and RF discharge parameters

Run #	Gas mixture	U_{DC}, kV	I_{DC}, mA	DC power, W	RF power, W	U_{RF}, kV (RMS)	I_{RF}, mA (RMS)
1	30% N_2 70% He	17.0	25.2	175	100	0.78	72
2					200	1.28	111
3					250	1.42	119
4	70% N_2 30% He	20.0	17.3	225	200	1.28	130
5					300	1.70	176
6					350	1.84	184
7	N_2	25.0	15.3	290	200	1.28	122
8					300	1.70	173

The results of the electron density measurements are summarized in Table 2. The electron-neutral collision frequency required for the electron density inference, ν_c, was obtained from the Boltzmann equation solution at $E/N=10\cdot10^{-16}$ V·cm^2 [33] using the experimental cross-sections of elastic and inelastic electron-molecule collision processes available in the literature. At P=20 torr and T=150 K, the collision frequencies in N_2, 30% He mixture, and 70% He mixture are $\nu_c=1.74\cdot10^{11}$ s^{-1}, $1.47\cdot10^{11}$ s^{-1}, and $1.10\cdot10^{11}$ s^{-1}, respectively. It can be seen that the electron density in the RF discharge in pure nitrogen is nearly independent of the RF power (within ~25%), $n_e\cong(1.5\text{-}2.0)\cdot10^{11}$ cm^{-3}. The observed electric current increase with the applied RF power (see Table 1) is likely to be due to the electron drift velocity increase at a higher E/N. Increase of helium partial pressure in the gas mixture up to 70% resulted in the electron density rise of about

a factor of two, up to $n_e=3.6\cdot10^{11}$ cm^{-3}. These values of electron density correspond to the test section ionization fraction of $n_e/N=(1.2\text{-}3.0)\cdot10^{-7}$, which are in the same range as the ionization fractions in previous plasma shock experiments [1,2,12,13].

In contrast, the test section electron density produced by the DC discharge afterglow in the nozzle plenum (with the RF discharge off) is much lower, $n_e<3\cdot10^9$ cm^{-3}. In fact, in this case microwave absorption measurements did not show detectable absorption above the noise level. This dramatic difference between the electron densities in the DC discharge afterglow and in the RF discharge is mainly due to two factors, (i) the lower reduced electric field in the DC discharge, and (ii) the flow expansion between the nozzle plenum and the test section. Basically, the value of E/N in nonequilibrium discharges in molecular gases controls the electron energy balance (e.g. see Fig. 2 [32]). Increase of E/N reduces the fraction of input power going into vibrational excitation and greatly increases the rates of both molecular dissociation and ionization (see Fig. 2). This is consistent with our previous measurements of a CO vibrational temperature in the supersonic plasma flows sustained by the DC and RF discharges [18]. Higher values of E/N in the transverse RF discharge are responsible for a higher electron impact ionization rate and therefore higher electron density. In addition, expansion of the DC afterglow plasma downstream of the nozzle throat reduces both the number density and the electron density in the test section. Note that the flow residence time in the nozzle, $\tau_{flow}\sim U/L\sim50\text{-}100$ μsec, is too short to allow significant electron-ion recombination downstream of the DC discharge (the recombination time is $\tau_{rec}\sim1/\beta n_e\sim1$ msec). Here U~500-1000 m/s is the flow velocity, L~5 cm is the nozzle length, $\beta\sim10^{-7}$ cm^3/s is the dissociative recombination rate, and $n_e\sim10^{10}$ cm^{-3} is the electron density in the DC discharge estimated from the DC measured DC voltage and current [17]. This result suggests that a transverse RF discharge can be efficiently used to produce rather high electron densities, as well atomic species and radical concentrations in supersonic flows of molecular gases.

Table 2. Electron density measurements

Run #	Gas mixture	DC power, W	RF power, W	δV/V	n_e, cm^{-3}
9	N_2	0	100	0.098	$1.93\cdot10^{11}$
10			150	0.079	$1.55\cdot10^{11}$
11			200	0.076	$1.49\cdot10^{11}$
12			250	0.077	$1.51\cdot10^{11}$
13	70% N_2, 30% He		200	0.096	$1.60\cdot10^{11}$
14	30% N_2, 70% He		200	0.29	$3.60\cdot10^{11}$
15	30% N_2, 70% He	175	0	$<2.5\cdot10^{-3}$	$<3\cdot10^9$

Figure 3 shows the results of the test section pressure measurements during the wind tunnel operation with both DC and RF discharges turned off. One can see that the static pressure remains stable and nearly constant (within 5%) for about 30 seconds before the back pressure starts rising. Turning the DC discharge on had almost no effect of the test section pressure, while

turning the RF discharge on resulted only in a slight pressure increase (within 1-3% depending on the RF power).

As in our previous experiments [18], with the DC and/or RF discharge on, the nozzle and the test section are filled with bright visible emission, arising primarily from the well-known second positive bands of nitrogen, $C^3\Pi_u \rightarrow B^3\Sigma_g$. This emission allowed straightforward supersonic plasma flow and shock visualization [17,18]. As a first-order approximation, neglecting kinetic processes of population and decay of electronically excited radiating species, we can assume that the observed emission intensity (i.e. the radiating species concentration) is simply proportional to the local number density. The rationale for this assumption is the fact that the excited electronic level populations of N_2 are strongly coupled with the ground state vibrational populations of nitrogen which relax extremely slowly. For example, the vibration-translation (V-T) relaxation time of N_2 by He at the conditions of the present experiment is of the order of seconds [31], while the flow residence time in the test section is of the order of tens of microseconds.

Figure 4 shows inverted B&W photographs of a supersonic N_2-He flow over a wedge in a quasi-two-dimensional plane nozzle [18] and a supersonic N_2-He flow over a cone in the nozzle shown in Fig. 1. Both flows are visualized by a DC discharge sustained in the nozzle plenum. Comparison of these two images shows significant qualitative differences. Indeed, the supersonic flow field over the wedge appears to be quite complicated. First, one can see that the visible oblique shock attached to the wedge nose extends only over about 1/4 of the wedge length. Second, there appears to be a fainter secondary shock formed about halfway along the wedge. Finally, there are two distinct bright features formed near the wedge surface, which look similar to boundary layers. On the other hand, the supersonic flow over the cone appears to be much less complicated. The entire region behind the shock is filled with bright, nearly uniform visible emission, with no apparent bright or dark structures (see Fig. 4). This observation is consistent with our assumption regarding the correlation between the emission intensity and the local number density. Indeed, in the absence of the shock perturbation by the nozzle walls the number density of the flow behind the conical shock is expected to be uniform. The conical shock front looks somewhat less distinct compared to the oblique shock front (see Fig. 4), since in the former case we are looking at a three dimensional object which is not entirely in focus.

This qualitative analysis suggests that the flow over a wedge in the quasi-two-dimensional plane nozzle studied in our previous experiment [17,18] is rather strongly perturbed by the nozzle side walls, which were only 4-5 mm apart. In the wedge flow shown in Fig. 4, the oblique shock angle of $\alpha=100^\circ$ indicates a test section Mach number of M=2.05. In the cone flow, the shock angle is $\alpha=68^\circ$, which corresponds to a Mach number of M=2.39. The shock angle is measured with an accuracy of $\pm 0.75^\circ$, which was found by comparing the angle determined from several frames of a high-resolution video camera taken during the same run at a rate of about 1 frame per second.

Unlike our previous experiments [18], turning the RF discharge on and off during the wind tunnel operation did not result in a measurable shock angle increase. These measurements have been done in all three gas mixtures considered. In these measurements, the DC discharge was on all the time to provide plasma flow visualization and enable shock angle measurements with the RF discharge off. The maximum RF discharge power applied was 350 W, which is almost twice

the maximum RF power used in our previous experiments in a quasi-two-dimensional plane nozzle (200 W) [18], which showed considerable shock weakening. As an example, Fig. 5 shows two typical flow images obtained in a 30% N_2 - 70% He flow over a cone with the 250 W RF discharge turned on and off. In all runs, the shock angle with the RF discharge turned on was within about 1° from its value with the RF discharge turned off, α=68°. At all experimental conditions, the shock front appeared sharp and well defined, with no evidence of splitting or dispersion (e.g. see Fig. 5).

In our previous shock weakening experiments in a supersonic flow over a 35° wedge [18], the oblique shock angle in a 30% N_2 - 70% He flow increased from $\alpha=99^0$ to $\alpha'=113^0$, which corresponds to an apparent Mach number reduction from M=2.06 to M'=1.88 (M'/M≅0.913). In a supersonic flow over a cone, the shock angle change that corresponds to such Mach number reduction, from M=2.39 to M'=2.18, is substantially smaller because of the three-dimensional relief effect, from $\alpha=68^0$ to $\alpha'=72^0$. However, a 4^0 angle change considerably exceeds the accuracy of the shock angle measurements, and a consistent shock angle increase of such magnitude would certainly be detected.

Thus, removal of the heated boundary layers, which contributed to the shock weakening in our previous plasma wind tunnel experiments [18] and the resultant reduction of the gas temperature gradients in the supersonic test section essentially resulted in disappearance of the effect of plasma on the shock strength. Although in the present experiments the RF discharge power substantially exceeded the power used in our previous work [18], this did not produce any detectable shock weakening. Therefore we conclude that the heated boundary layer / oblique shock interaction was indeed the only reason for the previously reported shock weakening in the plasma wind tunnel. Also, since in the present experiments both the flow and the plasma parameters (P=10-20 torr, M=2.4, $n_e/N=(1.2\text{-}3.0)\cdot10^{-7}$) are comparable with their values in the previous plasma shock experiments [1,2,12,13], these results strongly suggest that previously reported anomalous shock behavior in nonequilibrium plasmas is due to thermal effects alone.

4. Acknowledgements

Support from the Air Force Office of Scientific Research (AFOSR Grant No. 49620-99-1-0023) is gratefully acknowledged.

5. References

1. Klimov, A.I., Koblov, A.N., Mishin, G.I., Yu.L. Serov, and I.P. Yavor, "Shock Wave Propagation in a Glow Discharge", Soviet Technical Physics Letters, vol. 8, No. 4, 1982, pp. 192-194
2. A.I. Klimov, A.N. Koblov, G.I. Mishin, Yu.L. Serov, K.V. Khodataev, and I.P. Yavor, "Shock Wave Propagation in a Decaying Plasma", Soviet Technical Physics Letters, vol. 8, No. 5, 1982, pp. 240-241
3. I.V. Basargin and G.I. Mishin, "Probe Studies of Shock Waves in the Plasma of a Transverse Glow Discharge", Soviet Technical Physics Letters, vol. 11, No. 11, 1985, pp. 535-538

4. V.A. Gorshkov, A.I. Klimov, G.I. Mishin, A.B.Fedotov, and I.P. Yavor, "Behavior of Electron Density in a Weakly Ionized Nonequilibrium Plasma with a Propagating Shock Wave", Soviet Physics - Technical Physics, vol. 32, No. 10, 1987, pp. 1138-1141
5. A.P. Ershov, S.V. Klishin, A.A. Kuzovnikov, S.E. Ponomareva, and Yu.P. Pyt'ev, "Application of the Reduction Method to the Microwave Interferometry of Shock Waves in Weakly Ionized Plasma", Soviet Physics - Techical Physics, vol. 34, No. 8, 1989, p. 936-937
6. I.V. Basargin and G.I. Mishin, "Precursor of Shock Wave in Glow-Discharge Plasma", Soviet Technical Physics Letters, vol. 15, No. 4, 1989, p. 311-313
7. S.A. Bystrov, I.S. Zaslonko, Yu.K. Mukoseev, and F.V. Shugaev, "Precursor Ahead of a Shock Front in an RF Discharge Plasma", Soviet Physics - Doklady, vol. 35, No. 1, 1990, pp. 39-40
8. G.I. Mishin, Yu.L. Serov, and I.P. Yavor, "Flow Around a Sphere Moving Supersonically in a Glow Discharge Plasma", Soviet Technical Physics Letters, vol. 17, No. 6, 1991, pp. 413-416
9. G.I. Mishin, A.I. Klimov, and A.Yu. Gridin, "Measurements of the Pressure and Density in Shock Waves in a Gas Discharge Plasma", Soviet Technical Physics Letters, vol. 17, No. 8, 1992, pp. 602-604
10. A.Yu. Gridin, A.I. Klimov, and K.V. Khodataev, "Propagation of Shock Waves in a Nonuniform Transverse Pulsed Discharge", High Temperature, vol. 32, No. 4, 1994, pp. 454-457
11. A.P. Bedin and G.I. Mishin, "Ballistic Studies of the Aerodynamic Drag on a Sphere in Ionized Air", Technical Physics Letters, vol. 21, 1995, pp. 5-7
12. B.N. Ganguly, P. Bletzinger, and A. Grascadden, "Shock Wave Dispersion in Nonequilibrium Plasmas", Physics Letters A, vol. 230, No. 3-4, 1997, pp. 218-222
13. P. Bletzinger and B.N. Ganguly, "Local Acoustic Shock Velocity and Shock Structure Recovery Measurements in Glow Discharges", Physics Letters A, vol. 258, No. 4-6, 1999, pp. 342-348
14. H. Lowry, M. Smith, P. Sherrouse, J. Felderman, J. Drakes, M. Bauer, D. Pruitt, and D. Keefer, "Ballistic Range Tests in Weakly Ionized Argon", AIAA Paper 99-4822, AIAA 30th Plasmadynamics and Lasers Conference, Norfolk, VA, June 28-July 1, 1999
15. Yu.Z. Ionikh, N.V. Chernysheva, A.V. Meshchanov, A.P. Yalin, and R.B. Miles, "Direct Evidence for Thermal Mechanism of Plasma Influence on Shock Wave Propagation", Physics Letters A, vol. 259, 1999, pp. 387-392
16. A. R. White, S. M. Aithal, and V. V. Subramaniam, "Experimental Studies of Spark Generated Shock Waves", paper AIAA 99-3670 presented at the 30th AIAA Plasmadynamics and Lasers Conference, Norfolk, Virginia, June 28-July 1, 1999
17. Yano. R., Contini, V., Ploenjes, E., Palm, P., Merriman, S., Aithal, S., Adamovich, I., Lempert. W., Subramaniam. V., and Rich, J.W., "Supersonic Nonequilibrium Plasma Wind Tunnel Measurements of Shock Modification and Flow Visualization", AIAA Journal, vol. 38, No. 10, 2000, pp. 1879-1888
18. I.V. Adamovich, S. Merriman, E. Ploenjes, and P. Palm, "Shock Wave Control by Nonequilibrium Plasmas in Cold Supersonic Gas Flows", Paper 00-2327, presented at special session on high-speed flow control, AIAA Fluids 2000 Conference, Denver, CO, June 19-22, 2000; accepted for publication in AIAA Journal, 2001
19. S. Merriman, A. Christian, R. Meyer, B. Kowalczyk, P. Palm, and I.V. Adamovich, "Studies of Conical Shock Modification by Nonequilibrium RF Discharge Plasma", AIAA Paper

2001-0347, presented at 39th Aerospace Sciences Meeting and Exhibit, January 2001, Reno, NV
20. A. R. White and V. V. Subramaniam, "Shock Propagation through a Low Pressure Glow Discharge in Argon", accepted for publication in J. Thermophysics & Heat Transfer, 2001
21. R.F. Avramenko, A.A. Rukhadze, and S.F. Teselkin, "Structure of a Shock Wave in a Weakyly Ionized Nonisothermal Plasma", Soviet Physics - ZhETP Letters, vol. 34, No. 9, pp. 463-466, 1981
22. G.V. Vstovskii and G.I. Kozlov, "Propagation of Weak Shock Waves in a Vibrationally Excited Gas", Sov. Tech. Phys., vol.31, No. 8, pp. 911-914, 1986
23. V. Soloviev, V. Krivtsov, A. Konchakov, and N. D. Malmuth, "Mechanisms of Shock Wave Dispersion and Attenuation in Weakly Ionized Cold Discharge Plasmas", AIAA Paper 99-4908, AIAA 30th Plasmadynamics and Lasers Conference, Norfolk, VA, June 28-July 1, 1999
24. V. Bychkov, and N. Malmuth, "Shock Wave Structure in Nonequilibrium Ar Discharge Plasma", AIAA Paper 99-4938, AIAA 30th Plasmadynamics and Lasers Conference, Norfolk, VA, June 28-July 1, 1999
25. W.F. Bailey and W.M. Hilbun, "Baseline of Thermal Effects on Shock Propagation in Glow Discharges", Proceedings of Workshop on Weakly Ionized Gases, pp. GG3-GG18, U.S. Air Force Academy, June 9-13, 1997
26. Y.Z. Ionikh, N.V. Chernysheva, A.P. Yalin, S.O. Macheret, L. Martinelli, and R.B. Miles", "Shock Wave Propagation Through Glow Discharge Plasmas - Evidence of Thermal Mechanism of Shock Dispersion", AIAA Paper 2000-0714, 38th AIAA Aerospace Sciences Meeting and Exhibit, Reno, NV, January 10-13, 2000
27. S. Aithal and V.V. Subramaniam, "On the Characteristics of a Spark Generated Shock Wave", Physics of Fluids, vol. 12, 2000, pp. 924-934
28. I.V. Adamovich, V.V. Subramaniam, J.W. Rich, and S.O. Macheret, "Phenomenological Analysis of Shock Wave Propagation in Weakly Ionized Plasmas", AIAA Journal, vol. 36, No.5, 1998, pp. 816-822
29. Raizer, Yu.P., "Gas Discharge Physics", Springer, Berlin, 1991
30. P. Palm, E. Plönjes, M. Buoni, V.V. Subramaniam, and I.V. Adamovich, "Electron Density and Recombination Rate Measurements in CO-Seeded Optically Pumped Plasmas", accepted for publication in Journal of Applied Physics, 2001
31. Billing, G.D., "Vibration-Vibration and Vibration-Translation Energy Transfer, Including Multiquantum Transitions in Atom-Diatom and Diatom-Diatom Collisions", Nonequilibrium Vibrational Kinetics, Springer-Verlag, Berlin, 1986, Chap. 4, pp. 85-111
32. N.L. Aleksandrov, F.I. Vysikailo, R.Sh. Islamov, I.V. Kochetov, A.P. Napartovich, and V.G. Pevgov, "Electron Distribution Function in a N_2:O_2=4:1 Mixture", Sov. High Temperature, Vol. 19, 1981, p. 22
33. I.V. Adamovich and J.W. Rich, "The Effect of Superelastic Electron-Molecule Collisions on the Vibrational Energy Distribution Function", Journal of Physics D: Applied Physics, vol. 30, No. 12, 1997, pp. 1741-1745

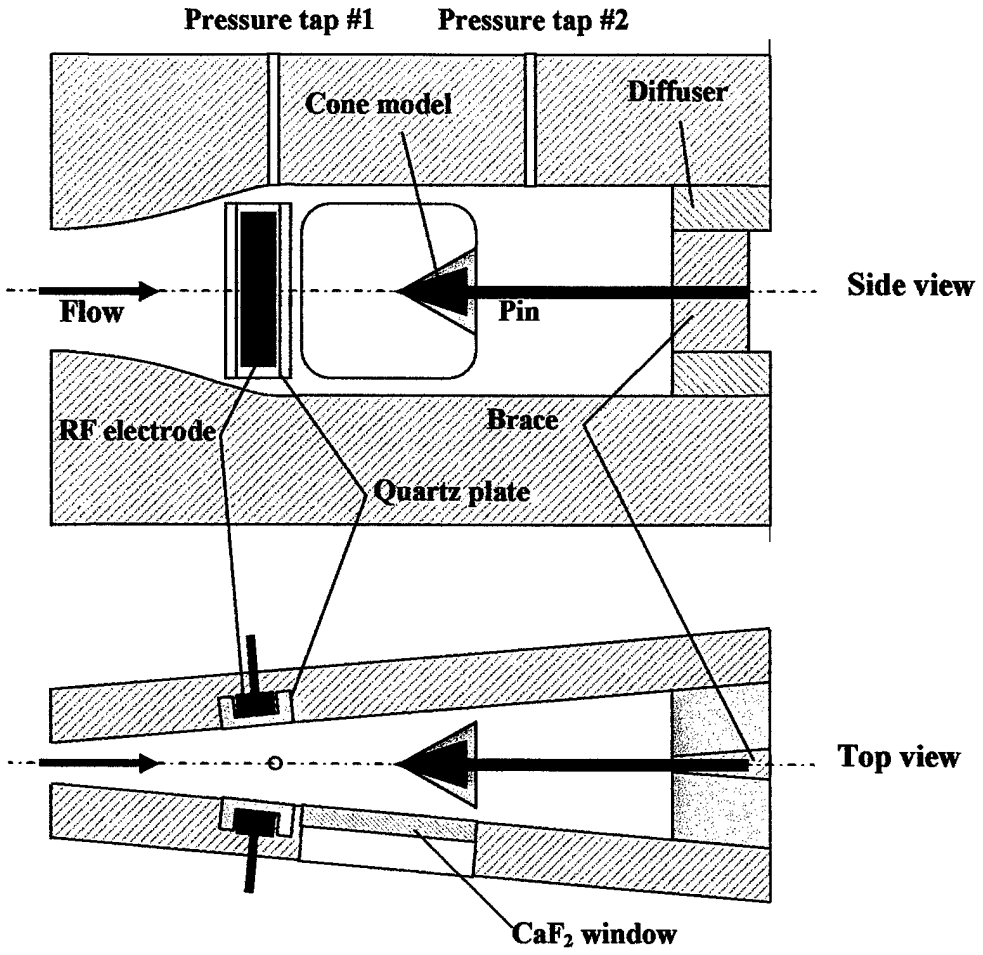

Figure 1. Schematic of the supersonic RF discharge / test section

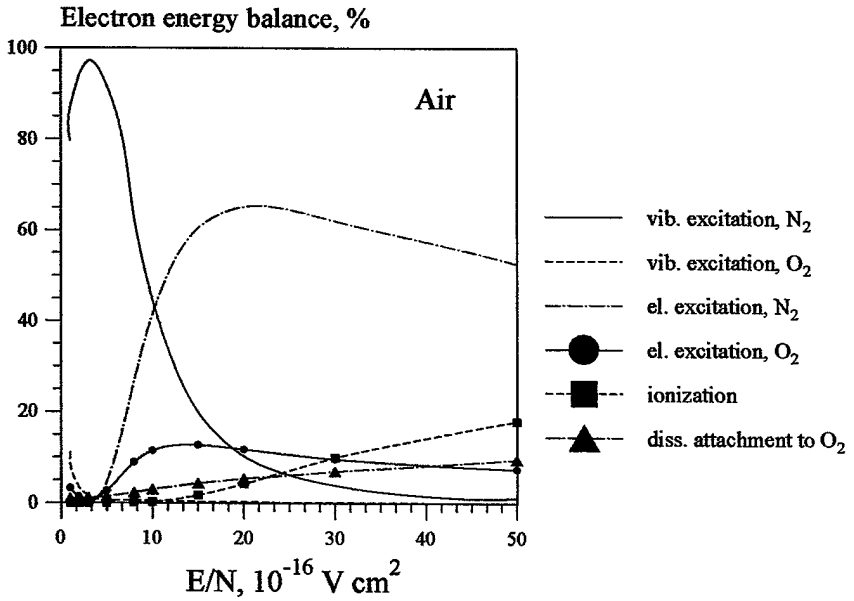

Figure 2. Electron energy balance in air plasmas [32]

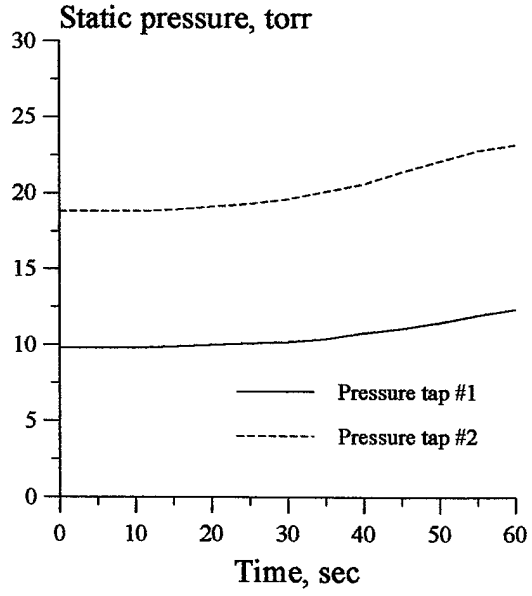

Figure 3. Results of test section static pressure measurements. Air at P_0=250 torr

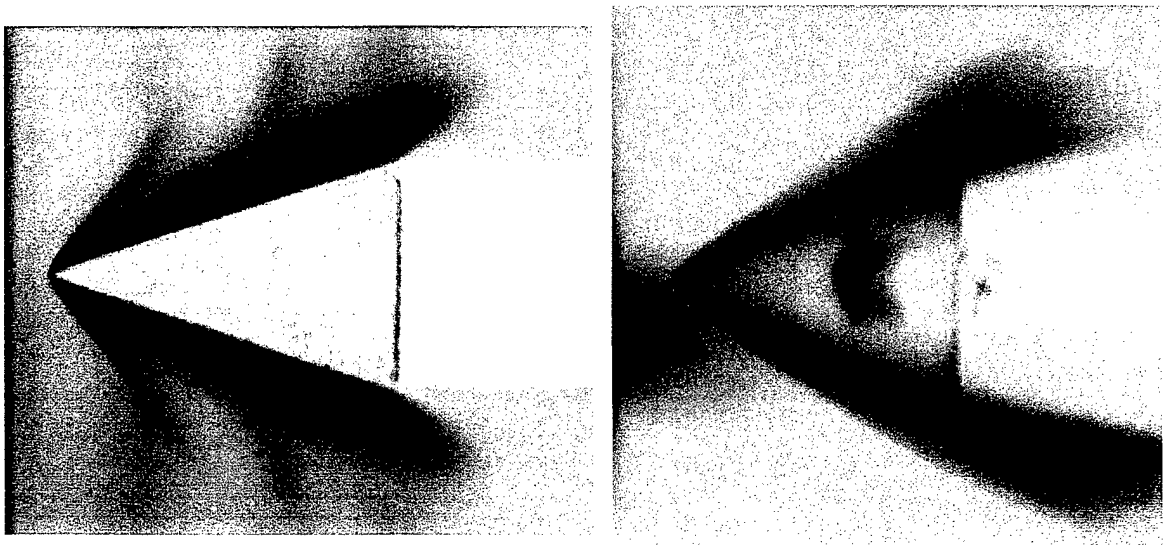

Figure 4. Inverted photographs of the supersonic flows visualized by the plasma generated by a DC discharge in the nozzle plenum at P_0=250 torr.
Left: 50% N_2 – 50% He flow over a 35^0 wedge [18]. The shock angle is 100^0 (M=2.05).
Right: 30% N_2 – 70% He flow over a 40^0 cone. The shock angle is 69^0 (M=2.39).

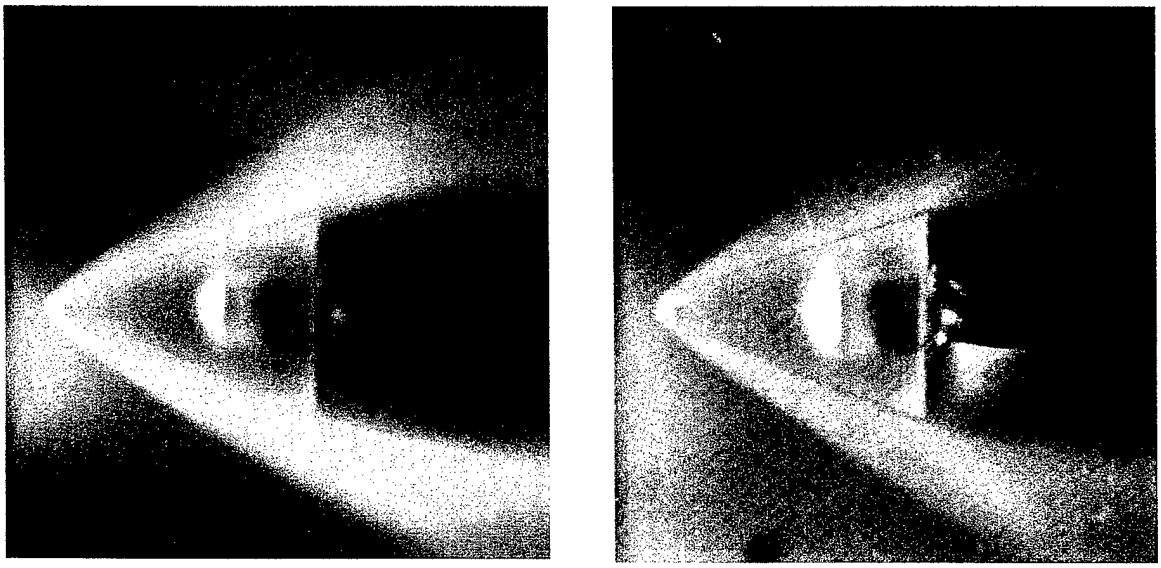

Figure 5. Photographs of the supersonic flow over a cone visualized by the plasma generated by a DC and an RF discharges in a 30% N_2 – 70% He flow at P_0=250 torr
Left: only the 175 W DC discharge is on.
Right: both the 175 W DC and the 250 W RF discharge are on.